AD723350

Bulletin 41
(Part 5 of 7 Parts)

THE SHOCK AND VIBRATION BULLETIN

Part 5
Shock, Fragility

DECEMBER 1970

A Publication of
THE SHOCK AND VIBRATION
INFORMATION CENTER
Naval Research Laboratory, Washington, D.C.

DDC
RECEIVED
MAY 21 1971
C

Office of
The Director of Defense
Research and Engineering

Reproduced by
NATIONAL TECHNICAL
INFORMATION SERVICE
Springfield, Va. 22151

This document has been approved for public release and sale; its distribution is unlimited.

89

ACCESSION for
CFSTI WHITE SECTION ☑
DDC BUFF SECTION ☐
UNANNOUNCED ☐
JUSTIFICATION .....
BY .....
DISTRIBUTION/AVAILABILITY CODES
DIST. AVAIL. and/or SPECIAL
A 21

SYMPOSIUM MANAGEMENT

THE SHOCK AND VIBRATION INFORMATION CENTER

William W. Mutch, Director
Henry C. Pusey, Coordinator
Rudolph H. Volin, Coordinator
Edward H. Schell, Coordinator
Katherine G. Jahnel, Clerk Typist

Bulletin Production

Graphic Arts Branch, Technical Information Division,
Naval Research Laboratory

Bulletin 41
(Part 5 of 7 Parts)

THE SHOCK AND VIBRATION BULLETIN

DECEMBER 1970

A Publication of
THE SHOCK AND VIBRATION
INFORMATION CENTER
Naval Research Laboratory, Washington, D.C.

The 41st Symposium on Shock and Vibration was held at the Air Force Academy, Air Force Academy, Colorado, on 27-29 October 1970. The U.S. Air Force was host.

Office of
The Director of Defense
Research and Engineering

CONTENTS

PAPERS APPEARING IN PART 5

Shock

A DISCUSSION OF PYROTECHNIC SHOCK CRITERIA 1
M. B. McGrath, Martin Marietta Corporation, Denver, Colorado

A SUMMARY OF PYROTECHNIC SHOCK IN THE AEROSPACE INDUSTRY 9
W. P. Rader, Martin Marietta Corporation, Denver, Colorado and William F. Bangs, Goddard Space Flight Center, Greenbelt, Maryland

MEASURES OF BLAST WAVE DAMAGE POTENTIAL 17
C. T. Morrow, LTV Research Center, Western Division, Anaheim, California

SHOCK RESPONSE OF A BILINEAR, HYSTERETIC BEAM AND SUPPORT SYSTEM 27
Bruce E. Burton, Ohio Northern University and Robert S. Ayre, University of Colorado, Boulder, Colorado

DIGITAL FOURIER ANALYSIS OF MECHANICAL SHOCK DATA 39
H. A. Gaberson, and D. Pal, Naval Civil Engineering Laboratory, Port Hueneme, California

THE COMPUTER DETERMINATION OF MECHANICAL IMPEDANCE FOR SMALL ARMS FROM THE RESPONSE TO RECOIL 53
L. B. Gardner, R. K. Young, and D. E. Frericks, U.S. Army Weapons Command, Rock Island, Illinois

SHOCK PULSE SHAPING USING DROP TEST TECHNIQUES 59
R. E. Keeffe and E. A. Bathke, Kaman Sciences Corporation, Colorado Springs, Colorado

ANALYSIS OF PROJECTILE IMPACT ON COMPOSITE ARMOR 69
Richard A. Fine, IBM Corporation, Rochester, Minnesota and Raymond R. Hagglund, Worcester Polytechnic Institute, Worcester, Massachusetts

A SYSTEMATIC APPROACH TO SHOCK HARDENING 77
J. L. Lipeles, Littleton Research and Engineering Corporation, Littleton, Massachusetts and D. Hoffman, Naval Ammunition Depot, Crane, Indiana

THE DEVELOPMENT OF SHOCK TEST CRITERIA FOR AIRCRAFT DISPENSER WEAPON EJECTION MECHANISMS 89
K. D. Denton, K. A. Herzing, and S. N. Schwantes, Honeywell, Inc., Ordnance Division, Hopkins, Minnesota

SHOCK LOAD RESPONSE OF AN ELASTIC ANNULAR PLATE ON A DISTRIBUTED FOUNDATION 101
John R. Mays, Department of Civil and Environmental Engineering, University of Colorado, Denver, Colorado and James E. Nelson, Space Systems Dynamics, Martin Marietta Corporation, Denver, Colorado

Fragility

METHODOLOGY AND STANDARDIZATION FOR FRAGILITY EVALUATION 111
R. C. Rountree, Logicon, San Pedro, California and F. B. Safford, TRW Systems Group, Redondo Beach, California

CONTROLLING PARAMETERS FOR THE STRUCTURAL FRAGILITY OF LARGE SHOCK ISOLATION SYSTEMS 129
Robert J. Port, Air Force Weapons Laboratory, Kirtland Air Force Base, New Mexico

HARDNESS EVALUATION 135
W. H. Rowan, TRW Systems Group, Redondo Beach, California

FRAGILITY TESTING FOR HYDRAULIC SURGE EFFECTS. 143
D. M. Eckblad, The Boeing Company, Seattle, Washington and W. L. Hedrick, TRW Systems Group, Redondo Beach, California

INITIAL DESIGN CONSIDERING STATISTICAL FRAGILITY ASSESSMENT. 155
R. L. Grant, the Boeing Company, Seattle, Washington

TRANSIENT PULSE DEVELOPMENT 167
J. Crum and R. L. Grant, The Boeing Company, Seattle, Washington

PAPERS APPEARING IN PART 1
Part 1 - Classified
(Unclassified Titles)

CASC (CAPTIVE AIR SPACE CRAFT) — A POSSIBLE CONCEPT FOR RIVERINE BOAT DESIGN
V. H. Van Bibber, Naval Ship Research and Development Laboratory, Panama City, Florida, and N. Elmore, Naval Ship Research and Development Center, Portsmouth, Va.

PROBLEMS OF DAMPING THE WINDOW AREAS OF SONAR DOMES
Howard N. Phelps, Jr., Naval Underwater Systems Center, New London, Connecticut

APPLICATION OF THE FINITE ELEMENT METHOD TO THE SHOCK ANALYSIS OF SONAR TRANSDUCERS
Vincent D. Godino and George A. Ziegra, General Dynamics/Electric Boat Division, Groton, Connecticut

DYNAMIC RESPONSE OF ABOVE-GROUND TARGETS TO A BLAST WAVE
P. N. Mathur, D. M. Rogers, R. H. Lee, and J. W. Murdock, The Aerospace Corporation, San Bernardino, California

PAPERS APPEARING IN PART 2

Keynote Talk

THE DYNAMIC CENTURY
D. Zonars, Air Force Dynamics Laboratory, Wright-Patterson Air Force Base, Ohio

Physiological Effects

TESTING AND MODELING STANDING MAN'S RESPONSE TO IMPACT
Joseph Gesswein and Paul Corrao, Naval Ship Research and Development Center, Washington, D.C.

EQUAL ANNOYANCE CONTOURS FOR THE EFFECT OF SINUSOIDAL VIBRATION ON MAN
C. Ashley, Mechanical Engineering Department, University of Birmingham, England

Isolation

ISOLATION FROM MECHANICAL SHOCK WITH A MOUNTING SYSTEM HAVING NONLINEAR DUAL-PHASE DAMPING
J. C. Snowdon, Ordnance Research Laboratory, The Pennsylvania State University, University Park, Pennsylvania

INTERACTIVE OPTIMAL DESIGN OF SHOCK ISOLATION SYSTEMS
W. D. Pilkey, University of Virginia, Charlottesville, Virginia

DESIGN OF HIGH-PERFORMANCE SHOCK ISOLATION SYSTEMS
Ronald L. Eshleman, IIT Research Institute, Chicago, Illinois

ELASTIC WAVE PROPAGATION IN A HELICAL COIL WITH VARYING CURVATURE AND ITS APPLICATION AS AN IMPACT LOAD DISPERSER
Nam P. Suh, Department of Mechanical Engineering, Massachusetts Institute of Technology, Cambridge, Massachusetts

ANALYSIS OF THE INVERTING TUBE ENERGY ABSORBER
J. M. Alcone, Sandia Laboratories, Livermore, California

THE EFFECTS OF PAYLOAD PENETRATION AND VARIOUS ANALYTICAL MODELS ON THE DESIGN OF A SPHERICAL CRUSHABLE CASING FOR LANDING ENERGY ABSORPTION
Robert W. Warner and Margaret Covert, NASA Ames Research Center

Damping

EFFECT OF FREE LAYER DAMPING ON RESPONSE OF STIFFENED PLATE STRUCTURES
David I. G. Jones, Air Force Materials Laboratory, Wright-Patterson AFB, Ohio

VIBRATION CONTROL BY A MULTIPLE-LAYERED DAMPING TREATMENT
A. D. Nashif, University of Dayton Research Institute, Dayton, Ohio and T. Nicholas, Air Force Materials Laboratory, Wright-Patterson Air Force Base, Ohio

DETERMINATION OF DAMPING PROPERTIES OF SOFT VISCOELASTIC MATERIALS
Fakhruddin Abdulhadi, IBM General Systems Division, Rochester, Minnesota

IMPROVING RELIABILITY AND ELIMINATING MAINTENANCE WITH ELASTOMERIC DAMPERS FOR ROTOR SYSTEMS
J. L. Potter, Lord Manufacturing Company, Erie, Pennsylvania

EFFECT OF HIGH POLYMER ADDITIVES ON DIFFUSER FLOW NOISE
B. M. Ishino, California State College, Fullerton, California and R. C. Binder, University of Southern California, Los Angeles, California

HAWK SUSPENSION SYSTEM PERFORMANCE ON M754 TRACKED VEHICLE
Paul V. Roberts, Raytheon Company, Missile Systems Division, Bedford, Massachusetts

PAPERS APPEARING IN PART 3

Instrumentation

A PRACTICAL APPLICATION OF ACCELEROMETER CALIBRATIONS
R. R. Bouche, Endevco, Dynamic Instrument Division, Pasadena, California

DESIGNING AN INSTRUMENTED TEST EGG FOR DETECTING IMPACT BREAKAGE
William L. Shupe, USDA, Agricultural Research Service, Transportation and Facilities Research Div., University of California, Davis, California and Robert M. Lake, Mayo Clinic, Rochester, Minnesota

AN ACCELEROMETER DESIGN USING FERROFLUID ULTRASONIC INTERFEROMETRY
Jack G. Parks, U.S. Army Tank-Automotive Command, Warren, Michigan

HYBRID TECHNIQUES FOR MODAL SURVEY CONTROL AND DATA APPRAISAL
Robert A. Salyer, TRW Systems, Inc., Redondo Beach, California

OBJECTIVE CRITERIA FOR COMPARISON OF RANDOM VIBRATION ENVIRONMENTS
F. F. Kazmierczak, Lockheed Missiles and Space Company, Sunnyvale, California

THE APPLICATION OF ANALOG TECHNIQUES TO REAL TIME ANALYSIS AND SCREENING OF DYNAMIC DATA
Roger C. Crites, McDonnell Aircraft Co., St. Louis, Mo.

SHOCK LOADING AND HOLOGRAPHIC INTERFEROMETRY IN NDT
R. L. Johnson, R. Aprahamian and P. G. Bhuta, TRW Systems Group, Redondo Beach, California

Data Analysis

A NEW SYNTHESIS TECHNIQUE FOR SHOCK SPECTRUM ANALYSIS
William G. Pollard, Spectral Dynamics Corporation of San Diego, San Diego, California

THE ROLE OF LATENT INFORMATION IN INFORMATION PROCESSING IN MEASURING SYSTEMS
Peter K. Stein, Arizona State University, Tempe, Arizona

Test Facilities

USBR VIBRATION TEST SYSTEM
R. M. McCafferty, U.S. Bureau of Reclamation, Denver, Colorado

MULTI-DEGREE OF FREEDOM MOTION SIMULATOR SYSTEMS FOR TRANSPORTATION ENVIRONMENTS
T. K. DeClue, R. A. Arone and C. E. Deckard, Wyle Laboratories, Huntsville, Alabama

DESIGN AND FABRICATION OF AN AIRCRAFT SEAT CRASH SIMULATOR
Nelson M. Isada, State University of New York at Buffalo, Buffalo, New York

DESCRIPTION OF A SHOCK AND VIBRATION DISPLACEMENT AMPLIFIER
D. Cerasuolo and J. Chin, Raytheon Company, Sudbury, Massachusetts

ARTILLERY SIMULATOR FOR FUZE EVALUATION
H. D. Curchack, Harry Diamond Laboratories, Washington, D.C.

GAS SPRING FIRING AND THE SOFT RECOVERY OF A HARD-WIRE INSTRUMENTED 155 MM PROJECTILE
S. L. Fluent, Heat, Plasma, Climatic, Towers Division, Sandia Laboratories, Albuquerque, New Mexico

FULL-SCALE RECOIL MECHANISM SIMULATOR (FORCED FLUID FLOW THROUGH A CONCENTRIC ORIFICE)
W. J. Courtney, IIT Research Institute, Chicago, Illinois and R. Rossmiller and R. Reade, U.S. Army Weapons Command, Rock Island, Illinois

ISOTOPE FUEL IMPACT FACILITY
Larry O. Seamons, Sandia Laboratories, Albuquerque, New Mexico

A REVERBERATION CHAMBER FOR USE AT REDUCED PRESSURES
M. H. Hieken, J. N. Olson, and G. W. Olmsted, McDonnell Aircraft Company, St. Louis, Missouri

DESIGN OF AN OFF-ROAD VEHICLE MOTION SIMULATOR
Nelson M. Isada, Cornell Aeronautical Laboratory, Inc., and State University of New York at Buffalo, Buffalo, New York and Robert C. Sugarman, and E. Donald Sussman, Cornell Aeronautical Laboratory, Inc., Buffalo, New York

AN AERIAL CABLE TEST FACILITY USING ROCKET POWER
C. G. Coalson, Sandia Laboratories, Albuquerque, New Mexico

PAPERS APPEARING IN PART 4

Vibration

SURVEY OF SPACE VEHICLE VIBRATION ANALYSIS AND TEST TECHNIQUES
W. Henricks, R. J. Herzberg, B. G. Wrenn, Lockheed Missiles and Space Company, Sunnyvale, California

METHODS USED TO REALISTICALLY SIMULATE VIBRATION ENVIRONMENTS
J. V. Otts, Centrifuge, Vibration, and Acoustics Division, Sandia Laboratories, Albuquerque, New Mexico

SIMULATION OF COMPLEX-WAVE PERIODIC VIBRATION
A. J. Curtis, H. T. Abstein, Jr., and N. G. Tinling, Hughes Aircraft Company, Culver City, California

RATIONALES APPLYING TO VIBRATION FOR MAINTENANCE
A. H. Grundy, Canadian Forces Headquarters, Ottawa, Canada

SPECIFICATION OF SINE VIBRATION TEST LEVELS USING A FORCE-ACCELERATION PRODUCT TECHNIQUE
A. F. Witte, Vibration and Acoustics Test Division, Sandia Laboratories, Albuquerque, New Mexico

SOME EFFECTS OF EQUALIZATION WITH A SINGLE MASS VS AN ELASTIC SYSTEM ON ACCELERATIONS AND STRESSES
R. M. Mains, Washington University

A METHOD FOR PREDICTING STRUCTURAL RESPONSES FROM LOWER LEVEL ACOUSTIC TESTS
D. O. Smallwood, Centrifuge, Vibration, Acoustics Division, Sandia Laboratories, Albuquerque, New Mexico

SWEEP SPEED EFFECTS IN RESONANT SYSTEMS
Ronald V. Trull, USAF, 4750th Test Squadron, Tyndall AFB, Florida

THE DYNAMIC RESPONSE OF A STEEL EYEBAR CHAIN SUSPENSION BRIDGE OVER THE OHIO RIVER TO VARIOUS EXCITATIONS
R. F. Varney, J. G. Viner, Federal Highway Administration, Department of Transportation, Washington, D.C.

DUAL SPECIFICATIONS IN RANDOM VIBRATION TESTING, AN APPLICATION OF MECHANICAL IMPEDANCE
A. F. Witte, Vibration and Acoustics Test Division, Sandia Laboratories, Albuquerque, New Mexico and R. Rodeman, Applied Mechanics Division, Sandia Laboratories, Albuquerque, New Mexico

VIBRATION – A DIAGNOSTIC TOOL FOR SHOCK DESIGN
Culver J. Floyd, Raytheon Company, Submarine Signal Division, Portsmouth, Rhode Island

THE RESONANT RESPONSE OF A MECHANICAL SYSTEM SUBJECTED TO LOGARITHMICALLY SWEPT AND NOTCHED BASE EXCITATION, USING ASYMPTOTIC EXPANSION
B. N. Agrawal, COMSAT Laboratories, Clarksburg, Maryland

EFFECTS OF FLIGHT CONDITIONS UPON GUNFIRE INDUCED VIBRATION ENVIRONMENT
J. A. Hutchinson and B. G. Masson, LTV Aerospace Corporation, Vought Aeronautics Division, Dallas, Texas

THE BOX CAR DYNAMIC ENVIRONMENT
Robert W. Luebke, C and O B and O Railroad Companies, Baltimore, Maryland

THE NOISE ENVIRONMENT OF A DEFLECTED-JET VTOL AIRCRAFT
S. L. McFarland and D. L. Smith, Air Force Flight Dynamics Laboratory, Wright-Patterson Air Force Base, Ohio

VIBRATION SIGNATURE ANALYSIS OF BEARINGS AND ELECTRONIC PACKAGES
Charles H. Roos, General Electric Company, Aerospace Electronic Systems, Utica, New York

OUTER LOOP CONTROL FOR VIBRATION TESTING
Gordon Lester, Perkin-Elmer Corporation, Danbury, Connecticut and James Gay Helmuth, Chadwick-Helmuth Company, Inc., Monrovia, California

EMPIRICAL PREDICTION OF MISSILE FLIGHT RANDOM VIBRATION
A. F. Kartman, The Bendix Corporation, Mishawaka, Indiana

STRUCTURAL VIBRATIONS IN THE BELL AH-1G HELICOPTER DURING WEAPON FIRING
R. Holland, Kinetic Systems, Inc., Boston, Massachusetts and D. Marcus and J. Wiland, U.S. Army Frankford Arsenal, Philadelphia, Pennsylvania

CHARACTERISTICS OF GUNFIRE INDUCED VIBRATION IN HELICOPTERS
C. E. Thomas and V. C. McIntosh, Air Force Flight Dynamics Laboratory, Wright-Patterson Air Force Base, Ohio

INFLIGHT VIBRATION AND NOISE STUDY OF THREE HELICOPTERS
Phyllis G. Bolds and John T. Ach, Air Force Flight Dynamics Laboratory, Wright-Patterson Air Force Base, Ohio

PAPERS APPEARING IN PART 6

Dynamics

PARAMETRIC RESPONSE OF MONOSYMMETRIC IMPERFECT THIN-WALLED COLUMNS UNDER SINUSOIDAL LOADING
Stanley G. Ebner, USAF Academy, Colorado and Martin L. Moody, University of Colorado, Denver, Colorado

PREDICTION OF UPSTAGE RANDOM VIBRATION ENVIRONMENT USING A STATISTICAL ENERGY APPROACH
D. E. Hines, G. R. Parker, and R. D. Hellweg, McDonnell Douglas Astronautics Company-West, Santa Monica, California

ON THE REDUCTION AND PREVENTION OF THE FLUID-INDUCED VIBRATIONS OF CIRCULAR CYLINDERS OF FINITE LENGTH
Dirse W. Sallet, Department of Mechanical Engineering, University of Maryland, College Park, Maryland and U.S. Naval Ordnance Laboratory, White Oak, Silver Spring, Maryland

EFFECTS OF LOOSENESS ON DYNAMIC BEHAVIOR
R. E. Beckett, K. C. Pan, U.S. Army Weapons Command, Rock Island, Illinois and D. D. Penrod, The University of Iowa, Iowa City, Iowa

DYNAMIC DEFLECTIONS OF MULTIPLE-SPAN GUIDEWAYS UNDER HIGH SPEED, AIR CUSHION VEHICLES
James F. Wilson, Duke University, Durham, North Carolina

ANALYSIS OF THE MOTION OF A LONG WIRE TOWED FROM AN ORBITING AIRCRAFT
S. A. Crist, Department of Engineering Mechanics, USAF Academy, Colorado

A POSTSHOT STUDY OF THE DYNAMIC RESPONSE OF THE LASL MOBILE TOWER DURING THE PLIERS EVENT
R. E. Bachman, E. F. Smith, Holmes and Narver, Inc., Las Vegas, Nevada and R. P. Kennedy, Holmes and Narver, Inc., Los Angeles, California

BOUNDS FOR THE RESPONSE OF A CONSERVATIVE SYSTEM UNDER DYNAMIC LOADING
H. Brauchli, The University of Alabama in Huntsville, Huntsville, Alabama

THREE DEGREE OF FREEDOM SPRING MASS EJECTION SYSTEM
R. Muskat, Aerospace Corporation, San Bernardino, California

STRUCTURAL DYNAMICS OF A PARABOLOIDAL ANTENNA
Myron L. Gossard and William B. Haile, Jr., Lockheed Missiles and Space Company, Sunnyvale, California

AN APPLICATION OF COMPONENT MODE SYNTHESIS TO ROCKET MOTOR VIBRATION ANALYSIS
F. R. Jensen, Hercules Inc., and H. N. Christiansen, Brigham Young University

COMPARISON OF CONSISTENT AND LUMPED MASS MATRIX SOLUTIONS WITH THE EXACT SOLUTION FOR A SIMPLY-SUPPORTED TIMOSHENKO BEAM
C. Baum, J. T. Higney, Gibbs and Cox, Inc., New York, New York and A. Jenks, Esso International Inc., New York, New York

APPLICATION OF APPROXIMATE TRANSMISSION MATRICES TO DESCRIBE TRANSVERSE BEAM VIBRATIONS
R. D. Rocke and Ranjit Roy, University of Missouri-Rolla, Rolla, Missouri

MEASUREMENT OF MOMENT-CURVATURE RELATIONSHIP FOR STEEL BEAMS
V. H. Neubert and W. Vogel, The Pennsylvania State University, University Park, Pennsylvania

SELF-SYNCHRONIZATION OF TWO ECCENTRIC ROTORS ON A BODY IN PLANE MOTION
Mario Paz, Associate Professor, University of Louisville, Louisville, Kentucky

PROPAGATION OF THE ERROR IN COMPUTED FREQUENCIES AND MODE SHAPES RESULTING FROM A DISCRETE MASS REPRESENTATION OF UNIFORM, SLENDER BEAMS WITH VARYING HEIGHT-TO-LENGTH RATIOS
Francis M. Henderson, Naval Ship Research and Development Center, Washington, D. C.

Dynamic Stress Analysis

A DISCUSSION ON THE ANALYTICAL DYNAMICS, STRESS, AND DESIGN INTERFACES
Irvin P. Vatz, Teledyne Brown Engineering, Huntsville, Alabama

DYNAMIC STRESS ANALYSIS IN A STRATIFIED MEDIUM
Jackson C.S. Yang, Ames Research Center, NASA, Moffett Field, California

COMPARISON OF STRUCTURAL LOADS: STATIC VERSUS DYNAMIC
Paul J. Jones and William J. Kacena, III, Martin Marietta Corporation, Denver, Colorado

EGGSHELLING AND VIBRATIONS OF A HIGH SPEED SHAFT WITH NASTRAN ANALYSIS
Dennis J. Martin and William C. Walton, Jr., NASA Langley Research Center, Hampton, Virginia

PARAMETRIC STUDY OF A BEAM WITH A COMPOUND SIDE-BRANCH RESONATOR AS A DEVICE TO EVALUATE PRELIMINARY DESIGN LOADS
J. Roger Ravenscraft, Teledyne Brown Engineering, Huntsville, Alabama

RAIL LAUNCHING DYNAMICS OF THE SAM-D SURFACE-TO-AIR MISSILE
Martin Wohltmann, Leonard A. Van Gulick, H. Carlton Sutphin, Martin Marietta Corporation, Orlando, Florida

PAPERS APPEARING IN PART 7

Mathematical Analysis

ROCKET-SLED MODEL STUDY OF PREDICTION TECHNIQUES FOR FLUCTUATING PRESSURES AND PANEL RESPONSE
Eric E. Ungar, Bolt Beranek and Newman Inc., Cambridge, Massachusetts

DETERMINATION OF STRUCTURAL PROPERTIES FROM TEST DATA
A. E. Galef and D. L. Cronin, TRW Systems Group, Redondo Beach, California

VALIDITY OF MATHEMATICAL MODELS OF DYNAMIC RESPONSE OF STRUCTURES TO TRANSIENT LOADS
Wilfred E. Baker, Southwest Research Institute, San Antonio, Texas

DYNAMIC RESPONSE OF PLATES WITH CUT-OUTS
Nicholas L. Basdekas, Office of Naval Research, Arlington, Virginia and Michael Chi, Catholic University of America, Washington, D. C.

NATURAL FREQUENCIES AND MODE SHAPES OF PLATES WITH INTERIOR CUT-OUTS
Jon Monahan, P. J. Nemergut, USAF Air Force Institute of Technology, G.E. Maddux, Air Force Flight Dynamics Laboratory Wright-Patterson AFB, Ohio

FINITE BEAM ELEMENTS FOR DYNAMIC ANALYSIS
V. H. Neubert, The Pennsylvania State University, State College, Pennsylvania and H. Lee, Westinghouse Research Laboratory, Pittsburgh, Pennsylvania

EVALUATION OF MODELS FOR ONE-DIMENSIONAL VIBRATION SYSTEMS
R. D. Rocke, University of Missouri-Rolla, Rolla, Missouri

DYNAMIC ELASTOPLASTIC RESPONSE OF GEOMETRICALLY NONLINEAR ARBITRARY SHELLS OF REVOLUTION UNDER IMPULSIVE AND THERMAL LOADINGS
T. J. Chung, J. T. Oden, R. L. Eidson, J. F. Jenkins, and A. E. Masters, Research Institute, The University of Alabama in Huntsville, Huntsville, Alabama

RIGID BODY MOTIONS OF ELASTICALLY RESTRAINED UNDERWATER STRUCTURES FROM DETONATION-INDUCED SHOCK
H. S. Zwibel and J. G. Hammer, Naval Civil Engineering Laboratory, Port Hueneme, California

EXTENSION OF CLASSICAL BINARY FLUTTER MODEL USING ROOT LOCUS
J. C. Hornbuckle, and R. L. Sierakowski, University of Florida, Gainesville, Florida

STIFFNESS AND MASS MATRICES FOR A TRIANGULAR ELEMENT
Mario Paz, Associate Professor, Civil Engineering Department, University of Louisville, Louisville, Kentucky and Earl Berry, Jr., Graduate Student, University of Louisville, Louisville, Kentucky

HELICOPTER FUSELAGE VIBRATION RESPONSE ANALYSIS USING THE HYBRID COMPUTER
James D. Cronkhite, Bell Helicopter Company, Fort Worth, Texas

VIBRATION OF A CLASS OF NONCONSERVATIVE SYSTEMS WITH TIME-DEPENDENT BOUNDARY CONDITIONS
Shoei-sheng Chen, Argonne National Laboratory, Argonne, Illinois

Fluid-Structure Interactions

A VARIATIONAL APPROACH TO THE FLUID-SHELL DYNAMIC INTERACTION PROBLEM
A. S. Benson, Lockheed Missiles and Space Company, Sunnyvale, California

EQUIVALENT MECHANICAL MODEL OF PROPELLANT FREE-SURFACE VIBRATIONS IN THE SATURN S-IVB WORKSHOP CONFIGURATION
Franklin T. Dodge and Luis R. Garza, Southwest Research Institute, San Antonio, Texas

THE EFFECT OF LIQUID OSCILLATIONS ON THE LM PROPELLANT QUANTITY GAUGE SYSTEM
M. Rimer, Grumman Aerospace Corporation, Bethpage, New York and D. G. Stephens, NASA Langley Research Center, Hampton Virginia

DERIVATION OF SKYLAB PROPELLANT STORAGE MODULE RANDOM VIBRATION ENVIRONMENT
A. E. Chirby, R. A. Stevens, H.C. Allen and W.R. Wood, Jr., North American Rockwell Corporation, Space Division, Downey, California

THE FLUTTER OF A HYDROFOIL
Thomas M. Ward, California Institute of Technology, Pasadena, California and Raymond C. Binder, University of Southern California, Los Angeles, California

SUPPLEMENT

AN AIR PULSER FOR VIBRATION TESTING
J. R. Peoples, Naval Ship Research and Development Center, Washington, D.C. and J. G. Viner, Federal Highway Administration, Washington, D. C.,

STATISTICAL APPROACH TO OPTIMIZE RANDOM VIBRATION TEST SPECTRA
David L. Earls and John F. Dreher, Air Force Flight Dynamics Laboratory, Wright-Patterson AFB, Ohio

STATISTICAL APPROACH TO OPTIMIZE RANDOM VIBRATION TEST SPECTRA
David L. Earls and John F. Dreher, Air Force Flight Dynamics Laboratory, Wright-Patterson AFB, Ohio

THE EFFECT OF TAILFINS ON THE VIBRACOUSTIC ENVIRONMENT OF EXTERNALLY CARRIED AIRCRAFT STORES
John F. Dreher, Air Force Flight Dynamics Laboratory, Wright-Patterson Air Force Base, Ohio

THE EFFECTS OF VISCOUS DAMPING ON DYNAMIC LOAD FACTORS FOR SINGLE DEGREE-OF-FREEDOM SYSTEMS
Harry Price Gray, Naval Ship Research and Development Center, Washington, D.C.

THE EFFECT OF CAVITATION ON THE FLAT PLATE HULL UNDERWATER SHOCK MODEL
R. J. Scavuzzo, Rensselaer Polytechnic Institute, Hartford Graduate Center, East Windsor Hill, Connecticut, and D. D. Raftopoulos, The University of Toledo, Toledo, Ohio

A DISCUSSION OF PYROTECHNIC SHOCK CRITERIA

M. B. McGrath
Martin Marietta Corporation
Denver, Colorado

This paper presents and discusses a set of criteria for predicting pyrotechnic shock environments. The spectra to be expected near the source are presented for a variety of pyrotechnic devices, along with a set of attenuation curves for various types of aerospace structures.

INTRODUCTION

In recent years, pyrotechnic devices have been used extensively in the aerospace industry. These devices include linear shaped charges, explosive bolts, separation nuts and bolts, and cartridge-actuated devices such as pin-pullers and bolt cutters. The environments producted by these pyrotechnics can cause damage and/or failure to equipment and structure. As a result, the technology to evaluate these environments is currently being developed.

Today the state-of-the-art of this technology is limited mainly to testing techniques, both to predict the environment and to qualify equipment to the predicted environment. Current testing techniques utilize a variety of simple and complex shock pulse generators and simulated or prototype hardware. The literature depicts many testing methods; and, once an environment has been established, a reasonable test can be produced. The method of predicting the shock environment makes use of available test data to empirically establish the environment.

A recently completed NASA contract with Goddard Space Flight Center involved the compilation and analysis of pyrotechnic shock data collected from the aerospace industry. The data are in the form of acceleration time histories and their related shock spectra for a wide variety of pyrotechnic devices and aerospace structures. A summary of the total program was presented in a paper by W. P. Radar and W. F. Bangs entitled "A Summary of Pyrotechnic Shock in the Aerospace Industry" during the 41st Shock and Vibration Symposium. One aspect of this contract involved using the data to develop criteria for predicting pyrotechnic shock environments. The criteria are presented as a set of source shock spectra for a variety of pyrotechni devices and as a set of attenuation curves for various types of aerospace structures.

This paper presents and discusses these criteria. The types of pyrotechnic devices commonly used and the spectra to be expected near the source for each device are described. The order of severity of the various devices is presented and a set of attenuation curves is given for a variety of aerospace structures. And finally, an attenuation curve for a constant velocity line is presented and discussed.

DATA SOURCE

The principal purpose of Contract NAS5-15208 with Goddard Space Flight Center was to compile and analyze pyrotechnic shock data from the aerospace industry to provide a single reference for shock data and to develop an understanding of the parameters involved. A total of 2837 measurements were compiled, reduced, and presented in four data volumes [1]. A separate volume describes the work accomplished and summarizes the analyses. A sixth volume contains guidelines defining the design information applicable to structure and equipment subjected to a pyrotechnic shock environment.

The guidelines include empirical curves obtained from the data for various types of explosive devices and for a variety of aerospace structures. The empirical curves are not to be considered a statistical estimate but do suggest a representative sample from a limited number of tests. The guidelines can be used most effectively in conjunction with the remaining five volumes of Ref. [1], where each individual test is described and the test data are presented.

SHOCK SPECTRUM CHARACTERISTICS

In a normal pyrotechnic shock test program, the time histories of acceleration at a number of locations are measured and recorded. Because the signature of the time history is quite complex due to the nature of the shock and the intervening structure, the frequency content is not immediately obvious. Therefore, spectral analyses are performed to obtain the frequency information. An acceleration shock spectrum is a plot of the maximum response acceleration of a single-degree-of-freedom oscillator versus the resonant frequency of the oscillator, where base excitation of the oscillator is assumed. A shock spectrum displays both amplitude and frequency information characteristic of the time history, a concept used extensively in the aerospace industry to specify shock environments.

Near the explosive source the acceleration shock spectrum is characterized by a high-amplitude curve that peaks in the high-frequency range, usually well above 1000 Hz. In the low-frequency range, a shock spectrum shows a definite tendency of a constant velocity line, which on a logarithmic plot of the acceleration shock spectrum has a numerical slope of one.

As the shock pulse propagates through the structure, the acceleration amplitude is attenuated. This attenuation is directly proportional to the distance from the source as measured along the shock path. However, the amplitude attenuation is a function of frequency, and the high-frequency range attenuates more rapidly than the low. An example of this characteristic can be seen in Fig. 1, which shows two spectra, one measured near the shock source and the second more than 100 in. from the source. The high-frequency amplitude can attenuate from one to two orders of magnitude in 100 in., while the low-frequency amplitude usually attenuates less than an order of magnitude.

The effect of different attenuation rates can be accounted for by determining two parameters: the attenuation rates of the peak acceleration and of a constant velocity line in the low-frequency range. However, the constant velocity line can be difficult to estimate from a spectrum because of resonant acceleration peaks due to the response of the local structure.

SPECTRUM DETERMINATION

A shock spectrum is used primarily for specifying equipment qualification levels. These levels can be obtained from a full-scale test of the actual structure, but a full-scale test is not always possible. A preliminary estimate of a spectrum can be obtained from the expected level of the explosive device at the source by using empirical attenuation curves. The information for estimating the spectrum level is given in the following sections. These guidelines are strictly empirical and are not intended to represent all applications. Best results can be obtained by using these curves and referring to the data in Ref. [1].

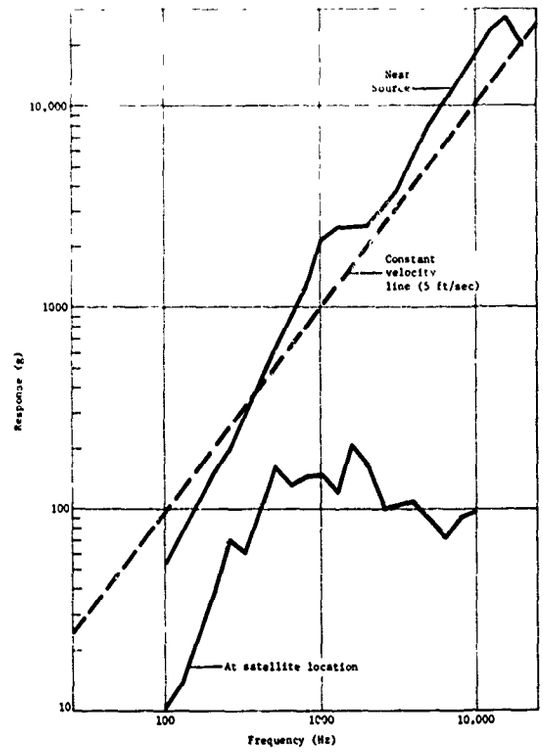

Fig. 1 - Shock spectra at source and satellite location

SOURCE SPECTRA

The following pyrotechnic devices are used in the aerospace industry to affect flight events. The devices are listed in their estimated order of severity.

1. Linear charges (mild detonating fuse and flexible linear shaped charge);
2. Separation nuts and explosive bolts;
3. Pin-pullers and pin pushers;
4. Bolt-cutters, pin-cutters, and cable-cutters.

Absolute acceleration shock spectra for these four devices are discussed below and presented in Figs. 2 through 5. The suggested environments are based on data measured within 10 in. of the explosive source, and the shock spectrum analyses are presented for a damping factor of 5%, i.e., an amplification factor (Q) of 10. These curves represent an envelope of a few measurements and cannot be considered a statistical estimate.

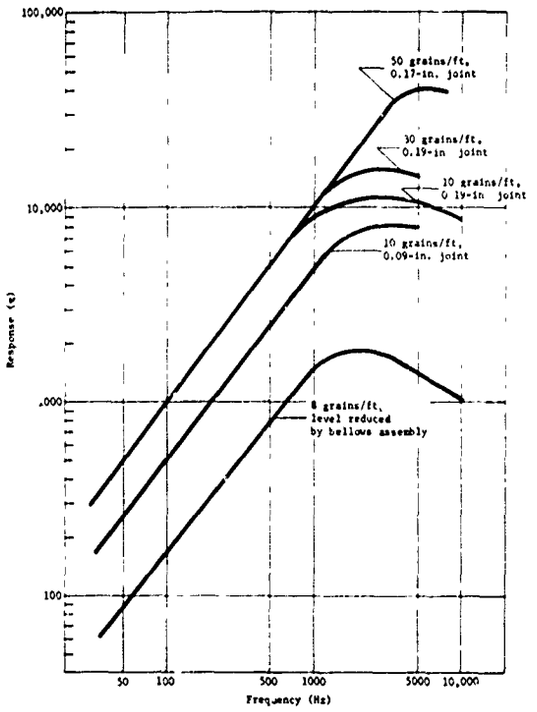

Fig. 2 - Suggested environment produced by linear pyrotechnic devices

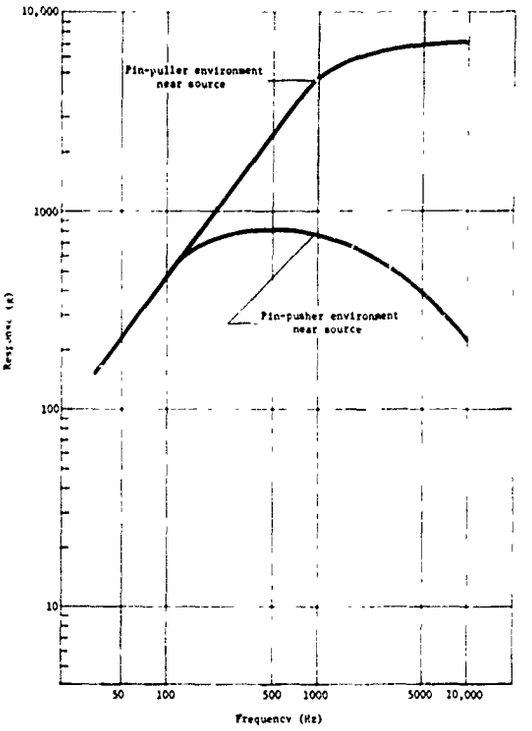

Fig. 4 - Suggested environments produced by pin-pullers and pin-pushers

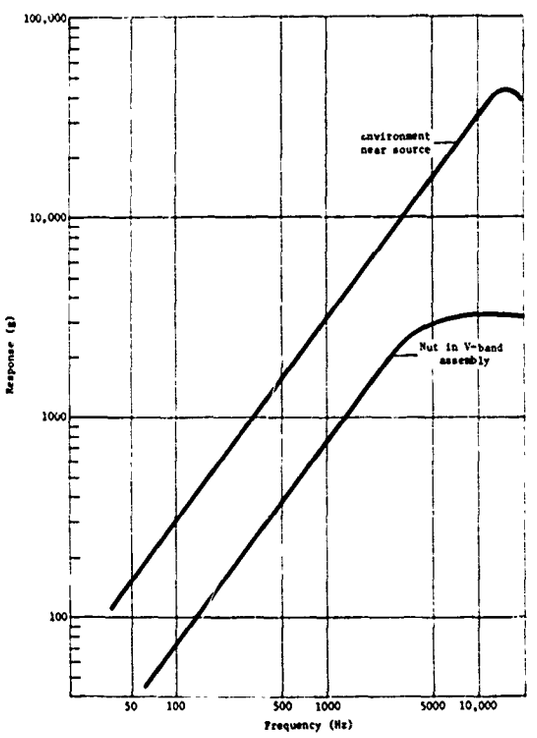

Fig. 3 - Suggested environment produced by separation nuts and explosive bolts

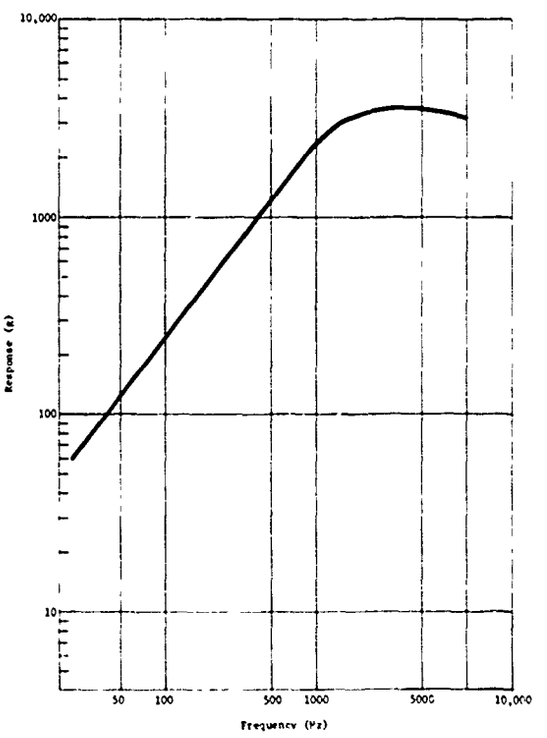

Fig. 5 - Suggested environment produced by bolt-, pin-, and cable-cutters

Linear Explosives

Linear explosive pyrotechnic devices are usually used in separation joints. The level of the environment produced by such a joint separation depends on the thickness of the material cut and the size of the explosive charge. The level of the spectrum increases with an increase of either of these parameters. Figure 2 presents the suggested environment produced by separation joints for several combinations of joint thickness and charge size. Also included is the environment for a bellows assembly, a separation device designed to lower the shock level.

The acceleration time histories characteristic of linear explosive devices have an effective duration of approximately 3 msec.

Separation Nuts and Explosive Bolts

Figure 3 presents the suggested shock environments produced by the detonation of a separation nut or explosive bolt. Two levels are shown: one for the device alone and one for a V-band assembly employing separation nuts or explosive bolts.

The acceleration time histories near the shock source characteristically decay in about 3 msec due to the presence of high-frequencies.

Pin-Pullers and Pin Pushers

Figure 4 presents the suggested shock environments produced by the detonation of pin-pulling and pin pushing pyrotechnic devices.

The acceleration-time histories characteristic of pin-pullers have an effective duration of 5 to 15 msec, while the pin-pusher is a softer, lower-frequency device that may have an effective duration of up to 50 msec.

Bolt-, Pin-, and Cable-Cutters

Figure 5 presents the suggested environments produced by the detonation of bolt-, pin-, and cable-cutting devices.

ATTENUATION CURVES

This section contains attenuation curves for the various types of structures listed in Table 1. These curves relate the predicted attenuation of the peak acceleration level of a shock spectrum to the distance from the shock source. These curves are normalized to a factor of one at the source and are to be used with the spectra curves given for the shock sources above. The normalization measurements are assumed to be 5 in. from the source.

TABLE 1
List of Structures for Attenuation Curves

Structure	Description	Fig. No.
Cylindrical shell	Without stringers or ring/frame	6
Skin ring frame	Longeron or stringer of skin/ring frame	7
Ring/frame	Circumferential ring frame of skin/ring frame with longeron	8
Primary truss	Truss members, including the effects of joints	9
Complex airframe	Airframe structure, including skin and truss structure	10
Complex equipment	Equipment mounting, such as a payload truss network	11
Honeycomb	Honeycomb used as load-carrying structure	12

Because these curves are generated from limited data for each type of structure, they are to be used with discretion; since structures vary so greatly, the levels predicted by these curves can be in error. Consequently, we recommend that the shock levels be confirmed by a full-scale verification test on the flight-configured hardware.

CONSTANT VELOCITY ATTENUATION

As shown in Fig. 1, low-frequency accelerations attenuate with distance less rapidly than those at high frequencies. One way to account for this effect is to specify the attenuation of a constant velocity line with distance. A shock spectrum for a location removed from the source can then be predicted by specifying the two attenuated parameters -- the acceleration peak and a constant velocity line.

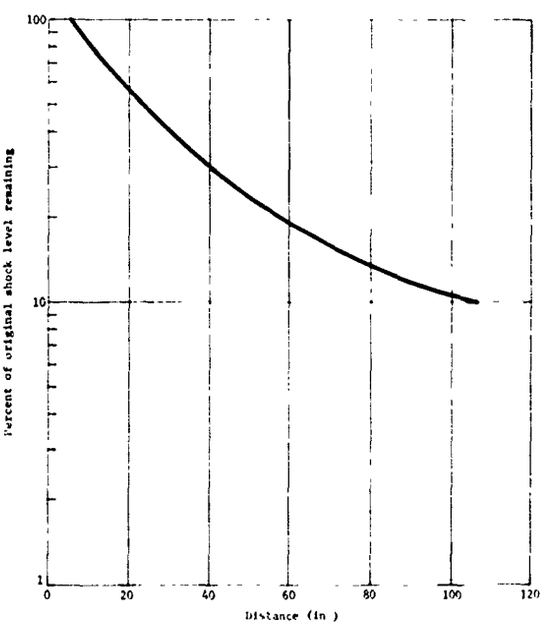

Fig. 6 - Attenuation for cylindrical shell

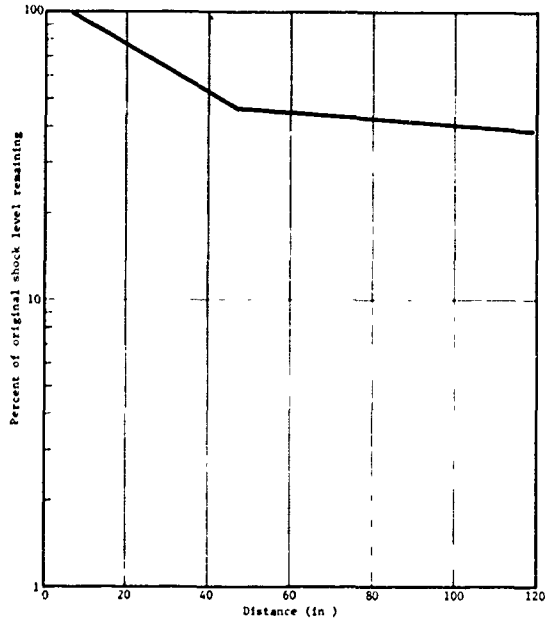

Fig. 7 - Attenuation for longeron or stringer

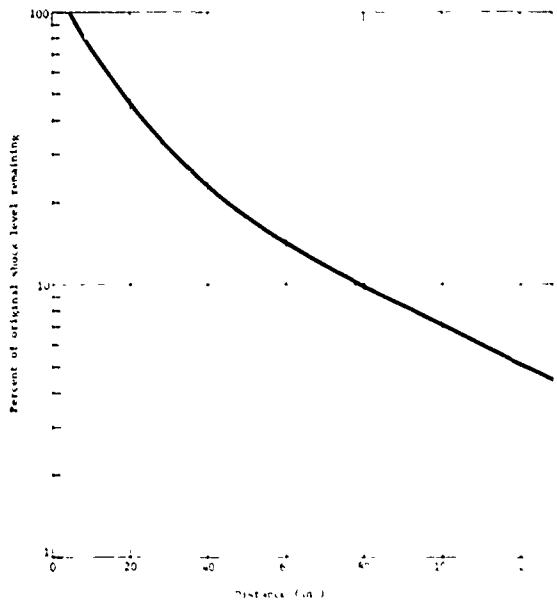

Fig. 8 - Attenuation for ring frame

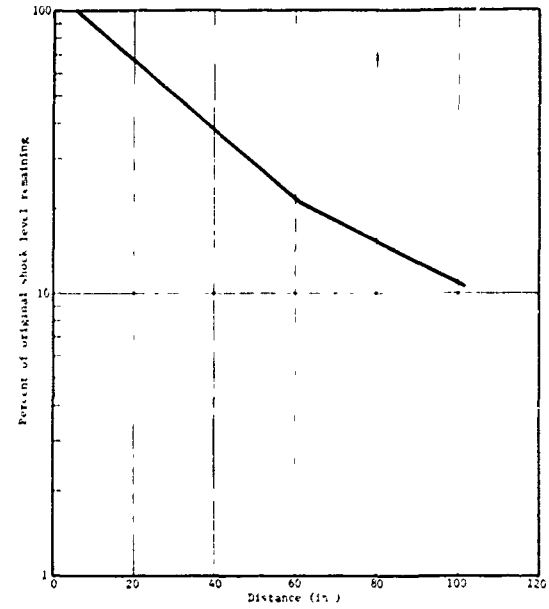

Fig. 9 - Attenuation for primary truss

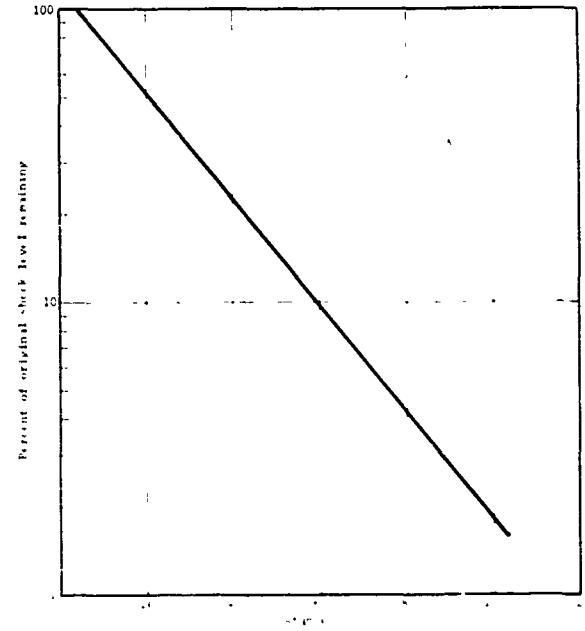

Fig. 10 - Attenuation for complex airframe

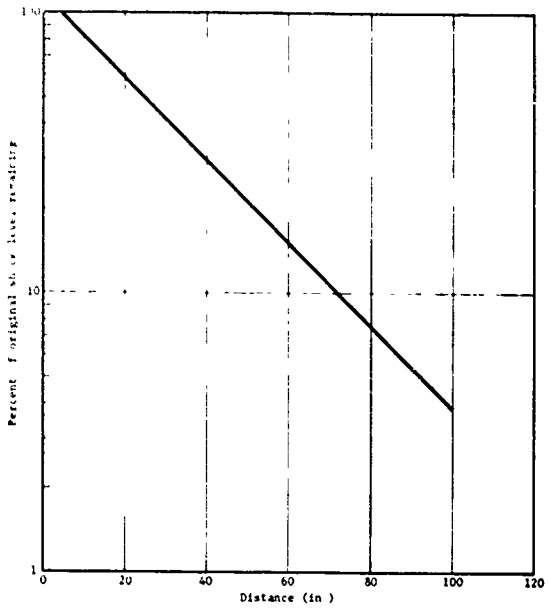

Fig. 11 - Attenuation for equipment mounting structure

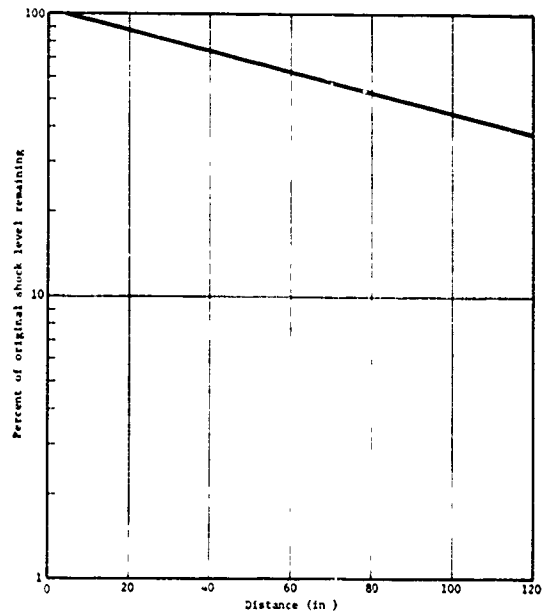

Fig. 12 - Attenuation for honeycomb

Volume one of Ref. [1] discusses the constant velocity concept and presents attenuation curves for this parameter taken from data on a truss structure. A composite of these curves is presented in Fig. 13, where the attenuation curve is normalized to a factor of one. Notice that the curve becomes flat, reflecting the fact that the constant velocity reduces to a certain level and stops. The constant velocity line is sometimes difficult to observe on spectra for locations far removed from the source since resonant peaks will appear in the low-frequency range of the spectrum, as in Fig. 1. It must be emphasized that this curve is obtained from limited data and also that the concept of a constant velocity line is not well established. Two recent articles discuss this concept in detail [2, 3] and relate it to damage potential. The curve in Fig. 13 is presented to account for the difference in attenuation rates over the frequency range of the spectra. Hopefully, the concept of constant velocity as applied to the shock spectra of complex time histories will be studied in more detail in the future.

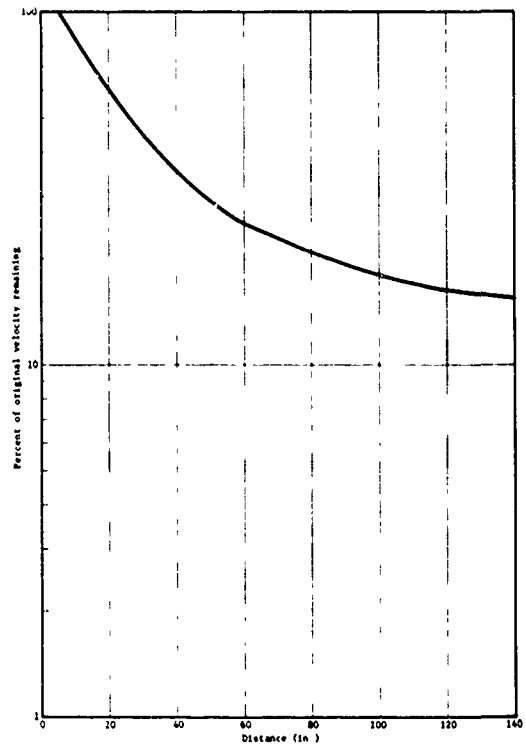

Fig. 13 - Attenuation for constant velocity line

DISCUSSION

results presented in this paper represent an attempt to provide design criteria for pyrotechnic shock. The results are empirical and, due to the large variations among structural configurations, do not provide all the answers. The curves must be used with caution.

The subject of constant velocity lines is currently being studied in the industry, and there is strong evidence of its relationship to damage potential. In this paper the attenuation of this line is used to account for the variation in acceleration with frequency. The data used to predict this attenuation curve are limited, and the entire subject of a constant velocity line needs a great deal of attention.

ACKNOWLEDGEMENTS

The work on which this paper is based has been sponsored by the National Aeronautics and Space Administration's Goddard Space Flight Center under Contract NAS5-15208. The contributors are too numerous to mention here, but are listed in the acknowledgements of Ref. [1].

REFERENCES

1. W. J. Kacena, M. B. McGrath, and W. P. Radar, "Aerospace Systems Pyrotechnic Shock Data, Ground Test and Flight," Martin Marietta Corporation Report MCR-69-611, March 7, 1970.

2. W. H. Roberts, "Explosive Shock," Shock and Vibration Bulletin, No. 40, Part 2, Dec. 1969.

3. H. A. Gaberson and R. H. Chalmers, "Modal Velocity as a Criterion of Shock Severity," Shock and Vibration Bulletin, No. 40, Part 2, Dec. 1969.

DISCUSSION

Mr. Schell (Shock Vibration Information Center): I am puzzled on the modifications to the original spectrum. You reduced both the peak acceleration and the velocity according to criteria determined from the data. I thought that I saw also, in some of the graphs, an attenuation of the high frequency content that differed from plain peak reduction. In other words, you were taking into account the fact that the high frequencies attenuate more rapidly than the low frequencies, is that right?

Mr. McGrath: This is what we are trying to account for. It is a very complex phenomenon. The high frequencies attenuate at different rates throughout the range. We are trying to account for this by a simple and empirical method. Let me also emphasize that the information we presented was envelopes taken from quite a bit of data. We take data, envelope it with one curve, and then use that curve as the attenuation curve. So we are trying to account for a rather complex situation with two simple parameters.

A SUMMARY OF PYROTECHNIC SHOCK IN THE AEROSPACE INDUSTRY

W. P. Rader
Martin Marietta Corporation
Denver, Colorado

and

William F. Bangs
Goddard Space Flight Center
Greenbelt, Maryland

Pyrotechnic shock data have been obtained from a survey of the aerospace industry and government agencies. Over 2800 measurements from 30 contributors have been compiled and categorized according to type of pyrotechnic device and structure. These data were analyzed to provide a reference document and establish guidelines for designing and testing to the pyrotechnic shock environment.

This paper presents a summary of the total program and a discussion of pyrotechnic test simulation techniques. Further results from the study, including guidelines for design and for predicting shock environments, are presented in a paper by Dr. Michael B. McGrath, entitled "A Discussion of Pyrotechnic Shock Criteria" during the 41st Shock and Vibration Symposium.

INTRODUCTION

Pyrotechnic shock is perhaps the least understood of the dynamic environments associated with the operation of aerospace vehicles and components. To date, the problem of predicting or even adequately explaining pyrotechnic shock has defied solution by rigorous mathematical treatments. Prediction of the environment and testing techniques are currently based primarily on empirical methods. Recent observations showed that reliable data were widely scattered among many companies and agencies, and that testing technology was not openly discussed between organizations. Therefore, the Goddard Space Flight Center, recognizing that a large amount of data existed in the industry, sponsored a program to collect and categorize these data and establish guidelines for designing structure and equipment to the pyrotechnic shock environment. The study was performed by the Martin Marietta Corporation under Contracts NAS5-15208 and NAS5-21241.

The specific tasks performed in the course of the program were:

A. Compilation of "reduced" pyrotechnic shock data representative of aerospace systems.

B. Definition of distinctive characteristics of pyrotechnic shock transients.

C. Evaluation of the "quality" of typically available pyrotechnic shock data.

D. Recommendation of measurement systems for ground test and flight.

E. Preparation of guidelines defining design information applicable to structure and equipment design.

F. Recommendation of test simulation techniques.

G. Classification of pyrotechnic systems according to the nature of resulting shock and damaging effects.

H. Evaluation of effects of structural configurations and materials on resulting shock characteristics.

I. Formulation of a follow-on research program.

J. Application of shock propagation theory to at least one class of pyrotechnic systems compiled in task C and comparison of results with measured data.

K. Performance of a ground test program using full scale Titan III structure to provide specific information that will aid in the understanding of basic pyrotechnic shock transient phenomena.

F. Investigation of the effects of mass loading on the pyrotechnic shock environment.

A complete description of each of these tasks and the results have been published in a six volume report [1]. This paper presents a brief description of results of selected tasks with emphasis on test simulation of pyrotechnic shock.

DATA COMPILATION AND CATEGORIZATION

Over 2800 pyrotechnic shock measurements were compiled and categorized according to the type of device and type of structure through which the shocks propagated as listed in Table 1. Each measurement is presented in MCR-69-011 [1] showing the acceleration time history, the shock spectrum (using a standard format with an analysis Q of 10 for most cases) and a drawing showing structural configuration including the locations of the pyrotechnic device and the transducers.

Table 1. Outline of Data Classification

A.	Structure cutting charges (mild detonating fuse, flexible linear shaped charge, primachord, etc.)
	1. Skin-ring-frame structure
	2. Truss structure
	3. Other structure
B.	Explosive nuts and bolts
	1. Skin-ring-frame structure
	2. Truss structure
	3. Other structure
C.	Cartridge actuated devices (pin pullers, bolt cutters, cable cutters, etc.)
	1. Skin-ring-frame structure
	2. Truss structure
	3. Other structure
D.	Space Vehicle test data
E.	Flight measurements

CHARACTERISTICS OF PYROTECHNIC SHOCK TRANSIENTS

The compiled pyrotechnic shock data were used to determine discinctive characteristics of the shock transients including propagation velocity, frequency content, and attenuation of amplitude with distance.

The propagation velocity was measured for several different structures. Velocities corresponding to both compressional and shear waves were found to exist in the measured data. Near the shock source, the acceleration time histories are characterized by high amplitude, high frequency complex waves. As the distance between the shock source and the measurement location increases, the high frequency energy is rapidly attenuated, and structural resonances begin to control the shock spectrum. The effect is illustrated by the shock spectra in Fig. 1. It should be recognized that accelerometer installations can seriously influence the measured data, particularly at locations near the shock source. The effect on transducer resonance frequency of several mounting installations has been investigated by Rasanen [2]. This work indicated that the use of aluminum blocks for accelerometer installations could lower the mounted resonance frequency by a factor of 2 to 3 from the transducer resonance specified by the manufacturer.

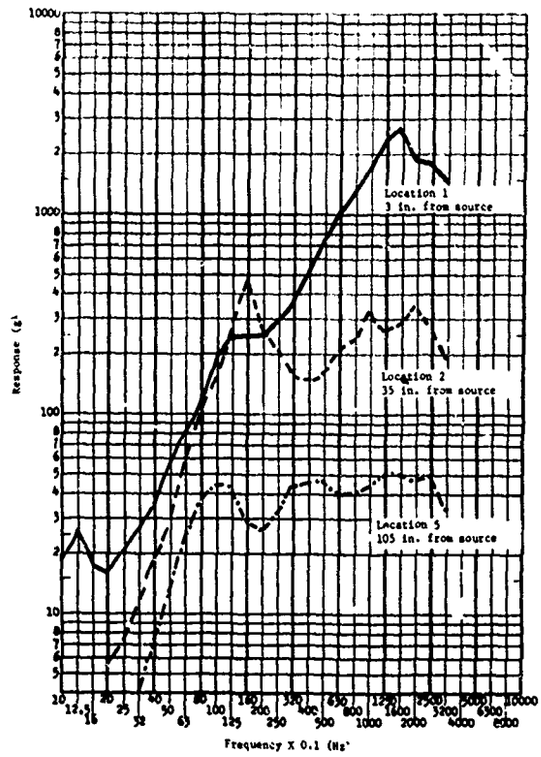

Fig. 1 - Comparison of shock spectra at various propagation distances

DAMAGE EFFECTS

Information concerning damage effects related to shock amplitude is extremely limited because of lack of documented failure histories. One of the perplexing aspects of this study was that in spite of the magnitude of the survey and the response in contribution of data, only 29 miscellaneous anomalies and 17 cases of relay chatter were reported. As a result, methods for relating pyrotechnic shock damage potential with structure and equipment fragility levels do not exist, although some preliminary information indicates shock velocity may be a significant parameter.

Generally, structural failures are confined to small fittings, brackets, bonds, and electrical connectors to small components such as diodes and transistors. Most damage effects are seen in equipment malfunction such as chatter or transfer of relays and switches, frequency shift in subcarrier oscillators, and transients induced in signal outputs. Usually, the design deficiency or workmanship problem is quite simple to correct. This characteristic may make the anomalies appear insignificant, especially in the development phase, and may partially explain the small number of reported problems.

TEST SIMULATION

The test firing of pyrotechnic systems may be performed for many reasons. For those interested in the shock environment, the pyrotechnic firing may be used as an equipment qualification test or may be the source of data from which individual equipment shock specifications may be derived. Individual equipment test specifications are implemented using a variety of simulation techniques, including conventional shock machines based on pulse shape reproduction, electrodynamic shakers controlled by synthesis/analysis hardware, and, to a lesser degree, airframe type test beds excited by explosive charges.

Full-scale qualification and flight acceptance tests of many NASA spacecraft are performed by detonation of the actual pyrotechnic devices in an installation incorporating actual structure. A margin of safety in number of stresses applied can be obtained by simply repeating the events as many times as desired. However, a margin of safety in shock amplitude is not achieved and, furthermore, repetition of some events, such as shroud separation, can be extremely expensive.

A ground test program was conducted to gain some insight into the degree of structural simulation required for full scale tests and to determine whether or not one could achieve a margin of safety by proper installation of the test hardware.

A test series was conducted on the following configurations:

A. Payload truss attached to Titan IIIC Transtage Skirt (Baseline Configuration);

B. Payload truss freely suspended;

C. Payload truss attached to rigid support fixture;

D. Payload truss attached to channel adapters (Adapters were designed to simulate the longitudinal stiffness of the payload skirt).

Photographs of the four configurations are shown in Fig. 2-5. Accelerometer locations on the payload truss are shown in Fig. 6. Examples of the average shock spectra obtained at locations 7 and 8 (satellite mounting points) for the four different configurations are shown in Fig. 7 and 8. Comparison of these data indicates that the use of the simple channel adapters to simulate the transtage skirt structure would provide a reasonable, conservative test of the satellite. The results, although inconclusive, are encouraging because they indicate that it may not be necessary to always include an expensive, complex structure in full scale testing.

Fig. 2 - Test configuration I - payload truss installed on transtage skirt

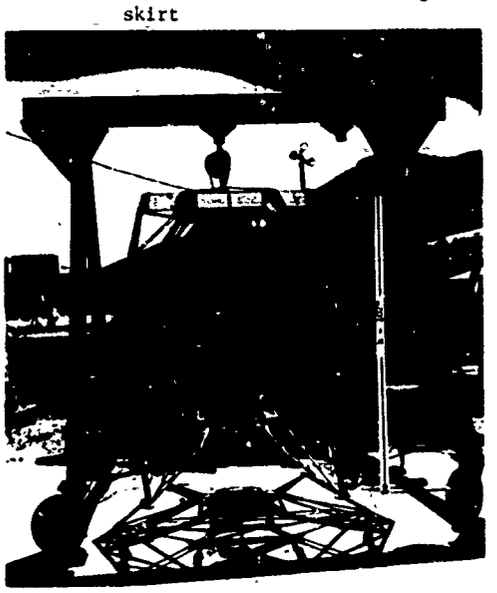

Fig. 3 - Test configuration II - payload truss freely suspended

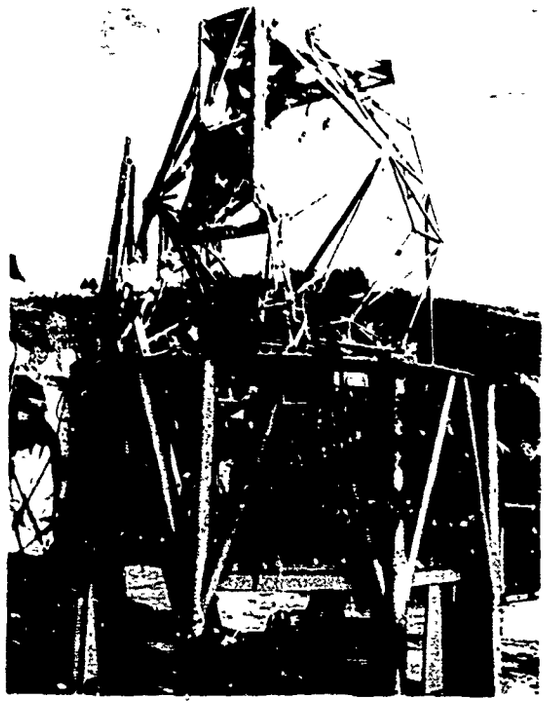

Fig. 4 - Test configuration III - payload truss attached to rigid support fixture

Fig. 5 - Test configuration IV - payload truss attached to channel adapters

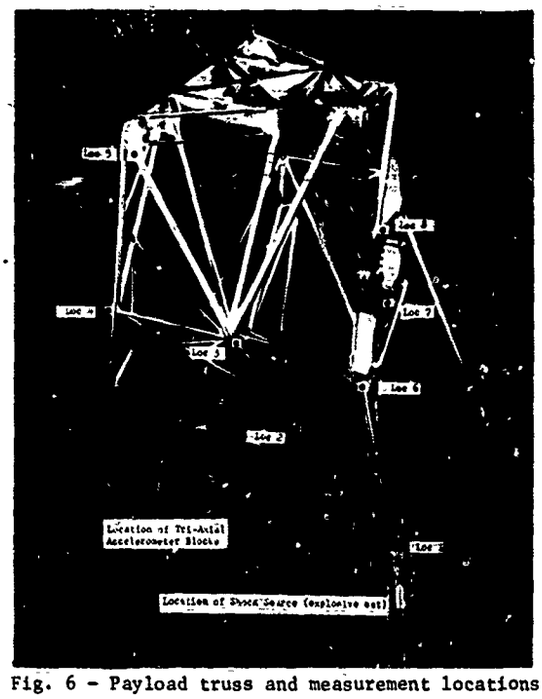

Fig. 6 - Payload truss and measurement locations

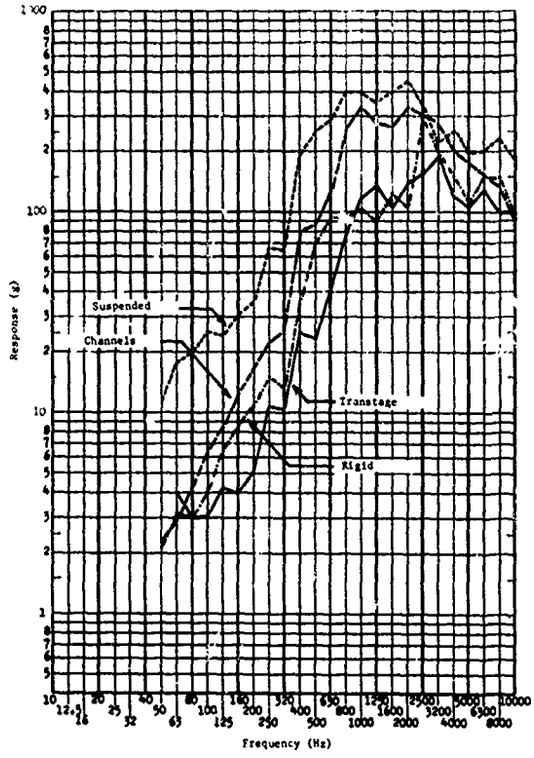

Fig. 7 - Shock spectra comparison for configurations at location 7, longitudinal axis

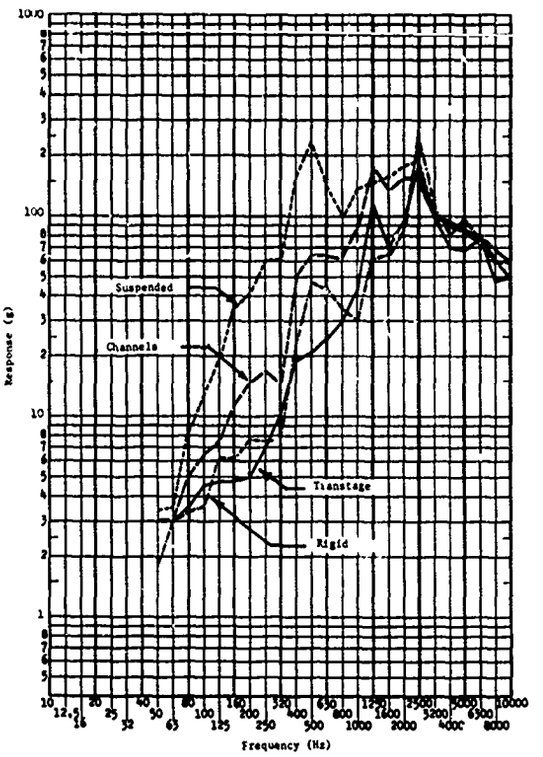

Fig. 8 - Shock spectra comparison for test configurations at location 8, longitudinal axis

MASS LOADING EFFECTS

A test and analysis program was conducted to determine the effect of weight variations in mounted subassemblies on the pyrotechnic shock environment. The effect, for both single and distributed mass loading, was evaluated at the interface of the subassembly and the mounting structure for two types of structures:

A. Airframe, skin and stringer construction;

B. Truss structure.

Final results of this study are not complete. However, preliminary results from the single mass loading tests are presented.

A full scale skirt and truss structure was used as the test fixture. Prototype components were installed on the airframe and on the truss as shown in Fig. 9 and high frequency accelerometers were installed in a triaxial configuration at component mounting points. Changes in weights of the two components were accomplished by the addition of small steel plates distributed throughout the equipment chassis (Fig. 10) to simulate electronic modules. A summary of the weight configurations tested is given in Table 2.

Fig. 9 - Locations of equipment installations and shock source

Fig. 10 - Component A showing installation of Weight

Table 2 Weight Configurations

	Component Weight (lb)	
	Component A Airframe Mounted	Component T Truss Mounted
Bare Structure*	0	0
Configuration 1	11.5	10.0
Configuration 2	23.0	20.0
Configuration 3	46.0	40.0

*Note: The total weight of the truss and skirt was 485 lb.

The pyrotechnic shock source consisted of a blasting cap and 50 grains of RDX explosive contained in a small plastic vial. The vial was inserted in a steel receptacle bolted to a longeron. This relatively inexpensive device produced excellent repeatability and provided an adequate simulation of typical data from ordnance devices used in the aerospace industry.

The tape recorded shock transients were digitized (100,000 samples/sec) and shock spectrum analyses were performed. The shock spectra were normalized to a reference accelerometer location and comparison plots made for the different weight configurations. An example of the results is shown in Fig. 11.

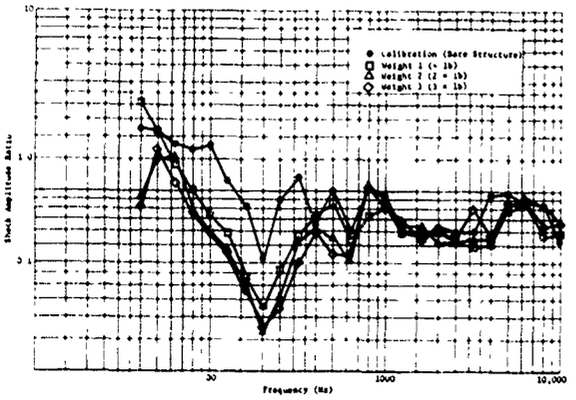

Fig. 11 - Comparison of normalized shock spectra for different component weights

The preliminary results of this study indicate that the primary effect on the shock environment occurs when an equipment item is installed on a previously unloaded structure. For the structure and component weights analyzed in this study, increasing the component weight by a factor of 2 or 4 has relatively little effect on the shock environment at the mounting point.

CONCLUSIONS AND RECOMMENDATIONS

The aerospace industry is presently using a variety of testing techniques to simulate pyrotechnic shock, most of which assume that duplication of the shock spectrum represents an adequate test. It is not clearly understood which parameters are related to damage potential. Additional efforts are needed to accumulate and disseminate failure information and to establish standardized methods for shock testing. Until such information is available it is recommended that the test methods used simulate the shock wave form as well as the shock spectrum. When this is impossible, the next alternative is matching the spectrum and the general character of the wave form; that is using a long duration, complex test for a long duration, complex environment.

From the preliminary results of this study it appears feasible to use relatively simple fixtures to simulate complex airframe structures in full scale tests. Additionally, it may be possible to obtain a test margin of safety for full-scale tests through proper design of such fixtures. Suggestions have been made to vary the amount of explosive charge or the tension in separation bolts to achieve a margin, but these techniques have not been proven.

The results of mass loading tests indicate that it is important to include prototype or "dummy" components in full scale tests if the correct pyrotechnic shock environment is to be achieved. However, after the components have been installed the effect of weight variations is relatively small and would not affect an established shock test specification. Final results from the mass loading effects study will be published in November 1970, as an addendum to Ref [1].

ACKNOWLEDGMENT

The total program briefly discussed in this paper had contributors too numerous to list here. Many individuals throughout the aerospace industry contributed data, correspondence, and discussions. The authors wish to express their gratitude for the cooperation and assistance provided by the individuals and the companies and agencies which they represent.

REFERENCES

1. W. J. Kacena, III, Dr. M. B. McGrath, and W. P. Rader, "Aerospace Systems Pyrotechnic Shock Data (Ground Test and Flight)," MCR-69-611. Martin Marietta Corporation, Denver, Colorado, March 7, 1970.

2. George K. Rasanen, "Installation Effects on the Resonant Frequencies of Shock Accelerometers," Martin Marietta Corporation, Orlando, Florida, Unpublished.

DISCUSSION

Mr. Zell (Picatinny Arsenal): I think most of us feel that the shock spectrum is a pretty useful tool for giving a feel for the relative severity of different shock pulses of widely different character. But I wonder if perhaps the emphasis on presenting actual data, and in trying to analyze the data in terms of shock spectra has not actually created a clouding or an obfuscation that actually complicates analysis. If these data had not been in a Fourier spectrum type of presentation would not the effect of frequency on attenuation, or the effect of structural modes be much more easily analyzed? Perhaps the time has come when the shock spectrum should be used more as an engineering tool.

Mr. Rader: If I understand correctly — you are suggesting that the Fourier spectrum may give more basic engineering information than does the shock spectrum. Is that right?

Mr. Zell: Yes. The effects of frequency on attenuation and mode shapes might be more easily evaluated. In terms of analyzing what is actually happening, it seems that by having the data in terms of a shock spectrum, which is a method of looking at it through a certain type of colored glasses for convenience sake, this type of basic analysis actually clouds the issue rather than clarifies it.

Mr. Rader: During the course of this program one of the tasks was a comparison of Fourier spectra versus standard shock spectra. The Fourier spectra gave essentially no more information than the shock spectra for the complex waves that are generated by pyrotechnic shock devices. This is not true for simple pulses since the Fourier and the shock spectra can be quite different. But for the complex waves that one sees in typical pyrotechnic shock devices the Fourier and shock spectra yielded essentially the same information in our experience.

Mr. Zell: The various analysis methods for determining structural properties, such as mechanical impedance and transmissibility as a function of frequency, cannot be applied directly to a shock spectrum in data that is generally acquired in the course of a development and test program on a particular structure.

Mr. Rader: Yes. I think that is a good point. However, again as I mentioned in the introduction, the definition of, or even adequately explaining pyrotechnic shock analytically has just not been possible to date. Hopefully this will be a subject for future examination. perhaps the Fourier spectrum may be more useful to relate to structural parameters.

Mr. Smith (Bell Aerospace Corporation): Some time ago Bill Roberts did a more modest study suggesting that the shock spectrum showed an additional characteristic at the low frequency end which tended to be more of a constant displacement type of behavior, and I noticed that perhaps this was present in some of your curves. It is important I think to know where the constant velocity line is likely to become inapplicable at the low frequency end. Do you have a short observation on that?

Mr. McGrath: We were in correspondence with Bill Roberts and we looked for this characteristic of a constant displacement line at a very low frequency, but quite often the data confuses the issue at very low frequencies because of faulty techniques of obtaining the spectrum. We found that the constant acceleration lines, constant velocity lines, constant displacement, just did not lead to any definite results that we could see. The constant velocity lines that we are referring to are almost a subjective approximation in the low frequency range, which might go from approximately 100 Hz up to as high as a thousand Hz. This is what we observed. Someone else might observe something else, but it probably takes a specific type of a data reduction.

Mr. Smith: It seems to me that probably within all of these data there may be another important piece of data that is required; and that is, with respect to the various classifications of structure and distance from the source, to what sort of bounds on the mass would you expect to apply the acceleration data in attempting to apply this in a realistic design sense? Obviously one might be happy to apply some particular value of acceleration to a 2 pound mass under some circumstance and never dream of doing the same thing with a 100 pound mass. There is some boundary somewhere that I think might be developable from all this information. If I want to use your curves of acceleration against distance from some source, for how large an item or how heavy an item, are they applicable?

Mr. Rader: The curves presented by Dr. McGrath were developed on a number of different types of structures including spacecraft, booster skirt structure, complex truss structures and the like. So we feel that the curves are applicable for typical aerospace structures as they exist today. The effect of mass loading from the preliminary work which was shown here essentially has very little effect on the shock environment as shown in the last slide. Once the component is installed on the structure or on the truss, this constitutes the major effect on the shock environment. Changing that weight by a factor of 2 or 4 had practically no effect on the basic shock spectrum.

MEASURES OF BLAST WAVE DAMAGE POTENTIAL

C. T. Morrow
LTV Research Center, Western Division
Anaheim, California

Shock excitation by a blast wave differs in two respects from mechanical shock as known in conventional shock tests. First, the excitation is clearly in the form of a pressure rather than a motion (acceleration). Second, the excitation of a typical structure is clearly at multiple points (antinodes) rather than at the base of an item of equipment, treated conventionally as a single mounting point. Relative phase is important. Yet, a spectral description of the blast wave is desirable. It must be selected with these two considerations in mind.

The shock spectrum is conventionally defined in terms of a physical model (a simple mechanical resonator, usually undamped) but can be considered as a purely mathematical operation on the input excitation. Carried out on an input force or pressure, it yields the peak force in the spring of the simple resonator. This is also a criterion of severity. However, unless phase information is added, it is not suitable for describing multiple point excitation. In high-intensity noise testing, the phase information is contained in the cross-power spectrum.

The Fourier spectrum is defined entirely in terms of a mathematical operation to be performed on acceleration, force, pressure, or any variable of interest. It is expressed as a density in that variable, simply related to the generalized residual shock spectrum, but it is a complex number and expresses phase information. The use of the Fourier spectrum as a criterion of severity for sonic booms and blast waves is explored.

INTRODUCTION

It is common to describe blast waves by their peak overpressure and duration. These criteria of severity are simple, readily obtained from a pressure-vs-time trace without appreciable data processing, and sufficient to describe a blast wave uniquely if its pulse shape is known a priori and identical to that of other blast waves with which it may be compared. However, such criteria are not directly indicative of damage potential if wave shapes are dissimilar, as they may well be at different radii from a blast or when reflections occur.

Consequently, two spectral descriptions will be considered--the shock spectrum [1,2,3] as redefined for the purpose, and the Fourier spectrum or Fourier transform. Of particular importance is their adaptability to describing force or pressure inputs as opposed to mechanical motion (acceleration) and to incorporation of relative phase information when a structure is shock excited simultaneously at many points.

THE SHOCK SPECTRUM

In mechanical shock technology, the first descriptions of severity were in terms of peak acceleration, rise time,

and effective duration. Application of these criteria to such diverse wave shapes as the decaying transients typical of field conditions and the standard pulses favored for laboratory testing frequently resulted in unrealistic simulation. Consequently, there has been an increasing trend toward the comparison of severities in terms of spectra.

The shock spectrum was first conceived by Biot [4] as a means for prediction of earthquake damage, was used for many years by Vigness and his associates at the Naval Research Laboratory, and was applied by Morrow to the specification of equipment shock tests for the ICBM program. For data-reduction purposes, it is generally presumed that the shock input to an item of equipment is available as an acceleration-vs-time curve. The shock spectrum is defined as the largest acceleration (in g's) of the mass of a simple mechanical resonator, in response to the shock, plotted as a function of the resonance frequency of the resonator, but is usually obtained from the acceleration-time data by computer processing. Many engineers use it rather literally as an indication of mechanical system response for design purposes and therefore like the spectrum to be obtained in terms of a resonator that has damping typical of the hardware in mind. Such a viewpoint is easily extended beyond its scope of validity in dealing with complex systems, and the undamped-resonator spectrum is more fundamental. Consequently, only the undamped shock spectrum will be considered here.

Thus, if the data were actually to be reduced by a mechanical resonator instead of an electronic computer, the shock would be applied to an undamped mechanical resonator, and the largest positive response peak of the mass and the largest negative peak would be plotted against the particular resonance frequency. Then the undamped resonator would be retuned and the operation repeated to yield more points until the two curves are filled out in sufficient detail. If desired, the maximum of the absolute values for each frequency could be determined and plotted to yield a third curve.

The operator would have the option of restricting his response observations to certain time intervals relative to the applied shock. For example, he could confine his observations to the interval in which the shock occurs to obtain what is known as the <u>initial spectrum</u>, or to the interval beginning at the end of the shock to obtain the <u>residual spectrum</u>. Some authors use the word primary, rather than initial, but this implies that the residual spectrum is a secondary measure of damage potential. Much the reverse is true when the shock is applied to a complex mechanical system. The residual spectrum, while simpler in some respects than the initial, comes close to being a complete description of the shock, except for phase, which, for single point excitation, is a secondary factor in damage potential.

GENERALIZATIONS OF THE SHOCK SPECTRUM

In practice, the shock spectrum is obtained today not by the clumsy operation used as a basis for the definition, but by an analog computer that simulates the tunable mechanical resonator or by a digital computer. It is possible to consider the shock spectrum not as the result of observations of a resonating mass, but the result of a mathematical operation performed on an acceleration-time signal. It becomes of interest to ask what is the physical significance of the same mathematical operation applied to other than acceleration signals. For example, if the operation is applied to a shock force acting on the mass in a simple undamped resonator, it yields the peak force in the spring as a function of resonance frequency. For shocks applied in this general way, this is an acceptable measure of stress in the simplified system. A spectrum obtained in this way, when divided by the mass in appropriate units, yields the peak acceleration of the mass.

That the physical interpretation of this particular generalization of the shock spectrum is valid may be seen from a comparison of differential equations. If a shock force F(t) is applied to a mass m attached by a spring k to a fixed base as in Fig. 1, the differential equation is:

$$ma + kx = F$$

or

$$\frac{d^2x}{dt^2} + \omega^2 x = \frac{F}{m}$$

or

$$\frac{d^2(kx)}{dt^2} + \omega^2 kx = \omega^2 F, \qquad (1)$$

where a is the acceleration of the mass, x is the displacement of the mass from its neutral position, and ω is 2π times the resonance frequency in Hz. If, on

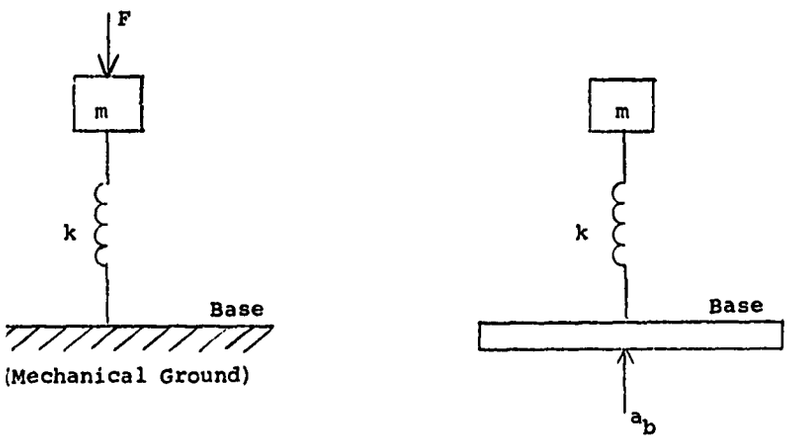

(a) Shock Force F (b) Shock Acceleration a_b

Fig. 1 Shocks Applied to a Simple Mechanical Resonator

the other hand, a shock acceleration $a_b(t)$ is applied to the base, as in Fig. 1b, the differential equation is:

$$ma + k(x-x_b) = 0$$

or by double differentiation, followed by transposition of m

$$\frac{d^2a}{dt^2} + \omega^2 a = \omega^2 a_b, \qquad (2)$$

where x_b is the displacement of the base as a function of time, from its neutral position, and a is the acceleration of the mass. Equations (1) and (2) involve different variables but otherwise are identical in mathematical form. The mathematical operation associated with taking the shock spectrum is to solve for the variable on the left and maximize it, within specified time intervals, as a function of ω or the resonance frequency $\omega/2\pi$. This variable is the force kx in the spring in Eq. (1) and the acceleration a of the mass in Eq. (2). This completes the proof.

There is no ambiguity if the result of Eq. (1) is identified as the "shock spectrum of the applied force" and the result of Eq. (2) is called the "shock spectrum of the applied acceleration." It is understood that the input force and acceleration are applied to different places in the simplified mechanical system.

What is the physical significance of the curves obtained when the mathematical operation of the shock spectrum is performed on the pressure-time pulse of a sonic boom or blast wave? An interpretation could be given in terms of a Helmholtz resonator, but such devices are seldom involved in shock damage. It is more useful to base the interpretation on the response of a mechanical system excited by the pulse. Airborne noise and shock waves tend to excite a structure at its antinodes. If a single antinode is considered, the shock excitation is much like that of a force acting on a mass. The force is the pressure multiplied by the effective area of the antinode, or by the area of the effective mass of the antinode. The shock spectrum of the applied pressure, when multiplied by the area of the mass in the simplified mechanical system, yields the peak force in the spring. In a slightly less direct way than in the previous cases, this generalization of the shock spectrum becomes an acceptable measure of damage potential. At least, it is reasonable to infer that if two different pressure pulses are applied to the same mechanical system, the pulse with the higher residual shock spectrum is more likely to damage a mechanical resonator tuned to that frequency. If one spectrum is higher than the other over all frequencies of interest, one can infer with even greater confidence that the associated pulse is the more severe, regardless of the mechanical system to which it is applied. However, the shock spectrum as usually reduced, provides no information on relative phase of excitations at two or more antinodes.

THE FOURIER SPECTRUM

The basic objective of the shock spectrum was to describe possible responses of a mechanical system to a shock. It will be evident later that the result is almost a direct description of the input shock itself.

However, a more fundamental approach is to set out from the beginning to describe the input directly. For periodic vibration inputs, this is commonly done by recording the various amplitudes and frequencies that can be identified by a wave analyzer or by means of a Fourier analysis. For the special case in which the wave shape repeats itself at a fundamental frequency, Fourier's theorem shows that the vibration is equivalent to a series of sinusoids (called harmonics) at multiples of the fundamental frequency, and is described by the amplitude and phase of each sinusoid. Phase information is necessary for complete reconstruction of the wave shape. For single-point excitation, it is seldom recorded as it has no general simple relation to damage potential. A mechanical system responding to vibration excitation shifts the phase as a function of frequency in a complicated way that is unpredictable unless the system dynamics are known. Consequently, there is no reason to expect one phase relation among the harmonics to indicate generally more or less damage potential than another. At any one harmonic frequency, the response of a linear mechanical system is proportional to the input. The ratio of the two amplitudes is calculable from theory if the system dynamics are known, or measured as a function of frequency, if they are not. Consequently, the spectral description is adequate for the computation of responses when this is desired, or for comparison of one periodic vibration with another in respect to damage potential. Fourier analysis is an entirely mathematical operation, which needs no major reinterpretation according to whether the variable processed is acceleration, force, or pressure.

Extensions of Fourier analysis permit the direct description of shock inputs and random excitation. The Fourier coefficients (amplitudes for the various harmonics) involve an integral of the original time function times a trigonometric or exponential function, over the fundamental period. If a shock is made to repeat itself at some fundamental period, the resulting time function can be expressed as a Fourier series. Then if the period is increased beyond limit, it should be possible to derive a spectral description of an isolated pulse. As the period is increased, the harmonics become more numerous and decrease in amplitude. However, the integral that appears in each Fourier coefficient is independent of the period provided the period is longer than the shock duration--it is exactly equal to the integral over that duration. Consequently, this integral, known as the Fourier transform or Fourier spectrum, which has the same value for an infinite period as for any finite period equal to or greater than the pulse duration, and has the units of a density in frequency (g/Hz, lb/Hz, or lb/in^2 Hz, etc., depending on the variable used) is the spectral description sought.

As the period increases beyond limit, the summation of harmonics, with one over the period divided out from each term, approaches an integral of the Fourier spectrum over all frequencies. This inverse transform permits the reconstruction of the wave shape.

DERIVATION OF THE FOURIER SPECTRUM

This derivation and its interpretation is accomplished most simply in terms of a complex exponential, once one is used to the notation, rather than in terms of trigonometric functions. A complex number is regarded as a vector at a particular angle to the axis of reals, as in Fig. 2, and expressible in terms of magnitude (amplitude) and angle, or as the vector sum of its projections on the real and imaginary axes, which are proportional to the cosine or the sine of the angle, respectively. Examination of the Taylor's series for

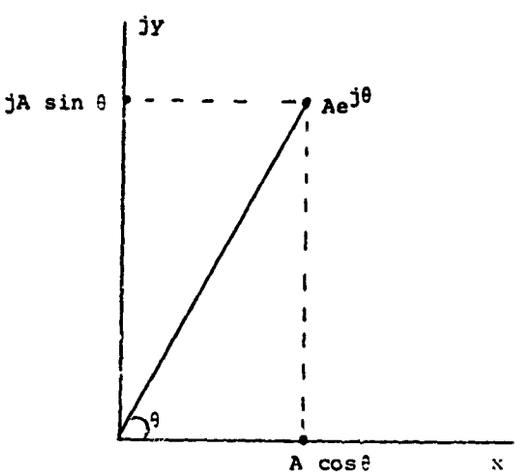

Fig. 2 Complex Vector

exponential and trigonometric functions discloses a particularly simple way of expressing this:

$$Ae^{j\theta} = A\cos\theta + jA\sin\theta, \qquad (3)$$

where e is the base of natural logarithms and where j is a unit vector along the imaginary axis. It follows that

$$\cos\theta = \frac{e^{j\theta} + e^{-j\theta}}{2} \qquad (4)$$

and

$$\sin\theta = \frac{e^{j\theta} - e^{-j\theta}}{2j} \qquad (5)$$

Furthermore,

$$Ae^{j\theta} \cdot Be^{j\phi} = AB\, e^{j(\theta+\phi)}, \qquad (6)$$

If, now, $\theta=2\pi ft$, where f is the frequency and t is the time, $Ae^{j\theta}$ becomes a counterclockwise rotating vector whose projections are the cosine and sine functions. However, it is easier than the trigonometric functions to manipulate in a differential equation, since

$$\frac{d}{dt} e^{j2\pi ft} = j2\pi fe^{j2\pi ft}, \text{ very simply.}$$

If ϕ is interpreted as a constant angle, Eq. (6) provides a simple way of expressing phase shifts as well as amplitude changes that may be produced by a mechanical system. The quantity $Be^{j\phi}$ may be determined theoretically or experimentally as a function of frequency for transmission between any two points in a linear mechanical system.

The Fourier series can be written, by application of Eq. (4), as

$$a(t) = \sum_{k=1}^{n} A_k \cos(2\pi kf_1 t - \phi_k)$$

$$= \tfrac{1}{2}\sum_{k=-n}^{n} A_k\, e^{j(2\pi kf_1 t - \phi_k)}$$

$$= \tfrac{1}{2}\sum_{k=-n}^{n} C_k\, e^{j2\pi kf_1 t} \qquad (7)$$

where

$$C_k = A_k\, e^{-j\phi_k} \qquad (8)$$

is a complex amplitude expressing the amplitude and phase of the harmonic, and it is readily shown that

$$C_k = \frac{2}{T}\int_{-T/2}^{+T/2} a(t)\, e^{-j2\pi kf_1 t}\, dt$$

$$= \frac{2}{T}\int_{-T/2}^{+T/2} a(t)\, e^{-j2\pi f_k t}\, dt \qquad (9)$$

where T is the period and $f_k=kf$, where f is the fundamental frequency or repetition rate. The integral, which becomes independent of T for long periods, is the Fourier spectrum:

$$S(f) = \int_{-\infty}^{\infty} a(s)e^{-j2\pi fs}\, ds, \qquad (10)$$

where the variable t is replaced by S to avoid confusion in derivations that might be undertaken later. Now, if $2\Delta f=2/T$ is factored out of each C_k and the period is allowed to increase beyond limit, the Fourier series approaches

$$a(t) = \int_{-\infty}^{\infty} S(f)e^{j2\pi ft}\, df. \qquad (11)$$

If S(f) is known for an applied shock, the response at any point within a linear mechanical system is obtained by evaluating

$$a_r(t) = \int_{-\infty}^{\infty} Be^{j\phi}\, S(f)e^{j2\pi ft}\, df,$$

where the complex transmission coefficient $Be^{j\phi}$, which expresses both amplitude change and phase shift as a function of frequency, is applicable to S(f) as a multiplier just as it would be to an individual harmonic in periodic excitation. In other words, one multiplies by the complex transmission factor and integrates the resulting Fourier spectrum with the appropriate complex exponential over the frequency range of interest.

If S(f) and the transmission characteristic are known, in terms of both amplitude and phase, both the applied shock and the response can be computed. The magnitude of S(f) is the primary indication of damage potential for single-point excitation and can be shown [5] to equal the residual undamped shock spectrum divided by $2\pi f$. Thus, two concepts that originated in quite different ways turn out to be very similar mathematically.

It is illuminating to ask how much energy is contained in a particular shock. If a periodic signal were applied to a one-ohm resistor (acoustical, mechanical, or electrical, as appropriate), the energy dissipated in one period would be

$$\int_{-T/2}^{T/2} a^2(t)\,dt = \frac{T^2}{4}\sum_{k=-n}^{n}|C_k|^2 = \frac{T^2}{2}\sum_{k=1}^{n}A_k^2 ,$$

which is readily shown by multiplying out the exponential form of Fourier's series, as in Eq. (7), term by term, observing that all other products integrate to zero, and noting that $C_k=C_{-k}$. For a sustained signal, the total energy over all time would be unbounded. For a shock, if $2\Delta f=2/T$ is factored out of each C_k and T is allowed to increase beyond limit,

$$\int_{-\infty}^{\infty} a^2(t)\,dt=\int_{-\infty}^{\infty}|S(f)|^2 df,=2\int_{0}^{\infty}|S(f)|^2 df \qquad (12)$$

which is a form of Parseval's theorem. The square of the magnitude of the Fourier spectrum of a shock is therefore referred to as the <u>energy spectral density</u> and is finite.

In passing, Eq. (12) suggests a comment about the spectral description of a stationary random vibration or signal. While the total energy is unbounded, the total power is finite:

$$\lim_{T\to\infty} 1/T \int_{-T/2}^{T/2} a^2(t)\,dt=\lim_{n\to\infty}\sum_{k=n}^{n_T}\frac{|C_k|^2}{4}$$

$$=\int_{-\infty}^{\infty}\lim_{n\to\infty}\frac{|S(t)|^2}{T}dt=\int_{0}^{\infty}\lim_{T\to\infty}\frac{2|S(f)|^2}{T}dt \qquad (13)$$

Therefore the familiar power spectral density for a random signal is given by

$$w(f) = \lim_{T\to\infty}\frac{2\,S(f)^2}{T} \qquad (14)$$

In any event, the Fourier transform is a fundamental description of a shock and a good measure of damage potential. So, for single-point excitation, is the closely related residual shock spectrum.

EFFECTS OF RELATIVE TIME DELAY OR PHASE SHIFT

Whether a structure is excited by random noise or a shock front, the excitations at the various antinodes for a particular mode of vibration or shock response are not necessarily directly additive in terms of magnitudes. For example, two pressures that push in step or in phase at adjacent antinodes tend to nullify each other. Two pressures that are exactly out of step or 180 degrees out of phase and therefore conform to the relative motions of two adjacent structural antinodes will be highly effective in exciting the structure. In high-intensity sound testing of airframes, it is becoming evident that such considerations can influence which modes of a structure are excited. Similar effects should be expected in shock-wave excitation.

RELATIVE PHASE IN RANDOM NOISE

Relative phase is important in blast wave excitation for the same reasons that it is coming to be accepted as important in high-intensity noise testing. A brief review of the latter consideration may be in order.

$$w_{1+2} = w_1 + 2w_{12} = w_2$$

$$= w_1 + 2c_{12}\,(w_1w_2)^{\frac{1}{2}} + w_2$$

$$= w_1 + 2c_{12}\,(w_1w_2)^{\frac{1}{2}}\cos\phi_{12} + w_2 \qquad (15)$$

and that of the difference by

$$w_{1-2} = w_1 - 2w_{12} + w_2$$

$$= w_1 - 2c_{12}\,(w_1w_2)^{\frac{1}{2}} + w_2$$

$$= w_1 + 2G_{12}\,(w_1w_2)^{\frac{1}{2}}\cos\phi_{12} + w_2 \qquad (16)$$

where

w_1 = power spectral density of first noise;

w_2 = power spectral density of second noise;

w_{12} = correlation density or real part of cross-power spectrum, obtained by multiplying the two noises in the same frequency band and averaging sufficiently in time to suppress fluctuations of the order of half the bandwidth;

$c_{12} = w_{12}\,(w_1 w_2)^{\frac{1}{2}}$ is the correlation density coefficient, of value between +1 and -1;

$\phi_{12}(f)$ is the dominant phase angle, if any, between the two noises as a function of frequency; and

G_{12}, a coefficient between zero and unity, is the value if ϕ_{12} were shifted to zero, as the magnitude of the cross-power spectrum and describes the magnitude of correlated noise.

Equation (15) governs the excitation of alternate antinodes by random noise and Eq. (16) that of adjacent antinodes in a structure.

Two random noises are considered to be at least partially correlated in the neighborhood of a given frequency, if any phase angle dominates because of relative time delay or any other reason. Thus c_{12} may be small because of the particular value of ϕ_{12} or because part of one noise or the other is of independent origin, reducing the value of G_{12}. The sinusoids describing a finite-duration sample of one random noise have a random phase relation to each other, but may have a simple relation, respectively, to the corresponding sinusoids of the second random noise, if the two are of the same origin. If the second is of independent origin, this phase relation too becomes random; in a narrow band containing many sinusoids, no angle ϕ_{12} is evident, and $C_{12}=0$. If only part of the noise is of independent origin, some value of ϕ_{12} dominates, and G_{12} is between zero and unity.

ENERGY SPECTRAL DENSITY OF THE SUM OF TWO SHOCK WAVES

Within one shock or in the comparison of two shocks, there are no random phase angles. Nevertheless, utilizing the Fourier spectrum and a derivation similar to that for Parseval's theorem, it is possible to set up equalities analogous to Eqs. (15) and (16). If $a_1(t)$ and $a_2(t)$ represent two shocks transmitted to the same failure point, the energy sum is, from Eq. (7),

$$\int_{-T/2}^{T/2} |a_1(t) + a_2(t)|^2 \, dt$$

$$= \int_{-T/2}^{T/2} |a_1^2(t) + 2a_1(t)a_2(t) + a_2^2(t)| \, dt$$

$$= \int_{-T/2}^{T/2} a_1^2(t)\,dt + 2\int_{-T/2}^{T/2} a_1(t)a_2(t)\,dt$$

$$+ \int_{-T/2}^{T/2} a_2^2(t)\,dt$$

$$= \frac{T}{4}\sum_{k=-\infty}^{\infty} C_{k1}C_{-k1} + \frac{T}{2}\sum_{k=-\infty}^{\infty} C_{k1}C_{-k2}$$

$$+ \frac{T}{4}\sum_{k=-\infty}^{\infty} C_{k2}C_{-k2} \, ,$$

$$= \frac{T}{4}\sum_{k=-\infty}^{\infty} |C_{k1}|^2 + \frac{T}{2}\sum_{k=-\infty}^{\infty} |C_{k1}| \cdot |C_{-k2}| \, e^{j(\phi_1 - \phi_2)}$$

$$+ \frac{T}{4}\sum_{k=-\infty}^{\infty} |C_{k2}|^2$$

$$= \frac{T}{4}\sum_{k=-\infty}^{\infty} |C_{k1}|^2 + \frac{T}{2}\sum_{k=0}^{\infty} |C_{k1}| \cdot |C_{-k2}| \cos\,(\phi_1 - \phi_2)$$

$$+ \frac{T}{4}\sum_{k=-\infty}^{\infty} |C_{k2}|^2$$

$$= \frac{T}{4}\sum_{k=-\infty}^{\infty} |C_{k1}|^2 + \frac{T}{2}\sum_{k=-\infty}^{\infty} |C_{k1}| \cdot |C_{k2}| \cos\,(\phi_1 - \phi_2)$$

$$+ \frac{T}{4}\sum |C_{k2}|^2$$

If now, $2\Delta f=2/T$ is factored out of each C_{k1} and each C_{k2},

$$\int_{-\infty}^{\infty}|a_1(t) + a_2(t)|^2\,dt = \int_{-\infty}^{\infty}|S_1(f)|^2\,df$$

$$+ 2\int_{-\infty}^{\infty}|S_1(f)|\cdot|S_2(f)|\cos(\phi_1-\phi_2)\,df$$

$$+\int_{-\infty}^{\infty}|S_2(f)|^2\,df,$$

and similarly,

$$\int_{-\infty}^{\infty}|a_1(t)-a_2(t)|^2\,dt \qquad (18)$$

$$=\int_{-\infty}^{\infty}|S_1(f)|^2\,df-2\int_{-\infty}^{\infty}|S_1(f)|\cdot|S_2(f)|\cos(\phi_1-\phi_2)\,df$$

$$+\int_{-\infty}^{\infty}|S_2(f)|^2\,df \qquad (19)$$

where the phase difference $\phi_1-\phi_2$ is always a determinate function of frequency.

If $a_2(t)$ is later than $a_1(t)$, $\phi_1-\phi_2$ may pass through 360 degrees or more in the frequency region containing significant energy, making the middle integrand negative over portions of the range. Further, if the time difference is such that the two shocks do not overlap, it follows simply from the time integral that the total energies must add directly. This amounts to saying that $\cos(\phi_1-\phi_2)$ must tumble in such a way that the middle integral is zero. However, for wider time-separated shocks, such that the response to the first shock decays before the second arrives, the magnitudes of the individual Fourier spectra are more indicative of peak stress than the energy spectrum of the sum or difference. Furthermore, if they are overlapping in time, the vector sum of their Fourier spectra, as transmitted to the same failure point, is a more fundamental indication of severity.

FOURIER SPECTRUM OF THE SUM OF TWO SHOCK WAVES

It follows from Eqs. (12), (18), and (19) that the magnitude of the Fourier spectrum for the sum or difference of two shocks is dependent only on the magnitudes of the individual Fourier spectra and their phase difference:

$$\left|S_{1+2}\right| = \left[\left|S_1\right|^2+2\left|S_1\right|\cdot\left|S_2\right|\cos(\phi_1-\phi_2)+\left|S_2\right|^2\right]^{1/2} \qquad (20)$$

$$\left|S_{1-2}\right| = \left[\left|S_1\right|^2-2\left|S_1\right|\cdot\left|S_2\right|\cos(\phi_1-\phi_2)+\left|S_2\right|^2\right]^{1/2} \qquad (21)$$

For two shocks not too widely separated in time and transmitted to the same failure point, this is a satisfactory measure of severity of excitation. However, if one wishes to compute accurately the response of a known mechanical system, absolute phase information will be beneficial in many cases. It follows immediately from Eq. (10) that the Fourier spectrum for the sum of two shocks is

$$S_{1+2}(f) = S_1(f) + S_2(f), \qquad (22)$$

and that for the difference is

$$S_{1-2}(f) = S_1(f) = S_2(f). \qquad (23)$$

It should be remembered that these are vector sums and differences in the complex plane. For example, if $a_2(t)$ is simply $a_1(f)$ delayed by a time τ, it follows from Eq. (10) that these become

$$S_{1+2}(f) = \left[1+e^{-j2\pi f\tau}\right] S_1(f) \qquad (24)$$

and

$$S_{1-2}(f) = \left[1-e^{-j2\pi f\tau}\right] S_1(f). \qquad (25)$$

CONCLUSION

The computation of the response of aerospace structures to blast is a

current problem. There will be an increasing interest in the testing of aerospace systems to blast conditions, as there has been in testing with high-intensity noise.

Blast is a distributed excitation for a structure, and should exhibit coincidence effects and other phenomena that are found with high-intensity noise of various types of point-to-point correlation. In short, the variation of relative phase angle with position may be as important as the magnitude. The complex Fourier spectrum, expressed as a function of position over an aerospace structure, permits accurate computation of response.

For the simulation of blast phenomena, it is important to understand, by as simple calculations as possible, how the severity of excitation depends generally on the orientation of the test item, on any reflections, and on the distance from the blast source. The complex Fourier spectrum is essential to such an understanding in the same way that the cross-power spectrum is essential to understanding of high-intensity noise testing. The relative phase versus frequency curve will influence which structural modes are excited and which suppressed.

In principle, the Fourier spectrum is equivalent in information to the residual shock spectrum with phase information added by a supplementary circuit in the shock spectrum computer. However, Fourier spectra may be obtained with computers that are commercially available now.

REFERENCES

1. I. Vigness, "Some Characteristics of Navy 'High Impact' Type Shock Machines," Proceedings of the SESA, Vol. 5, No. 1, pp. 101-110, 1947

2. C.T. Morrow, "The Shock Spectrum as a Criterion of Severity of Shock Impulses," J. Acoust. Soc. Amer., Vol. 29, No. 5, pp. 596-602, May 1957

3. Charles T. Morrow, Shock and Vibration Engineering, Volume I, Wiley, 1963

4. M.A. Biot, "Analytical and Experimental Methods in Engineering Seismology," Transactions of the ASCE, No. 108, pp. 365-385, 1943

5. G. O'Hara, "Impedance and Shock Spectra," J. Acoust. Soc. Amer., Vol. 31, No. 10, pp. 1300-1303, Oct. 1959

DISCUSSION

Mr. Zell (Picatinny Arsenal): In relating Dr. Morrow's attack to the pyrotechnic problem, has any attempt been made to define the actual impulse energy generated by these pyrotechnic devices in terms of the Fourier transform? Could these then be related by mechanical impedance techniques to effects occurring elsewhere in the structure?

Mr. McGrath (Martin Marietta Corporation): There is a paper by Fung, and quite a few other people have noted this, that at very low frequencies, as you approach zero the Fourier transform gives the impulse energy. And as Dr. Morrow just pointed out, the residual shock spectrum and the Fourier spectrum are the same; and usually in the low frequency range the residual shock spectrum governs. So we looked into this, but we found we had difficulties in reducing the data. If you reduce it either by an analog procedure or a digital procedure (we used the digital procedure) to produce both a Fourier spectrum and a shock spectrum, we found that a very slight dc bias, or a little bit of noise, in the low frequency range pretty well obscured the information, and we could not come to any conclusion as to what impulse energy was contained in a complex wave. One can do this very simply for a simple wave, such as a half sine pulse. It can be done analytically, but we just were not able to come to any conclusion in what we did.

Mr. Zell: Could these devices be tested on a very rigid block? Perhaps the acceleration of the rigid block would yield more of a spectrum of the impulse, rather than a spectrum that was altered by the response of a complex structure?

Mr. McGrath: The point, I think, is that one wants to attach the measurement device to a very rigid piece that would feel only the initial impulse and not the later complex part of the wave. Is that correct?

Mr. Zell: Yes. In other words, if one has an explosive bolt and if one mounted it on a very rigid block and measured the acceleration of the very rigid block one could then relate this to the force and determine the spectrum.

Mr. Naylor (Defense Research Establishment, Suffield, Canada): I would like to take this opportunity to cover the whole of the morning session. There seems to be a recurrent question that the accelerations are not really representative of damage. It is movement that causes damage — strains — either bending strains or tension strains. It is very easy to record acceleration but the results are not always satisfactory. Mr Grundy from Canada commented on this yesterd and put in a plea for stating results in velocity, so I would suggest that we lean on the instrumentation people to integrate accelerations and obtain a better dynamic range, either before or after recording, and if you have to deal with acceleration data in your spectrum analysis, convert to velocity and thus get this automatic roll-off against the high frequencies which are not important structurally. We should forget about this acceleration kick — it is not really useful to us in understanding what is happening to structures.

Mr. McGrath: This is a very important point, namely, that it is velocity and not acceleration that seems to be the important parameter related to damage, for which we are actually looking. Until now it has been acceleration.

Dr. Morrow: As we make use of acceleration and other criteria of severity, we most commonly do it on a relative basis. We are comparing two conditions and are trying to tell which is more severe, and the criteria we have are in many respects less useful on an absolute basis than on a relative basis. On a relative basis the factor of $2\pi f$ cancels out in both — and so you are about as well off if you forget about it from the beginning. I did want to add one other comment on the papers I have heard. I have noticed quite a few shock spectra which are extended all the way to 10,000 Hz, or higher, and my comment about the residual shock spectrum a little earlier is related to this. There is one other consideration. It is very difficult to get valid data up to 10,000 Hz, the accelerometer may not resonate until 20,000 or 50,000 Hz, and that looks very fine, but that is not the limiting factor. What usually happens is that one introduces a resonance below 10,000 Hz in the structure by adding the accelerometer and if one makes comparisons, again on a relative basis, in situations where the loading effect remains constant, this again does not matter; but on an absolute basis it can be entirely misleading.

Mr. McGrath: You could probably do this if your measurement system had the proper roll-off characteristics. However, there is no such thing as a rigid block. Everything has a natural frequency. The accelerometers we used had quite a high useful frequency range.

SHOCK RESPONSE OF A BILINEAR, HYSTERETIC BEAM AND SUPPORT SYSTEM

Bruce E. Burton
Ohio Northern University
Ada, Ohio

and

Robert S. Ayre
University of Colorado
Boulder, Colorado

Shock spectra are presented for an elasto-inelastic beam simply supported at each end on elasto-inelastic supports which are subjected to a half-sine ground acceleration pulse. The beam and supports have, respectively, bilinear, hysteretic moment-curvature and bilinear, hysteretic force-displacement characteristics. Since the beam-support system and the ground excitation are mutually symmetrical, the system response is also symmetrical. The maximum relative displacement at the ends of the beam and the maximum relative displacement and maximum bending moment at the midspan are presented for six cases in which the beam-support system has different elasto-inelastic properties. A lumped flexibility and lumped mass model was used to represent the continuous system.

INTRODUCTION

The purpose is to present an analysis for the response of a bilinear hysteretic beam and support system subjected to a ground acceleration pulse, and to show response spectra for relative displacement and bending moment. This study is related to an earlier one by Tauchert and Ayre [8,9] in which the beam remained elastic while the supports alone exhibited bilinear, hysteretic, elasto-plastic characteristics. It is a considerable extension of the earlier one in that both the beam and the supports may exhibit bilinear hysteretic characteristics. Furthermore, this investigation was carried into the more general elasto-inelastic range rather than limiting it to the usual elasto-plastic assumption. Pertinent publications dealing with the transient, dynamic response of a structural system having an elasto-inelastic beam or beams are indicated in Refs. [1,2,3,5,7,10]. The research reported herein was a part of the doctoral investigation carried on at the University of Colorado by the first named author.

METHOD OF ANALYSIS

Model Representation. The physical system is shown in Fig. 1. It consists of an elasto-inelastic beam simply supported at each end by identical elasto-inelastic supports. The constant properties of the beam are:

E = modulus of elasticity;

I = second-moment-of-area of cross-section;

ℓ = length of beam between supports;

μ = mass per unit length of beam.

The ground input $u_g(t)$ is the half-sine acceleration pulse:

$$\ddot{u}_g = A_g \sin \frac{\pi t}{t_g} \qquad 0 \le t \le t_g \qquad (1)$$

$$\ddot{u}_g = 0 \qquad t \ge t_g \qquad (2)$$

where

$\ddot{u}_g$ = ground acceleration;

A_g = amplitude of ground acceleration;

t = time;

t_g = duration of ground pulse.

The corresponding expressions for ground displacement are:

$$u_g = \frac{U_g}{2}\left(\frac{t}{t_g} - \frac{1}{\pi}\sin\frac{\pi t}{t_g}\right) \qquad 0 \le t \le t_g \qquad (3)$$

$$u_g = U_g\left(\frac{t}{t_g} - \frac{1}{2}\right) \qquad t \ge t_g \qquad (4)$$

where

u_g = ground displacement;

$U_g = 2t_g^2 A_g/\pi$.

Since both the structure and the excitation are symmetrical, the response is also symmetrical.

A lumped-flexibility, lumped-mass model (Figs. 2 and 3) was used. Wen and Toridis [10] found this type of model to be more effective than the lumped-flexibility and continuous-mass model or the continuous-flexibility and lumped-mass model for the type of structure considered in this study. Symbols relating to the model beam are:

N = number of beam segments;

$h = \ell/N$ = constant length of beam segments;

$N+1$ = number of masses;

$i = 1,2...N+1$ = subscript designating beam station (mass point);

$m_i = m = \mu h$ = any interior mass (constant), where $i = 2,3..N$;

$m_1 = m_{N+1} = m/2$ = end masses;

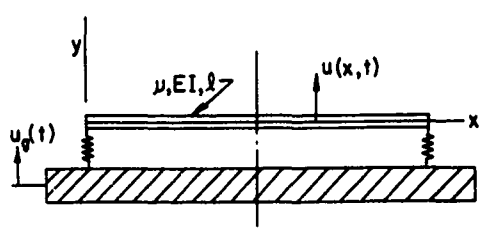

FIG. 1.—EQUILIBRIUM POSITION FOR DISTRIBUTED PARAMETER BEAM ON CONCENTRATED SUPPORTS.

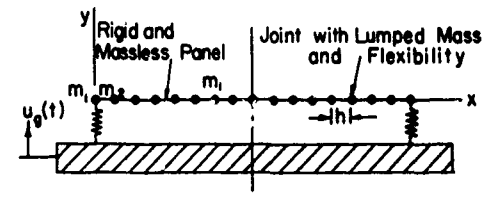

FIG. 2.—EQUILIBRIUM POSITION FOR LUMPED PARAMETER MODEL BEAM ON SUPPORTS.

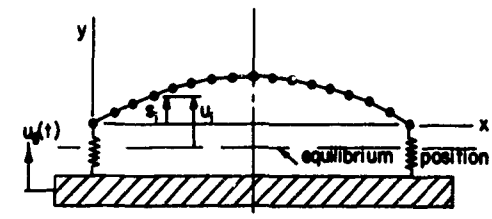

FIG. 3.—DISPLACED POSITION FOR LUMPED PARAMETER SYSTEM.

u_i = absolute displacement of mass at station i;

$s_i = u_i - u_1$ = displacement of beam relative to its ends.

Nonlinear Restoring Forces. The restoring force-displacement function $r(w_1)$ for the supports is bilinear and hysteretic, as shown in Fig. 4, where

$w_1 = u_1 - u_g$ = displacement of beam ends relative to ground;

$r = r(w_1)$ = restoring force in support;

r_y = restoring force at yield point in support;

q_1 = elastic-range stiffness (constant) of support;

$q_2 = \alpha q_1$ = inelastic-range stiffness (constant) of support;

$\alpha = q_2/q_1$ = support stiffness bilinearity ratio, $0 \le \alpha \le 1$.

When $\alpha = 0$, the supports are elastoplastic. When $\alpha = 1$, the supports are linearly elastic over the full range of support relative deflection.

The bending moment-curvature function M(K) for the beam is also bilinear and hysteretic, as shown in Fig. 5, where

$K_i = -\frac{1}{h^2}(s_{i-1} - 2s_i + s_{i+1}) =$ beam curvature;

M_i = bending moment;

M_y = bending moment at yield point in beam;

k_1 = EI = elastic-range stiffness (constant) of beam;

$k_2 = \beta k_1$ = inelastic-range stiffness (constant) of beam;

$\beta = k_2/k_1$ = beam stiffness bilinearity ratio, $0 \leq \beta \leq 1$.

When $\beta = 0$, the beam is elasto-plastic. When $\beta = 1$, the beam is linearly elastic over the full range of beam curvature.

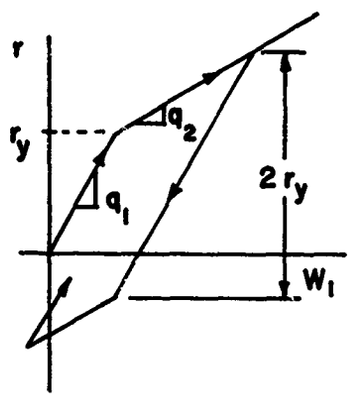

FIG. 4.–RESTORING FORCE-DISPLACEMENT FUNCTION FOR THE SUPPORTS.

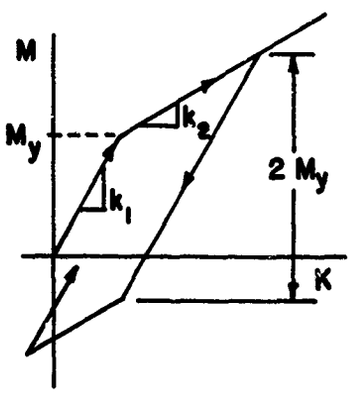

FIG. 5.–BENDING MOMENT-CURVATURE FUNCTION FOR THE BEAM.

Equations of Motion. For the model beam (Fig. 3) the differential equation of motion for the left end mass m_1 is

$$m_1 \ddot{u}_1 = M_2/h - r(w_1) \qquad (5)$$

Due to symmetry a similar expression can be written for the right end mass, i.e., $u_1 = u_{N+1}$. The differential equation of motion for any interior mass is

$$m_i \ddot{u}_i = (M_{i-1} - 2M_i + M_{i+1})/h, \qquad (6)$$
$$i = 2,3...N.$$

Equations (5) and (6) may be nondimensionalized by use of the following nondimensional quantities:

$\bar{u}_i = u_i/U_g$, absolute displacement of beam;

$\bar{u}_g = u_g/U_g$, displacement of ground;

$\bar{w}_i = w_i/U_g = (u_i - u_g)/U_g$, displacement of beam relative to ground;

$\tau = t/t_g$, time;

$\bar{M}_i = M_i \ell^2/EIU_g$, bending moment in beam;

$\ddot{\bar{u}}_i = \ddot{u}_i t_g^2/U_g$, absolute acceleration of beam;

$\bar{r} = r/q_1 U_g$, support restoring force.

Equation (6) becomes:

$$\ddot{\bar{u}}_i = C_1 \bar{R}_i, \; i = 2,3 \ldots N, \qquad (7)$$

where $C_1 = Nt_g^2 EI/m\ell^3$;

$$\bar{R}_i = \bar{M}_{i-1} - 2\bar{M}_i + \bar{M}_{i+1}.$$

Similarly, Eq. (5) becomes:

$$\ddot{\bar{u}}_1 = 2C_1\bar{R}_1 - 2C_2\bar{r} \qquad (8)$$

where $C_2 = t_g^2 q_1/2m_1$.

By using the dimensionless ratios, γ and ρ, defined below, the physical quantities in the dimensionless constants C_1 and C_2 need not be specified:

$\gamma = q_1/48\, EI/\ell^3$ = ratio of support stiffness to beam stiffness;

$\rho = t_g/T_{ss}$ = ratio of pulse duration to "fundamental period" of beam;

$T_{ss} = (4mN\ell^3/\pi^2 EI)^{\frac{1}{2}}$ = fundamental natural period of elastic beam simply supported on rigid supports ($q_1 \to \infty$).

The constants C_1 and C_2 then become:

$$C_1 = (4/\pi^2)\, N^2\rho^2;$$

$$C_2 = (192/\pi^2)\, N\gamma\rho^2.$$

The numerical procedure used to obtain the response quantities is the same as that used in an earlier publication [8]. Norris et al. [6], refer to this procedure as a special case of the Adams-Stormer method. In order to verify the results using the Adams-Stormer method, the fourth-order version of the Runge-Kutta method was also used to obtain the response quantities for a few cases. The calculations were performed on the CDC 6400 digital computer at the University of Colorado.

The model beam contained 16 segments (N=16) so that there were 17 point masses equally spaced. A 9-mass model had been used in an earlier study [8], and it was found by a trial increase to 33 masses that the 17-mass model was more than adequate for the purposes of this investigation.

For each application of the ground pulse the beam response was explored for maxima occurring in the time interval, $0 \le t \le 1.5\ T_1$, where T_1 is the fundamental natural period of the beam simply supported on elastic supports at each end. The ratio of ground pulse duration to fundamental natural period of the beam simply supported on rigid supports at each end, $\rho = t_g/T_{ss}$, which is the abscissa of the response spectra, was varied from 0.1 to 1.0. The terminal computational time of $1.5\ T_1$ was found by trial extended computations to be adequate.

In the computational time increment, $\Delta t = T_q/\Phi$, where T_q is the smallest natural period for the system, the divisor Φ was taken equal to 4. Others have used values of Φ ranging from π to 10. It was found by trial calculation that $\Phi = 4$ is satisfactory for the purposes of this investigation.

A detailed presentation of the procedure, study of errors, decisions regarding beam increments and time increments, etc., can be found in the thesis [11] on which this paper is based. Direct comparisons of numerical results are shown in the second section following this one.

COMPUTED RESULTS

Response spectra present the nondimensional response quantities. Two parameters, ρ and γ, define the system if it is elastic. For the elasto-inelastic beam and support system, six non-dimensional parameters, including ρ and γ, are required. They are repeated here for convenience:

$\overline{M}_y = M_y\ell^2/EIU_g$, bending moment at yield point in beam;

$\overline{r}_y = r_y/q_1U_g$, restoring force at yield point in supports;

$\alpha = q_2/q_1$ = support stiffness bilinearity ratio;

$\beta = k_2/k_1$ = beam stiffness bilinearity ratio;

$\gamma = q_1/48EI/\ell^3$ = ratio of support stiffness to beam stiffness;

$\rho = t_g/T_{ss}$ = ratio of pulse duration to "fundamental period" of beam.

For the response spectra, the ordinate is a response quantity and the abscissa is the parameter $\rho = t_g/T_{ss}$. The response quantities are the following:

$|\overline{w}_1|_{max}$ = greatest maximum, disregarding sign, of nondimensional displacement at ends of beam, relative to ground;

$|\overline{w}_c|_{max}$ = greatest maximum, disregarding sign, of nondimensional displacement at center of beam, relative to ground;

$|\overline{M}_c|_{max}$ = greatest maximum, disregarding sign, of nondimensional bending moment at center of beam.

A value of 4.0 was selected for the support-beam stiffness ratio γ, and only this value was used. (Time did not permit the investigation of more than one value for γ.) For any given response spectra plot, three of the following four nonlinear parameters, $\overline{M}_y$, $\overline{r}_y$, α and β, are held fixed while the remaining one, which is the family parameter, is varied. Table 1, Index to Response Spectra, indicates the six cases of beam and support characteristics and the three response quantities. A short vertical line on a response spectrum is used to indicate the minimum value of ρ which results in elastic action in the system.

The first three families of response spectra (Figs. 6, 7, 8) show the results for the elastic beam on elasto-plastic supports ($\alpha = 0$) (family parameter, $\overline{r}_y$). The close agreement with the results of an earlier investigation [8] is not surprising since the mathematical models used in the two investigations are similar.

Figures 9, 10, and 11 indicate the results of investigating the elastic beam on elasto-inelastic supports (family parameter, α). It should be noted that each of these sets of response curves results from an investigation of the region on the corresponding response curves (see Figs. 6, 7, and 8) between the curve for $\overline{r}_y = 0.05$ and the curve for the elastic case.

Figures 12, 13, and 14 present the spectra for the elasto-plastic beam on elastic supports (family parameter, $\overline{M}_y$); Figs. 15, 16 and 17, for the elasto-inelastic beam on elastic supports (family parameter, β); Figs. 18, 19 and 20, for the elasto-inelastic beam on elasto-plastic supports (family parameter, $\overline{r}_y$); and in Figs. 21, 22 and 23 are shown the spectra for the most general case, the elasto-inelastic beam on elasto-inelastic supports (family parameter, α).

VERIFICATION OF NUMERICAL RESULTS

Comparison of Numerical Results with Series Solution Results for the Elastic Beam and Support System. A series solution was obtained for the response of the linear, elastic, distributed parameter Bernoulli-Euler beam simply supported on linear, elastic supports. A comparison of the results obtained by the series solution, using the first four symmetric modes, with the results obtained for the lumped-parameter model by the Adams-Stormer method indicates that the average difference in the relative displacement at the beam ends is 1.23%, and in relative midspan displacement is 1.33%. The average difference for the bending moment response is 4.06%. The maximum differences, all of which occur for the particular case when ρ equals 0.2 are: 2.73% in the relative displacement at the beam ends; and 2.28% in the relative displacement and 7.59% in the bending moment at the beam midspan.

Comparison of Numerical Results with the Results from an Earlier Study for an Elasto-Plastic System. Figures 6, 7 and 8 present, respectively, the response spectra for the relative displacement at the ends of the beam and the relative displacement and bending moment at the beam midspan. The response results, as shown on these graphs, are in close agreement with the results obtained in an earlier study[8]. This comparison is limited to the case of an elastic beam on elasto-plastic supports.

Comparison of Results Obtained by the Adams-Stormer Method with Those Obtained by the Runge-Kutta Method. For the linearly elastic beam-support system the response results were obtained for five values of ρ and three different response quantities using both the Adams-Stormer and the Runge-Kutta methods. In all cases of comparison the differences between the Adams-Stormer results and the Runge-Kutta results are less than 1%. It should be noted that for these problems the Runge-Kutta method required almost twice as much computer time as the Adams-Stormer method.

Due to the large amount of computer time required, only one nonlinear case (elasto-plastic beam on elastic supports) was calculated using the Runge-Kutta method. The parameters γ, ρ, and $\overline{M}_y$ were assigned arbitrary values of 4.0, 0.3, and 5.0, respectively. In comparing the results for this case with the results for the same case using the Adams-Stormer method, it was found that the maximum relative displacement at the ends of the beam and also at the midspan differed by much less than 1%. For this elasto-plastic case, the Runge-Kutta method required about 3.5 times as much computational time as the Adams-Stormer method.

CONCLUSIONS

The response spectra for relative displacement and bending moment are regular in all six cases investigated. Because of the complexity of the nonlinear system and its response it is not feasible to compose a brief statement describing the transient response in three variables as affected by six combinations of the system parameters. A few characteristics, however, of the elasto-inelastic beam-support system are noted. Referring to Fig. 10 (case 2) (see Table 1), it is seen that even though inelastic action begins in the supports when ρ is decreased to 0.52, as indicated by the short vertical line, the relative displacement at the beam midspan is not affected significantly until ρ is reduced below 0.3 in value. As seen in Fig. 11, however, the bending moment at the midspan is affected by any value of ρ that results in inelastic action in the supports.

It can be seen from Fig. 12 (case 3), that the relative displacement at the ends of the beam decreases as $\overline{M}_y$ (bending moment at yield point) is decreased, provided the beam is forced into yielding. This decrease in relative displacement indicates that when yielding takes place in some part of the structure, the displacement does not necessarily increase in all parts of the structure, but may decrease as in this case. Figure 13, however, shows that the relative displacement at the midspan of the beam increases as $\overline{M}_y$ is decreased.

A question to consider for case 5 is: for a given value of the pulse duration where yielding occurs in the system, does inelastic action occur in both the beam and beam supports? Although only a limited amount of data is available, the question may be answered by observing the point where the spectrum for the inelastic system branches off the spectrum for the elastic system. In comparing the actual branch points for the spectrum where $\overline{T}_y = 0.03$ with the location of the short vertical lines in Figs. 18 and 20, it seems apparent that as ρ is decreased to a value of 0.72, yielding occurs in both the beam and the supports, since the actual branch points coincide with the vertical lines. For the spectrum in which $\overline{T}_y$ equals 0.05, however, yielding takes place in the beam when ρ equals 0.57 followed by yielding in the supports when ρ is reduced to 0.50.

Also, in comparing the spectra in Fig. 18 (case 5) with the spectra in Fig. 6 (case 1), it is seen that there is little difference in the response quantities. From the above comparison it is concluded that elasto-inelastic action occurring in the beam, within the range investigated, has only a slight effect on the displacement at the ends of the beam. If a similar comparison is made for the relative displacement and the bending moment spectra at the beam midspan using Figs. 19 and 7 and Figs. 20 and 8, respectively, it is concluded that the inelastic action in the beam has a relatively small effect on the midspan displacement and bending moment.

Observing the spectra in Fig. 21 (case 6) for the relative displacement at the ends of the beam, it is seen that as the family parameter is increased in value, the displacement decreases. When α equals 0.7, however, the displacement spectrum for the inelastic system falls below the spectrum for the elastic system. This anomaly may be due to the fact that as α increases in value, the inelastic action in the beam exerts a proportionately greater influence on the dynamic response of the system. It was found in Fig. 15, for the elasto-inelastic beam on elastic supports, that all spectra for the relative displacement at the ends of the beam fall below the spectrum for the elastic system.

Other types of hysteretic, beam-moment-curvature functions involving curvilinear branches in place of the linear branches used in this investigation [4] should be studied in order to determine the effect that the sharp discontinuities in the hysteretic, moment-curvature function may have on the response quantities.

TABLE 1: INDEX TO RESPONSE SPECTRA

Case	Beam**					Supports**					Response Quantity*			Fig. No.
	Elastic	Elasto-Plastic	Elasto-Inelastic	β	$\bar{M}_y$	Elastic	Elasto-Plastic	Elasto-Inelastic	α	$\bar{r}_y$	$\lvert\bar{w}_1\rvert_{max}$	$\lvert\bar{w}_c\rvert_{max}$	$\lvert\bar{M}_c\rvert_{max}$	
1	X			1.0	∞		X		0	† v	X	X	X	6 7 8
2	X			1.0	∞			X	v	0.05	X	X	X	9 10 11
3		X		0	v	X			1.0	∞	X	X	X	12 13 14
4			X	v	5.0	X			1.0	∞	X	X	X	15 16 17
5			X	0.3	2.5		X		0	v	X	X	X	18 19 20
6			X	0.3	2.5			X	v	0.05	X	X	X	21 22 23

† v = variable (family parameter)
* Greatest maximum without regard for sign; subscript (1) refers to either end of beam; subscript (c) refers to midspan.
** Ratio of support stiffness to beam stiffness, γ = 4.0, constant for all cases

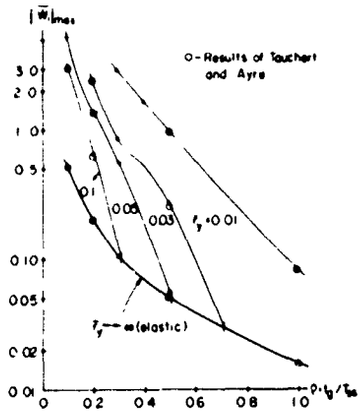

FIG. 6.-RELATIVE DISPLACEMENT AT ENDS OF BEAM, ELASTIC BEAM ON ELASTO-PLASTIC SUPPORTS, $\alpha = 0.0$, $\gamma = 4.0$.

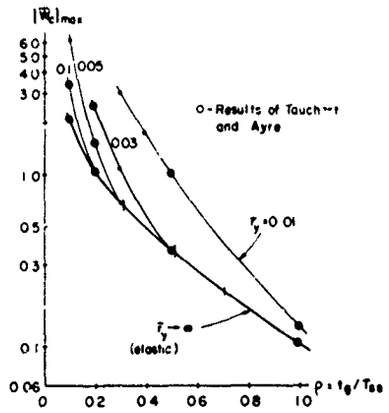

FIG. 7.-RELATIVE DISPLACEMENT AT MID-SPAN, ELASTIC BEAM ON ELASTO-PLASTIC SUPPORTS, $\alpha = 0.0$, $\gamma = 4.0$.

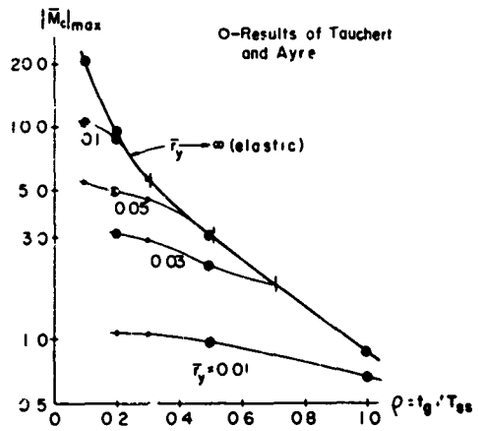

FIG. 8.-BENDING MOMENT AT MIDSPAN, ELASTIC BEAM ON ELASTO-PLASTIC SUPPORTS, $\alpha = 0.0$, $\gamma = 4.0$.

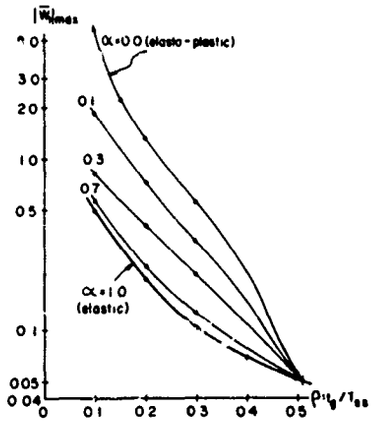

FIG. 9.-RELATIVE DISPLACEMENT AT ENDS OF BEAM, ELASTIC BEAM ON ELASTO-INELASTIC SUPPORTS, $\bar{r}_y = 0.05$, $\gamma = 4.0$.

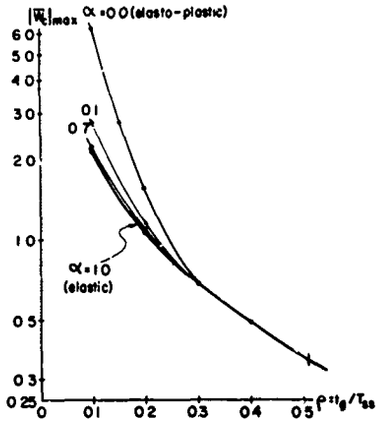

FIG. 10.-RELATIVE DISPLACEMENT AT MIDSPAN, ELASTIC BEAM ON ELASTO-INELASTIC SUPPORTS, $\bar{r}_y = 0.05$, $\gamma = 4.0$.

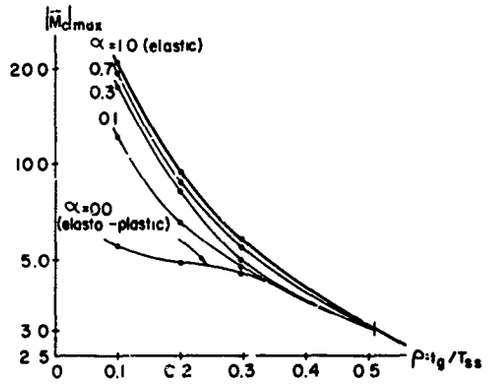

FIG. 11.-BENDING MOMENT AT MIDSPAN, ELASTIC BEAM ON ELASTO-INELASTIC SUPPORTS, $\bar{r}_y = 0.05$, $\gamma = 4.0$.

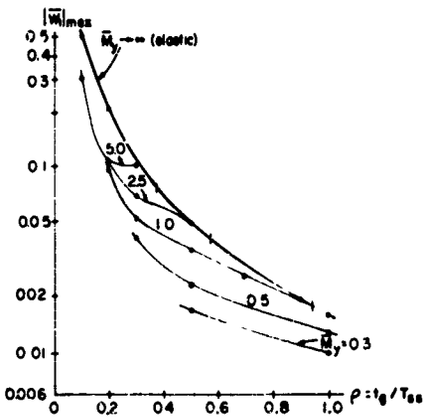

FIG. 12.—RELATIVE DISPLACEMENT AT ENDS OF BEAM, ELASTO-PLASTIC BEAM ON ELASTIC SUPPORTS, β = 0.0, γ = 4.0.

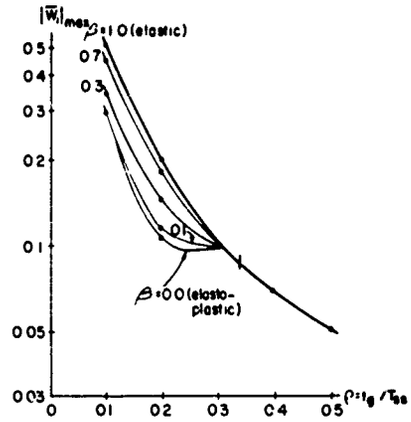

FIG. 15.—RELATIVE DISPLACEMENT AT ENDS OF BEAM, ELASTO-INELASTIC BEAM ON ELASTIC SUPPORTS, $\bar{M}_y$ = 5.0, γ = 4.0.

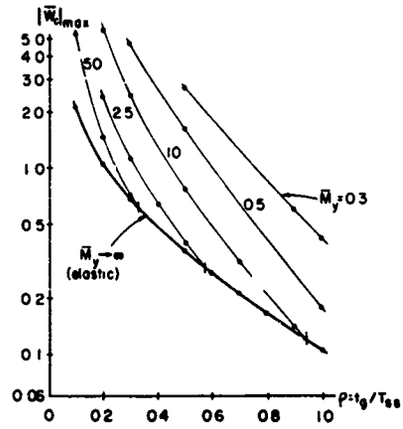

FIG. 13.—RELATIVE DISPLACEMENT AT MIDSPAN, ELASTO-PLASTIC BEAM ON ELASTIC SUPPORTS, β = 0.0, γ = 4.0.

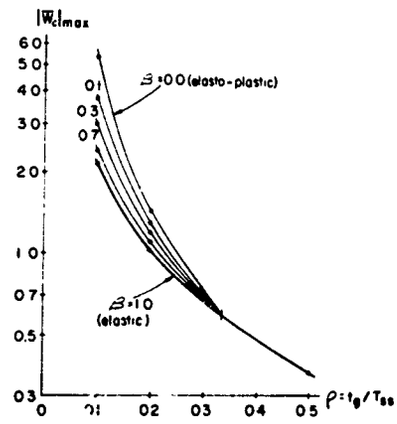

FIG. 16.—RELATIVE DISPLACEMENT AT MIDSPAN, ELASTO-INELASTIC BEAM ON ELASTIC SUPPORTS, $\bar{M}_y$ = 5.0, γ = 4.0.

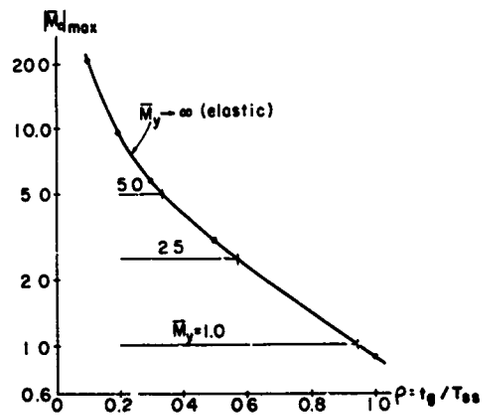

FIG. 14.—BENDING MOMENT AT MIDSPAN, ELASTO-PLASTIC BEAM ON ELASTIC SUPPORTS, β = 0.0, γ = 4.0.

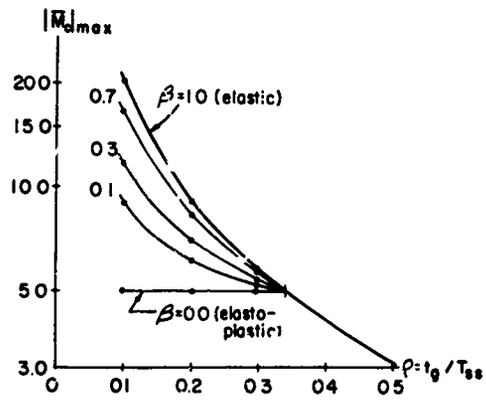

FIG. 17.—BENDING MOMENT AT MIDSPAN, ELASTO-INELASTIC BEAM ON ELASTIC SUPPORTS, $\bar{M}_y$ = 5.0, γ = 4.0.

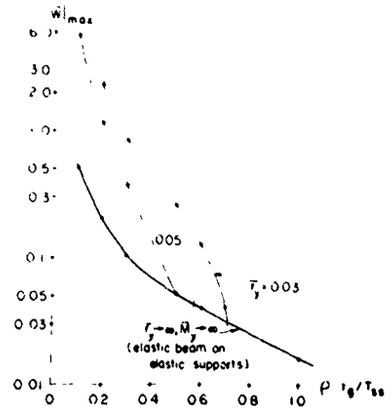

FIG. 18.–RELATIVE DISPLACEMENT AT ENDS OF BEAM, ELASTO-INELASTIC BEAM ON ELASTO-PLASTIC SUPPORTS, $\bar{M}_y$ = 2.5, β = 0.3, α = 0.0, γ = 4.0.

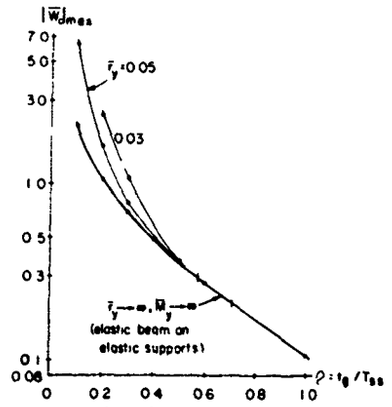

FIG. 19.–RELATIVE DISPLACEMENT AT MIDSPAN, ELASTO-INELASTIC BEAM ON ELASTO-PLASTIC SUPPORTS, $\bar{M}_y$ = 2.5, β = 0.3, α = 0.0, γ = 4.0.

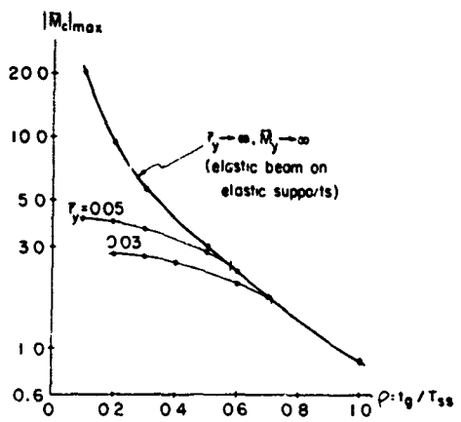

FIG. 20.–BENDING MOMENT AT MIDSPAN, ELASTO-INELASTIC BEAM ON ELASTO-PLASTIC SUPPORTS, $\bar{M}_y$ = 2.5, β = 0.3, α = 0.0, γ = 4.0.

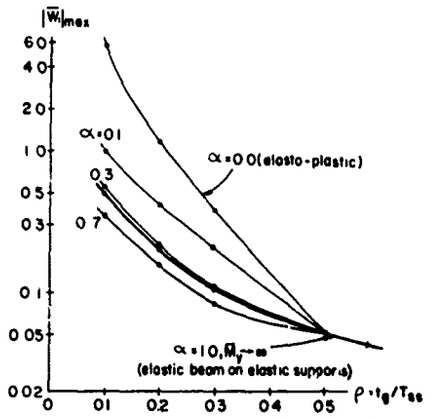

FIG. 21.–RELATIVE DISPLACEMENT AT ENDS OF BEAM, ELASTO-INELASTIC BEAM ON ELASTO-INELASTIC SUPPORTS, $\bar{M}_y$ = 2.5, β = 0.3, $\bar{r}_y$ = 0.05, γ = 4.0.

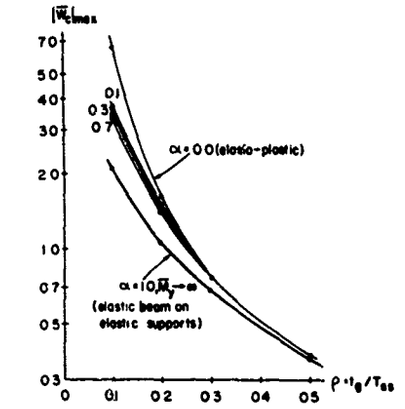

FIG. 22.–RELATIVE DISPLACEMENT AT MIDSPAN, ELASTO-INELASTIC BEAM ON ELASTO-INELASTIC SUPPORTS, $\bar{M}_y$ = 2.5, β = 0.3, $\bar{r}_y$ = 0.05, γ = 4.0.

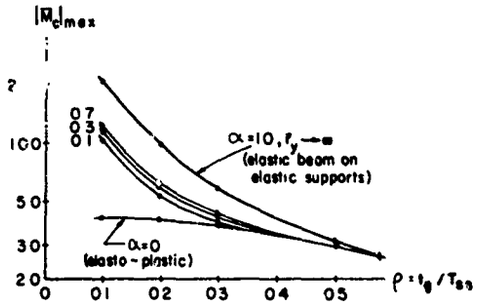

FIG. 23.–BENDING MOMENT AT MIDSPAN, ELASTO-INELASTIC BEAM ON ELASTO-INELASTIC SUPPORTS, $\bar{M}_y$ = 2.5, β = 0.3, $\bar{r}_y$ = 0.05, γ = 4.0.

REFERENCES

1. M.L. Baron, H.H. Bleich and P. Weidlinger, "Dynamic Elastic-Plastic Analysis of Structures", J. Eng. Mechanics Div., ASCE, Vol. 87, pp. 23-42, Feb. 1961

2. G.V. Berg and D.A. DaDeppo, "Dynamic Analysis of Elasto-Plastic Structures", J. Eng. Mechanics Div., ASCE, Vol. 86, pp. 35-58, April 1960

3. A.C. Heidebrecht, J.F. Fleming and S.L. Lee, "Dynamic Analysis of Inelastic Multi-Degree Systems", J. Eng. Mechanics Div., ASCE, Vol. 89, pp. 193-215, Dec. 1963

4. M.J. Kaldjian, "Moment Curvature of Beams as Ramberg-Osgood Functions", J. Structural Div., ASCE, Vol. 93, pp. 53-65, Oct. 1967

5. J.R. Mays and R.S. Ayre, "Shock Load Response of a Beam on a Distributed Foundation with Yielding Bilinear, Hysteretic Action in Either Member", Developments in Mechanics, Vol. 4, pp. 681-701, 1968; Proc., 10th Midwestern Mechanics Conf.

6. C.H. Norris, et al., Structural Design for Dynamic Loads, pp. 196-207. McGraw-Hill, New York, 1959

7. A.B. Schultz, "Nonlinear Response of a Beam to Shock Pulse", J. Franklin Inst., Vol. 276, pp. 385-393, 1963

8. T.R. Tauchert and R.S. Ayre, "Shock Response of a Simple Beam on Nonlinear Supports", J. Eng. Mechanics Div., ASCE, Vol. 91, pp. 91-109, Dec. 1965

9. T.R. Tauchert and R.S. Ayre, "Shock Resistant Design of Simple Beams on Yielding, Nonlinear Supports", Int. J. Mech. Sci., Vol. 8, pp. 479-490, 1965

10. R.K. Wen and T. Toridis, "Discrete Dynamic Models for Elasto-Inelastic Beams", J. Eng. Mechanics Div., ASCE, Vol. 90, pp. 71-102, Oct. 1964

11. B.E. Burton, Shock Response of an Elasto-Inelastic Beam on Elasto-Inelastic Supports, Ph.D. thesis. Univ. of Colorado, Boulder, 1968.

DISCUSSION

Mr. Ripperger (University of Texas): I can not add anything to this paper except that I thought it was very interesting. I want to make an observation that one of my students and I published a paper that is related to this problem in the 30th Shock and Vibration Symposium Bulletin about ten years ago in which we looked into the permanent deformation that was developed in tip loaded cantilever beams subjected to shock loading at the support of the tip. If anybody is interested in related information to this paper they might want to look at that one. (Editors Note: 30th Shock and Vibration Bulletin Part III, p302, February 1962).

Mr. Burton: Thank you for that information.

Mr. Ayer (University of Colorado): This paper is really part of a series that has been generated by various people. There is another one on a cantilever beam problem by a man by the name of Shultz which came out in 1964 or 1965, and there have been some others relating to other configurations. In introducing it I remarked that it was more of an academic sort of paper, not with any intention of apologizing for it in any way, but with the aim of trying to understand some of the nonlinear phenomena with which we are faced without necessarily relating the problem to a specific application. It is really a sort of quantitative study from which we hope to derive some qualitative conclusions that may give us a basis for judgment.

DIGITAL FOURIER ANALYSIS OF MECHANICAL SHOCK DATA

H. A. Gaberson, Ph.D. and D. Pal
Naval Civil Engineering Laboratory
Port Hueneme, California

Fourier transforms of recorded shock motions show promise as classifiable descriptors of mechanical shock hardness, and the transforms have become inexpensive to compute due to the availability of various Fast Fourier Transform computer programs. However, confusing differences exist between the continuous Fourier transform and that actually produced by the computer programs. Interestingly, it is the fact of sampling or discretization itself which causes the difficulty. This paper presents a self-contained development of the discrete Fourier transform, and relates the computed transform to the continuous version. The finiteness of the transient makes possible an exact representation of the transform at a sequence of discrete frequencies. Computer programs generally report only these discrete values which are often too widely spaced to be related to mechanical systems. Interpretation formulas are derived that permit the intermediate values to be computed. Finally, the basic unresolvability of errors due to too coarse sampling (aliasing) is discussed. It is concluded that change of sampling rate can indicate the absence of aliasing errors.

INTRODUCTION

NCEL is evaluating methods to determine the hardness of routinely installed shore based equipment and to this end seeks improved descriptors of environmental shock severity as well as the potential of equipment to withstand that environment, the equipment SHOCK HARDNESS. This report presents a theoretical development of the digitally computable discrete Fourier transform, a descriptor of mechanical shock that holds great promise for use in the measurement of equipment shock hardness.

The Fourier transform of a mechanical shock motion is expected to be a useful description for many reasons. It is an alternate means of recording the motion; whereas such a motion is normally thought of as velocity, acceleration or displacement as a function of time, the transform records the motion as a function of frequency. The transform is the usual input to theoretical calculations of shock response, hence one might expect it to have experimental usefulness. The shock spectrum, a related frequency domain function, has had wide acceptance as a measure of shock severity. Since the Fourier transform contains a complete description of the original motion, as opposed to the shock spectrum which only retains about half of the information, it is felt that the transform offers greater potential as a complete descriptor. Furthermore, the Fourier amplitudes and phases, that are necessarily computed, are required in the computation of many related frequency domain functions, such as the power spectral density, cross and auto correlations, frequency response, and the like. Therefore, the Fourier transform and its related functions must be evaluated for use as a means for organizing and classifying the shock hardness of equipment.

In addition, the dynamic test instrumentation industry has recently come forth with many analyzers and special purpose computers to "instantly" compute frequency domain functions. The logic circuits or calculation routines are difficult to evaluate and verify. A thorough understanding of the readily available digitally computed Fourier transform is also useful to prove the fidelity of the output of the various analyzers.

In 1964, Cooley and Tukey[1] published an efficient Fourier transform computing algorithm which has made inexpensive Fourier transform calculations a reality. Bergland[2] presented a comprehensive discussion of the Fast Fourier Transform, or "FFT" as the Cooley-Tukey algorithm is now called. In it, he reports that the cost of doing a 2^{10} or 1024 sample analysis has dropped from a few dollars to a few cents as a

result of this computing method. In fact, special purpose hardware has reduced the cost to a few hundredths of a cent. Thus we can look forward to very economical frequency domain calculations if these methods prove to be of value in the measurement of equipment shock hardness.

Inherent peculiarities and differences exist between a digitally computed transform and the ideal continuously integrated version. Therefore, this paper presents a self-contained development of the discrete Fourier transform in a form sufficiently detailed to be understandable to the test engineer. The paper begins by reviewing a few properties of the continuous Fourier transform and then develops the discrete transform along lines suggested by Cooley, Lewis, and Welch.[3] The available computer programs present results in various trigonometric forms, and these forms are developed in the next section. The computer results are returned at discrete frequencies which in the case of shock data may only include a few frequencies within the range of interest; therefore, formulas that permit determination of values at any intermediate frequency are developed. Finally, in the last section, the subject of sampling and procedures to avoid aliasing are described. The paper substantially covers the preparatory study that must be done before embarking on a program of digital Fourier analysis of mechanical shock data.

CONTINUOUS FOURIER TRANSFORM

Many presentations[4,5,6] of the continuous Fourier transform are available for use as a point of departure. We shall cite Bracewell[4] as presenting the precise forms with which we begin, the adequate expositions of mathematical existence, and the proof that all practical waveforms do indeed have Fourier transforms. Therefore, we begin by considering a function of time, x(t), which has a Fourier transform F(f) given by:

$$F(f) = \int_{-\infty}^{\infty} x(t)\, e^{-2\pi ift}\, dt. \qquad (1)$$

Here, f is the frequency in cycles per second (Hertz, Hz), t is the time in seconds and i is the imaginary constant, $i = \sqrt{-1}$. The function F(f) is complex, requiring amplitude and phase, or real and imaginary functions to represent it. Figures 1 and 2 represent such a function and its Fourier transform. The transform F(f) can be inverse transformed back to x(t) by taking the inverse transform of F as follows:

$$x(t) = \int_{-\infty}^{\infty} F(f)\, e^{2\pi ift}\, df. \qquad (2)$$

The above two expressions constitute a continuous Fourier transform pair; x(t) transforms to F(f) and vice versa according to the above expressions.

It is necessary to recall some properties of the Fourier transforms of real functions to efficiently present the forthcoming development. Equation (1) may be written as:

$$F(f) = \int_{-\infty}^{\infty} x(t)\, [\cos(2\pi ft) - i \sin(2\pi ft)]dt. \qquad (3)$$

Since F(f) is a complex function, it may be written in terms of its real and imaginary parts:

$$F(f) = R(f) + i\, I(f) \qquad (4)$$

Since x(t) is a real function, the real and imaginary parts of F(f) can be written as:

$$R(f) = \int_{-\infty}^{\infty} x(t) \cos(2\pi ft)\, dt \qquad (5)$$

$$I(f) = \int_{-\infty}^{\infty} x(t) \sin(2\pi ft)\, dt. \qquad (6)$$

Now observe from Equations (5) and (6) that, since R and I are functions of f alone, and since the cosine is an even function and the sine is odd, the real part of the transform (of a real function) is even and the imaginary part is odd; in symbols:

$$R(f) = R(-f) \qquad (7)$$

$$I(f) = -\, I(-f)\ . \qquad (8)$$

In other words, F(-f) is the complex conjugate of F(f). This being the case, only positive or negative values are required to fully specify the Fourier transform of a real function. Finally, noting Equations (5) and (6) at f = 0, the imaginary part goes to zero at zero frequency, which means the Fourier transform is real at zero frequency.

DISCRETE TRANSFORM THEORY

We now proceed to develop a discrete formulation of the above pair. The following development is an expanded and specialized presentation of an original proof by Cooley, Lewis and Welch.[3] Consider the function obtained by sampling x(t) at the rate, S (samples per second), as shown in Figure 1. The time interval between the samples will be:

$$\Delta t = \frac{1}{S}\ . \qquad (9)$$

This new function (the sampled version of the continuous function, x(t)) may be exactly written by restricting Equation 2 to only discrete values of time. This is accomplished by expressing time as:

$$t = j\Delta t, \qquad (9a)$$

where $j = 0, \pm 1, \pm 2, \pm 3, \ldots \pm\infty$.

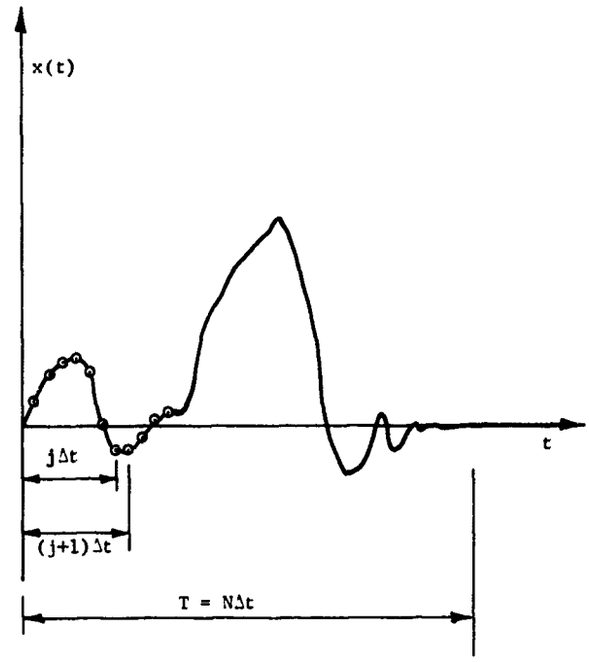

Figure 1. A function of time of duration T, and an indication of digitizing.

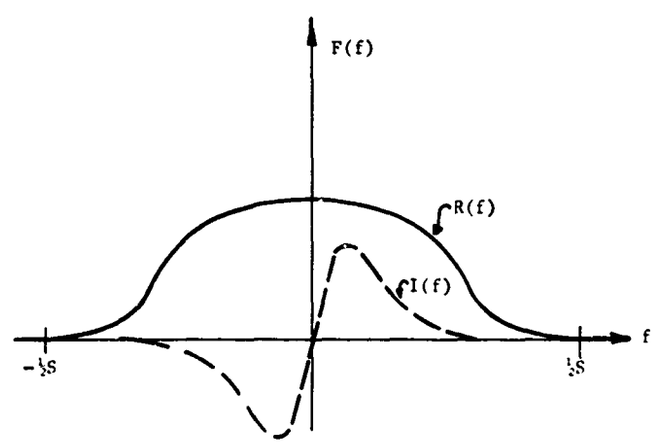

Figure 2. Plot of a Fourier Transform in which F(f) = 0 for |f| > ½S.

Thus by substituting Equations (9a) and (9) into Equation (2), the sampled version of $x(t)$ is:

$$x(j\Delta t) = \int_{-\infty}^{\infty} F(f)\, e^{2\pi ijf/S}\, df. \qquad (10)$$

This infinite integral is now written as an infinite sum of many finite integrals, each of duration S, indexed by the integer k, as follows:

$$x(j\Delta t) = \sum_{k=-\infty}^{\infty} \left[\int_{kS}^{(k+1)S} F(f)\, e^{2\pi ijf/S}\, df \right]. \qquad (11)$$

Since $e^{2\pi ijf/S}$ is a periodic function of period S, it is advantageous to change the variable of integration in Equation (11) as follows. Let:

$$f = f' + kS. \qquad (12)$$

Therefore,

$$df = df'. \qquad (12a)$$

The new integration limits are found by noting in Equation (12) that $f' = 0$, when $f = kS$, and that $f' = S$, when $f = (k + 1)S$. The substitution of these integration limits, Equations (12) and (12a) into (11), and noting that $e^{2\pi ijk} = 1$ for integral values of j and k, yields:

$$x(j\Delta t) = \sum_{k=-\infty}^{\infty} \left[\int_{0}^{S} F(f' + kS)\, e^{2\pi ijf'/S}\, df' \right]. \qquad (13)$$

Thus the change of variable eliminates k from the limits of integration and will permit the interchanging of the summation and integral signs. This can be seen by writing a few terms of the summation of Equation (13), grouping these terms under one integral sign, and factoring the exponential and the differential factors from each term; thus Equation (13) becomes:

$$x(j\Delta t) = \int_{0}^{S} \left[\sum_{k=-\infty}^{\infty} F(f' + kS) \right] e^{2\pi ijf'/S}\, df'. \qquad (14)$$

The inner summation may be used as the definition of a new function,

$$F_p(f') = \sum_{k=-\infty}^{\infty} F(f' + kS). \qquad (15)$$

Using this definition in Equation (14), we obtain:

$$x(j\Delta t) = \int_{0}^{S} F_p(f')\, e^{2\pi ijf'/S}\, df'. \qquad (16)$$

Equation (14) is written in terms of a variable f' which required a range of values from 0 to S, as was implied in Equation (12). Now, consider the ramifications of permitting f' in $F_p(f')$ to take on all values. The effect is to make Equation (15) applicable for wider values of f and in fact $F_p(f)$ becomes periodic of period S. Note that from Equation (15):

$$F_p(f + S) = \sum_{k=-\infty}^{\infty} F(f + S + kS)$$

$$= \sum_{k=-\infty}^{\infty} F[f + (k + 1)\, S]. \qquad (17)$$

Since $(k + 1)$ is an integer and also varies from $-\infty$ to ∞:

$$\sum_{k=-\infty}^{\infty} F[f + (k + 1)\, S] = \sum_{k=-\infty}^{\infty} F(f + kS). \qquad (17a)$$

Thus from Equations (15, 17, 17a), it can be seen that:

$$F_p(f) = F_p(f + S) \qquad (18)$$

and therefore, $F_p(f)$ is a periodic function with period S as shown in Figure 3. As will be seen, this development requires the periodicity of $F_p(f)$. Thus we drop the primes in Equation (15) and rewrite it in terms of the original f, anticipating that we shall account for the effects later in the section on aliasing:

$$F_p(f) = \sum_{k=-\infty}^{\infty} F(f + kS). \qquad (15a)$$

The other primes in Equation (16) may be dropped since the integration has the limits 0 and S:

$$x(j\Delta t) = \int_{0}^{S} F_p(f)\, e^{2\pi ijf/S}\, df. \qquad (16a)$$

Now, since $F_p(f)$ is periodic, it has a Fourier series expansion (see Reference 5, p. 43); hence we can write:

$$F_p(f) = \sum_{j=-\infty}^{\infty} C_j\, e^{-2\pi ijf/S} \qquad (19)$$

where the coefficients, C_j, are given by:

$$C_j = \frac{1}{S} \int_{0}^{S} F_p(f)\, e^{2\pi ijf/S}\, df. \qquad (20)$$

By comparing Equation (16a) and Equation (20) it becomes clear that:

$$C_j = \frac{1}{S}\, x(j\Delta t). \qquad (21)$$

Therefore, Equation (19) becomes:

$$F_p(f) = \frac{1}{S} \sum_{j=-\infty}^{\infty} x(j\Delta t)\, e^{-2\pi ijf/S}. \qquad (22)$$

$F_p(f)$ given by Equation (22) is a continuous function of frequency represented by an infinite series. To obtain the finite Fourier transform, we sample $F_p(f)$ between 0 and S at N intervals, Δf apart, such that:

$$\Delta f = S/N. \qquad (23)$$

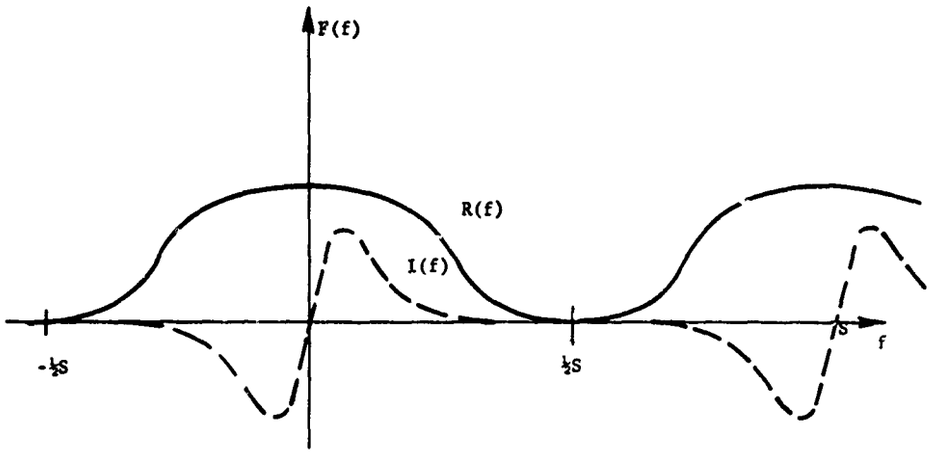

Figure 3. The different transform regions.

Frequency at the sampling points is expressed as:

$$f = n\Delta f, \tag{24}$$

where $n = 0, 1, 2, 3, \ldots, N - 1$.

Substitution of Equations (23) and (24) into (22) yields:

$$F_p(n\Delta f) = \frac{1}{S} \sum_{j=-\infty}^{\infty} x(j\Delta t)\, e^{-2\pi ijn/N}. \tag{25}$$

In Equation (25), the quantity $e^{-2\pi ijn/N}$ is a periodic function of n with period N. Accordingly, the summation is expanded into an infinite sequence of short sums each of N terms, with each sum indexed by ℓ, as follows:

$$F_p(n\Delta f) = \frac{1}{S} \sum_{\ell=-\infty}^{\infty} \left[\sum_{j=\ell N}^{\ell N+N-1} x(j\Delta t)\, e^{-2\pi ijn/N} \right]. \tag{25a}$$

Let $j = j' + \ell N$. Now when $j = \ell N$, $j' = 0$, and when $j = \ell N + N - 1$, $j' = N - 1$. Also note that $e^{-2\pi i\ell n} = 1$ for all values of the integers ℓ and n. Substitution of the above into Equation (25a) yields:

$$F_p(n\Delta f) = \frac{1}{S} \sum_{\ell=-\infty}^{\infty} \left[\sum_{j'=0}^{N-1} x[(j' + \ell N)\Delta t]\, e^{-2\pi ij'n/N} \right]. \tag{25b}$$

By an expansion and regrouping as was done in justifying the interchange of the sum and integral in Equation (13), it can be shown that the two summations in Equation (25b) can be interchanged. Also the primes need not be retained on the j's as will be explained below. Hence, Equation (25b) becomes:

$$F_p(n\Delta f) = \frac{1}{S} \sum_{j=0}^{N-1} \left[\sum_{\ell=-\infty}^{\infty} x(j\Delta t + \ell N\Delta t) \right] e^{-2\pi ijn/N}. \tag{26}$$

As in Equation (15), one can define:

$$x_p(j\Delta t) = \sum_{\ell=-\infty}^{\infty} x(j\Delta t + \ell N\Delta t). \tag{27}$$

Including this final concept into Equation (26), we obtain:

$$F_p(n\Delta f) = \frac{1}{S} \sum_{j=0}^{N-1} x_p(j\Delta t)\, e^{-2\pi ijn/N}. \tag{28}$$

Equation (28) is finally the discrete Fourier transform of the discrete sequence of points $x_p(j\Delta t)$, the result sought. The dropping of the primes on j is explained in the same way as in the dropping of the primes on f' following Equation (16). Considering j in Equation (27) as taking on all values similarly results in $x_p(n\Delta t)$ becoming periodic in this case with period $N\Delta t$.

Equation (27), which is similar to Equation (15a), is a device that permits us to evaluate the effects of truncating the infinite summation of the mathematical concept of the continuous Fourier Transform. Thus while Equation (1) requires integration over all time, Equation (27) in an understandable way, eliminates this requirement. Referring again to Figure 1, in

any practical case the transient of interest has a finite duration, T, and at all other times is zero. Thus while Equation(27) formally includes all time, it permits us to include all time with a finite number of samples. Figure 4 illustrates this more clearly. We define $T = N\Delta t$. Now consider the summation of Equation (27) for one of the values of j. The equation requires the sum of the x's at $j\Delta t$, $j\Delta t+T$, $j\Delta t + 2T$, and so one, as well as at $j\Delta t - T$, $j\Delta t - 2T$, etc. But, if the transient is all contained within the interval 0-T, the value of x_p for this j is merely the value of the transient at $t = j\Delta t$, all the other values are zero. Additionally, the periodicity of x_p is also made apparent by Figure 4, it is clear that x_p as given by Equation (27) will have the same values $j\Delta t$, $j\Delta t + T$, $j\Delta t + 2T$, etc. This periodicity is required in the development of the inverse transform relation.

The inverse discrete Fourier transform relation can be obtained by redoing the above series of steps, except that this time Equation (1) is sampled. The complete set of analogous steps leads to the result:

$$x_p(j\Delta t) = \frac{1}{T}\sum_{n=0}^{N-1} F_p(r\Delta f)\, e^{2\pi ijn/N} . \qquad (29)$$

Recalling the definitions of S (the sampling rate), N (the number of frequency samples) and T (the duration of x_p), Equations (27) and (28) may be rewritten in the following more convenient forms:

$$F_p(n\Delta f) = \frac{1}{N}\sum_{j=0}^{N-1} T\, x_p(j\Delta t)\, e^{-2\pi ijn/N} \qquad (30)$$

$$T\, x_p(j\Delta t) = \sum_{n=0}^{N-1} F_p(n\Delta f)\, e^{2\pi ijn/N} . \qquad (31)$$

The discrete Fourier transform pair, Equations (30) and (31), constitutes the primary result of this section. It is reassuring to show that Equations (30) and (31) do indeed transform to each other. This can be shown by direct substitution which is carried out in the Appendix and in Reference 7

Some final explanation is yet required. The discrete transform pair $x_p(j\Delta t)$ and $F_p(n\Delta f)$ will equal the corresponding continuous functions x(t) and F(f) at the sampling points according to the following precise rules:

$$x_p(j\Delta t) = \sum_{\ell=-\infty}^{\infty} x(j\Delta t + \ell N\Delta t) \qquad 0 \le j \le N-1 \quad (27)$$

$$F_p(n\Delta f) = \sum_{k=-\infty}^{\infty} F(n\Delta f + kS) \qquad 0 \le n \le N-1. \quad (32)$$

Thus so long as x(t) is non-zero only in the interval $0-N\Delta t$, $x_p(j\Delta t)$ will equal the function at the discrete points. We must be careful however in examining Equation (32) to establish the relation between the two transforms. From the previous discussion of the characteristics of Fourier transforms of real functions, it was established that the transform for negative values was the complex conjugate of that for positive values. This fact leads to the conclusion that the sampling rate, S, must be high enough so that the Fourier transform has no values for frequencies in excess of S/2. Consider a Fourier transform of a real function that has the values shown in Figure 3 between 0 and S/2. Because its values for negative arguments must be complex conjugates of those for positive values, it must also appear as shown between 0 and -S/2. Now if the values of the discrete transform are formed according to Equation (32), the function must be periodic of period S as shown in Figure 3 for the full range of S. If the function is such that its Fourier transform has non-zero values outside the range $-\frac{1}{2}S \le f \le \frac{1}{2}S$, discrete transformation will form the sum indicated in Equation (32) and what are termed "aliasing" errors will occur. These will be discussed later under sampling. Finally, then, on Figure 3, the values returned by the various standard computer programs usually lie in the range $0 \le f \le \frac{1}{2}S$; the actual corresponding continuous transform would have values in the range $-\frac{1}{2}S \le f \le \frac{1}{2}S$; and the $F_p(f)$, which is periodic, has values all along the axis. The symmetry of the transform resolves a superficial inconsistancy in that Equations (30) and (31) appear to return N complex values of the transform, F(f), for N samples of x(t), and since the F's are complex this would indicate a return of two values for each unknown entered. As explained above no such situation occurs; half the indicated values of the transform between 0 and S are redundent.

In summary, we selected a sampling rate S which in turn set the time interval between samples since:

$$\Delta t = 1/S. \qquad (9)$$

This resulted in making our computed transform periodic with period S. We sampled the values of this periodic transform at N frequencies, thus the interval between sampled values of the transform became in Equation (23):

$$\Delta f = S/N . \qquad (23)$$

This sampling in turn caused the time function to be considered periodic with period $N\Delta t$. The duration of the time function, T, is taken equal to this period, thus.

$$T = N\Delta t \qquad (33)$$

Combining Equations (9), (23) and (33) we see that the frequency interval is given by:

$$\Delta f = 1/T . \qquad (34)$$

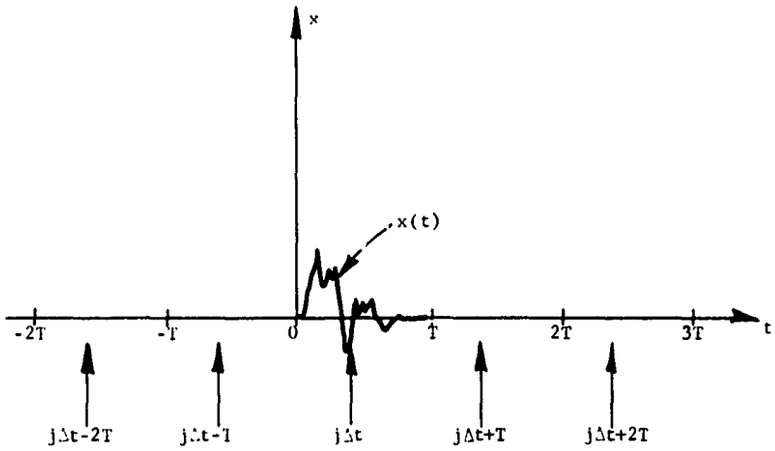

Figure 4. The development of $x_p(j\Delta t)$ from $x(t)$.

Thus the sampling rate set the upper frequency limit (S/2) of the Fourier Transform and the duration of the transient set the frequency increment between the computed values of the transform.

TRIGONOMETRIC FORMS

A trigonometric form of Equation (31) will now be developed, since most results from the computers are returned in these forms. It is helpful to consider the sum on the basis of 2M points rather than N and to simplify the notation of Equation (31) as follows:

$$G_n = F_p(n\Delta f)/T \tag{35}$$

$$X_j = x_p(j\Delta t). \tag{36}$$

Thus Equation (31) may be written:

$$X_j = \sum_{n=0}^{2M-1} G_n \, e^{i\pi jn/M} . \tag{37}$$

This sum can be written as follows:

$$X_j = G_0 + \sum_{n=1}^{M-1} G_n \, e^{i\pi jn/M} + G_M \, e^{i\pi j}$$

$$+ \sum_{n=M+1}^{2M-1} G_n \, e^{i\pi jn/M} . \tag{38}$$

Consider a new summation index m such that:

$$m = 2M - n. \tag{39}$$

When $n = M + 1$, $m = M - 1$, and when $n = 2M - 1$, $m = 1$. Substituting this new index into the second sum of Equation (38) (noting that $e^{2\pi ij} = 1$) yields:

$$X_j = G_0 + \sum_{n=1}^{M-1} G_n \, e^{i\pi jn/M}$$

$$+ \sum_{m=1}^{M-1} G_{(2M-m)} \, e^{-i\pi jm/M} + G_M \, e^{i\pi j} . \tag{40}$$

The two summations of Equation (40) can be combined and the complex exponentials written trigonometrically such that they become:

$$\sum_{n=1}^{M-1} \Big\{ G_n \, [\cos(\pi jn/M) + i \sin(\pi jn/M)]$$

$$+ G_{(2M-n)} [\cos(\pi jn/M) - i \sin(\pi jn/M)] \Big\}.$$

This can be simplified to yield:

$$\sum_{n=1}^{M-1} \Big\{ [G_n + G_{2M-n}] \cos(\pi jn/M)$$

$$+ i \, [G_n - G_{2M-n}] \sin(\pi jn/M) \Big\}.$$

Finally define:

$$c_n = G_n + G_{2M-n} \tag{41}$$

$$b_n = i(G_n - G_{2M-n}) \tag{42}$$

and note that $e^{i\pi j} = (-1)^j$. Making the indicated substitutions yeilds:

$$X_j = G_0 + \sum_{n=1}^{M-1} [c_n \cos(\pi jn/M)$$

$$+ b_n \sin(\pi jn/M)] + G_M(-1)^j, \tag{43}$$

the general trigonometric form.

The most compact trigonometric form is developed by noting the consequences of extending the summation in Equation (43) from 0 to M. The coefficients b_0 and b_M would not be involved since the sine would be zero for both values of n. When n=M, the cosine term would behave identically to $(-1)^j$ and the extension is complete. Thus the compact form is:

$$X_j = \sum_{n=0}^{M} [c_n \cos(\pi jn/M) + b_n \sin(\pi jn/M)]. \quad (44)$$

From Equations (35), (41) and (42) the c's, b's, and original F_p's are related by:

$$c_n = \left\{F_p(n\Delta f) + F_p[(2M-n)\Delta f]\right\}/T \quad (45)$$

$$b_n = i\left\{F_p(n\Delta f) - F_p[(2M-n)\Delta f]\right\}/T \quad (46)$$

except for the two special cases of n:

$$c_0 = F_p(0)/T \quad (47)$$

$$c_M = F_p(M\Delta f)/T. \quad (48)$$

Since the IBM Corporation makes many of its programs available to its large number of users, the form of the output of the IBM Subroutine RHARM[8] is automatically a common form and must be referenced. RHARM[8] uses the Cooley-Tukey[1] Fast Fourier Transform (FFT) Algorithm by calling subroutine HARM[7] which uses the FFT algorithm and was written by Cooley. The transform computed by RHARM is returned as a set of a's and b's such that the original 2N input amplitudes are given by:

$$X_j = \tfrac{1}{2}a_0 + \sum_{k=1}^{N-1} [a_k \cos(\pi jk/N)$$

$$+ b_k \sin(\pi jk/N)] + \tfrac{1}{2}a_N(-1)^j. \quad (49)$$

By comparing Equation (49) and (44) one finds that:

$$\tfrac{1}{2}a_0 = c_0 = F_p(0)/T \quad (50)$$

$$\tfrac{1}{2}a_M = c_M = F_p(M)/T \quad (51)$$

$$a_k = c_n \quad (52)$$

$$b_k = b_n \quad (53)$$

Actual values of the continuous transform are obtained as follows. Since it has been shown that the $F_p(n\Delta f)$'s equal the continuous integral transform at the discrete frequency values $(n\Delta f)$, we should specifically derive the relationship between the F_p's and the a's, b's and c's. Following Equation (8) it was concluded that for real functions negative values of the transform were complex conjugates of the positive values, and since we have shown in the text following Equation (32) that values of F_p between M and 2M are identical to the negative values (since F_p is periodic, see Figure 3) one may write:

$$F_p(n) = F_p^*(2M-n) \quad (54)$$

where F_p^* indicates the complex conjugate. Thus if F_p has a real and imaginary part given by:

$$F_p(n) = R(n) + I(n) \quad (55)$$

one may also conclude that:

$$F_p(2M-n) = R(n) - I(n). \quad (56)$$

Rearranging Equations (45) and (46) yields:

$$T\, c_n = F_p(n) + F_p(2M-n) \quad (57)$$

$$-i\, T\, b_n = F_p(n) - F_p(2M-n). \quad (58)$$

Addition of Equations (57) and (58) yields:

$$F_p(n) = \tfrac{1}{2}T(c_n - i\, b_n). \quad (59)$$

For completeness, we repeat Equations (47) and (48):

$$F_p(0) = T\, c_0 \quad (47)$$

$$F_p(M) = T\, c_M. \quad (48)$$

INTERMEDIATE VALUES OF THE TRANSFORM

Any discrete Fourier transform computation of necessity only returns values at discrete frequencies and, as was shown in Equation (34), the frequency increment is 1/T the duration of x(t). In the analysis of mechanical shock data where the duration is often only milliseconds, the resulting frequency increment is undesirably coarse. In this section we develop the formulae for the determination of intermediate values of the transform.

Thus, utilizing the computed discrete values of the Fourier transform, we seek the values of the transform for any value of the frequency, f. Equation (1), the defining equation, is repeated below:

$$F(f) = \int_{-\infty}^{\infty} x(t)\, e^{-2\pi ift}\, dt. \quad (1)$$

For the case where x(t) is non-zero only when t is between 0 and T, Equation (1) becomes.

$$F(f) = \int_0^T x(t)\, e^{-2\pi ift}\, dt. \quad (60)$$

The values of F(f) for the discrete points $n\Delta f$ or by Equation (34) n/T, have previously been computed. These discrete values may be expressed as (since $f = n\Delta f = n/T$):

$$F(n) = \int_0^T x(t)\, e^{-2\pi int/T}\, dt. \qquad (61)$$

Since x(t) has non-zero values only between 0 and T, we take it to be a periodic function with period T and expand it as a Fourier series as follows:

$$x(t) = \sum_{n=-\infty}^{\infty} A_n\, e^{i2\pi nt/T} \qquad (62)$$

where the A_n are given by:

$$A_n = \frac{1}{T}\int_0^T x(t)\, e^{-i2\pi nt}\, dt. \qquad (63)$$

Equation (63) is equivalent to Equation (61) if A_n is given by:

$$A_n = \frac{F_n}{T}. \qquad (64)$$

Using Equation (64) in (62), we form an expression for $x_p(t)$, a periodic function that equals the original x(t) in the interval $0 \le t \le T$, as follows:

$$x_p(t) = \sum_{n=-\infty}^{\infty} \frac{F_n}{T}\, e^{2\pi int/T}. \qquad (65)$$

For any case in which we take 2M samples at a rate S such that $F(f) = 0$ for $f > \frac{1}{2}S$ (i.e., at a rate to preclude "aliasing"), $F(n) = 0$ for $n > M$ and Equation (65) becomes:

$$x_p(t) = \sum_{n=-M}^{+M} \frac{F_n}{T}\, e^{2\pi int/T}. \qquad (65a)$$

Now define a rectangular function, $p_t(t)$ such that:

$$p_t(t) = 1, \text{ when } 0 \le t \le T$$
$$p_t(t) = 0 \text{ for all other } t. \qquad (66)$$

By forming a product of Equations (65a) and (66) we obtain a useful expression for the original x(t):

$$x(t) = p_t(t)\, x_p(t) = p_t(t) \sum_{n=-M}^{M} \frac{F_n}{T}\, e^{2\pi int/T}. \qquad (67)$$

Form the Fourier transform of Equation (67) as follows:

$$F(f) = \int_{-\infty}^{\infty} p_t(t) \sum_{n=-M}^{M} \frac{F_n}{T}\, e^{2\pi int/T} \cdot e^{-2\pi ift}\, dt. \qquad (68)$$

By Equation (66) this becomes:

$$F(f) = \int_0^T \sum_{n=-M}^{M} \frac{F_n}{T}\, e^{2\pi int/T} \cdot e^{-2\pi ift}\, dt. \qquad (68a)$$

Expanding the first few terms of the sum shows that the sum and integral sign can be interchanged. Making that interchange and performing the integration yields:

$$F(f) = \sum_{n=-M}^{M} \frac{F_n}{T} \cdot \frac{(e^{-2\pi ifT} - 1)}{2\pi i(n/T - f)}. \qquad (69)$$

Equation (69) is the final result and proves that the intermediate values are recoverable from the discrete values.

In order to use Equation (69) it must be expressed in terms of the a's, b's and c's that are computed by the computer programs. Recall that, from Equation (59):

$$F_p(n) = \tfrac{1}{2}T(c_n - i\, b_n). \qquad (59)$$

Following Equation (8), it was shown that $F_p(-n)$ was the complex conjugate of $F_p(n)$; hence:

$$F_p(-n) = \tfrac{1}{2}T(c_n + i\, b_n). \qquad (70)$$

Equations (59) and (70) are applicable for all n between 0 and M. At the limits of n, from Equations (47) and (48) and the complex conjugate result, one obtains:

$$F_p(0) = T\, c_0 \qquad (70a)$$

$$F_p(M) = T\, c_M \qquad (70b)$$

$$F_p(-M) = T\, c_M. \qquad (70c)$$

Substitution of the above relations for the F_p's in Equation (69) yields, after some simplification:

$$F(f) = \frac{(1 - e^{-2\pi if\, T})}{2\pi i}\left\{\frac{c_0}{f} + \frac{2fc_M}{f^2 - M^2/T^2} + \sum_{n=1}^{M-1} \frac{(fc_n - i\, b_n\, n/T)}{(f^2 - n^2/T^2)}\right\}. \qquad (71)$$

By adopting the convention that $b_0 = 0$, we can slightly condense Equation (71) to:

$$F(f) = \frac{(1 - e^{-2\pi ifT})}{2\pi i}\left\{\frac{2fc_M}{f^2 - M^2/T^2} + \sum_{n=0}^{M-1} \frac{(fc_n - i\, b_n\, n/T)}{(f^2 - n^2/T^2)}\right\}. \qquad (72)$$

At first inspection, Equation (72) appears to have zeros in denominators at the integer frequencies, $f = 0, M/T, n/T$. A zero is also formed in the numerator by the exponential term thus yielding an indeterminate form. Application of standard rules for evaluating indeterminate forms[9] yields the correct value, thus checking the accuracy of the algebra.

Finally, Equation (71) may also be written in terms of the a's and b's of the output of Subroutine PHARM.[8] Substitution of Equations (50) through (53) in Equation (71) yields:

$$F(f) = \frac{(1 - e^{-2\pi i f T})}{2\pi i}\left\{\frac{1}{2}\frac{a_0}{f} + \frac{f\, a_M}{f^2 - M^2/T^2} + \sum_{k=1}^{M-1} \frac{(f\, a_k - i\, b_k\, k/T)}{(f^2 - k^2/T^2)}\right\}. \qquad (73)$$

By adopting the convention that $b_M = 0$, the above may be written more simply as:

$$F(f) \frac{(1 - e^{-2\pi i f T})}{2\pi i}\left\{\frac{1}{2}\frac{a_0}{f} + \sum_{k=1}^{M} \frac{(f\, a_k - i\, b_k\, k/T)}{(f^2 - k^2/T^2)}\right\}. \qquad (74)$$

Thus, any of the Equations (71) through (74) can be used with a set of the computed constants to compute intermediate values of F(f) at intermediate frequency values. NCEL has found it helpful to plot the Fourier transform as a function of the log of the frequency, and to this end selects frequencies for F(f) evaluation from the following formula:

$$f = 10^{0.01(j-1)} \qquad (75)$$

where j = 1, 2, 3, . . . k, the interpolation index. It will be noted that integer values of j generate 100 frequencies between each power of 10. The interpolation index, k, selects the maximum frequency computed.

SAMPLING AND DIGITIZATION

Most generally, shock data is delivered in analog continuous form on magnetic tape. The data has already been filtered to some extent by the instrumentation and the upper frequency capabilities of the transducer instrumentation combination. We then digitize this analog data into a sequence of digits for analysis. It is well to stop and reflect on any inherent inaccuracies in digitization.

All realizable mechanical shock transients have Fourier transforms, and the magnitude of the transform at any frequency is generally referred to as the frequency content of the pulse. Of necessity, the data recording system has upper frequency limitations; thus all recorded data is band limited. At least some upper frequency exists beyond which information contained has nothing to do with the shock transient. Thus we say that the recorded analog signal is band limited meaning, that the magnitude of its Fourier transform is zero above some upper frequency which is termed the cut-off frequency.

The sampling theorem of information theory[10] then provides a most useful tool in discussing accuracy of sampled data, and we quote Shannon's original statement of it:[10] "If a function f(t) contains no frequencies higher than W cps, it is completely determined by giving its ordinates at a series of points spaced 1/2W seconds apart." The proof is given in many references[1-3,6,9-11] and was substantially followed in the development on intermediate values here. Thus if we assure that the sampled function had zero frequency content beyond the cutoff frequency which was indeed half our sampling rate, we are assured that our digitized function is a complete representation of the recorded shock transient and that no inaccuracies were inherently introduced due to digitizing. A converse theorem which has been proved[9] states that if a function is finite its transform is completely determined by values at a series of points. This predicts the existence of the preceeding derivation of formulae that do indeed yield intermediate values for the discretely defined transform returned by the digital computer FFT algorithms.

To assure that the recorded signal has no frequency content beyond the cut-off frequency is difficult, however, and means must be sought to assure this. Therefore, the ramifications of too low a sampling rate or "aliasing" must be considered. Since many fine presentations already exist, we shall only touch upon it briefly. Hamming[11] presents a helpful explanation and theoretical development to show the inception of aliasing when the frequency content exceeds half the sampling rate. To illustrate for those not already familiar with aliasing, consider that a motion picture samples a continuous event at about 16 frames per second. According to the sampling theorem, as such it will offer distinguishable information on phenomena with frequency content less than 8 cycles per second. When a spoked wheel rolls such that more than 8 spokes per second pass an observable position, the viewer is unable to distinguish the actual frequency; the wheel often appears to be rolling unrealistically slow or even backwards. This is often referred to as a stroboscopic effect.

Aliasing can also be appreciated with reference to our development of the finite Fourier transform. Discretization of continuous data at a sampling rate, S, effectively results in forcing the transform of the sampled data to be cumulatively composed of the spectrum of the continuous data according to Equation (15a) repeated below:

$$F_p(f) = \sum_{k=-\infty}^{\infty} F(f + k\, S). \qquad (15a)$$

Thus, thinking for illustrative purposes of amplitude only, imagine the transform of a function sampled at too low a rate as shown in Figure 5. The actual transform of the continuous function has non-zero values for frequencies greater than ½S, shown as a solid line in the

Figure. The computed transform, $F_p(f)$, shown dotted, is formed according to Equation (15a). For example, the value at f_1 is composed of the value of actual transform at f_1 and f_1-S. One can easily see that these errors become severe as the sampling rate S is decreased.

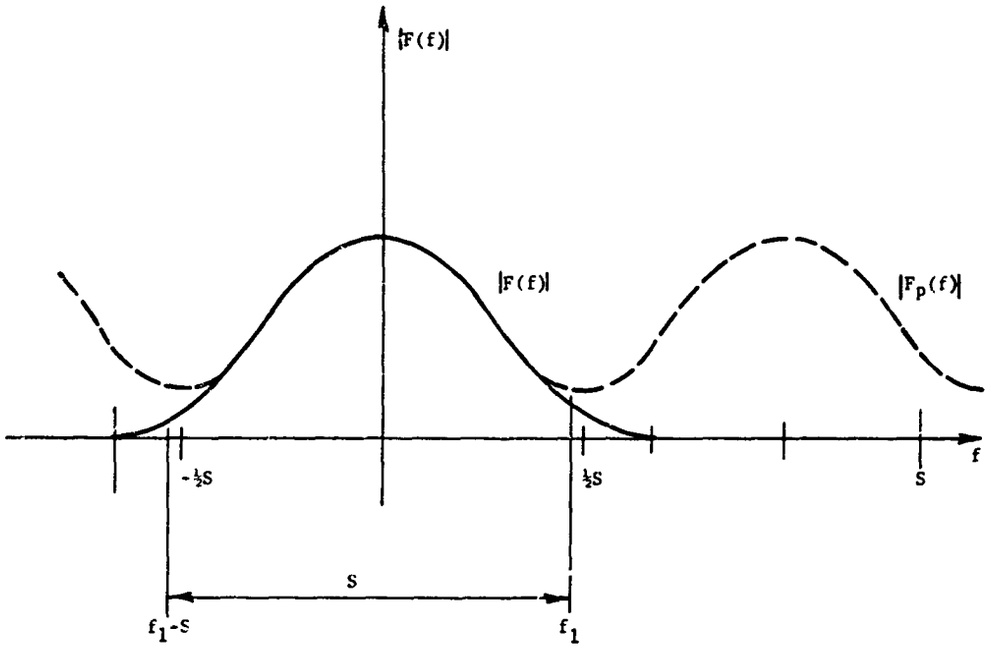

Figure 5. Illustration of transforms indicating aliasing problems.

Finally, even though one may have many reasons to believe that recorded data will contain no frequencies beyond some reasonable limit entirely compatable with reasonable sampling rates, one must be assured that extraneous effects have not introduced high frequency signals that may give rise to aliasing errors. Filtering is often suggested as a means to assure the absence of unwanted high frequency, but filtering may introduce undesirable phase shifts in transient data. Test runs with vastly increased sampling rates to note differences in the resulting computed transforms appear to be the only reasonable means to use for indicating the absence of aliasing errors. One is certainly comforted if the amplitudes approach zero with increasing frequency, and while one can be fairly certain of errors if this is not the case, one cannot be assured of accuracy even though it is.

CONCLUSION

In summary, increased use of digitally computed Fourier transforms and related functions for mechanical shock analysis is expected. For example, since modal velocity has been shown a strong indicator of stress and damage,[12] transforms of velocity are expected to indicate shock hardness. The theoretical transition from the continuous to the discrete Fourier transform is subtle and complicated. This report has presented that theory written specifically for mechanical engineers. The report begins with the continuous Fourier transform pair and presents a self-contained development of the discrete Fourier transform pair, Equations (30) and (31). This discrete pair is written in terms of periodic or "aliased" extensions of the original continuous transform pair defined by Equations (15a) and (27). Various trigonometric forms that are more commonly generated by the available computer programs are given in Equations (43), (44) and (49). Formulae for the exact determination of transform values at intermediate frequencies are given in Equations (69), (72) and (74). Finally, the theory to predict sampling rate adequacy and maximum "aliasing" errors is given. The material has been organized to enable a test engineer to use and evaluate the results of a digital Fourier analysis of digitized mechanical shock data.

ACKNOWLEDGMENT

This work was supported by the Naval Facilities Engineering Command under the cognizance of CAPT P. A. Phelps, Assistant Commander of Research and Development (Code 03).

SYMBOLS

C_j	Fourier series coefficient, Equation (20)
$F(f)$	Fourier transform, see Equation (1)
F_n	$F_p(n\Delta f)$
F_p^*	Complex conjugate of F_p
$F_p(f)$	Periodic transform, "aliased" version, see Equation (15a)
$F_p(n)$	$F_p(n\Delta f)$
G_n	Simplified notation for discrete transform values, see Equation (35)
$I(f)$	Imaginary part of $F(f)$, Equation (8)
$I(n)$	$I(n\Delta f)$
M	$N/2$, Equation (37)
N	Total number of intervals in duration of function, Equation (23)
$R(f)$	Real part of $F(f)$, Equation (7)
$R(n)$	$R(n\Delta f)$
S	Sampling rate, samples per unit time, Equation (9)
T	Duration of $x_p(t)$, Equation (33)
X_j	Simplified notation for discrete time function, see Equation (36)
a_k	Trigonometric form coefficient, Equation (49)
b_n	Trigonometric form coefficient, Equation (42)
c_n	Trigonometric form coefficient, Equation (41)
e	Base of natural logarithms
f	Frequency, cycles per unit time
f'	Reduced range frequency, Equation (12)
i	Imaginary constant, $\sqrt{-1}$
j	Time index integer such that incremental time is denoted. $t = j\Delta t$, $j = 0, \pm 1, 2, 3, \ldots$
j'	Reduced range time index integer, Equation (25c)
k	Summation integer, Equation (11)
ℓ	Summation integer, Equation (25b)
m	Summation index integer, Equation (39)
n	Frequency index integer, such that frequency is denoted, $f = n\Delta f$, $n = 0, \pm 1, 2, 3, \ldots$
p_t	Rectangular function, Equation (66)
t	Time
$x(t)$	A function of time
$x_p(t)$	Periodic "aliased" version of $x(t)$, Equation (4)
Δf	Frequency increment, Equation (24), also shown equal to $1/T$, Equation (34)
Δt	Time increment, Equation (9)

REFERENCES

1. Cooley, J. W. and Tukey, J. W., "An Algorithm for the Machine Calculation of Complex Fourier Series"; Mathematics of Computation, Vol. 19, pp. 297-301; April 1965.

2. Bergland, G. D., "A Guided Tour of the Fast Fourier Transform"; IEEE Spectrum, July 1969, pp. 41-52.

3. Cooley, J. W. and Lewis, P. A. and Welch, P. D., "Application of the Fast Fourier Transform to Computation of Fourier Integrals, Fourier Series, and Convolution Integrals," IEEE Trans. on Audio and Electroacoustics, Vol. AU-15, No. 2, June 1967, pp. 79-85.

4. Bracewell, R., "The Fourier Transform and Its Applications," McGraw-Hill Book Co., New York, 1965.

5. Papoulis, A., "The Fourier Integral and Its Applications," McGraw-Hill Book Co., New York, 1962.

6. Sneddon, I. A., "Fourier Transforms," McGraw-Hill Book Co., New York, 1951.

7. Gaberson, H. A. and Pal, D., "Digital Fourier Analysis of Mechanical Shock Data," Naval Civil Engineering Laboratory, August 1970.

8. "System/360 Scientific Subroutine Package, (360A-CM-03X) Version III, Programmer's Manual; Publication number H20-0205-3; International Business Machines Corporation; Technical Publications Department; 112 East Post Road, White Plains, New York, 1968.

9. Burington, R. S., "Handbook of Mathematical Tables and Formulas," Handbook Publishers, Inc., Sandusky, Ohio, 1950.

10. Shannon, C. E., "Communication in the Presence of Noise," Proc. IRE, January 1949.

11. Hamming, R. W., "Numerical Methods for Scientists and Engineers," McGraw-Hill Book Company, New York, 1962.

12. Gaberson, H. A. and Chalmers, R. H., "Modal Velocity as a Criterion of Shock Severity," The Shock and Vibration Bulletin, No. 40, Part 2, Naval Research Laboratory, Washington, D. C., Dec 1969; pp. 31-49.

APPENDIX

In order to prove that Equations (30) and (31) constitute a transform pair, the right hand side of Equation (30) is substituted into (31) and the result is shown to be an identity. First, a symbol simplification is made by letting:

$$x_p(j\Delta t) = x_j. \qquad \text{(A-1)}$$

Now making the above substitutions yields:

$$T\,x_j = \sum_{n=0}^{N-1}\left[\frac{1}{N}\sum_{j=0}^{N-1} T\,x_j\,e^{-2\pi ijn/N}\right]\cdot e^{2\pi ijn/N}. \qquad \text{(A-2)}$$

Since T and N are constant, they can be factored out of the summations to yield:

$$N\,x_j = \sum_{n=0}^{N-1}\left[\sum_{j=0}^{N-1} x_j\,e^{-2\pi ijn/N}\right]\cdot e^{2\pi ijn/N}. \qquad \text{(A-3)}$$

The first step to prove this an identify is to expand the inner sum:

$$N\,x_j = \sum_{n=0}^{N-1}\left\{x_0 + x_1\,e^{-2\pi in/N} + x_2\,e^{-2\pi i2n/N} + \ldots \ldots + x_{(N-1)}\,e^{-2\pi i(N-1)n/N}\right\}e^{2\pi ijn/N}. \qquad \text{(A-4)}$$

The above sum forms a row of terms; expanding it yields a set of rows of terms that can be arranged in an array as follows:

The right hand side of Equation (A-5) is an N x N array of terms that for any value of j should all add up to Nx_j, the left hand side. To make the proof clear recall that the formula for the sum of a geometric progression[9] of n terms is:

$$S_n = (rL - a)/(r - 1), \qquad \text{(A-6)}$$

where a is the first term,

r is the common ratio,

n is the number of terms,

L is the last term.

What shall now be found is that for each j, the jth column will total Nx_j and all other columns will total zero. Consider the sums of the following columns for the indicated values of j:

<u>Column 0 when j = 0</u>. The exponentials are all unity and the column totals Nx_0.

<u>Column 1 when j = 0</u>. This is a geometric progression with: $a = x_1$; $r = e^{-2\pi i/N}$; $n = N$; $L = x_1\,e^{-2\pi i(N-1)/N}$. Substitution of the above values into Equation (A-6) yields zero.

<u>Column (N-1) when j = 0</u>. This is again the progression with: $a = x_{N-1}$; $r = e^{-2\pi i(N-1)/N}$; $n = N$; $L = x_{N-1}\,e^{-2\pi i(N-1)^2/N}$. Substitution of the above values into Equation (A-6) yields zero.

<u>Column 1 when j = 1</u>. Note that all exponents add to zero, yielding Nx_1.

<u>Column (N-1) when j = 1</u>. This is again the progression with: $a = x_{N-1}$; $r = e^{-2\pi i(N-2)/N}$; $n = N$; $L = x_{N-1}\,e^{-2\pi i(N^2-N+2)/N}$. Substitution of the above values into Equation (A-6) yields zero.

<u>Finally for Column N-1 when j = N-1</u>. The exponents all become zero, yielding Nx_{N-1}.

Thus for all values of j it can be similarly shown that Equations (A-2) thru (A-5) are identities, and the transform, inverse transform relationship of Equations (30) and (31) is proved.

$$\begin{array}{llll}
Nx_j = x_0 & + x_1 & + x_2 + \ldots\ldots & + \ldots + x_{N-1} \\
\quad + x_0\,e^{2\pi ijn/N} & + x_1\,e^{-2\pi i/N+2\pi ij/N} & + x_2\,e^{-2\pi i2/N+2\pi ij/N} + \ldots\ldots & + \ldots + x_{N-1}\,e^{-2\pi i(N-1)/N+2\pi ij/N} \\
\quad + x_0\,e^{2\pi ij2/N} & + x_1\,e^{-2\pi i2/N+2\pi ij2/N} & + x_2\,e^{-2\pi i4/N+2\pi ij2/N} + \ldots\ldots & + \ldots + x_{N-1}\,e^{-2\pi i(N-1)2/N+2\pi ij2/N} \\
\quad + \ldots\ldots & + \ldots\ldots & + \ldots\ldots & + \ldots + \ldots\ldots \\
\quad \ldots\ldots & \ldots\ldots & \ldots\ldots & \ldots\ldots \\
\quad + x_0\,e^{2\pi ij(N-1)/N} & + x_1\,e^{-2\pi i(N-1)/N+2\pi ij(N-1)/N} & + x_2\,e^{-2\pi i2(N-1)/N+2\pi ij(N-1)/N} & \ldots + x_{N-1}\,e^{-2\pi i(N-1)^2/N+2\pi ij(N-1)/N}
\end{array} \qquad \text{(A-5)}$$

Mr. Zell (Picatinny Arsenal): This is probably very trivial but for a predetermined sampling rate should we not pass all data through a low pass filter as a matter of principle?

Mr. Gaberson: I believe that is a good idea but I am unsure of the effect of the filter on the phases of the transient near the cutoff frequency of the filter.

Mr. Galef (TRW Systems): I can add a little bit to what you just said. Since we ordinarily know what kind of filter we have, it is easy enough to take the transform of that filter and multiply it by the transform obtained using the filter and thereby correct for it. I have another question. Could you clarify please, did you indicate that your program yields Fourier spectrum results and frequencies in addition to the reciprocal of time interval?

Mr. Gaberson: Yes, any frequency desired at all. Every frequency.

Mr. Galef: Is this an interpolation or is it an actual result?

Mr. Gaberson: It is an exact result. The derivation is in the paper.

Mr. Naylor (Defense Research Establishment, Suffield): I am interested in reading your full paper but I had some indications this summer that the integration time is related to the resonant frequencies of the object. If one takes an integrated time which includes an exact number of cycles of the object which is vibrating, the Fourier transform apparently looks very different from one where there is an extra part of a cycle included. It starts to look more like a continuous frequency spectrum. If these transforms are going to be as cheap as you indicate, I would ask people who are doing these to vary the length of time of integration to include the exact number of cycles and they may be surprised by their results.

Mr. Gaberson: Yes, you are referring to the amount of the transient that one chooses to analyze, where one should cut it off since one cannot keep integrating forever. There is some question as to how much of the transient is significant, how much of it one should digitize and analyze.

Mr. Cronin (University of Missouri, Rolla): Regarding this problem of aliasing, generally speaking a transient is defined as a function which stops in time. That is, it goes to zero and from thenceforward it remains zero. Fourier representations for these functions will have frequency components out to infinity so that when one is dealing with a signal wherein the Fourier representation goes to zero, such as at the folding frequency, these functions are characterized by a time history which goes out to infinity. So in handling any real signals one will always have this aliasing problem. Perhaps it could be helped or alleviated somewhat by choosing a cutoff for analysis of the signal by including sufficient null time, that is, terminate the signal and then add into the data sufficient length of null time or zeros representing the data to reduce the contribution of aliasing and the associated error and that would help as much as using a filter.

Mr. Caberson: We were operating on band limited functions from Popoulos' book mainly, and he does quite readily talk about band limited functions that are transients. Certainly, in any real system would you believe any frequency content above 20,000 Hz? So you would have to say that the function is band limited at 20,000 Hz. Therefore, if I sample at 40, I am in there.

Mr. Cronin: I am talking about theory as opposed to practice.

THE COMPUTER DETERMINATION OF MECHANICAL IMPEDANCE FOR SMALL ARMS FROM THE RESPONSE TO RECOIL

L. B. Gardner, R. K. Young, and D. E. Frericks
U. S. Army Weapons Command
Rock Island, Illinois

A digital technique was developed for determining the mechanical impedance at a weapon-mount interface from data obtained during an actual firing on the test mount. This technique was applied to data obtained from a test firing of the XM207 automatic weapon, tripod mounted on sand bags. From the mechanical impedance, the spring constant, seen at the interface, was found to be 380 lb/in. and the damping coefficient at this interface was found to be 1.15 lb/in. In addition power spectral densities of the force and velocity at the interface were obtained. The use of this information for mount simulation studies is described.

INTRODUCTION

Personnel in the Science and Technology Laboratory of the Army Weapons Command became involved in the measurement of mechanical impedance as a consequence of investigations to determine the validity of weapon-mount simulation techniques.

To define valid simulations, two criteria are proposed. The first criterion is the requirement of very nearly the same dynamics of the weapon-mount interface on both the test and field mounts. This criterion is met by a comparison of the frequency spectrums of the displacement, velocity, and acceleration of the interface.

The second criterion for determination of valid simulation is the requirement of the same mechanical impedance at the weapon-mount interface on both mounts. Only the point impedance is considered (rather than the transfer impedance tensor) since the center of interest is the simulation of the weapon-mount interface that can be characterized by a point. The application of these two criteria are necessary in order that the two mount systems, as seen from the weapon-mount interface, be equivalent.

METHODS OF MEASURING MECHANICAL IMPEDANCE

The method generally used for the measurement of mechanical impedance, hereafter referred to as the "standard" method, yields a continuous function of frequency since all frequencies in a given range are excited by forcing functions with the same amplitude.[1] The second method, discussed in this paper referred to as the "impulse" method, yields the value of the mechanical impedance at particular values of the frequency within a given band of frequencies.

The "standard" method for the determination of the mechanical impedance of a system is to apply a sinusoidal forcing function of known frequency and magnitude to the system and to measure the acceleration of the system at the point of application of the force. The velocity is obtained by the integration of the acceleration. The ratio of the force to the velocity is defined as the mechanical impedance at the frequency of the forcing function. To obtain the frequency distribution of the mechanical impedance, the magnitude of the forcing function is held constant while the frequency is swept over the range of interest.

A simulation can be termed successful if the weapon system operates in the same manner as it does on a field mount. In an actual firing all frequencies within the range of frequencies observed in the firing test are not excited thus the requirement that the mechanical impedance of the test mount must be the same as that of the field mount at all frequencies is too stringent. Consequently, the "standard" method of mechanical impedance measurement yields more information than is needed for a simulation test. In addition, each attachment point of the weapon would have to be tested individually when the "standard" method is utilized.

The "impulse" method makes use of

measurements taken during an actual firing from the test mount. This method provides values of the mechanical impedance only at the frequencies excited by the firing of the weapon thus providing a minimal test of the simulation. In addition, not only the mechanical impedance of the test mount may be determined from such a test firing but also the dynamics of the weapon-mount interface may also be determined. Consequently, a double check of the validity of the simulation provided by the test mount is made available from one experiment. The greatest weakness in the "impulse" method of mechanical impedance measurements lies in the reproducibility of the measurements. Since the test is dependent upon the ammunition used in the test firing, inconsistencies may appear due to the variation in the ammunition from round to round. To minimize this effect one lot of ammunition is used for an entire series of tests.

The standard means of mechanical impedance measurement has been adequately described elsewhere,[1] therefore, the remainder of this paper is concerned with the "impulse" method.

ANALYSIS OF MECHANICAL IMPEDANCE DATA

In the "impulse" method of mechanical impedance measurements, the test system can be instrumented such that all parameters useful to the analysis of the system are measured simultaneously. The parameters necessary for the determination of the point impedance are the force and the velocity obtained from parameters measured at the point of interest. In addition, the displacement and acceleration of the point are needed to yield the total dynamics of that point. Each point of attachment should be instrumented in the same way such that the impedances of all points of attachment can be simultaneously measured during the same firing test.

In the analysis procedure used in the simulation studies the output signals of the transducers used to instrument the test mount are recorded on analog magnetic tape and played back at a later time for computer analysis.

Computer analysis of the test data provides a wide variety of techniques for the treatment of data that could be used to furnish more information than just the mechanical impedance. The number of different parameters measured during one test is only dependent upon the recording facilities available for the test, since the signals are recorded and can be analyzed one channel at a time during playback. In addition, the number of data samples taken on a given test is completely arbitrary since a selection of digitizing rates and time base expansions of the recorded data through a selection of playback speeds are available.

The parameters generally measured in a firing test are the force, the acceleration, and the displacement at a point. These parameters are recorded as a function of time and are at least piecewise continuous functions of time. Therefore, each of these parameters can be represented by a Fourier series whose coefficients are determined from the recorded data. Therefore, the data can be represented as an analytical function. Since such an analytic function can be obtained for both the displacement and the acceleration, the velocity can either be obtained by differentiating the displacement function or by integrating the acceleration function. The force as a function of time can then be represented as

$$f(t) = \frac{a_0}{2} + \sum_n \left(a_n \cos \frac{n\pi t}{p} + b_n \sin \frac{n\pi t}{p}\right)$$

or equivalently as

$$f(t) = \sum_n C_n e^{\frac{in\pi t}{p}}$$

where $C_n = \frac{a_n - ib_n}{2}$

and $C_0 = \frac{a_0}{2}$

Now the force can be considered a superposition of forces, $f_n(t)$, with only one frequency associated with each component, that is

$$f(t) = \sum_n f_n(t)$$

where $f_n(t) = a_n \cos \frac{n\pi t}{p} + b_n \sin \frac{n\pi t}{p}$

or $f_n(t) = C_n e^{\frac{in\pi t}{p}}$

where n is the number of the overtone and p is the period of the function. Similarly the velocity can be represented by

$$v(t) = \sum_n v_n(t)$$

where $v_n(t) = A_n \cos \frac{n\pi t}{p} + B_n \sin \frac{n\pi t}{p}$

or $v_n(t) = D_n e^{\frac{in\pi t}{p}}$

$$D_n = \frac{A_n - iB_n}{2}$$

The number of terms used in the series to represent the data is determined by considering the decrease in the sum of the square of the deviations of the Fourier

series from the data points as compared to the decrease in the difference between the number of data points and the number of overtones used as each succeeding term of the series is added, or in other words requiring that the quantity M, be a minimum,

$$M = \frac{\sum_i \delta_i^2}{N-n}$$

where δ_i is the deviation of the i th data point, N is the total number of data points, and n is the number of terms used in the series.

After the Fourier coefficients have been determined from the data points, the power spectral density P_n can be obtained since

$$P_n = 2p\,(a_n^2 + b_n^2)$$

where p is the period of the function and a_n and b_n are the Fourier coefficients for the function being considered. The power spectral density provides a ready means of comparing the dynamics of the weapon-mount interface.

Also from the Fourier coefficient of the force and velocity functions the complex mechanical impedance can be obtained. The complex mechanical impedance, MZ, is defined as the ratio of the root means square force and the root mean square velocity at a particular frequency. Therefore,

$$MZ_n = \frac{\sqrt{\langle f_n^2 \rangle}}{\sqrt{\langle v_n^2 \rangle}}$$

or $$MZ_n = \frac{C_n}{D_n} = \frac{a_n - ib_n}{A_n - iB_n}$$

Therefore $$MZ_n = \frac{A_n a_n + B_n b_n + i(a_n B_n - A_n b_n)}{A_n^2 + B_n^2}$$

but $$MZ_n = |\,MZ_n\,|\, e^{i\phi_n}$$

where ϕ is the phase difference between f_n and v_n.

Therefore the magnitude and phase angle are

$$\phi_n = \mathrm{Tan}^{-1}\left[\frac{\mathrm{Im}(MZ_n)}{\mathrm{Re}(MZ_n)}\right] = \mathrm{Tan}^{-1}\left[\frac{a_n B_n - A_n b_n}{a_n A_n + b_n B_n}\right] \quad (1)$$

and $$|\,MZ_n\,| = [(MZ_n)(MZ_n)^*]^{1/2} = \left[\frac{a_n^2 + b_n^2}{A_n^2 + B_n^2}\right]^{1/2} \quad (2)$$

The complex mechanical impedance can therefore be expressed in terms of the coefficients of the Fourier series representation of the force and velocity measured at one point. In addition, during the same analysis procedure the power spectral densities of these functions are acquired for use in comparisons of the dynamics of the weapon-mount interface on both the test mount and the field mount.

This digital analysis technique has been applied to data obtained from a test firing of the XM207 automatic weapon with the tripod mount resting on sandbags. The force and displacement were measured at the interface between one of the tripod legs and the sandbag. The velocity of the interface was obtained by a numeric differentiation of the Fourier series fitted to the displacement-time curve. Fourier series were also fitted to the force-time and the velocity-time curves. The power spectral density (PSD) of the force-time curve was computed from the spectral coefficients of the Fourier series fitted to this curve and is shown in Figure 1.

The power spectral density (PSD) of the velocity-time curve was computed in a similar manner and is shown in Figure 2.

From the spectral coefficients of the force-time curve and the velocity-time curve, the point mechanical impedance was calculated from Equation 2 and Equation 1. The magnitude of the mechanical impedance is shown in Figure 3 and the phase angle of the mechanical impedance is shown in Figure 4.

RESULTS AND CONCLUSIONS

The information made available in Figures 1 through 4 provides a means of comparing a weapon-mount interface measurement for a field mount with a simulation mount. The data taken for this study also provides information for the selection of spring constants and damping coefficients to be used in the simulation mount.

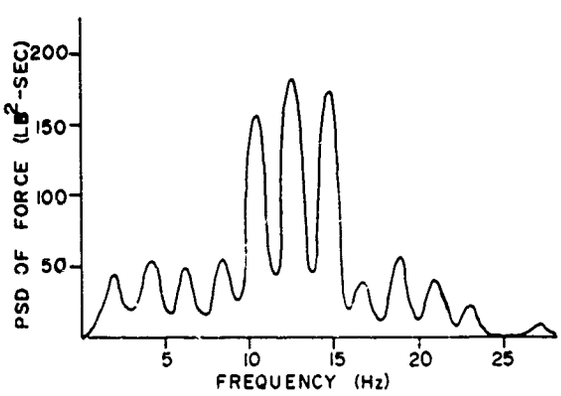

Fig. 1 - Graph of the Power Spectral Density (PSD) of the Force at the XM207 Weapon-Mount Interface as a Function of the Frequency

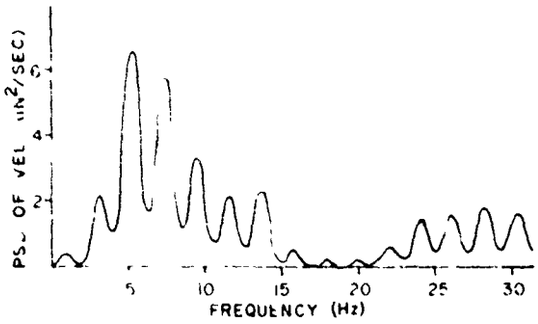

Fig. 2 - Graph of the Power Spectral Density of the Velocity of the XM207 Weapon-Mount Interface as a Function of the Frequency

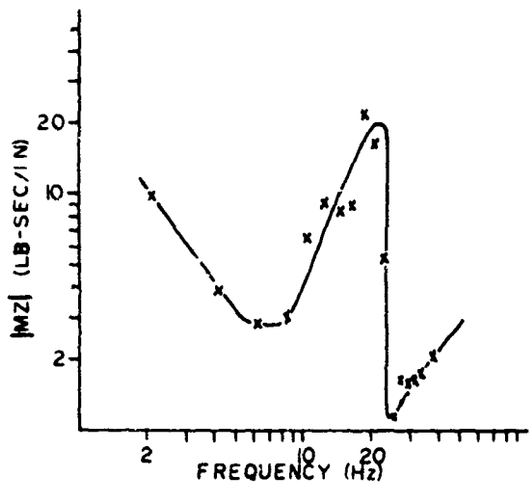

Fig. 3 - Graph of the Magnitude of the Mechanical Impedance as a Function of the Frequency at the XM207 Weapon-Mount Interface

The power spectral densities shown in Figures 1 and 2 show the frequencies at which the power is transmitted through the interface. If a simulation is successful, the power should be transmitted through the interface at these same frequencies.

In addition to providing a basis of comparison of the field mount test to future simulation tests, Figures 3 and 4 provide information which can be used as a guide in simulation. Consideration of Figures 3 and 4 shows that the antiresonance frequency is at 21 Hz and the resonant frequency is at 25 Hz; at the resonance frequency the spring constant of the weapon-sand interface for the XM207 is calculated and found to be 380 lb/in. Previous measurements made at this

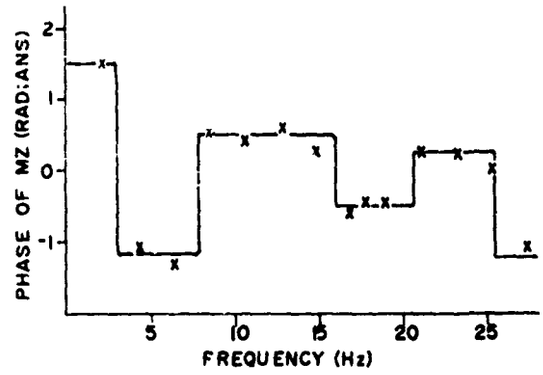

Fig. 4 - Graph of the Phase Angle of the Mechanical Impedance as a Function of Frequency at the XM207 Weapon-Mount Interface

interface have shown the spring constant to be between 300 and 400 pounds per inch. From Figure 3 the damping coefficient is seen to be 1.15 lb/in./sec which is also consistent with earlier tests of this same interface. By using these values of the spring constant and the damping coefficient, a first attempt at a simulation of this interface can be made.

The digital analysis technique thus makes available to the technical staff of the Science and Technology Laboratory not only a means of evaluating a simulated mount through comparisons of PSD and mechanical impedance curves but also a means of obtaining initial values of the spring constant and damping coefficient for the simulated mount.

1. R.E. Kerfoot, "Solutions for Mechanical Impedance Measurement Problems," Spectral Dynamics Corp. Technical Publication No. M-1, 9-66.

DISCUSSION

Mr. Ashley (University of Birmingham): How did you actually measure the force at the stand-tripod interface in this particular experiment?

Mr. Young: We mounted a strain gauge along one of the tripod legs to give the force along that leg, then we used the component of that force in the direction in which we measured the displacement. This, of course, is an approximation. It is not exactly the force at the foot itself but it is as near as we could come.

Mr. Ashley: Did you bother to use any mass cancellation technique or did you think it was so small as not to be necessary?

Mr. Young: The mass of the strain gauge compared to the mass of the weapons system is so small as to be virtually negligible. One knows the weight of a strain gauge, and weapons system weighed about 19 pounds so we did not attempt any mass cancellation. Perhaps when we get to our simulation and we find we cannot simulate it we might be tempted to go back and try it again.

Mr. Ashley: While I am pursuing this one, I was thinking actually of the small mass of the tripod leg itself after the strain gauge and before it actually digs into the sand.

Mr. Young: Are you referring to the foot itself?

Mr. Ashley: Yes.

Mr. Young: The foot weighs excess of one pound. They are fairly massive, they have a part that actually digs down into the sand. The foot sits on top of the sand and then it has another part that digs down into the sand. An interesting point about this particular weapons system -- it is one of the machine guns of the Stoner family -- is that they found that it works well in sand; however, they wanted to know how it works in Viet Nam mud. So we got in four bags of Viet Nam mud to try this weapon in and we found very nearly the same behavior as for sand.

SHOCK PULSE SHAPING USING DROP TEST TECHNIQUES*

R. E. Keeffe and E. A. Bathke
Kaman Sciences Corporation
Colorado Springs, Colorado

An analytic technique is described for designing a drop test experiment in which transient acceleration time histories are simulated. Verification of the developed methodology is qualitatively demonstrated by an experimental test program.

INTRODUCTION

The basic concept of using laboratory shock testing techniques for qualifying components which in service are subject to transient vibratory environments is, in itself, a well developed technology. However, the majority of the past work done in this area has concentrated on the development of test techniques for reproducing either basic acceleration pulse shapes, as for example a half sine or terminal sawtooth, or equivalent pulses with the objective to envelop a desired shock response spectrum. Various forms of shock testing machines have been developed to perform these types of tests [1] and, in general, perform adequately the tasks for which they were designed.

In the technique under discussion here, we are concerned with the somewhat more specific task of developing a test method for reproducing time histories of acceleration pulses. Recently a considerable amount of effort has been expended in this general area, although it appears to have been performed primarily using electromagnetic shakers. For example, Favour, et al [2] describe a technique in which desired transient waveforms are generated by pre-programming an electromagnetic shaker with a driving signal computed via Fourier transform techniques and knowledge of the shaker transfer function. Excellent results were obtained in a prototype setup in which a transient acceleration-time history (with peak accelerations in the range of 40 g) were accurately reproduced. Similarly Moser and Garner [3] discuss a method of frequency compensation in an electromagnetic shaker system which will allow generation of shaker pulse response which is nearly identical to the input pulse into the shaker amplifier. Numerous other investigators have used electromagnetic shakers for reproducing shock response spectra rather than specific time history waveforms (see, for example, References [4] and [5]).

There are, however, practical limitations on the magnitudes of acceleration pulses which can be reproduced using shakers. Typically, current large shaker systems can be used to generate shock pulses in test hardware (approximate weight 50 lb.) having peak magnitudes on the order of 100 g's. In some instances, a need exists for developing pulse shaping techniques wherein shock pulse histories having peak accelerations on the order of several hundred g's can be simulated.

The test technique under consideration here was developed to fill this need. It employs a standard drop test apparatus used in conjunction with a receiver assembly, consisting of alternating layers of linear springs and

*This work was accomplished under Army Contract DAAH 01-69-C-1809 in cooperation with U. S. Army Missile Command and the Defense Atomic Support Agency.

rigid masses, designed so as to shape a desired acceleration pulse experienced by the drop table (and associated test hardware). In the following discussion a review of the analytic modeling and system design techniques is first presented. Next, a discussion of a test program designed to verify the method is given, followed by comparisons between theory and test.

DISCUSSION

Basic Theory

Consider the basic drop test experiment illustrated in Figure 1.

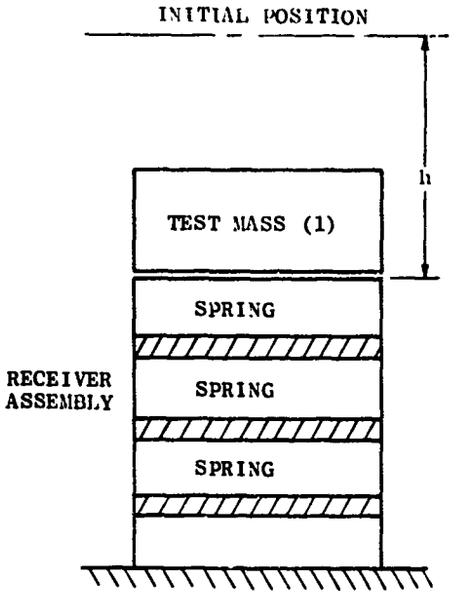

FIGURE 1

BASIC DROP TEST

The test mass (1), initially at position h, impacts the receiver assembly of springs and masses either at the free-fall or accelerated-fall velocity $\dot{X}_1$. If the springs are considered massless and the masses assumed to be infinitely stiff, the response of the test mass can be evaluated using a simple one-dimensional lumped mass model. For a N degree of freedom system, the lumped-mass model (excluding damping) can be diagrammed as in Figure 2 below.

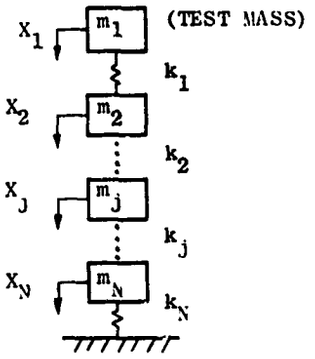

FIGURE 2

LUMPED MASS MODEL

The differential equations of motion for this system can be expressed in the following matrix form:

$$\begin{bmatrix} m_1 & & & \\ & m_2 & & \\ & & \ddots & \\ & & & m_N \end{bmatrix} \begin{Bmatrix} \ddot{X}_1 \\ \ddot{X}_2 \\ \vdots \\ \ddot{X}_N \end{Bmatrix} +$$

$$\begin{bmatrix} k_1 & -k_1 & & & \\ -k_1 & (k_1+k_2) & -k_2 & & \\ & -k_2 & \ddots & \ddots & \\ & & & (k_{N-1}+k_N) & -k_N \\ & & & -k_N & k_N \end{bmatrix} \begin{Bmatrix} X_1 \\ X_2 \\ \vdots \\ X_N \end{Bmatrix} = 0 \qquad (1)$$

with the initial condition on test mass $\dot{X}_1(0) = \dot{X}_1$. Define the normal mode frequencies, Ω_i, and the matrix of the normal mode vectors as $\left[\phi^{(i)}\right]$. Where this matrix defines the coordinate transformation from generalized to normal mode coordinates:

$$\{X\} = \left[\phi^{(i)}\right]\{n\} \qquad (2)$$

The initial conditions on normal mode velocities are expressed in the following vector form:

$$\begin{Bmatrix} \dot{n}_1 \\ \dot{n}_2 \\ \vdots \\ \dot{n}_n \end{Bmatrix} = \left[\phi^{(i)}\right]^{-1} \begin{Bmatrix} \dot{X}_1 \\ 0 \\ 0 \\ \vdots \\ 0 \end{Bmatrix} \qquad (3)$$

and the normal mode response of the jth mass is found to be

$$n_j(t) = \frac{\dot{n}_j}{\Omega_j} \sin \Omega_j t \ . \qquad (4)$$

In generalized coordinates, the displacement response of the test mass (#1) is given as

$$X_1(t) = \sum_{i=1}^{N} \frac{\varphi_1^{(i)} \dot{n}_i}{\Omega_i} \sin \Omega_i t, \qquad (5)$$

with the acceleration response given by

$$\ddot{X}_1(t) = \sum_{i=1}^{N} -\Omega_i \varphi_1^{(i)} \dot{n}_i \sin \Omega_i t \ . \qquad (6)$$

Equation (6) can be rewritten as follows:

$$\ddot{X}_1(t) = \sum_{i=1}^{N} A_i \sin \Omega_i t \qquad (7)$$

The form of Equation (7) is representative of an odd Fourier series expansion of the function $\ddot{X}_1(t)$, with the restriction that all values of A_i are of like signs. The application of a desired acceleration-time history is obvious; that is, the given acceleration-time history is approximated by an odd Fourier series expansion consisting of N harmonic contributions. Then the design problem of determining the values of m_i and k_i required to satisfy the system constraints on A_i and Ω_i remains to be solved.

In the following section the developed procedures for solving these design problems for N=2, and N=4 are presented. Similar procedures have been developed for N=3 and N=5 but are not presented here. It is important to note that, while in theory it is possible to extend this method to arbitrarily large values of N, there always are practical problems concerned with designing the corresponding test setup, which effectively imposes an upper bound on N. For the study discussed here, N=5 seemed to be a reasonable upper limit.

Analytic Design Procedures

The following discussion deals with the analytic formulations and solutions necessary to design component/receiver systems, for the simulation of acceleration-time shock pulses.

The following basic assumptions are pertinent to solution development.

1. The receiver assembly consisting of alternating layers of springs and masses can be analytically modeled as a lumped parameter system. This essentially implies that the springs are massless and the masses are perfectly rigid.

2. The springs used in the receiver assembly are linear and elastic.

3. The effects of damping are not included in the analytic system response.

The differential equations of motion and the solutions of these equations for the acceleration response of the test mass for a given initial condition on test mass velocity are presented for 2 and 4 degree of freedom systems. In all cases the test mass is identified as mass #1 while the receiver assembly is comprised of the remaining masses and springs in the system. In addition for all cases the initial conditions on velocity of the test mass is designated as $\dot{X}_1$(in/sec), with an initial displacement X_1(in) equal to zero. Spring stiffnesses (k) are in (lb/in) units while inclusion masses (m) are expressed in (lb sec^2/in).

The equations of motion for the 2 degree of freedom system are expressed as:

$$\begin{aligned} \ddot{X}_1 + \omega_1^2 X_1 - \omega_1^2 X_2 &= 0 \\ \ddot{X}_2 + \omega_2^2 X_2 - \omega_1^2 \frac{m_1}{m_2} X_1 &= 0 \end{aligned} \qquad (8)$$

where

$$\begin{aligned} \omega_1^2 &= k_1/m_1 \\ \omega_2^2 &= (k_1+k_2)/m_2 \end{aligned} \qquad (9)$$

Subject to the stated initial conditions the acceleration response of the test mass (#1) becomes:

$$\ddot{X}_1(t) = \sum_{\alpha=1}^{2} A_\alpha \sin \Omega_\alpha t \qquad (10a)$$

$$\text{where: } A_1 = -\frac{\dot{X}_1 \Omega_1 \left(\omega_2^2 - \Omega_1^2\right)}{\left(\Omega_2^2 - \Omega_1^2\right)} \qquad (10b)$$

$$\frac{A_2}{A_1} = -\frac{\Omega_2 \left(\omega_2^2 - \Omega_2^2\right)}{\Omega_1 \left(\omega_2^2 - \Omega_1^2\right)} \qquad (10c)$$

$$\sum_{\alpha=1}^{2} \Omega_\alpha^2 = \sum_{\alpha=1}^{2} \omega_\alpha^2 \tag{10d}$$

$$\prod_{\alpha=1}^{2} \Omega_\alpha^2 = \left[\prod_{\alpha=1}^{2} \omega_\alpha^2\right] - \omega_1^4 \frac{m_1}{m_2} \tag{10e}$$

Given the amplitude ratios and frequencies of response, the problem of determining the system masses and stiffness constants requires finding the solution to a set of nonlinear equations. The 2D system of equations has an algebraic solution which is readily apparent. The following substitution of variables is performed:

$$\begin{aligned} y_1 &= \omega_1^2 = \frac{k_1}{m_1} \\ y_2 &= \omega_2^2 = \frac{k_1+k_2}{m_2} \\ y_3 &= \omega_1^4 \frac{m_1}{m_2} = \frac{k_1^2}{m_1 m_2} \end{aligned} \tag{11}$$

The design system equations are then:

$$\begin{aligned} y_1+y_2 &= \Omega_1^2 + \Omega_2^2 \\ y_1 y_2 - y_3 &= \Omega_1^2 \Omega_2^2 \\ \Omega_2(y_2-\Omega_2^2) &+ \frac{A_2}{A_1}\Omega_1(y_2-\Omega_1^2) = 0 \end{aligned} \tag{12}$$

The algebraic solution is simple and direct:

$$y_2 = \left(\Omega_1^3 \frac{A_2}{A_1} + \Omega_2^3\right) \Big/ \left(\Omega_1 \frac{A_2}{A_1} + \Omega_2\right) \tag{13}$$

$$y_1 = \Omega_1^2 + \Omega_2^2 - y_2$$

$$y_3 = y_1 y_2 - \Omega_1^2 \Omega_2^2$$

$$k_1 = y_1 m_1$$

$$m_2 = y_1^2 m_1 / y_3$$

$$k_2 = y_2 m_2 - k_1$$

For any system with more than two masses, the complexity of the nonlinear equation system increases markedly. The normal approach of computer solution using numerical techniques could not be applied since the behavior of the equations was such that convergence was not attainable within a reasonable amount of computer time.

Fortunately, these nonlinear systems of equations possessed advantageous relationships among the parameters. Through a judicious choice of unknowns to be determined, inherent linear sub-systems were generated for which direct algebraic solutions were obtained. This procedure is illustrated with the 4D system. The equations of motion for the 4 degree of freedom system are:

$$\begin{aligned} \ddot{X}_1 + \omega_1^2 X_1 - \omega_1^2 X_2 &= 0 \\ \ddot{X}_2 + \omega_2^2 X_2 - \omega_1^2 \frac{m_1}{m_2} X_1 - \omega_5^2 X_3 &= 0 \\ \ddot{X}_3 + \omega_3^2 X_3 - \omega_5^2 \frac{m_2}{m_3} X_2 - \omega_6^2 X_4 &= 0 \\ \ddot{X}_4 + \omega_4^2 X_4 - \omega_6^2 \frac{m_3}{m_4} X_3 &= 0 \end{aligned} \tag{14}$$

where the following definitions are employed:

$$\begin{aligned} \omega_1^2 &= k_1/m_1 & \omega_4^2 &= (k_3+k_4)/m_4 \\ \omega_2^2 &= (k_1+k_2)/m_2 & \omega_5^2 &= k_2/m_2 \\ \omega_3^2 &= (k_2+k_3)/m_3 & \omega_6^2 &= k_3/m_3 \end{aligned} \tag{15}$$

Subject to the stated initial conditions, the acceleration response of the test mass (#1) becomes:

$$\ddot{X}_1(t) = \sum_{\alpha=1}^{4} A_\alpha \sin \Omega_\alpha t \tag{16a}$$

where:

$$A_1 = \frac{\dot{X}_1 \Omega_1 \left[\sum_{j=1}^{4} (-1)^{j-1} a_{4-j}\, \Omega_1^{2j-2}\right]}{\left[\pi\left(\Omega_j^2 - \Omega_1^2\right)\right]_{j=2,3,4}} \tag{16b}$$

$$\frac{A_2}{A_1} = -\frac{\Omega_2\left[\sum_{j=1}^{4}(-1)^{j-1}\ a_{4-j}\ \Omega_2^{2j-2}\right]\left[\pi\left(\Omega_j^2-\Omega_1^2\right)\right]_{j=3,4}}{\Omega_1\left[\sum_{j=1}^{4}(-1)^{j-1}\ a_{4-j}\ \Omega_1^{2j-2}\right]\left[\pi\left(\Omega_j^2-\Omega_2^2\right)\right]_{j=3,4}} \tag{16c}$$

$$\frac{A_3}{A_1} = -\frac{\Omega_3\left[\sum_{j=1}^{4}(-1)^{j-1}\ a_{4-j}\ \Omega_3^{2j-2}\right]\left[\pi\left(\Omega_j^2-\Omega_1^2\right)\right]_{j=2,4}}{\Omega_1\left[\sum_{j=1}^{4}(-1)^{j-1}\ a_{4-j}\ \Omega_1^{2j-2}\right]\left[\pi\left(\Omega_j^2-\Omega_3^2\right)\right]_{j=2,4}} \tag{16d}$$

$$\frac{A_4}{A_1} = -\frac{\Omega_4\left[\sum_{j=1}^{4}(-1)^{j-1}\ a_{4-j}\ \Omega_4^{2j-2}\right]\left[\pi\left(\Omega_j^2-\Omega_1^2\right)\right]_{j=2,3}}{\Omega_1\left[\sum_{j=1}^{4}(-1)^{j-1}\ a_{4-j}\ \Omega_1^{2j-2}\right]\left[\pi\left(\Omega_j^2-\Omega_4^2\right)\right]_{j=2,3}} \tag{16e}$$

$$\sum_{\alpha=1}^{4}\Omega_\alpha^2 = \sum_{\alpha=1}^{4}\omega_\alpha^2 \tag{16f}$$

$$\sum_{\beta=2}^{4}\sum_{\alpha=1}^{3}\Omega_\alpha^2\Omega_\beta^2 = \left[\sum_{\beta=2}^{4}\sum_{\alpha=1}^{3}\omega_\alpha^2\omega_\beta^2\right] - \omega_1^4\frac{m_1}{m_2} - \omega_5^4\frac{m_2}{m_3} - \omega_6^4\frac{m_3}{m_4}\ ; \quad \alpha < \beta \tag{16g}$$

$$\sum_{\gamma=3}^{4}\sum_{\beta=2}^{3}\sum_{\alpha=1}^{2}\Omega_\alpha^2\Omega_\beta^2\Omega_\gamma^2 = \left[\sum_{\gamma=3}^{4}\sum_{\beta=2}^{3}\sum_{\alpha=1}^{2}\omega_\alpha^2\omega_\beta^2\omega_\gamma^2\right] - \omega_6^4\frac{m_3}{m_4}\left(\omega_1^2+\omega_2^2\right) - \omega_5^4\frac{m_2}{m_3}\left(\omega_1^2+\omega_4^2\right) - \omega_1^4\frac{m_1}{m_2}\left(\omega_3^2+\omega_4^2\right);$$

$$\alpha < \beta < \gamma \tag{16h}$$

$$\prod_{\alpha=1}^{4}\Omega_\alpha^2 = \left[\prod_{\alpha=1}^{4}\omega_\alpha^2\right] - \omega_1^2\omega_2^2\omega_6^4\frac{m_3}{m_4} - \omega_1^2\omega_4^2\omega_5^4\frac{m_2}{m_3} - \omega_3^2\omega_4^2\omega_1^4\frac{m_1}{m_2} + \omega_1^4\omega_6^4\frac{m_1 m_3}{m_2 m_4} \tag{16i}$$

where the following definitions were used:

$$a_0 = 1$$

$$a_1 = \sum_{\alpha=2}^{4} \omega_\alpha^2$$

$$a_2 = \left[\sum_{\beta=3}^{4} \sum_{\alpha=2}^{3} \omega_\alpha^2 \omega_\beta^2\right] - \omega_6^4 \frac{m_3}{m_4} - \omega_5^4 \frac{m_2}{m_3} ; \quad \alpha < \beta \tag{17}$$

$$a_3 = \left[\prod_{\alpha=2}^{4} \omega_\alpha^2\right] - \omega_2^2 \omega_6^4 \frac{m_3}{m_4} - \omega_4^2 \omega_5^4 \frac{m_2}{m_5}$$

For the higher order systems a standard mathematical definition can be employed in simplifying expression of the systems of equations. A polynomial $P(x_1,x_2,\ldots,x_n)$ which is unchanged by any permutation of the indeterminates $x_1,x_2,\ldots,x_n$ is called a symmetric function of the variables $x_1,x_2,\ldots,x_n$. Introducing a new indeterminate z, we put

$$f(z) = (z-x_1)(z-x_2)\cdots(z-x_n) \tag{18}$$

$$= z^n - \sigma_1 z^{n-1} + \sigma_2 z^{n-2} - \ldots + (-1)^n \sigma_n .$$

The coefficients of the powers of z in this polynomial are

$$\sigma_1 = x_1 + x_2 + \cdots + x_n,$$

$$\sigma_2 = x_1x_2 + x_1x_3 + \cdots + x_2x_3 + \cdots + x_{n-1}x_n,$$

$$\sigma_3 = x_1x_2x_3 + x_1x_2x_4 + \cdots + x_{n-2}x_{n-1}x_n,$$

$$\cdots\cdots\cdots\cdots\cdots\cdots$$

$$\sigma_n = x_1x_2\ldots x_n. \tag{19}$$

$\sigma_1,\sigma_2,\ldots,\sigma_n$ are the elementary symmetric functions of $x_1,x_2,\ldots,x_n$. In the following work, the notation $\sigma_j(x_n)$ will be used to denote the elementary symmetric function σ_j of the variables $x_1,x_2,\ldots,x_n$.

For the four dimensional system, the following substitutions are employed:

$$y_1 = \omega_1^2 = \frac{k_1}{m_1}$$

$$y_2 = \omega_2^2 = \frac{k_1+k_2}{m_2}$$

$$y_3 = \omega_3^2 = \frac{k_2+k_3}{m_3}$$

$$y_4 = \omega_4^2 = \frac{k_3+k_4}{m_4}$$

$$y_5 = \omega_1^4 \frac{m_1}{m_2} = \frac{k_1^2}{m_1m_2} \tag{20}$$

$$y_6 = \omega_5^4 \frac{m_2}{m_3} = \frac{k_2^2}{m_2m_3}$$

$$y_7 = \omega_6^4 \frac{m_3}{m_4} = \frac{k_3^2}{m_3m_4}$$

The design system Equations (16b) to (16i) are then

$$y_1 + a_1 = \sigma_1(\Omega_4^2)$$

$$y_1a_1 + a_2 - y_5 = \sigma_2(\Omega_4^2)$$

$$y_1a_2 + a_3 - y_5(y_3+y_4) = \sigma_3(\Omega_4^2)$$

$$y_1a_3 + y_5(y_7-y_3y_4) = \sigma_4(\Omega_4^2) \tag{21}$$

$$y_2 + y_3 + y_4 = a_1$$

$$y_2y_3 + y_2y_4 + y_3y_4 - y_6 - y_7 = a_2$$

$$y_2y_3y_4 - y_4y_6 - y_2y_7 = a_3$$

The last three equations of (21) are the defining relationships for a_1, a_2, a_3. Equations (16c) to (16e) constitute a linear system in these three variables. Having solved this linear system, one can then obtain the solution to the four dimensional system from Equations (21) by the following steps:

$$y_1 = \sigma_1 - a$$

$$y_5 = y_1a_1 + a_2 - \sigma_2$$

$$(y_3+y_4) = \frac{1}{y_5}\left[y_1a_2 + a_3 - \sigma_3\right]$$

$$y_2 = a_1 - (y_3+y_4)$$

$$(y_7-y_3y_4) = \frac{1}{y_5}\left[\sigma_4 - y_1a_3\right]$$

$$y_6 = y_2(y_3+y_4) - (y_7-y_3y_4) - a_2$$

$$y_4 = \frac{1}{y_6}\left[-y_2(y_7-y_3y_4) - a_3\right]$$

$$y_3 = (y_3 + y_4) - y_4 \tag{22}$$

$$y_7 = y_3 y_4 + (y_7 - y_3 y_4)$$

$$k_1 = y_1 m_1$$

$$m_2 = k_1^2/(y_5 m_1)$$

$$k_2 = y_2 m_2 - k_1$$

$$m_3 = k_2^2/(y_6 m_2)$$

$$k_3 = y_3 m_3 - k_2$$

$$m_4 = k_3^2/(y_7 m_3)$$

$$k_4 = y_4 m_4 - k_3.$$

Experimental Program

In order to determine the feasibility of the developed analytic design method a test program was performed with the goal of simulating a number of three-degree (3D) and four-degree (4D) of freedom acceleration pulses. This section is devoted to a qualitative description of the overall test setup and a presentation of results for typical 3D and 4D experiments. Actual testing was carried out at the Sandia Corporation shock testing facility, Albuquerque, New Mexico, using a Model HVA 1212 drop test machine, manufactured by Monterey Research Laboratories, Monterey, California.

A typical 3D test setup is as shown in Figure 3. The inclusions were machined from 10" O.D., steel rod, while the spring elements were fabricated from 7" O.D. low and high density polyethylene rod. A docking fixture was designed and installed as shown. The purpose of the docking fixture was to maintain a positive lock between the drop table and the uppermost spring element after initial impact. During the course of testing, this docking collar performed successfully at impact velocities in the range of 6-10 fps.

The polyethylene material used for the spring materials, although having the desirable features of low cost and light weight exhibited some extremely undesirable characteristics which essentially ruled out its use for any further testing of this type. The basic problem with this material is that it is viscoelastic. Therefore, use of polyethylene violates the initial assumption used in the analytic development of linear elastic spring elements. This difficulty was overcome to some extent by using equivalent static

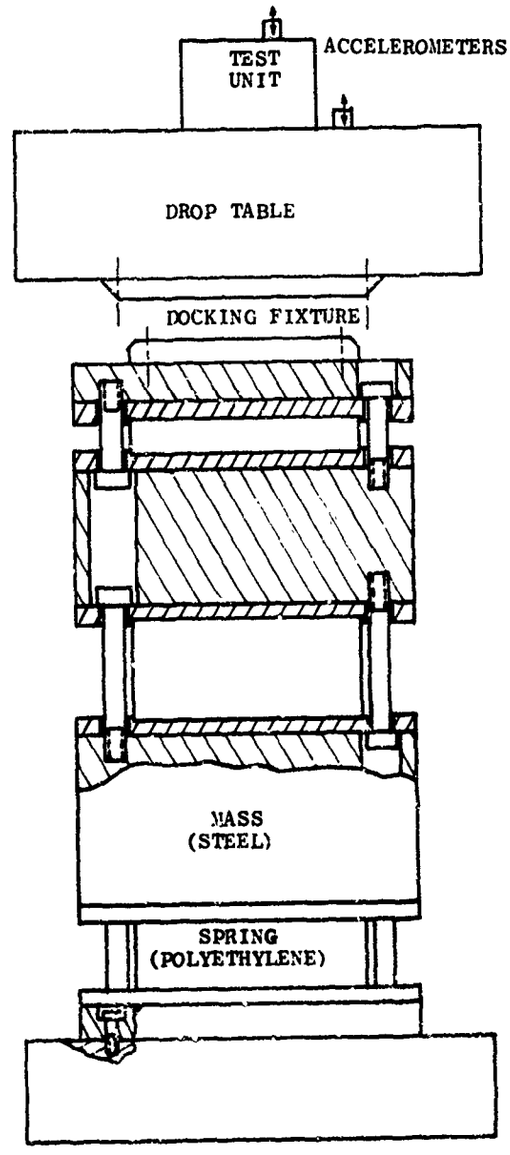

FIGURE 3

TYPICAL 3D TEST SETUP

stiffness values for various lengths of 7" polyethylene rods as determined from single-degree of freedom "calibration" drop tests. That is, a simple test involving impacting the drop table on a given length of rod at a specified impact velocity, resulted in a half sine acceleration response which was used to compute an equivalent static stiffness. These tests were repeated over a range

of impact velocities and the results averaged to give a design stiffness value for that particular length of polyethylene rod. Another problem with this material was its basic bilinear stiffness behavior between tension and compression loading. In order to eliminate the bilinear stiffness problem the springs were fixtured to operate always in a compressive mode regardless of the direction of relative motion between adjacent masses (see Figure 4).

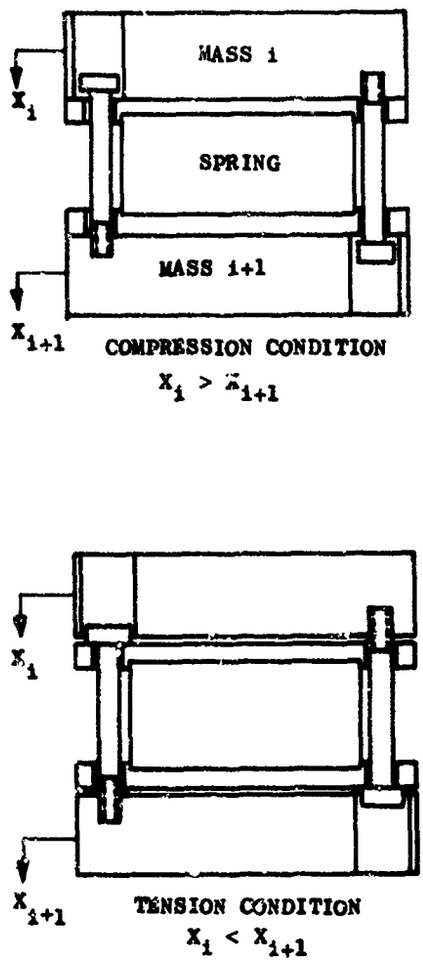

FIGURE 4
DETAILS OF SPRING ASSEMBLY

Physical parameters used in two experiments considered representative for 3D and 4D test configurations are summarized in Table I.

TABLE I
PHYSICAL TEST PARAMETERS

CONFIG.	MASS VALUES $\left(\frac{LB\ SEC^2}{IN}\right)$	STIFFNESS VALUES (LB/IN)
3D Test	$m_1 = .622$	$k_1 = 3.5 \times 10^6$
	$m_2 = .106$	$k_2 = 1.48 \times 10^6$
	$m_3 = .606$	$k_3 = 8.0 \times 10^5$
4D Test	$m_1 = .591$	$k_1 = 2.3 \times 10^6$
	$m_2 = .155$	$k_2 = 1.0 \times 10^6$
	$m_3 = .163$	$k_3 = 5.3 \times 10^5$
	$m_4 = .159$	$k_4 = 1.45 \times 10^6$

It should be pointed out that since the stiffness numbers given are nominal values obtained by averaging calibration tests at different impact velocities, a considerable range in effective stiffness (on the order of ±20%) can be expected for any particular spring.

Results obtained for the 3D and 4D test configurations, each tested at two different impact velocities, are presented in Figure 5 and Figure 6 respectively. These data, shown by the dashed and dotted lines, were traced directly from oscillograph records which were electronically filtered at 2500 Hz.

Also shown as the solid line in each figure are the computed acceleration response using the physical parameters listed in Table I and a viscous damping value for each spring equal to 7% of critical (as obtained from a logarithmic decrement test on a representative polyethylene pad).

In general the shape of the predicted and experimental acceleration pulses agree fairly well, particularly when the range of uncertainty in the spring stiffness values is considered. However, the test results do exhibit some degree of high frequency response not predicted by theory which, to some extent, is attributed to built-in nonlinearities in the test setup, e.g., the intermittent impacting between the retainer plates and inclusion as the

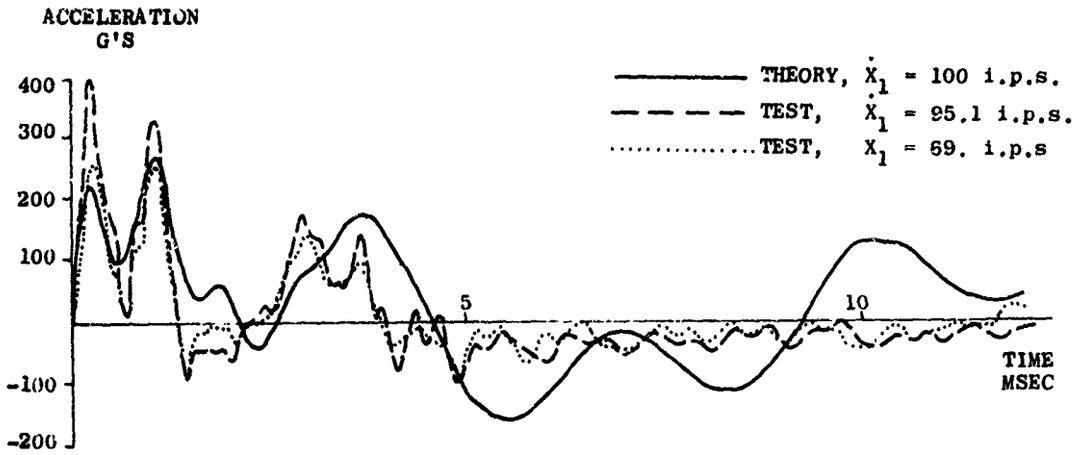

FIGURE 5
ACCELERATION VS. TIME FOR 3 DEGREE OF FREEDOM TEST

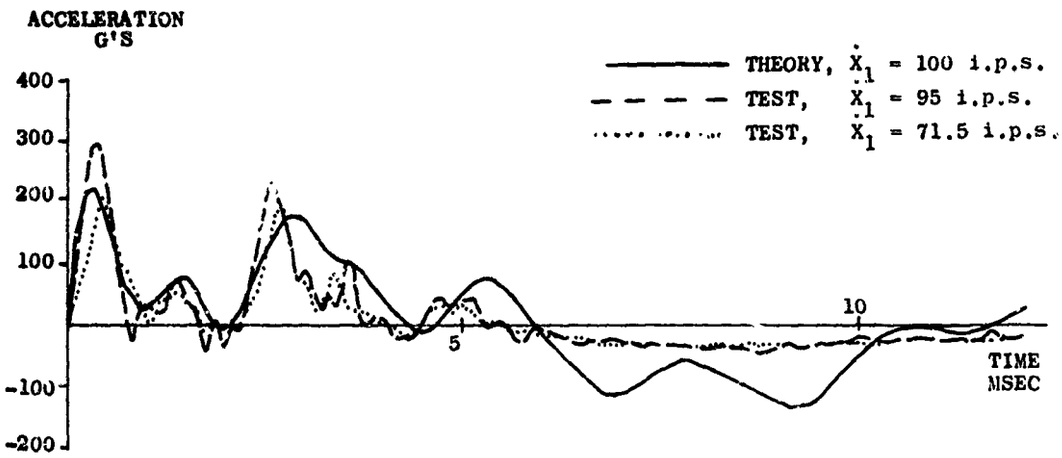

FIGURE 6
ACCELERATION VS. TIME FOR 4 DEGREE OF FREEDOM TEST

individual springs alternate between tension and compression conditions.

It is particularly interesting to note the degree of repeatability in basic pulse shape evident from the test results at the two separate impact velocities for each test setup. This result agrees with what is theoretically expected; examination of the design equations shows that relative amplitudes are independent of initial velocity but that absolute amplitudes are proportional to the impact velocity. In certain test programs this response behavior may be a desirable test

characteristic. That is, a drop test can be designed for a given acceleration time history and easily repeated at increasing values of impact velocity (peak accelerations) until failure or malfunction is noted.

CONCLUSIONS

The conclusions arrived at during the course of this study may be summarized as follows:

1. Using the developed analytic techniques, it is possible to design a drop test experiment for simulation of transient acceleration pulses containing up to five sine harmonics. The amplitudes of all harmonics must be of like sign.

2. An experimental program using a commercially available drop test machine was undertaken to demonstrate the feasibility of the technique, and met with a reasonable degree of success. Transient acclera-tion pulses containing 3 and 4 fundamental harmonics and having peak magnitudes on the order of 200 to 400 g's were produced which qualitatively matched the predicted or design accelerations.

3. In order to make this method a usable simulation technique, improvement in experimental procedure is required. In particular, design of light weight, linear and elastic spring elements appears to be the most important requirement.

4. To some extent the developed test method suffers from a certain degree of inflexibility. That is, a new test setup has to be designed, fabricated and assembled for each acceleration pulse to be simulated. However, once a test setup is in place, a number of tests can be rapidly run at increasing values of impact velocity (i.e. increasing acceleration levels) without changing the basic pulse shape. This capability is attractive if testing to determine fragility (failure) of a component under a basic form of acceleration pulse is desired.

ACKNOWLEDGMENT

The authors would like to acknowledge the assistance provided by the Sandia Corporation (Albuquerque) component shock testing laboratory in the performance of the experimental portion of this program. In particular the efforts of Mr. C. Endres, Mr. J. Cannon, and Mr. K. Campbell, Jr. are gratefully acknowledged.

REFERENCES

1. Harris and Crede, Shock and Vibration Handbook, Volume 2 Data Analysis, Testing and Methods Control, Chapter 26, McGraw-Hill, New York, 1961.

2. J. D. Favour, J. M. LeBrun, J. P. Young, "Transient Waveform Control of Electromagnetic Test Equipment," Shock and Vibration Bulletin #40, Part 2, pp. 157-171, December 1969.

3. J. R. Moser and D. Garner, "An Improved Electrodynamic Shaker Shock Technique," Shock and Vibration Bulletin #40, Part 2, pp. 173-181, December 1969.

4. D. A. Regillo, "Shock Testing with an Electrodynamic Exciter and Waveform Synthesizer," Shock and Vibration Bulletin #39, Part 5, pp. 67-72, December 1968.

5. J. Fagan and J. Sincavage, "Shock Testing and Analysis: A New Laboratory Technique," Shock and Vibration Bulletin #39, Part 5, pp. 83-83, December 1968.

DISCUSSION

Mr. Hughes (Naval Weapons Evaluation Facility): Why did you use polyethelene which is nonlinear in different directions when you are trying to simulate a linear spring? Why did you not use a linear spring?

Mr. Keeffe: That is a good question. We have asked ourselves that 200 times. There were some time considerations, and in the spring rates that we were looking for it turned out that the basic properties of polyethelene satisfied our requirements. Also when one starts looking in spring catalogues for Bellville springs and helical springs, we could not find anything that had the spring rates which we required. They were on the order of a million pounds per inch, so we had to look for something else. Now we feel that there are better ways to do it, but it was a matter of expediency.

ANALYSIS OF PROJECTILE IMPACT ON COMPOSITE ARMOR

Richard A Fine
IBM Corporation
Rochester, Minnesota

and

Raymond R Hagglund
Worcester Polytechnic Institute
Worcester, Massachusetts

Theoretical and experimental analyses are performed to investigate bullet impact effects on ceramic composite armor. The armor consists of ceramic tile bonded to fiberglass reinforced plastic backing. This type of armor is used to protect military personnel and equipment. Projectiles of one material and with separate core and casing (e.g. armor-piercing) are considered. Theoretical analysis is based on a quasi-static approximation of the event. The law of motion is used to predict the deceleration of the bullet and the force resisted by the armor during impact. Experimental data obtained by open-lens photography of the impact event are in good agreement with the theoretical analysis. The photographs clearly indicate ductile behavior of the bullet during impact, contrary to the generally accepted theory that materials such as hardened steel exhibit brittle characteristics at high strain rates.

INTRODUCTION

Ceramic composite armor was proven feasible by Goodyear Aero-Space in 1962. It has unusual ability to stop bullets and is relatively light in weight. An approximate comparison of the weight per square foot required to stop a .30 caliber armor piercing bullet at its muzzle velocity is shown in Table 1.

The development and improvement of ceramic composite armor has been largely by trial and error. First attempts at a fundamental understanding involved experiments to relate material properties to performance. An example is Foster's work, where he measured density, elastic modulus, strength, etc. of hundreds of armor samples, experimentally determined their performance, and attempted to correlate performance with properties and combinations of properties [2]. Studies of shock wave propogation in the bullet and armor have been pursued by several investigators [3,4,5]. These studies experimentally determine

TABLE 1
Approximate Armor Weight Required To Stop A .30 Cal. A/P Bullet At Its Muzzle Velocity [1]

Armor Material	Areal Density (lbs/sq. ft.)
Homogeneous Steel	20
Dual-hardness Steel	12
Alumina-fiberglass Composite	9.5-10
Silicon Carbide-fiberglass Composite	8.5-9
Boron Carbide-fiberglass Composite	7-7.5

the relationship between two properties such as pressure and particle velocity during the time a shock wave passes through a material, and apply this relationship in a mathematical model of the impact. The relationship, known as a Hugoniot curve [6] is used rather than the equations of state, motion, energy, and continuity because the equations of state for solids are rarely available and difficult to handle mathematically. One difficulty with this approach is that the Hugoniot relationship is valid only for waves constrained similarly to those where it was measured, generally plane waves. This type of work has now been abandoned as a means to improve the understanding of composite armor [7].

This paper studies the application of quasi-static theory to the impact event. This assumes dynamic equilibrium is attained during every instance of the impact. Justification for this approximation is first that photographs show that bullet fracture is caused by force at the tip, rather than spalling at the tail as would be expected if shock waves were the major factor. Second, while quasi-static theory predicts deceleration at the tail of the bullet before the shock wave reaches it, the predicted deceleration is negligible so this is not an important limitation. The quasi-static approximation can thus be expected to account for major effects, while neglecting less important non-equilibrium effects.

EQUATIONS FOR BULLET MOTION

This portion of the theoretical analysis establishes the deceleration rate of the bullet. Analysis is based on the law of motion:

$$a = F_s/m_s \qquad (1)$$

where a is the acceleration of the bullet, F_s is the force at the solid-particle interface of the bullet, and m_s is the mass remaining of the solid bullet. The mass m_s is equal to the initial mass minus the mass which has been fractured into particles. Considering the armor as a rigid surface, the volume fractured during a time increment is equal to the area of contact at that time multiplied by the distance the bullet moves. This assumption is reasonable until the ceramic fractures, and in fact for some time after the ceramic fractures, because even then the interface makes only very slow progress into the armor compared with the velocity of the bullet. Thus the mass remaining can be represented as

$$m_s = m - \int \rho A_t u_t dt \approx \Sigma \rho A_t u_t \Delta t \qquad (2)$$

where m is the mass of the whole bullet, ρ is the bullet density, A_t is the bullet to armor contact area, u_t is the velocity, and Δt is time increment.

The acceleration a is represented in finite difference form as the incremental change in velocity. Thus

$$a \approx \frac{u_{t+\Delta t} - u_t}{\Delta t} \qquad (3)$$

The limiting force on the bullet is its maximum strength multiplied by the interface area

$$F_s = -\sigma_{max} A_t \qquad (4)$$

where σ_{max} is the maximum strength of the bullet material. Substituting Eqs. (2), (3), and (4), into Eq. (1) gives

$$\frac{u_{t+\Delta t} - u_t}{\Delta t} \approx \frac{-\sigma_{max} A_t}{m - \rho \Delta t \Sigma A_t u_t} \qquad (5)$$

Solving for velocity after the time increment,

$$u_{t+\Delta t} \approx u_t - \frac{\sigma_{max} A_t \Delta t}{m - \rho \Delta t \Sigma A_t u_t} \qquad (6)$$

This equation can be solved iteratively, using a computer, until the velocity reaches zero or the bullet is entirely destroyed.

EXPERIMENTAL VERIFICATION

In this section predictions based on the preceding model for bullet motion are compared with experimental results.

Calculated motion of a .30 Cal. M2/AP bullet striking armor at 2732 ft/sec is shown in Fig. 1. The two-material bullet has been represented as two single-material bullets of appropriate cross-sectional areas

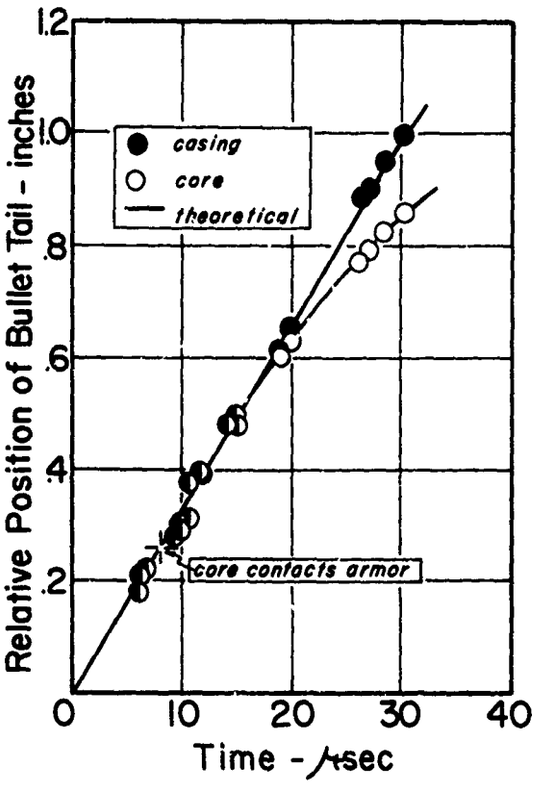

Fig. 1 - Predicted deceleration of .30 Cal. M2/AP bullets at 2732 ft/sec, with experimental verification

striking the armor in the appropriate time sequence. Frictional forces between the core and jacket are neglected. Material strengths used are 500,000 psi for the core (high-carbon steel hardened to Rockwell A 79-80) and 100,000 psi for the brass jacket. These values are arbitrarily chosen as about fifty percent greater than static strengths. The literature indicates that dynamic strengths of materials are considerably higher than static, but little specific data is available, particularly at the very high loading rates considered here.

Figure 2 shows calculated motion of a one-material bullet (cores fired without its jackets) at 2700 ft/sec. Again, the strength of 500,000 psi is used.

Experimental data for comparison is also included in Figures 1 and 2 and is found to be in good agreement with the theoretical predictions. These data are obtained by taking measurements from photographs of the impact event. Examples of the photographs are shown in Figures 3 and 4.

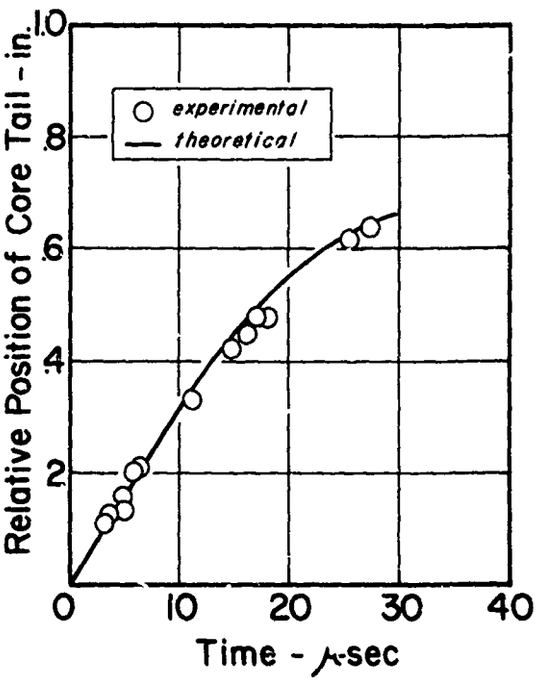

Fig. 2 - Predicted deceleration of .30 Cal. M2/AP cores at 2700 ft/sec, with experimental verification

The photographs are taken using an open-lens camera in a dark room. A high intensity flash of 1/2 microsecond duration illuminates the subject. The flash is triggered by the projectile penetrating a switch consisting of a non-conducting plastic film with aluminum foil on each side. Penetration completes a triggering circuit. Adjusting the distance between the switch and armor varies the timing of the photographs. Each photograph is of a separate ballistic test, and the timing is adjusted to provide sequences showing the progressive stages of impact.

Figure 3 shows .30 Cal. M2/AP projectiles at five points during impact. These are examples of photographs from which the experimental points in Figure 1 are derived. Figure 4 shows .30 Cal. M2/AP cores,

during impact. These provide an additional experimental data set and allow visual observation of core fracture. The back half of the casing is used as a carrier for firing the projectile. In this set of photographs two cameras were used to simultaneously provide an oblique and perpendicular view of the projectile. The perpendicular view improves the ease and accuracy of measurements while the oblique view facilitates visual observation.

Timing of the pictures is determined by measuring spall motion. The spall velocity is considered constant (although unknown) because it's deceleration is negligible compared with that of the bullet which is being resisted by armor. Thus the distance travelled by the spall is proportional to the elapsed time since initial contact. To determine the proportionality factor between spall distance and time, a curve of measured bullet position vs spall position (time) is drawn (similar to Figures 1 and 2). The slope of the curve at the origin must be equal to the incident velocity of the bullet, which defines the units on the time scale.

DISCUSSION OF PHOTOGRAPHS

Study of the photographs reveals several things about the impact. Perhaps most important is that extensive fracture occurs at the bullet tip. This indicates that the major factor in the event is compressive loading at the tip rather than reflected tensile shock waves.

Although it has been established that initial fracture of the armor occurs within the first few microseconds [3], the pictures show that the ceramic resists the bullet for a much longer time. Figure 3 shows that at 17 microseconds the spall is still directed parallel to the plate surface, indicating no penetration of the projectile. At 26 microseconds obliquely directed spall can be detected, indicating that penetration has begun. Similarly, in Figure 4, no penetration is evidenced at 15 microseconds. This indicates that the representation of the armor as a rigid surface for theoretical calculations is valid for a significant portion of the event.

Figure 3 shows that the jacket is decelerated less than the core. At the later times the core can be seen protruding at the back of the bullet. This is due to the material with higher strength sustaining a larger force and therefore, greater deceleration.

An important and unexpected result is best seen in Figure 4, at 15 microseconds. In this photograph ductile behavior of the forward portion of the bullet is clearly evident. This is contrary to the generally accepted theory that materials such as hardened steel exhibit brittle characteristics at high strain rates.

EQUATIONS FOR FORCE APPLIED TO THE ARMOR

In this section, equations are derived for the force applied to the armor. This force is different than the force on the solid portion of the bullet because there is a gradient through the particulate portion. The approach used is to apply the momentum form of the law of motion [8] to the entire bullet:

$$\underline{F} = \lim_{\Delta t \to o} \frac{\underline{G}_{t+\Delta t} - \underline{G}_t}{\Delta t} \qquad (7)$$

where $\underline{F}$ is the total force vector applied to a body in a given direction and $\underline{G}$ is the momentum in the same direction. For application of this equation, the projectile is subdivided as shown in Figure 5. Using these subdivisions, the equation can be rewritten:

$$-F(t) = \lim_{\Delta t \to o} \frac{\underline{G}_{A'} - (\underline{G}_A + \underline{G}_B)}{\Delta t} \qquad (8)$$

Expressing the momentum in terms of mass multiplied by volume gives

$$-F(t) = \lim_{\Delta t \to o} \frac{\rho V_{A'} u_{t+\Delta t} - \rho V_A u_t - \rho V_B u_t}{\Delta t} \qquad (9)$$

where v is volume and u is velocity. The volumes of A and A' are chosen to be equal, and the volume of B is $A_t u_t \Delta t$, so the equation can be rewritten

$$-F(t) = \lim_{\Delta t \to o} \frac{\rho V_A (u_{t+\Delta t} - u_t) - \rho (A_t u_t \Delta t) u_t}{\Delta t} \qquad (10)$$

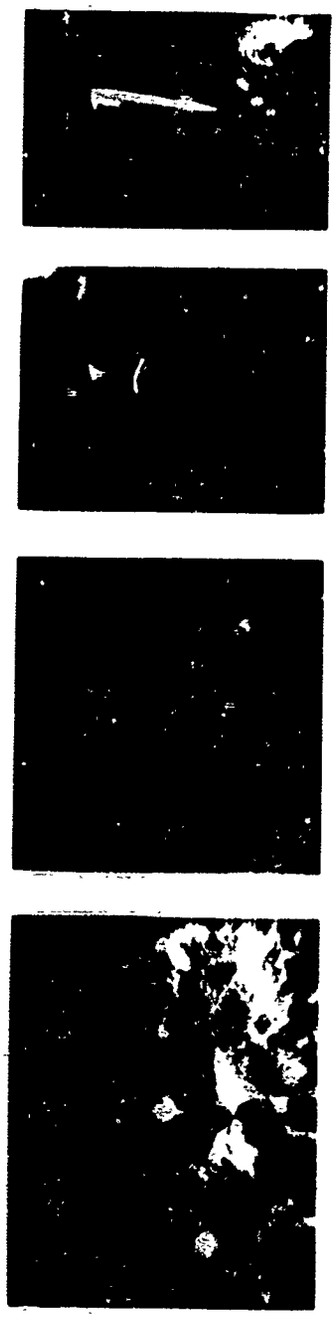

Fig. 3 - Examples of open-lens photographs of .30 Cal. M2/AP bullets striking boron carbide armor at 2732 ft/sec. Times: 6, 12, 17, and 26 microseconds

Fig. 4 - Examples of open-lens photographs of .30 Cal. M2/AP cores striking boron carbide armor at 2700 ft/sec. Right angle and oblique views are shown of each event. Times: 4, 6, 15, and 25 microseconds

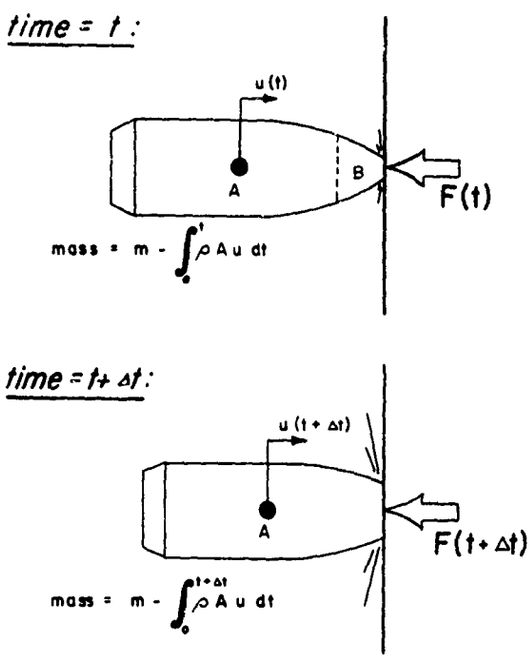

Fig. 5 - Projectile sub-divisions used in applying the momentum form of the law of motion

Dividing both the numerator and the denominator of the argument of the limit by Δt gives

$$-F(t) = \lim_{\Delta t \to 0} \left\{ \frac{\rho V_A u_{t+\Delta t} - u_t}{\Delta t} - \rho A_t u_t^2 \right\} \quad (11)$$

When the limit is taken, the incremental change in velocity divided by the incremental time becomes du/dt, which is the acceleration of the bullet

$$-F(t) = \rho V_A a - \rho A_t u_t^2 \quad (12)$$

ρV_A is, within an incremental unit, equal to m_s. Using the law of motion, equation (1), this is equal to F_s/a. Making this substitution,

$$F(t) = -F_s + \rho A_t u_t^2 \quad (13)$$

Using equation (4),

$$F(t) = -\sigma_{max} A_t + \rho A_t u_t^2 \quad (14)$$

With th equation the force applied to the arm.. facing at any time during this phase of the impact can be found. Required are values for the area of contact, A_t, and the velocity at the particular time u_t. These values are found using equation (6).

PROJECTILE DAMAGE THEORIES

In this section, three theories of projectile damage are examined. The motion of the projectile is computed until the completion point indicated by each theory. At this completion point, the predicted mass remaining (m_s) is noted for comparison with experimental values.

Theories considered are that pulverization is completed when a) the armor fractures at a given applied force, b) a fixed duration of impact passes, and c) the bullet is stopped. Predicted mass remaining for these theories, as a function of bullet velocity, are shown in Figure 6.

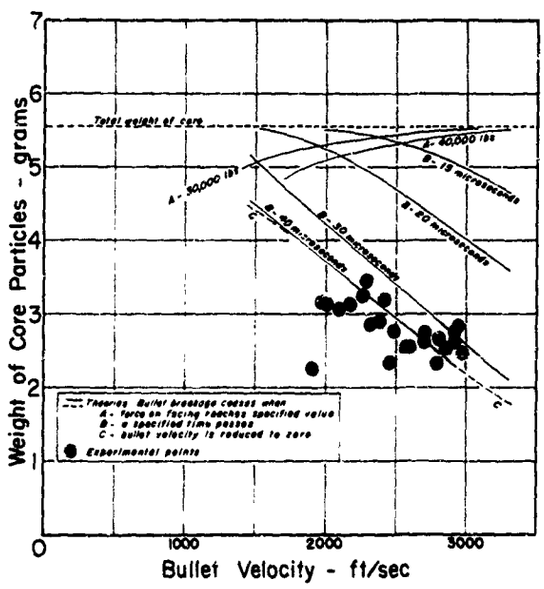

Fig. 6 - Three sets of predictions of the extent of bullet damage, with experimental values. The predicted weight of core not pulverized is shown, assuming bullet damage ceases when the a) force applied to the armor exceeds a given value, b) a constant time interval passes, and c) the velocity is reduced to zero

Also indicated in Figure 6 are experimental values. To obtain these values, bullets were shot at sample tiles. Provisions were made to collect all of the spall and to separate the bullet particles from the armor particles. The larger particles were then weighed to provide the experimental values in Figure 6.

Experimental data are widely scattered, so definite conclusions can not be drawn. The points agree best with the coincident predictions for completion of pulverization at a fixed duration of 40 microseconds and for completion when projectile velocity is reduced to zero. The latter is preferred for two reasons. First, no rationale has been proposed for damage stopping at a fixed time-other than an early time such as ten microseconds, often considered the time when armor fracture occurs [3]. Second, the 40 microsecond curve is limited to a velocity of about 2900 ft/sec. Beyond this projectile motion is reduced to zero in less than 40 microseconds.

CONCLUSIONS

This paper shows that the application of quasi-static theory to projectile impact is valid. The major damage is caused by compressive stresses at the bullet tip, rather than reflected stress waves at the tail.

Observation of spall direction in the photographs indicates that no significant penetration of the armor occurs until late in the event. This extends the duration of validity of the model and lends credibility to the theory that bullet damage continues until the bullet is stopped. Bullet damage studies agree better with this theory than others considered, but are not conclusive.

The armor designer should concentrate on developing materials to withstand the compressive load rather than arranging material impedances to reflect the maximum shock energy into the projectile.

ACKNOWLEDGEMENTS

This paper is derived from a thesis prepared at Worcester Polytechnic Institute [9]. The authors wish to express their appreciation to the Norton Company and the National Aeronautics and Space Administration for partial support of this work.

The authors are indebted to Mr James L Wotipka and to Dr Fakhruddin Abdulhadi for their valuable discussions on the subject. Sincere appreciations are due to Miss Mary E Daly who typed the manuscript.

BIBLIOGRAPHY

1. Torti, M. L. and R. A. Fine. "Composite Ceramic Armor", PROCEEDINGS OF THE 14th REFRACTORY COMPOSITES WORKING GROUP MEETING, 1968.

2. Foster, B. D. AREAL DENSITY PROJECT FINAL REPORT. Norton Company internal report, 1966.

3. Martin, D. M., U. S. Army Research and Engineering Command, Natick, Mass. Private Communications.

4. Wilkins, M. L. SECOND PROGRESS REPORT OF LIGHT ARMOR PROGRAM. Lawrence Radiation Laboratory, University of California, Livermore, 1967.

5. Wilkins, M., C. Honodel, and D. Sawle. AN APPROACH TO THE STUDY OF LIGHT ARMOR. Lawrence Radiation Laboratory, University of California, Livermore, 1967.

6. Duvall, G. E. "Some Properties and Applications of Shock Waves", RESPONSE OF METALS TO HIGH VELOCITY DEFORMATION, Technical Conference Proceedings. New York: Interscience Publishers, 1960.

7. AIR FORCE TECHNICAL OBJECTIVE DOCUMENT, MATERIALS. TOD 71-26. Air Force Materials Laboratory, Wright-Patterson Air Force Base, Ohio, 1970.

8. Housner, G. W. and Donald E. Hudson. APPLIED MECHANICS - DYNAMICS, Second Edition. New York: D. Van Nostrand Company, Inc., 1959.

9. Fine, R. A. AN ANALYSIS OF PROJECTILE IMPACT ON COMPOSITE ARMOR. Ph.D. Thesis, Worcester Polytechnic Institute, 1968.

A SYSTEMATIC APPROACH TO SHOCK HARDENING

J. L. Lipeles
Littleton Research and Engineering Corp.
Littleton, Massachusetts

and

D. Hoffman
U. S. Naval Ammunition Depot
Crane, Indiana

A general specification for the shock hardening of naval ordnance has been recommended. Some background leading to the recommendation is presented along with the salient features of the proposed specification.

INTRODUCTION

The Navy has had a shock program in operation since the early 1940's when the ancester of MIL-S-901 was first written and yet much of the shipboard equipment is still quite fragile. The Naval Ordnance Systems Command has sought to improve its approach to the shock problem. Working in close cooperation, the Naval Ammunition Research Depot at Crane, Indiana, and Littleton Research and Engineering Corp. have developed a general specification for shock hardening that constitutes a significant step toward attainment of the long-sought goal of shock resistance for shipboard equipment.

BACKGROUND

The basic weapon in the Navy's war against shock is MIL-S-901 and, while MIL-S-901 is a reasonably good test specification, it is by no means a complete arsenal.

1) MIL-S-901 is basically a test requirement. The tests are necessarily performed late in the development cycle and are included in the larger group of environmental tests, (rain, sand and dust, explosive atmosphere, etc.). Ordinarily these tests represent design conditions that are not given the same kind of intensive attention (analytic and developmental testing) as are lavished on performance and strength requirements.

When failures are discovered during testing, there is, ordinarily, no completed dynamic analysis in hand to guide the engineers in their fix and redesign efforts. The redesign process is hampered by the lack of knowledge and understanding that an analysis can provide.

The tests occur in a time frame in which schedule and budgetary pressures are at a maximum. When a problem is uncovered in the shock test, it is, therefore, very tempting to ask for waivers and deviations from the specification. In the past waivers and deviations have been readily available. The specification, therefore, promotes an atmosphere in which failures occur regularly and are accepted.

2) The definition of 'failure to perform essential function' (MIL-S-901) is left for the procuring agency to include among the Ordering Data. However, it is often missing, leaving the definition of failure a vacuous quantity.

3) MIL-S-901 is often inappropriate. It has its genesis early in World War II when, in response to the need created by the German mine attack, the British developed the lightweight shock machine. The design criteria of the machine was: produce a shock which simulates damage observed in the fleet. The great majority of that damage was below decks, in general, and in the engine room in particular. The important attribute that this criteria possessed was that the shock produced was

characterized by high frequency motions representative of the keel and lower deck response to underwater blast.

However, most ordnance equipment is located high up in the ship where it is exposed to shock motions that have been substantially filtered by the ship's structure. Upper deck shock motions are characterized by low (20-30 h) frequency motions due to the natural frequencies of the decks themselves.

One comical result of these conditions is that equipment to be mounted on the upper decks has often required shock isolation to pass the specification imposed test. But in the service installation the isolators amplify the input and often must be removed.

SYSTEMATIC GENERAL PROCEDURE

The deficiencies discussed above suggested the need for a more generally applicable, systematic approach. The proposed specification attempts to satisfy the need by offering a three prong procedure of planning, analysis, and test which is substantially different from that utilized in the past. The main features of the proposed specification (which is appended) are:

1) Shared technical responsibility between the contractor and the procuring agency;

2) Planning of a comprehensive program of substance to meet the shock requirements;

3) Compatibility between top specifications and those generated for procured components.

These features are discussed in detail below.

SHARED RESPONSIBILITY

The task of obtaining shock resistant equipment is divided between the procurement agency and the contractor. The part played by the procurement agency is not trivial or short range.

PROCUREMENT AGENCY TASKS

1) Determine design goals. The design goals are required for incorporation in the detail specification. Their development has been discussed above. Sufficient time and effort must be expended to do a thorough job. The procurer must assign appropriate levels and choose the best format (time, history, spectrum, etc.) for the particular application. In the event that the procuring agency is unable to obtain appropriate design goals, a minimum goal and test level are provided.

2) Determine test levels and acceptance criteria. The level of test as it is related to the design goal must be assigned. It will be incorporated in the detail specification. Usually, the procurement agency will specify the test method. If so, care must be taken that the design goal and the test are compatible. They should be different in level but not in spectrum. A substantial difference in spectrum between the two will make the design goal become of decreased importance, since the test is the primary acceptance device.

3) Accept the Program and System Test Plans. Acceptance of contractor formulated program and system test plans and their subsequent incorporation in the detail specification injects the procurement agency into the design and development planning cycle. The natural inclination of the reviewer will be to concentrate on the technical aspects of the plan - the the type and quality of the analyses and test proposed and the care with which they have been thought out. However, the schedule and manpower proposed to carry out the technical programs are direct measures of the contractor's ability to perform and the realism of these proposals will be subjected to close scrutiny.

The completeness and accuracy of the plan are major factors in determining the effectiveness of the whole shock hardening program. Great care will therefore be required in the evaluation of these plans.

4) Monitor progress. Once an acceptable program has been agreed upon, the procurement agency must monitor progress and essentially police the program. In particular, compatibility reports of GFE shock specifications must be reviewed and appropriate action taken. Witnessing of system tests is only one small part of the monitoring activity.

5) Accept the design.

The contractor's tasks are extended and enlarged to ensure the successful development of shock resistent equipment.

CONTRACTOR TASKS

1) Once the original statement of the shock requirement is made, a program can be formulated. This program is the single most important factor in ensuring the development of shock resistant hardware. A report must be

submitted very early in the program (perhaps two weeks after receipt of contract) describing the shock program to be pursued. The plan must delineate a program of subst[illegible] whose duration would be the length of th[illegible] contract. It must describe work to be accomplished and fix a schedule of intermediate reports. These reports would be required at various stages during the development (i.e. Analytic Model Report, Analysis Results Report, Laboratory Test Plan Report, Test Results Report, Ship Test Results Report, etc.). The importance of the plan and the intermediate reports is paramount. It requires that designers consider the shock environment from the very beginning rather than merely testing for it at the end. The effect of enforcing the plan would be the consideration, by contractors, of the shock environment during the initial design phases when the greatest potential for effective effort is present.

2) Both analyses and tests are required in several increments. Initially a preliminary analysis must be done. This would be followed by developmental testing of components and subassemblies. Information obtained would be utilized in a refined final analysis. Final acceptance would be based on a laboratory test. A requirement that both analysis and test be done is not to subvert the final requirement of the test but to make it more effective. The shock analysis provides several important benefits to the designer.

a) He gains a greater understanding of the equipment structure. This understanding becomes very important when a failure is observed during test. Failures are the more easily fixed and redesigns effected when there is an analysis in hand.

b) The analysis will aid the test engineer in his selection of instruments and their locations. Without an analysis, it is easy to select a wrong instrument or one with an inadequate range. The most critical locations or response parameters may not be obvious without an analysis.

c) The results of analyses will be used to write specifications for subcontractors that are meaningful and compatible with higher specifications. For this reason, analysis should be begun as early as possible in the program. Perhaps preliminary data would be used to allow the first analysis to be done quickly so that subcontractors' progress would be impeded as little as possible.

3) It is essential that the contractor demonstrate the compatibility of shock requirements between purchased (or GFE) items and top level specifications. It may be necessary to conduct dynamic analyses and tests of partial structures to obtain mechanical impedances of static analyses and tests to obtain influence coefficients. The purpose of these analyses and tests is to obtain information necessary to avoid the blind application of top level specifications to components or subassemblies when it is inappropriate to do so. The result of specification incompatibility is invariably schedule delay and increased cost, or unacceptably delicate equipment.

The results of all analyses and tests should be periodically reviewed from the point of view of possible changes to lower specifications (that is, the requirements placed on the subcontractors). This is essential if the assembled equipment (some parts of which are designed and manufactured by the prime contractor, and some parts purchased from vendors) is to meet the specifications. The practice of writing immutable specifications is self-defeating. Specifications should be written early with the understanding that later on in the program when more data are available, the requirements will be reviewed and their validity checked. Retaining an invalid specification is wasteful of time and money. In the present case many equipments are acquired to MIL-S-901 when it is inappropriate to do so. In many cases designers who are attempting to do a conscientious job must design equipment to meet an unrealistic test requirement, resulting in a corruption of the intended purpose of the specification.

CONCLUSION

Ordnance equipment is in general among the most shock sensitive equipment aboard ship. This need not be the case. A large part of past problems have been due to the fact that equipment has been procured with little or no regard to its shock resistance. It has been common practice among contractors to seek deviations or waivers to shock requirements. The shock requirement is usually in the form of a test required late in the development cycle. At that time tight budget and schedule pressures are the rule rather than the exception and when difficulty is experienced meeting the shock requirements, waivers and deviations are sought and often received.

The difficulties inherent with the application of MIL-S-901 to the procurement of naval ordnance have led to the proposal that a

systems approach be utilized in the procurement of shock proof equipment. This type of procurement would be more expensive than current practice in the short run, but would be more effective and develop tougher equipment which would be less expensive in the long run.

APPENDIX

MILITARY DEVELOPMENT SPECIFICATION

SHOCK HARDENING: NAVAL ORDNANCE, EQUIPMENT AND SYSTEMS, GENERAL SPECIFICATION FOR

1. SCOPE

1.1 Scope This specification defines the analysis test, data and reporting requirements for shock hardening of ordnance systems and levels of assembly.

1.2 Purpose The purpose of this specification is to establish a uniform approach to the hardening of ordnance to prevent mechanical shock damage due to transportation, handling or hull-transmitted shock from underwater non-contact explosions or from ship's own weapons.

1.3 Classification

1.3.1 Hull mounted Hull mounted items are all systems, equipment or components thereof, located below the main deck and supported principally by the main structural members of the ship, including structural bulkheads. Items located on light platforms, decks or similar structures are excluded.

1.3.2 Deck mounted Deck mounted items are systems, equipment or components thereof, located on main deck or above for surface ships and items located on light platforms, decks and non-structural bulkheads for all ships.

1.3.3 Shell mounted Shell mounted items are equipment or components thereof, attached directly to shell plating or hull side and bottom framing below the waterline.

1.3.4 Principal units Principal units are items of equipment or assemblies of equipment which are the major parts of a system such as gun mounts, antenna pedestals, missile launchers and similar items directly supported by ship's structure of foundations.

1.3.5 Subsidiary components Subsidiary components are items of equipment or assemblies of equipments which form a part of, or are supported on, a principal unit. These would include such items as the power supply section of a radar receiver, radar antenna, fire control panel or a circuit breaker mounted on a panel.

1.4 Definitions

1.4.1 Equipment shock grade

1.4.1.1 Grade A Grade A items are equipment and systems essential for the safety and the continued combat capability of ship and personnel, such as fire control systems, weapons stowage and handling equipment, gun mounts and launchers, electronic warfare items or night vision devices.

1.4.1.2 Grade B Grade B items are equipment and systems not required for the safety of ship and personnel or the continued combat capability of the ship and having only a limited shock hardening requirement.

1.4.1.3 Grade C Grade C items are those not required for safety of ship and personnel or the combat capability of the ship and having no shock hardening requirement imposed on their design or manufacture.

1.4.2 Equipment failures

1.4.2.1 Critical failure A critical failure to Grade A equipment is a failure that significantly degrades the performance of the equipment's function or creates a condition to exist that is hazardous to personnel or vital equipment. A critical failure to Grade B equipment is a failure that causes a condition to exist that is hazardous to personnel or to vital equipment. A critical failure cannot be experienced by Grade C equipment.

1.4.2.2 Non-critical failure A non-critical failure is a failure that significantly degrades the ability of Grade B or Grade C equipment to perform its specified function.

1.4.3 Levels of assembly As used in

this specification, levels of assembly shall be:

(a) System
(b) Subsystem
(c) Equipment
(d) Component
(e) Part

2. APPLICABLE DOCUMENTS

2.1 Government documents The following documents of the exact issue shown form a part of this specification to the extent specified herein. In the event of conflict between the documents referenced herein and the contents of this specification, the contents of this specification shall be considered a superseding requirement.

SPECIFICATIONS

MIL-S-901C of 15 January 1963 - Shock Tests, H. I. (High-Impact); Shipboard Machinery, Equipment and Systems, Requirements for

STANDARDS

MIL-STD-810B of 15 June 1967 - Environmental Test Methods
MIL-STD-202D of 14 April 1969 - Test Methods for Electronic and Electrical Component Parts

PUBLICATIONS

NAVSHIPS 250-423-30 of May 1961 - Shock Design of Shipboard Equipment, Dynamic Analysis Method (AD 265-425L)
NAVSHIPS 250-423-31 Shock Design of Shipboard Equipment, Interim Design Inputs for Submarine and Surface Ship Equipment
NAVSHIPS 250-660-30 of July 1949 - A Guide for Design of Shock Resist- and Naval Equipment
NAVSHIPS 900-185A of April 1957 - Guide for the Design of Shock and Vibration Resistant Electronic Equipment
Naval Research Laboratory Report 6267 of March 1965 - Background for Mechanical Shock Design of Ships Systems (AD 612 734)
Naval Research Laboratory Report 5618 of June 1961 - Navy High-Impact Shock Machines for Lightweight and Mediumweight equipment (AD 260 008)
Naval Ship Research and Development Center - Report C-2541 of May 1968 (Confidential) A Method for Explosion Shock Testing of Equipment Located in Upper Levels of Surface Ships (U) (AD 393 268)
David Taylor Model Basin, Underwater Explosions Research Div. Report 7-61 Floating Shock Platform for Shock Testing Equipment up to 30,000 Pounds
Naval Ship Research and Development Center-Report C-2391 of June 1967 Modification of a Navy High Impact Shock Machine to Simulate Shock at Upper Levels of Surface Ships (AD 817 812)

2.2 Non-government documents

Applied Technology Associates Report 124 of January 1969 Guide for Users of the Dynamic Design-Analysis Method (AD 350 895)

(Copies of specifications, standards and publications required by suppliers in connection with specific procurement functions should be obtained from the procuring activity or as directed by the contracting officer. Documents having an AD number may be obtained from the Defense Documentation Center, Cameron Station, Alexandria, Virginia 22314.)

3. REQUIREMENTS

3.1 Requirements Shock requirements for naval ordnance systems, equipment and components shall be as specified herein and in accordance with the applicable detail specification. In case of conflict, this specification shall take precedence over general equipment specifications in the determination of shock hardening design, development and testing requirements.

3.2.1 Principal units If design goals are unspecified in the detail specification or the contract, velocity-time history shown in Fig. 1a shall be used for deck mounted (1.3.2) principal units (1.3.4) and the shock spectrum shown in Fig. 1b for hull (1.3.1) or shell (1.3.3) mounted principal units.

3. 2. 2 Subsidiary Components The design goal for subsidiary components (1 3. 5) shall be compatible with the design goal of the principal units. Numerical values for design goals may be obtained by analysis, by test of principal units, or by extrapolation of data from full-scale ship tests of similar equipment or systems.

3. 3 Test level

3. 3. 1 Principal units The test level shall be as specified in the detail specification of the contract.

3. 3. 1. 1 Principal units If the test level is unspecified in the detail specification or contract, it shall be, nominally, two-thirds of the design goal, within the tolerances shown in Fig. 2a and 2b. Principal units that are hull or shell mounted may be tested in accorance with MIL-S-901C.

3. 3. 2 Subsidiary components Subsidiary components and other components or subassemblies not mounted on prinicpal units shall be tested by the application of a waveshape or a spectrum having a nominal amplitude of two-thirds the design goal (3. 2. 2), unless specified otherwise in the detail specification or contract.

3. 4 Shock hardening program The contractor shall establish and conduct a shock hardening program including, as a minimum, the elements required by this specification.

3. 4. 1 Shock hardening program plan The purpose of the shock hardening program plan, hereinafter called the plan, shall be to delineate a program which will assure the development of shock hardened equipment. The plan must be sufficiently complete and detailed that a reasonable assessment of the contractor's ability to meet the shock requirement can be performed. As a minimum the plan shall include the requirements of 3. 4. 3 to 3. 4. 7.

3. 4. 2 Upon approval by the procuring agency, the plan shall become a part of the detail specification.

3. 4. 3 The plan shall include a description of the preliminary analysis (3. 5. 1) to be performed. It shall include a statement of the input forces, a list of the response variables to be studied, a definition of the analytic model or models to be employed and a presentation of the method of solution.

3. 4. 4 The plan shall list and describe the system, subsystem, equipment, component and parts testing (4. 2. 1) required.

3. 4. 5 The plan shall outline the final analysis (3. 5. 3), list the subsystem and component data (4. 2. 1. 2) to be incorporated in the analysis, and list the response variables to be studied.

3. 4. 6 The plan shall state the analysis (3. 5) and test (4. 2) schedules.

3. 4. 7 The plan shall state the level and amount of engineering and supporting effort to be employed in the analysis and test efforts.

3. 5 Analysis

3. 5. 1 A preliminary analysis shall be performed to determine the dynamic response of the equipment to the shock loads defined as design goal (3. 2). The results shall be incorporated in component specifications (3. 8), intermediate analyses and test requirements at levels of assembly below the system level. Specifications of government furnished equipment, incorporated in the design, shall be reviewed to assess specification compatibility.

3. 5. 2 A preliminary shock analysis report shall be submitted in which there is a detailed description of the analytic model employed, the forcing functions used, the method of solution and the results.

3. 5. 3 A final analysis shall be performed to determine the dynamic response of the equipment to the shock loads defined as design goal in 3. 2. The results of subsystem and equipment tests (4. 2. 1) shall be incorporated. Specifications of components and government furnished equipment shall be reviewed to assess specification compatibility. The final analysis shall be sufficiently detailed that all failure criteria of 3. 6. 4 are accurately predictable. The final analysis shall be the basis for acceptance in the event no system test is performed (3. 11)

3. 5. 4 A final shock analysis report shall be submitted in which there is a detailed description of the analytic model, the forcing functions used, the method of solution and the results.

3. 5. 4. 1 The final shock analysis report shall include a detailed description of subsystem and component tests (4. 2. 1) and a statement of the results.

3. 5. 4. 2 Based upon the result of the system tests, a revised final shock analysis report

may be submitted.

3.6 System test plan

3.6.1 The system test plan shall describe, in detail, the methods, procedures and machinery by which the loads will be applied.

3.6.1.1 The system test plan shall, upon approval by the procuring agency, become a part of the detail specification.

3.6.2 The system test plan shall describe all jigs and fixtures to be used in testing.

3.6.3 Test instrumentation shall be described in detail. The description shall include, but shall not be limited to:

(a) Transducers, their amplitude and frequency ranges and their range of linearity.
(b) Signal processing equipments, their amplitude and frequency ranges and their range of linearity.
(c) Data processing methods and equipment, their amplitude and frequency ranges and their range of linearity.
(d) Transducer location shall be described and justified on the basis of analysis or test.

3.6.4 Definitions of equipment failure relating to structural and performance requirements shall be stated. They shall include, but not be limited to:

(a) Yielding. Is yielding permitted? If so, which members and to what extent?
(b) Misalignment (mechanical, electrical, optical, etc.). Is misalignment tolerable? If so, which elements and to what extent?
(c) Pressure. Are pressure variations acceptable? If so, to what extent?
(d) Friction. Are friction variations acceptable? If so, to what extent?
(e) Fasteners. Is fastener loosening tolerable? If so, to what extend?
(f) Performance requirements. What are the performance requirements prior and subsequent to test?

3.7 System test results

3.7.1 A system test report shall be submitted stating the results obtained in the system tests (3.6) and comparing them with those reported in the final analysis report (3.5.4.1)

3.7.2 Any repair or readjustment necessary to operate the equipment following the test shall be described in detail along with an account of the time required, the level of expertise required of the repairmen and the repair equipment required.

3.8 Component specifications

3.8.1 Component specifications shall be written by the contractor for all components purchased by the contractor for incorporation into the system.

3.8.2 The validity of the component specifications shall be initially justified by the preliminary analysis (3.5.1) and shall be verified by final analysis (3.5.3) or test results (3.4.3). Revisions shall be made as required.

3.9 Government furnished equipment

3.9.1 The shock specifications of government furnished equipment (if any) shall be reviewed to assess their compatibility with the equipment environment. The initial assessment shall be based on the preliminary analysis and shall be updated when the results of the final analysis and test programs become available.

3.9.2 The results of this review shall be reported in either the system test report (3.7.1) or the final shock analysis report (3.5.4).

3.10 Extensions No extensions shall be permitted unless they are justified by a detailed analysis and the accuracy of the analytic model has been established by prior system test.

3.11 Basis of acceptance Systems and equipment shall be accepted on the basis of

(a) System Test Report (3.7.1)
(b) Final Shock Analysis Report (3.5.4); when equipment is too large or too heavy to be tested
(c) Combination of test and analysis, when tests at a higher level of assembly verify the analysis at a lower level of assembly.

In no case, however, shall the acceptance on the basis of analysis at a certain level of assembly lead to the acceptance of a higher level of assembly without the interposition of a test.

3.12 Acceptance criteria Unless stated otherwise in the detail specification or contract, acceptance criteria shall be as follows:

(a) A minimum of 3 tests at the specified

test level (3. 3) shall be conducted; shocks shall be applied in each direction specified in the detail specification or contract.

(b) Critical failures (3. 6. 4 and 1. 4. 2. 1) shall be cause for rejection.

3. 13 Marking

3. 13. 1 Note for drawings Equipment which meets the requirements specified herein and has been approved by the procuring agency shall include the following marking, along with the applicable grade (1. 4. 1) either A or B, on the assembly drawing for the equipment:

(a) SHOCK HARDENED DESIGN, GRADE ____

4. QUALITY ASSURANCE PROVISIONS

4. 1 Data requirements

4. 1. 1 Shock hardening program plan A shock hardening program plan (3. 4) shall be submitted to the procuring agency not more than 30 days after award of the contract, unless a different time period is stated in the contract schedule.

4. 1. 2 Preliminary shock analysis report A preliminary shock analysis report (3. 5. 2) shall be submitted.

4. 1. 3 Final shock analysis report A final shock analysis report (3. 5. 4) shall be submitted at least 30 days prior to initiation of system tests.

4. 1. 4 System test plan A system test plan (3. 6) shall be submitted at least 30 days prior to system testing.

4. 1. 5 System test report A system test report (3. 7) shall be submitted not more than 30 days after completion of system tests.

4. 2 Test requirements

4. 2. 1 Development tests

4. 2. 1. 1 Vibration tests, mechanical impedance tests as well as shock tests of various types may be used at the discretion of the developer for the purpose of determining design data or other information useful to the development effort and to the attainment of the design goal. All such tests shall be described in detail in the system test plan.

4. 2. 1. 2 Subsystem and component tests Subsystem and component tests shall be conducted during development and shall include, but not be limited to, the tests of 4. 2. 1. 2 to 4. 2. 1. 2. 4.

4. 2. 1. 2. 1 Foundation test If a foundation is supplied by the contractor, a mechanical impedance test of the foundation shall be performed and the results incorporated in the final analysis (3. 5. 3).

4. 2. 1. 2. 2 Non-linear elements tests The force-deflection characteristics of non-linear elements (shock or vibration isolators, plastically deforming structural elements, pneumatic devices, viscoelastic elements, etc.) shall be determined by test. The effects of non-zero strain rate shall be included. The results of these tests shall be incorporated in the final analysis (3. 5. 3).

4. 2. 1. 2. 3 Elastic characteristics The elastic (or plastic) characteristics which cannot be predicted analytically with reasonable accuracy shall be determined by test.

4. 2. 1. 2. 4 Parts Electrical and mechanical parts (resistors, transistors, bearings, etc.) shall be tested in accordance with MIL-STD-202, Method 213A.

4. 2. 2 Qualification and acceptance tests

4. 2. 2. 1 Witnessing Witnesses from the procuring agency shall be invited to observe qualification and acceptance tests.

4. 2. 2. 2 Rough handling shock Bench-repairable equipment, weighing 100 pounds or less, shall be tested for resistance to rough handling shock in accordance with MIL-STD-810B, Method 516, Procedure V.

4. 2. 2. 3 Transportation Shock Equipment and components that may be shipped shall be tested for resistance to transportation shock in accordance with MIL-STD. 810B, Method 516, Procedure II.

4. 2. 2. 4 Hull-transmitted shock

4. 2. 2. 4. 1 Tests to determine resistance to damage from hull-transmitted shock shall be performed in accordance with the requirements of 3. 3 and 3. 6.

4. 2. 2. 4. 2 Tests shall be conducted with the equipment in a ready state. Electrical, hydraulic and penumatic power shall be on. Rotating parts shall be turning at rated speed.

4. 2. 2. 4. 2. 1 One test shall be conducted, in each direction specified, with the equipment in the dormant (power-off or non-operating) state.

4. 2. 2. 4. 3 Prior to each test and subsequent to each test the equipment shall be operated to determine whether the equipment is capable of meeting its performance specifications.

4. 2. 2. 4. 4 Structural damage and other damage of a non-critical nature (1. 4. 2. 2) shall be repaired before continuation of testing.

4. 2. 2. 5 Instrumentation Instrumentation shall be employed to serve the following ends:

(a) to verify that the test imput meets the requirements.
(b) to discover failures - particularly those itemized in 3. 6. 4.
(c) to obtain data necessary to verify component specifications (3. 8).

4. 2. 3 Production tests This specification is not applicable to production tests.

5. PREPARATION FOR DELIVERY

5. 1 This section is not applicable to this specification.

6. NOTES

6. 1 Design guidance The following references are provided for the assistance of the equipment designer and for the assistance of the approving agency. The application of this design guidance material shall not detract from or take precedence over the requirements of this specification or the detail specifications.

(a) NAVSHIPS 250-423-30 of May 1961
(b) NAVSHIPS 250-423-31
(c) NAVSHIPS 250-660-30 of July 1949
(d) NAVSHIPS 900-185A of April 1967
(e) ATA Report 124 of January 1969
(f) NRL Report 6267 of March 1965

6. 2 Test Guidance The following references are provided for the assistance of the test designer and for the assistance of the approving agency. The application of this test guidance material shall not detract from or take precedence over the requirements of this specification or the detail specifications.

(a) NRL Report 5618 of June 1961
(b) UERD Report 7-61
(c) NSRDC Report C-2541 of May 1968
(d) NSRDC Report C-2391 of June 1967

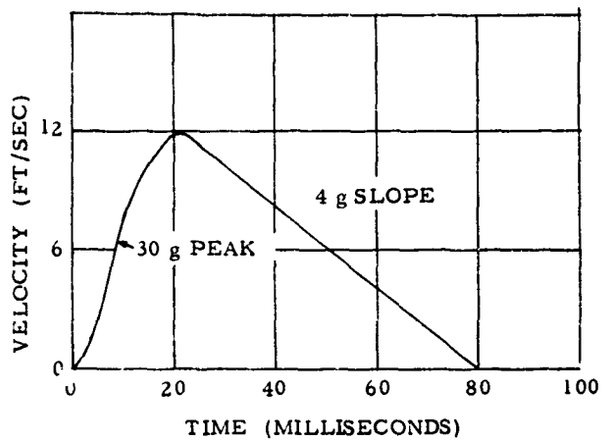

(a)

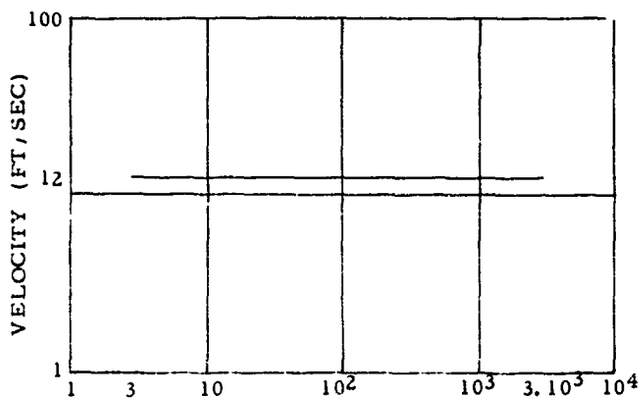

(b)

Figure 1

PRINCIPAL UNIT DESIGN GOAL

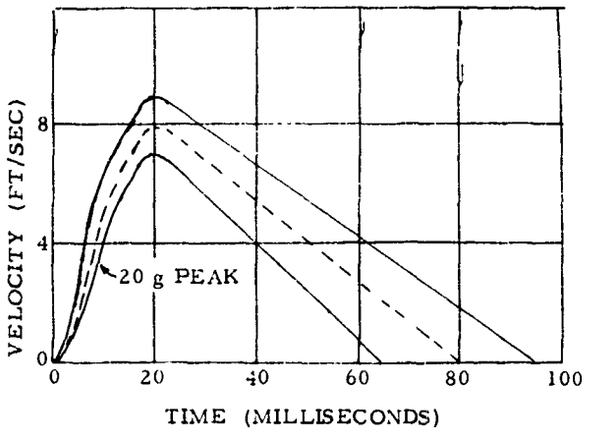

(a)

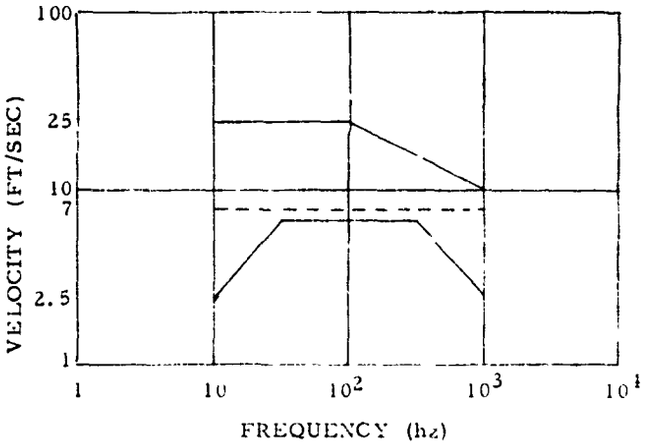

(b)

Figure 2

PRINCIPAL UNIT TEST LEVEL

Mr. Sullivan (NavSec): I gather you are familiar with Mil-S-901, and I believe there is a statement in it concerning the mounting of equipment in a manner that simulates shipboard installation. Is that correct?

Mr. Lipeles: Yes, that is true. The specification requires that. In the course of carrying out this study we surveyed a large number of ordnance programs, and one of the curious things that we found is that there are several details of Mil-S-901 that are invariably neglected, and that is one of the most important ones that is almost always neglected.

Mr. Sullivan: But it is a fixturing problem, not necessarily a basic fault of the machine. The specification permits you to introduce those frequencies, if they are critical parameters that are important to the equipment being tested. You also commented on determining the test levels as something that would be done for each particular piece of equipment. I wondered who would do this?

Mr. Lipeles: We envisioned that that would be a task of the procurement agency. We recognize that that in itself is a problem area. Many procurement agencies are not technically qualified to carry out that function, but there are many people in various laboratories outside of the procurement agencies who could carry out that function, and there is sufficient technical expertise so that that should not be a stumbling block.

Mr. Sullivan: I am sure you appreciate that procurement is spread out among several hundred procuring agencies, and having several hundred people specify inputs for different pieces of the same ship might lead to a little bit of confusion. Another point you mentioned concerned a combined effort of analysis and test, which is fine, but it has always been a problem. I gather you were proposing that we have some sort of definite schedule of running analytical studies and preliminary tests that would be a formal part of the contract, and I wonder, what happens when you get down to the final test which you referenced and the equipment fails? Who is responsible for correcting the failure?

Mr. Lipeles: Did I understand you to say that you questioned who was responsible for carrying it out?

Mr. Sullivan: No. You had a joint effort between the procuring agency and the supplier in ad hocing this piece of equipment up to the test and then you are going to run your final test. Hypothesizing that something happens during that test and the equipment fails, who fixes it.

Mr. Lipeles: The contractor. After all it is his job to build something that meets the specification since there are design levels. That is really one of the major problems. It is very common that a test will be run and there is a failure and nothing gets done about it.

Mr. Sullivan: Would you propose that the Navy in this case review and approve his analytical work leading up to this final test?

Mr. Lipeles: I did not mention all of the requirements of this specification. There are a number of reports that are required. All of the analytical results, both preliminary and final, are required to be reported, but none of them are the basis of acceptance except the final test.

Mr. Balan (Grumman Aircraft): There are cases in which it would be advantageous to mount these various items of equipment on shock mounts. To what extent, if any, do you propose that the contractors investigate the advantage in their analysis prior to fabrication?

Mr. Lipeles: I would expect that once the levels have been specified, if shock mounting is required to meet those levels then those shock mounts are part of the design and therefore the contractor's responsibility.

Mr. Balan: There are two alternatives: one possible way would be to hard-mount the equipment, and the other way would be to soft mount the equipment. The advantages and disadvantages of each method are not immediately apparent. It would seem to me as though it would be desirable for the prospective vendor, or the contractor, to be directed to analyze and to predict the advantage of soft mounting as opposed to the typical or usual way of hard mounting.

Mr. Lipeles: I would expect that a requirement that a piece of equipment be either hard mounted or soft mounted would be specified in the detailed specification. If a procurement agency wanted to go one particular way, they would say so.

THE DEVELOPMENT OF SHOCK TEST CRITERIA FOR AIRCRAFT DISPENSER WEAPON EJECTION MECHANISMS

K. D. Denton, K. A. Herzing, S. N. Schwantes
Honeywell Inc., Ordnance Division
Hopkins, Minnesota

External stores carried on aircraft are subjected to a number of dynamic environments from external sources. Typical external sources of exc''ation are boundary layer pressure fluctuations causing store [illegible] ock excitation from a hard or arrested landing. In additi.n, s[illegible] al stores have unique self-induced dynamic environr

One sign[illegible] induced environment occurs on the SUU-38 munitions dispenser [illegible] es pyrotechnic ejection mechanisms to eject thirty canisters in sequence during captive carriage. As each ejection occurs, the adjacent remaining canisters and the dispenser are subjected to a pyrotechnic induced shock environment. This paper describes a test program and the associated analysis which were conducted to develop both an impact shock test criteria and a shock spectrum simulation test for the SUU-38 dispenser ejection mechanism. The shock spectra of the dispenser response to canister ejection and the corresponding response to a MIL-STD-810B crash shock test are also compared.

INTRODUCTION

External stores carried on tactical aircraft are subjected to a number of different dynamic environments. The commonly recognized environments are those which produce vibration or shock transients through external excitation, such as fluctuating aerodynamic pressures which act upon the store surface or abrupt aircraft deceleration produced by a hard landing. Structural loads and stresses due to these sources are commonly included in the design calculations for external stores.

Certain external stores have significant self-induced environments which should also be considered during the design and test activities. One such self-induced environment occurs on external stores which eject cargo or munitions during captive carriage. The SUU-38 version of the Tactical Fighter Dispenser (TFD) sequentially ejects thirty cargo canisters downward during captive flight. An electrically initiated pressure cartridge is used in the ejection mechanisms to achieve sufficient canister ejection velocity for safe separation from the aircraft.

During the development program of the SUU-38, a qualification and acceptance specification was written for procurement of the pressure cartridge. At this time, it was felt that the MIL-STD-810B, 30-g crash shock requirement for the dispenser approximated the most severe operational shock environment experienced by the pressure cartridge. However, after the SUU-38 system was in production, laboratory testing of the dispenser indicated that unfired pressure cartridges experienced significantly higher induced shock from the ejection of adjacent canisters.

Self-induced environments are unique to the system in which they occur; therefore, no general shock specification can be expected to furnish appropriate test criteria for components in a system such as the SUU-38 dispenser. Consequently, the test program and associated analysis described in this paper were conducted to develop a more realistic component shock test specification for the SUU-38 pressure cartridge.

SYSTEM DESCRIPTION

1. Dispenser Description

Fig. 1 shows three empty SUU-38 dispensers mounted on an F-105 aircraft. Note the thirty small rectangular openings on the bottom of each dispenser. Each of these openings contained a canister prior to ejection.

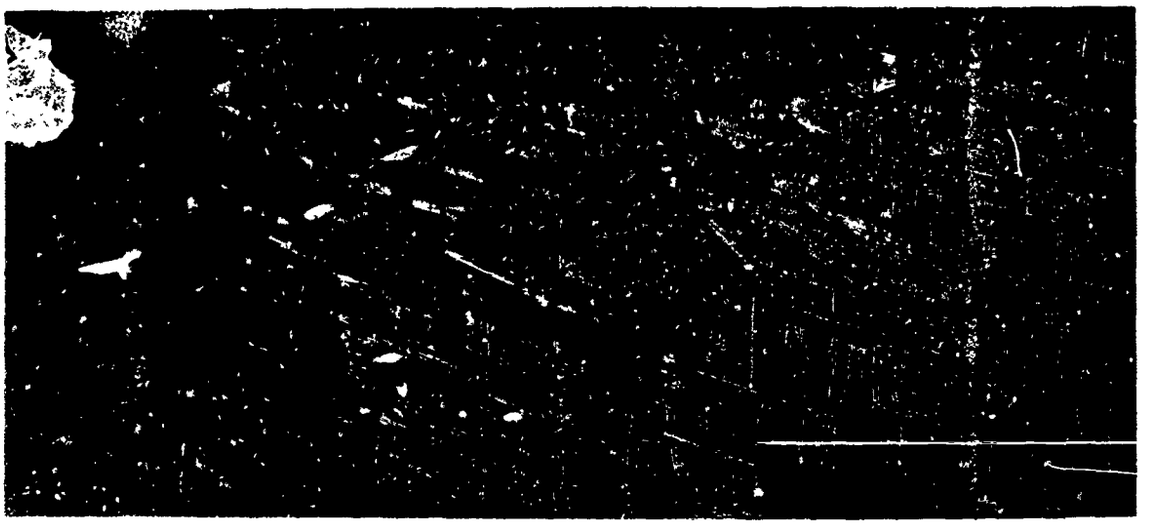

FIG. 1. SUU-38 Dispensers on F-105 Aircraft

The SUU-38 has been flown with and without tail fins. With the tail fins (see Fig. 2) the loaded dispenser weight is 931 pounds, and the empty weight, after all cargo is ejected, is 268 pounds. The basic TFD dispenser was designed with ten bays, each measuring 14.25 inches long, 6 inches wide, and 13.25 inches deep. An electromechanical stepping switch, called the intervalometer, is used to control the sequence and time interval between the canister ejections.

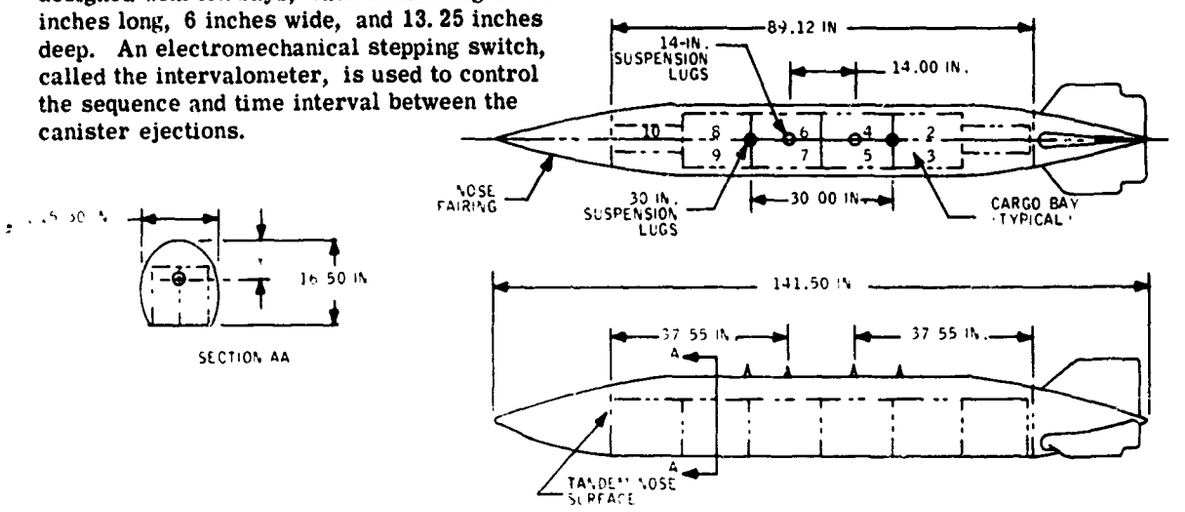

FIG. 2. Dispenser Physical Characteristics

2. Adapter Description

The SUU-38 version of the TFD dispenser was required to have 30 bays instead of ten so an adapter was designed which subdivides each bay into three sub-bays, (see Fig. 3). Each sub-bay, located on 4.74 inch centers, has a separate canister ejection retention system (see Fig. 4).

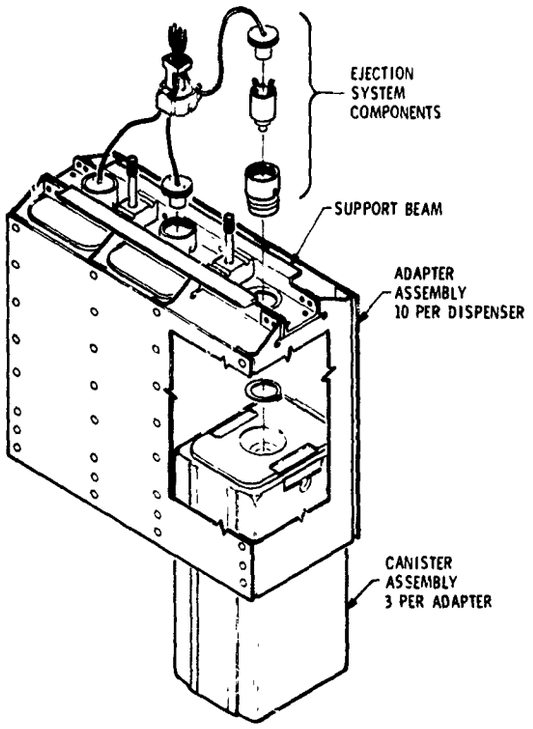

FIG. 3. Adapter Assembly SUU-38 Dispenser

Three canisters are loaded into each adapter. The adapters are attached to the dispenser by means of two 3/8-inch diameter bolts. The adapters remain in the dispenser after cargo ejection. Note that the ejection and retention forces are first transmitted to the adapter support beam. The support beam then transfers loads through the two 3/8-inch bolts into the primary dispenser structure.

3. Retention Ejector Assembly

This assembly (see Fig. 4) includes the thruster body and retaining ring, the piston assembly, and the pressure cartridge. The thruster body is attached to the adapter beam by means of a snap ring on the lower side and

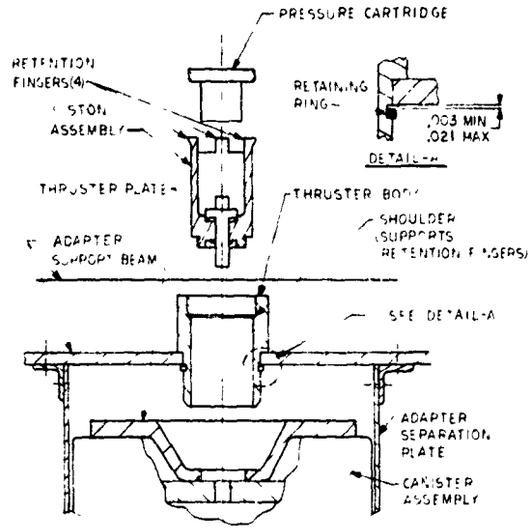

FIG. 4. Canister Adapter Interface (Exploded View)

a shoulder on the thruster body on the upper side (see Fig. 4). In order to assure installation of the snap ring, piece-part tolerances are such that a gap of about 0.012 inch will normally occur between the snap ring and the bottom of the adapter beam. The allowable gap ranges from 0.003 to 0.021 inch.

The piston assembly is threaded into the thruster plate of the canister to a predetermined torque. The four segmented flange sections or retention fingers will then bear out against the mating shoulder on the thruster body, and the thruster plate will also bear out on the bottom of the adapter support beam. The pressure cartridges are then threaded into the thruster body.

4. Pressure Cartridge Description

The SUU-38 pressure cartridge (see Fig. 5) is basically a threaded steel header with a thin metal cup containing the propellant. Two steel pins carry the signal through the header to the ends of the nichrome bridgewire. The bridgewire is welded to each end of the pins. The bridgewire bond is probably the part most susceptible to high level shock, but its small mass keeps inertia loads at a minimum. The bridgewire is much smaller in diameter than the pins, thus making it the high resistance element in the electrical circuit.

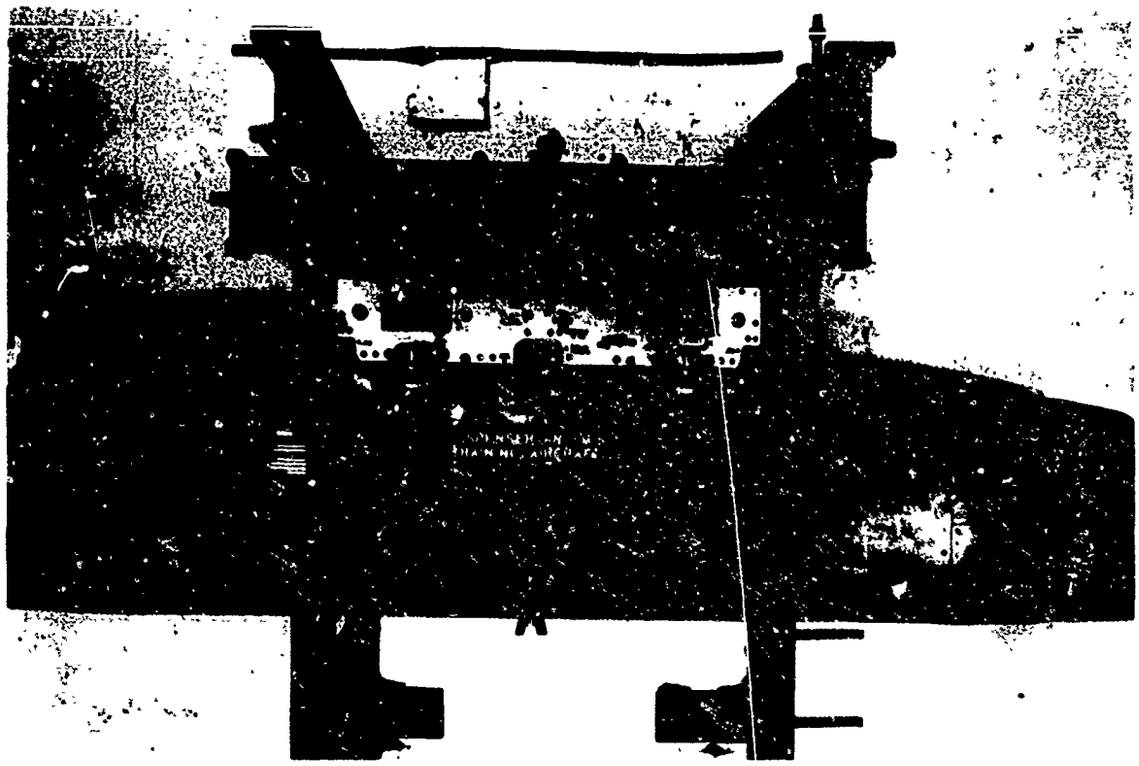

FIG. 6. SUU-38 Suspended In Ejection Fixture

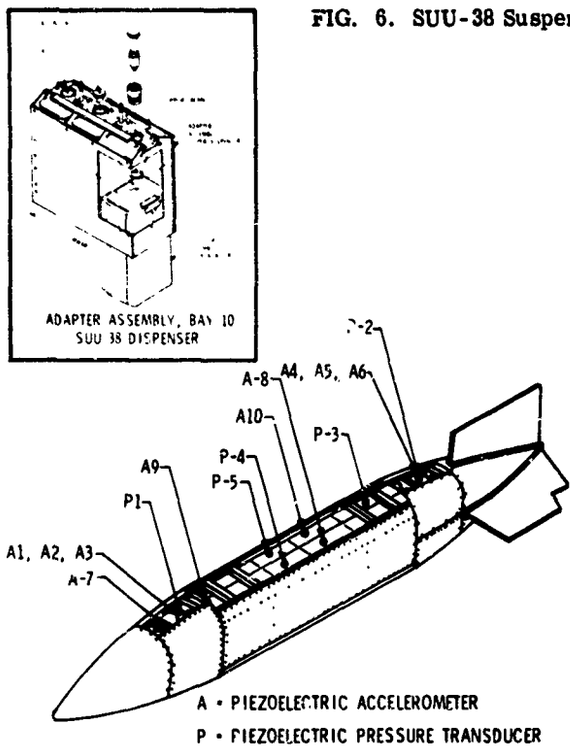

FIG. 7. Test Instrumentation Location

The ejection sequence was the same as the operational ejection sequence, which is automatically controlled by the intervalometer during in-flight ejections. During this sequence canisters are ejected from the aft, center, and forward sub-bays in each adapter. The bay-to-bay ejection sequence is designed to minimize the dispenser center-of-gravity shift during canister ejections. Table 1 illustrates the sequence employed during the pressure cartridge shock environment ejection tests. The second and third ejections were erroneously performed out of sequence. Based on subsequent review of all shock transients in other bays, this error had no significant effect on the validity of the data acquired in bay 10.

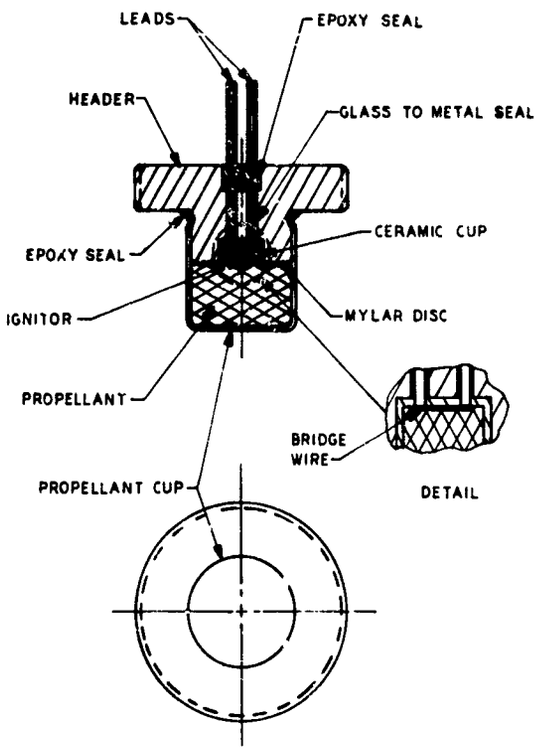

FIG. 5. Pressure Cartridge Construction (Typical)

5. Ejection Event Description

An electrical signal of the proper voltage heats the bridgewire, initiating the ignitor mixture which ignites the primary propellant in the cartridge. After the ignition is started, the propellant cup on the bottom of the cartridge bursts, allowing the gases to expand into and pressurize the thruster body and piston volume. The piston area exposed to the pressure is 0.635 square inch. At about 1400 psi, the gas pressure causes the segmented flange sections on the piston to bend inward and fail, allowing the piston assembly to be pushed through the thruster body. The 22 pound canister assembly and piston are then accelerated to a velocity of 27 to 34 feet-per-second over a piston stroke of 1.25 inches.

The peak pressure attained during ejection from the dispenser ranges from 7000 to 8000 psi. The corresponding peak ejection force range is from 4380 to 5000 pounds. The normal pressure pulse duration is from 7 to 8 milliseconds.

Once the piston starts moving through the thruster body, the upward reaction force on the thruster body causes it to move rapidly upward for a distance equal to the gap of 0.003 to 0.021 inch at the snap ring. The resulting impact with the bottom of the adapter beam contributes to the high frequency energy observed on adjacent pressure cartridge responses, as described in the following sections.

TEST PROCEDURE

A laboratory test was performed to measure the shock environment produced by cargo ejection. A full-scale SUU-38 dispenser with inert canisters was suspended from a MAU-12 bomb rack in an Explosives Test Laboratory (Fig. 6). The suspension arrangement locally simulates the store configuration when it is carried on the center-line station of a jet aircraft. Since the primary purpose of this test was to measure the pressure cartridge shock environment generated by canister ejection, only the pressure cartridge headers were instrumented.

The suspended dispenser was instrumented with ten piezoelectric accelerometers (see Fig. 7). Piezoelectric pressure transducers were used to measure pressure-time histories of five of the cartridges, shown as P1 through P5 in Fig. 7. The accelerometers were attached using both steel screws and dental cement. Transducer outputs were signal conditioned by charge amplifiers and the data were recorded on magnetic tape at a speed of 120 ips (Standard IRIG Mode, ±40 percent deviation, 0 - 20 kc frequency response). Along with the ten data channels (the appropriate pressure transducer output was recorded only when the monitored pressure cartridge was fired), a constant 1000 cps time base and an event pulse signaling initiation of current flow through the cartridge bridgewire were recorded on the 1-inch magnetic tape.

The test sequence consisted of ejecting canisters in the single step mode. Using this procedure, only one of the pressure cartridge firing circuits was energized at a time, and the fire signal was initiated manually. After each ejection, the firing line was attached to the next cartridge to be fired, and the instrumentation was inspected visually.

DATA ANALYSIS

Preliminary review of the tape recorded data was performed by examining expanded oscillograms of the acceleration and pressure time histories. Even though the data acquisition and recording system bandwidths were on the order of 20 kc, all the data were low pass filtered at 5 kc during playback. The low pass cutoff frequency corresponds to 20 percent of the test accelerometer's natural frequency.

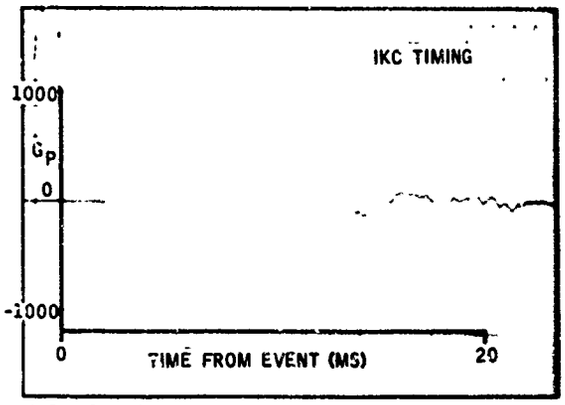

FIG. 8. Shock Response on Fired Cartridge (A3, Run 5)

Fig. 8 shows the shock time history from measurement location A3 (vertical) as the pressure cartridge to which the measuring accelerometer was mounted was fired. By comparison, the response at the adjacent cartridge (measurement location A7) and in an adjacent bay (measurement location A9) are shown in Fig. 9 and 10. The pressure time history (P1) for the ejection is shown in Fig. 11.

Run	Bay Fired	Run	Bay Fired
1	Aft Bay 10	19	Aft Bay 8
2	Fwd Bay 10	20	℄ Bay 8
3	℄ Bay 10	21	Fwd Bay 8
4	Aft Bay 10	22	Aft Bay 3
5	℄ Bay 10	23	℄ Bay 3
6	Fwd Bay 10	24	Fwd Bay 3
7	Aft Bay 1	25	Aft Bay 7
8	℄ Bay 1	26	℄ Bay 7
9	Fwd Bay 1	27	Fwd Bay 7
10	Aft Bay 1	28	Aft Bay 4
11	℄ Bay 1	29	℄ Bay 4
12	Fwd Bay 1	30	Fwd Bay 4
13	Aft Bay 9	31	Aft Bay 6
14	℄ Bay 9	32	Fwd Bay 6
15	Fwd Bay 9	33	Aft Bay 5
16	Aft Bay 2	34	℄ Bay 5
17	℄ Bay 2	35	Fwd Bay 5
18	Fwd Bay 2		

TABLE 1. Dispenser Ejection Sequence

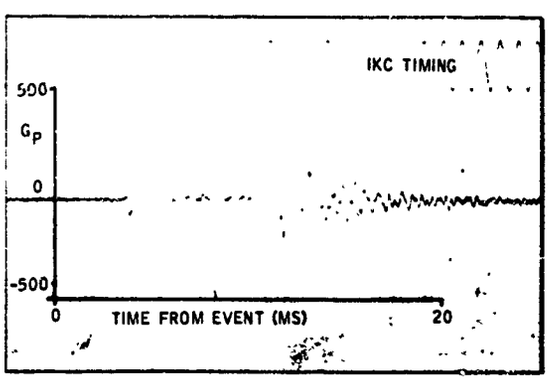

FIG. 9. Shock Response on Adjacent Cartridge (A7, Run 5)

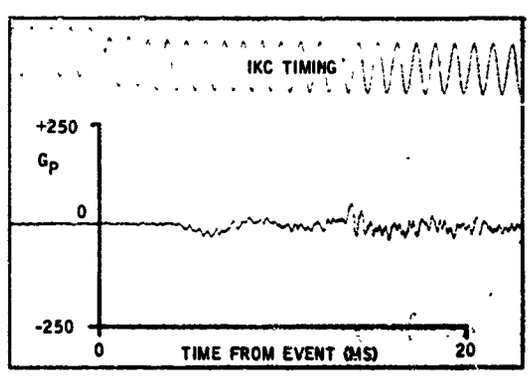

FIG. 10. Shock Response on Cartridge in Adjacent Bay (A9, Run 5)

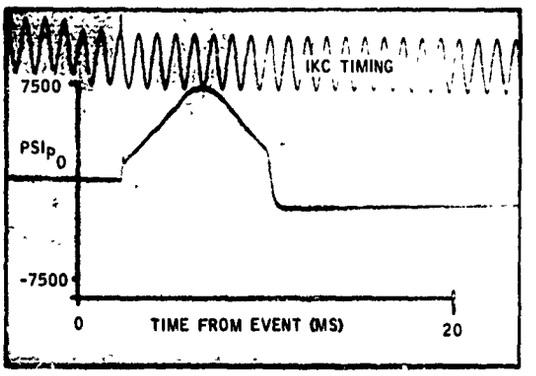

FIG. 11. Pressure Time History Measurement P1, Run 5

It was apparent from even a preliminary review of the data that significant shock levels were being generated by adjacent pressure cartridge firings; it was possible for a given cartridge to be exposed to this operational environment twice before it had to function successfully. Fig. 12 shows this situation in the acceleration time history of measurement location A3 during aft canister function in bay No. 10, and Fig. 13 repeats it as the center canister was functioned.

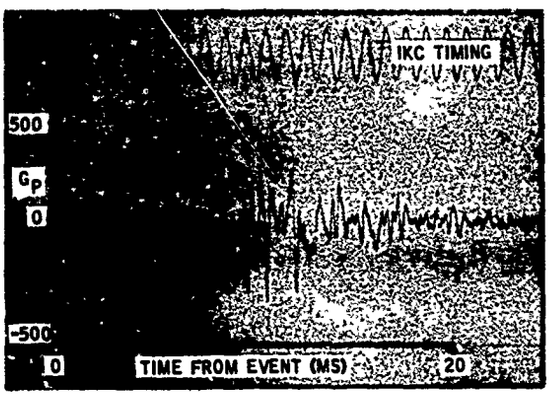

FIG. 12. Shock Response on Forward Cartridge When Aft Cartridge is Fired (A7, Run 4)

CRITERIA DEVELOPMENT

Because the measured levels exceeded the existing shock test criteria for the vendor supplied pressure cartridges, it was decided to revise these criteria to be more consistent with the measured environments. All the adjacent cartridge and bay composite time histories were reviewed, and the three most

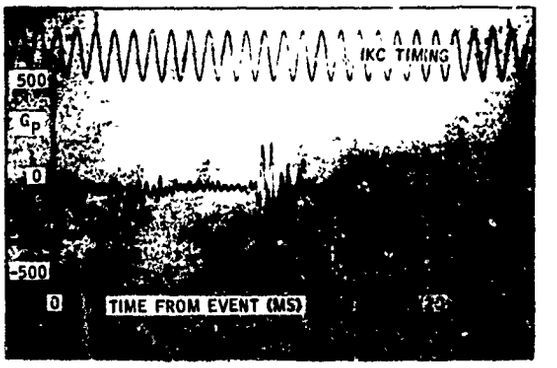

FIG. 13. Shock Response on Forward Cartridge When Center Cartridge is Fired (A7, Run 5)

significant amplitude responses were chosen for further analysis. These time histories, (see Fig. 14), were analyzed using the digital shock spectrum program, SFSPEC, to produce their respective undamped shock and Fourier magnitude spectra (Fig. 15 through 17). The computer program solves the response equation for a single degree-of-freedom system excited by the shock time history. The absolute maximum response at each natural frequency incrementally assigned to the single degree-of-freedom system constitutes the shock spectrum. Two types of analysis were chosen because both an impulse shock machine test criteria and an electrodynamic vibration machine shock synthesis were desired.

The requirement for an impact shock test criteria was based on the fact that the pressure cartridges are supplied by vendors who do not possess sophisticated shock test equipment. The Fourier magnitude spectra of three classical wave shapes which can be produced by most commercial impact shock machines were examined. Of the spectra examined, it was found that a half-sine pulse spectrum most closely fit the worst-case Fourier magnitude composite spectrum from the measured data. The fit of the spectrum for an 800 g (peak), 0.2 msec duration half-sine pulse is illustrated in Fig. 18. While these test criteria are an overtest in the low frequency portion of the spectrum, they are a distinct improvement over the previous 30 g (peak), 11 msec half-sine test criteria.

A6, Run 7

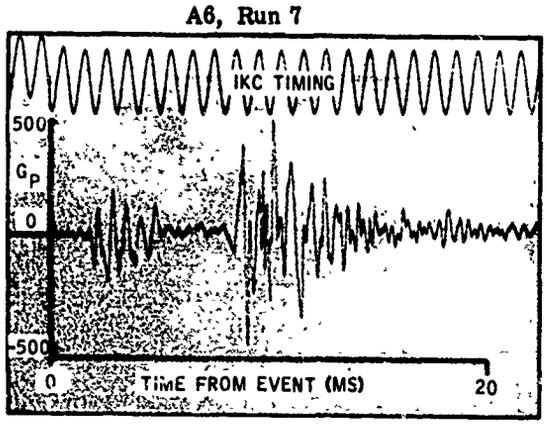

A3, Run 1

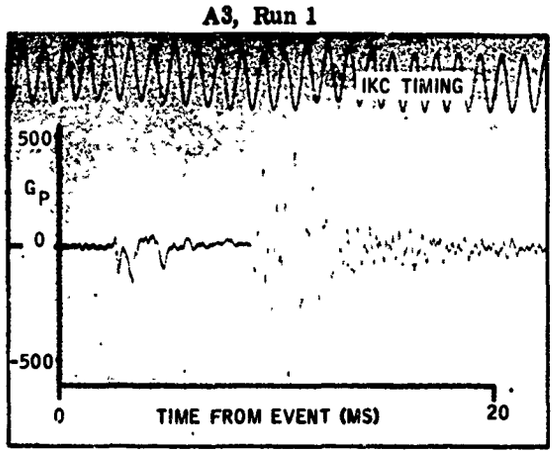

A8, Run 4

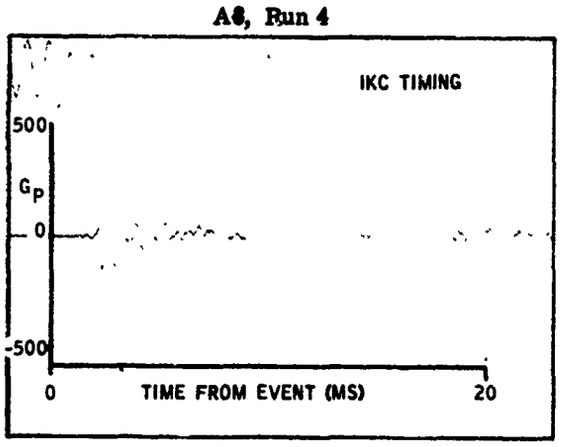

FIG. 14. Three Most Significant Time Histories Chosen for Spectral Analysis

A review of the shock spectra of the data acquired in all three axes indicated that the longitudinal and transverse axis data were generally lower at all frequencies than the vertical axis data. This same trend was exhibited in the time histories of these measurements.

An evaluation of the operational environment of the pressure cartridge dictated the use of two half-sine shocks in each of the six principal axes of the pressure cartridge. The improved shock test criteria are compatible with the present pressure cartridge construction and will provide the needed quality assurance that future mechanical changes or defects will be detected by the shock test.

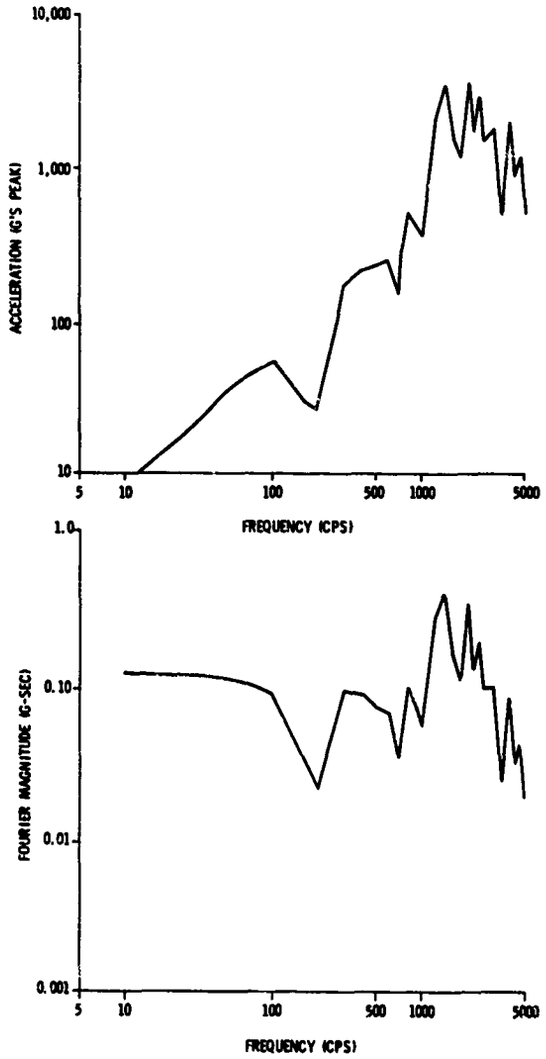

FIG. 15 Shock and Fourier Magnitude Spectra for Measurement A3, Run 1

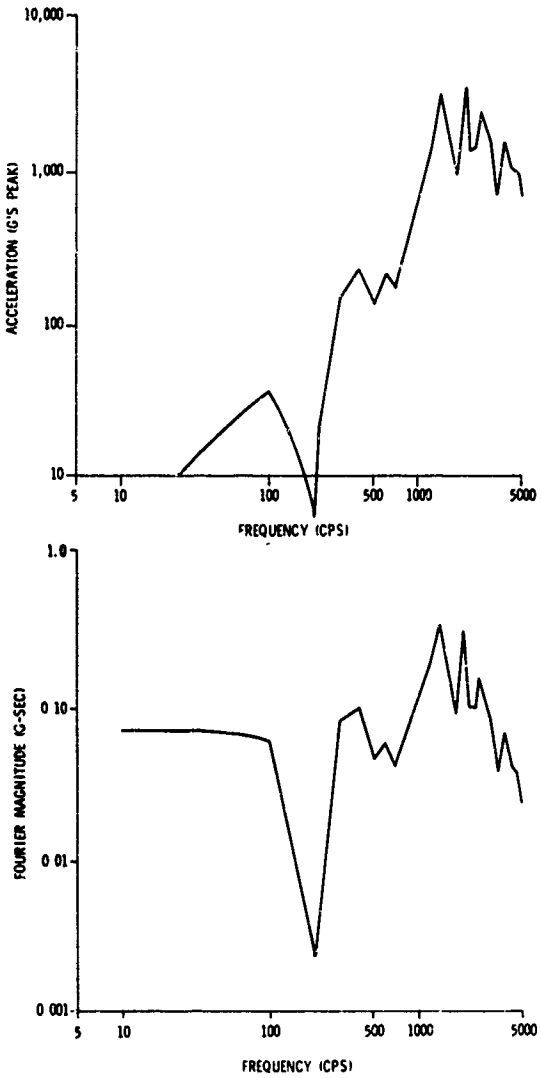

FIG. 16. Shock and Fourier Magnitude Spectra for Measurement A3, Run 4

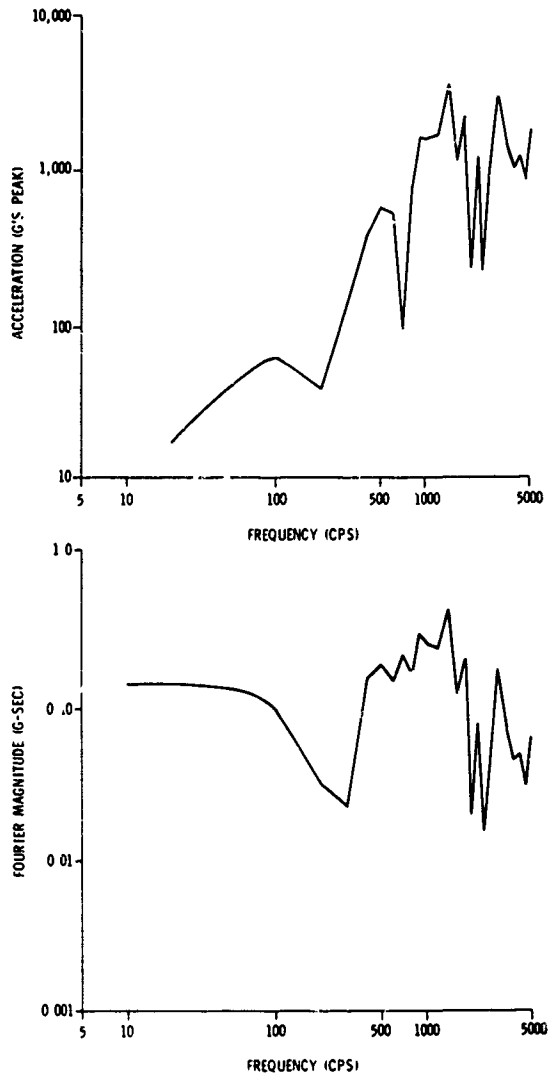

FIG. 17. Shock and Fourier Magnitude Spectra for Measurement A6, Run 7

An equivalent damage test criteria was also desired for use in subsequent product improvement. The simulation criterion can be used to reproduce the measured responses during laboratory tests on an electrodynamic vibration exciter. The criterion was generated by enveloping the undamped shock spectra of the three previously selected time histories as illustrated in Fig. 19.

COMPARISON OF EJECTION SHOCK AND MIL-STD-810B SHOCK TEST

The differences between the ejection shock environment and the shock response due to application of the MIL-STD-810B crash shock test to the dispenser is exemplified in Fig. 20. The crash shock spectrum was calculated from the accompanying time history response which was measured in the end bay of a full scale TFD dispenser that was subjected to a 30 g (peak), 11 msec, half-sine shock applied through the store/aircraft interface.

The reduced data spectrums point out the extreme spectral differences in the two environments. These differences are significant insofar as the pressure cartridge is concerned since its size and rigidity imply high resonant frequencies.

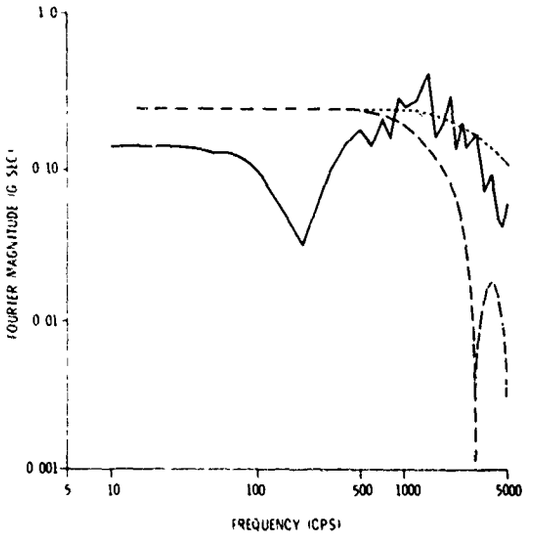

FIG. 18. Worst-Case Composite Fourier Magnitude Spectrum (——) vs 800-g (peak) Half-sine of 0.2 msec Duration (----) and 0.5 msec Duration (– – –)

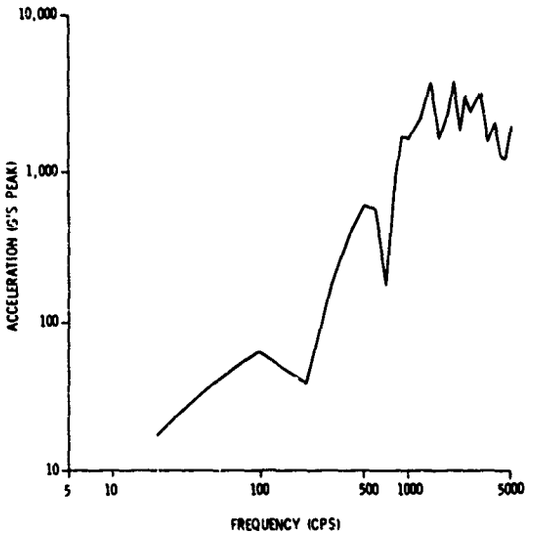

FIG. 19. Worst-Case Composite Shock Spectrum

POSSIBLE APPLICABILITY OF SUU-38 EJECTION SHOCK DATA TO SIMILAR SYSTEMS

Based on design experience with a number of other aircraft dispenser ejection mechanisms, each ejection mechanism design has certain unique features which can be expected to generate a distinct ejection shock spectrum on adjacent structure or canisters. For example, it would be of academic interest to conduct a similar ejection response measurement and analysis program on the SUU-38 dispenser using a modified thruster body which is rigidly attached to the adapter beams. The elimination of the thruster body-retention ring gap, shown

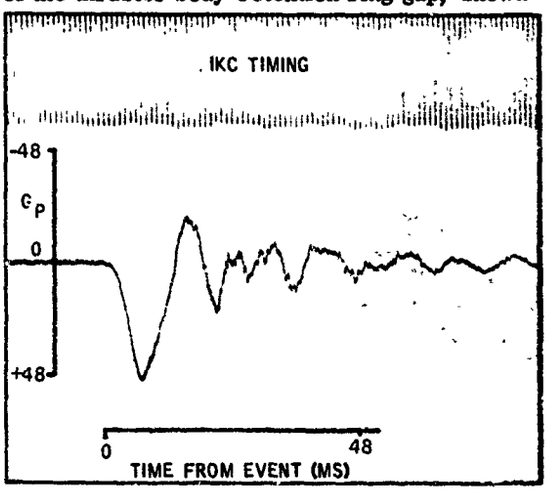

FIG. 20a. Shock Response of Dispenser End Bay to 810B Crash Shock

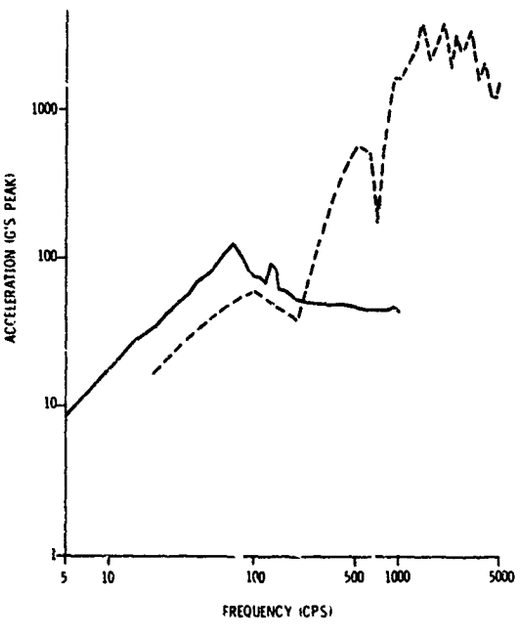

FIG. 20b. Shock Spectrum Comparisons Crash Shock Response (——) and Composite Ejection Response (– – –)

in Fig. 4, should reduce the high frequency shock spectrum levels. This change is not practical due to other considerations; furthermore, the existing SUU-38 retention ejection mechanism performs satisfactorily in the present environment.

The SUU-38 ejection shock response spectra should not be indiscriminantly used for other dispenser ejection mechanisms because of the unpredictable effect of seemingly insignificant hardware differences between dispenser ejection mechanisms. It is more realistic to develop individual shock response spectra and test criteria for each dispenser system unless ejection shock spectra are available for a number of similar dispenser ejection mechanisms.

CONCLUSIONS

1. The self-generated shock environment produced by dispenser ejection is the dominant shock environment experienced by the pressure cartridge. By comparison crash shock test levels (Fig. 20) contain relatively little energy in the high frequencies.

2. The shock environment produced by canister ejection is a highly localized phenomenon and only transmits significant energy to cartridges mounted on the same adapter thruster beam. There is no significant shock transmission to adjacent bays within a dispenser. Similarly, the lack of damage to the cargo in the canisters remaining in the functioned adapter indicates that the induced shock levels in the cargo are attenuated by the canister assembly.

3. The best fit Fourier magnitude curve of Fig. 18 suggested an optimum half-sine pulse duration of 0.2 msec. It was found, however, that the control limitations of commercial shock machines as well as problems with the test fixture's resonant frequencies made the use of a half-sine duration of 0.5 msec more practical. While the 0.5 msec, 800 g (peak) half-sine Fourier magnitude spectrum is not as good a fit as the 0.2 msec spectrum (also shown in Fig. 18), it is still a considerable improvement over the original 30 g (peak) 11 msec, half-sine criteria.

4. The adjacent canister ejection shock test described in this paper should be considered unique to the SUU-38 system. Individual ejection shock test criteria should be developed for other dispenser ejection mechanisms because of the influence of unique hardware differences on the shock spectra.

ACKNOWLEDGEMENTS

This work was supported under Air Force Contract Number F08-635-70C-001.

DISCUSSION

Mr. Zell (Picatinny Arsenal): What did the time history for the basic propulsion force of the cartridge look like? What was its overall duration?

Mr. Denton: The overall duration of the pressure level?

Mr. Zell: Right. In other words what did the force-time history look like for the basic ejection force created by the cartridge?

Mr. Denton: The duration of the half-sine pulse was approximately a half millisecond and the peak pressure was about 14,000 psi.

Mr. Zell: At one point we were testing something that mounted to the cannister, and at the time there was a question whether the ejection shock was affecting its operation. An attempt was made to simulate the pressure-time history and, as I recall, a pulse was on the order of 20 milliseconds in total duration and it was a skewed half sine. Apparently there is a difference in the basic pulses.

Mr. Herzing: I have the paper in my hand so maybe I can answer your question a little better. We do include the pressure-time history for the pressure cartridge for that measurement. It is about 61/2 milliseconds duration, 7500 psi and it is more of a haversine shape with a very sharp leading edge. I think, if you will recall the time-history of the acceleration measurement, it had a little glitch in the time-history initially, and that died down. Then there was the larger part of the time history and the little initial glitch correlates timewise with the steep rise on the pressure cartridge. We have definitely identified the characteristic frequencies in the acceleration shock spectra as being due to local structural response.

SHOCK LOAD RESPONSE OF AN ELASTIC ANNULAR PLATE

ON A DISTRIBUTED FOUNDATION

John R. Mays
Department of Civil and Environmental Engineering
University of Colorado, Denver, Colorado

and

James E. Nelson
Space System Dynamics
Martin Marietta Corporation, Denver, Colorado

Effects of system parameter variation on response spectra of an elastic annular plate supported by a distributed foundation when loaded by a dynamic pulse are presented.

INTRODUCTION

This paper presents a method of analysis for the response of an elastic annular plate on a distributed foundation subjected to a transverse force pulse applied at the inner edge of the plate. The pulse shape is a sine function of time having one-half cycle duration. The plate and the foundation have separate force-deformation characteristics. The effects of varying stiffnesses, pulse duration, and the ratio of inner to outer radii are presented. A finite difference technique is used to solve the nonlinear differential equations.

The effects of parameter variation are pictured by use of families of curves (response spectra), and results are shown in dimensionless form.

PROBLEM STATEMENT AND ANALYSIS

An elastic annular plate of uniform properties supported by a Winkler [1] foundation of negligible mass is shown in Fig. 1. The symmetric plate with inner radius b, outer radius a, and uniform thickness h is loaded uniformly along the inner surface by a sinusoidal shock load of amplitude I_0, duration t_1, and circular frequency ω. See Figs. 2 and 3.

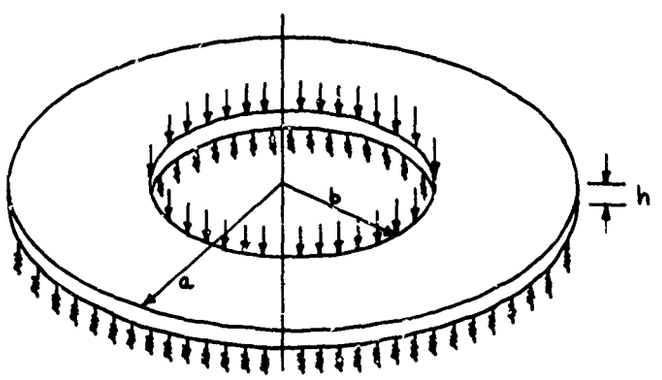

Fig. 1 - Elastic Annulus on Elastic Support

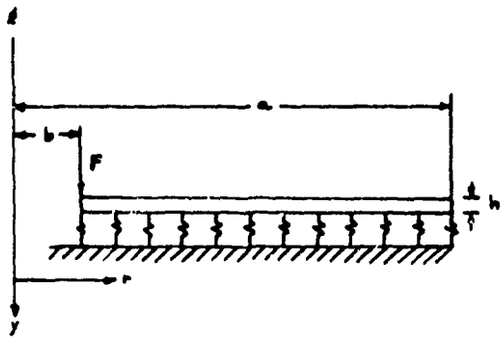

Fig. 2 - Elastic Annulus on Elastic Support

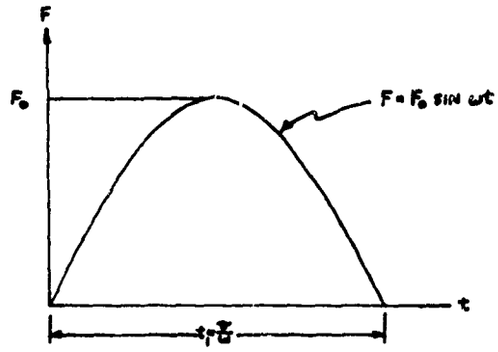

Fig. 3 - Force Pulse

The mode shape associated with the fundamental frequency is the rigid body mode corresponding to the limiting infinitely stiff plate [2]. The fundamental period (T_1) for the elastic system can be shown to be

$$T_1 = 2\pi\sqrt{\mu/q} \qquad (1)$$

where μ is the mass per unit area of the annular plate and q is the foundation modulus (intensity of reaction for a unit of deflection) [3]. Circumferential modes are not excited because of the symmetry of the plate and its loading.

The second order nonlinear partial differential equation of motion for the plate foundation system can be written as,

$$\frac{\partial^2 y}{\partial t^2} = \frac{1}{\mu}\left[\frac{2}{r}\frac{\partial M_r}{\partial r} + \frac{\partial^2 M_r}{\partial r^2} - \frac{1}{r}\frac{\partial M_\phi}{\partial r} - qy\right] \qquad (2)$$

where y and r represent the displacement and radial coordinates respectively, M_r and M_ϕ represent the radial and tangetial plate bending moments, and t represents time.

In order to express the problem and its solution in nondimensional form, the following dimensionless variables are defined:

Radial Coordinate	$\bar{r} = r/a$	
Displacement	$z = y/y_o$, where $y_o = \dfrac{F_o}{q\pi(a^2 - b^2)}$	
Time	$\tau = t/t_1$	
Radial Moment	$\bar{M}_r = M_r/F_o$	
Tangential Moment	$\bar{M}_\phi = M_\phi/F_o$	(3)
Radial Curvature	$\bar{\kappa}_r = \kappa_r/\kappa_o$, where $\kappa_o = \dfrac{12F_o}{Eh^3}$	
Tangential Curvature	$\bar{\kappa}_\phi = \kappa_\phi/\kappa_o$	

where E represents Young's Modulus for the plate, κ_r and κ_ϕ represent curvatures in the radial and tangential directions. The displacement reference quantity y_o is the rigid body displacement of the system when loaded statically by the force F_o. Assuming Poisson's ratio to be one-half, the governing differential equation when cast into nondimensional form becomes:

$$\frac{\partial^2 z}{\partial \tau^2} = 4\pi^3(1-\gamma^2)(T^2)\left\{\frac{\partial^2 \bar{M}_r}{\partial \bar{r}^2} + \frac{2}{\bar{r}}\frac{\partial \bar{M}_r}{\partial \bar{r}} - \frac{1}{\bar{r}}\frac{\partial \bar{M}_\phi}{\partial \bar{r}} - \frac{z}{\pi(1-\gamma^2)}\right\} \qquad (4)$$

where:

$$\bar{M}_r = \frac{2}{3}\left(2\kappa_r + \kappa_\phi\right) \qquad (4a)$$

$$\bar{M}_\phi = \frac{2}{3}\left(\kappa_r + 2\kappa_\phi\right) \qquad (4b)$$

$$\bar{\kappa}_r = \left(\frac{S}{\gamma^2-1}\right)\frac{\partial^2 z}{\partial \bar{r}^2} \qquad (4c)$$

$$\bar{\kappa}_\phi = \left(\frac{S}{\gamma^2-1}\right)\frac{1}{\bar{r}}\frac{\partial z}{\partial \bar{r}} \qquad (4d)$$

and s, γ, t are nondimensional system parameters defined in Table 1.

TABLE 1

Definition of System Parameters		
Ratio	Symbol	Terminology
$\dfrac{t_1}{T_1}$	T	Pulse Duration Ratio
$\dfrac{Eh^3/12}{q_1 a^4}$	S	Component Stiffness Ratio
$\dfrac{b}{a}$	γ	Radii Ratio

The obvious boundary conditions consist of zero values for shear and moment at the outer boundary and zero moment at the inner face. The forcing function is used to determine the shear at the inner face boundary.

The governing equation was expressed with the moment terms clearly isolated so that the case of the inelastic plate could be easily studied by replacing the elastic moment-curvature functions (4a) and (4b) by a definition of the moment-curvature relations for a particular yield theory.

NUMERICAL PROCEDURE

In order to solve the partial differential equation of motion, the plate is divided into N annular elements each with equal radial dimensions. If the displacement z at each point were known at a given time τ, then a finite-difference formulation of equations (4) and consideration of the boundary conditions provide values for the acceleration term, $\partial^2 z/\partial\tau^2$, at each element. These in turn are integrated over a small step in time, $\Delta\tau$, to obtain new values for displacements. The entire process is repeated continually until solutions of z, $\bar{M}_r$, and $\bar{M}_\phi$ versus τ are obtained for particular values of the system parameters γ, T, and S.

A Fortran IV program was run on the Control Data Corporation 6400 computer system at the Graduate School Computing Center of the University of Colorado. This program sought maximum values of z, $\bar{M}_r$, and $\bar{M}_\phi$ (z_{max}, $\bar{M}_{r\,max}$, and $\bar{M}_{\phi\,max}$) within a time period from initiation of the pulse to one fundamental period beyond pulse to one fundamental period beyond pulse termination ($0 \leq \tau \leq t_1 + T_1$) and along a radius ($b \leq r \leq a$). Therefore, maxima discussed in this paper refer to the maxima occurring at any point within the plate during this period of time.

The accuracy of the numerical solution for a given set of system parameters depend upon values of N and $\Delta\tau$. It was found that the selection of the time step for the integration procedure was critical; so that, once a time step was found to cause the procedure to converge, any smaller steps did not appreciably change the results. Such a fortunate conclusion could not, however, be reached in the case of varying the number of divisions. Figs. 4, 5, and 6 demonstrate the effect of N on convergence of z, $\bar{M}_r$, and $\bar{M}_\phi$ for particular values of T, γ, and S. Because the convergence was slow with N and because the computing expense increases rapidly with increasing N, a method of projecting the convergence was determined. In general, the finite-difference expressions used in the numerical procedures were three-point, central differences whose error term is inversely proportional to the square of N. Therefore, given data for two values of N, the value at $N \to \infty$ could be calculated with confidence. The accuracy versus savings in computational effort of this extrapolation can be demonstrated by consideration of the data available from Figs. 4, 5, and 6. Two asymptotes corresponding to values projected from data at N's of 18 & 24 and 30 & 40 are shown in each of the three figures. The cost of obtaining the 30 & 40 projection is five times that for the 18 & 24 projection while their values differ by 1%, 2%, and 2.5% respectively for z_{max}, $\bar{M}_{r\,max}$, and $\bar{M}_{\phi\,max}$.

VERIFICATION

Checks on the analysis are provided by consideration of limiting values of the system parameters γ, S, and T. As the ratio of inner

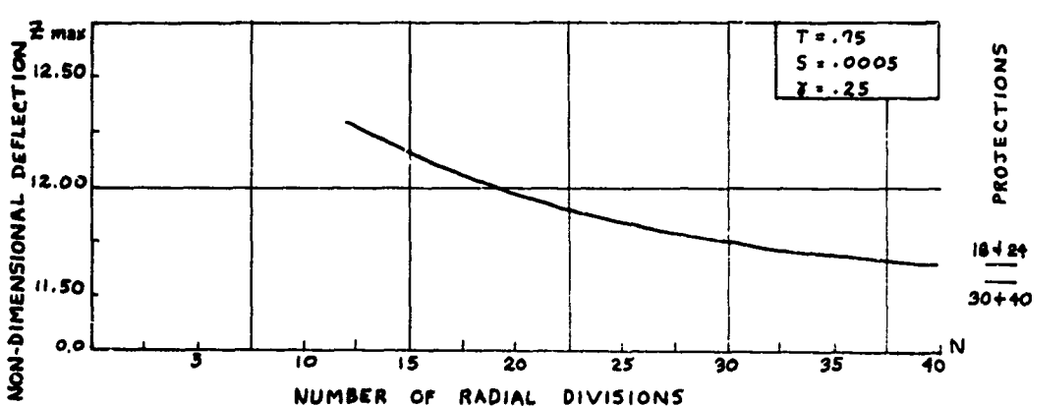

Fig. 4 - Convergence of Solution (z) with N

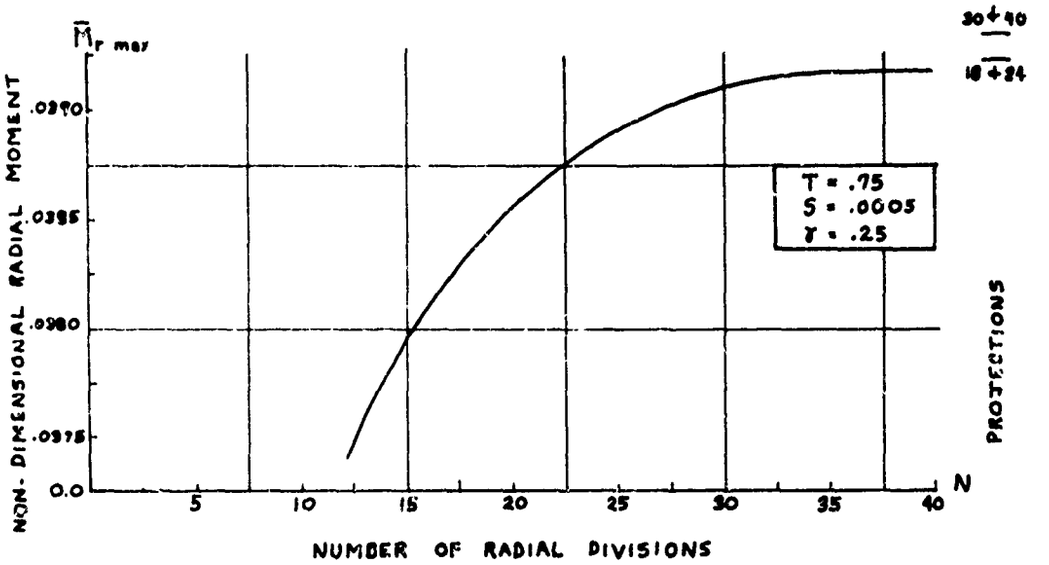

Fig. 5 - Convergence of Solution ($\bar{M}_r$) with N

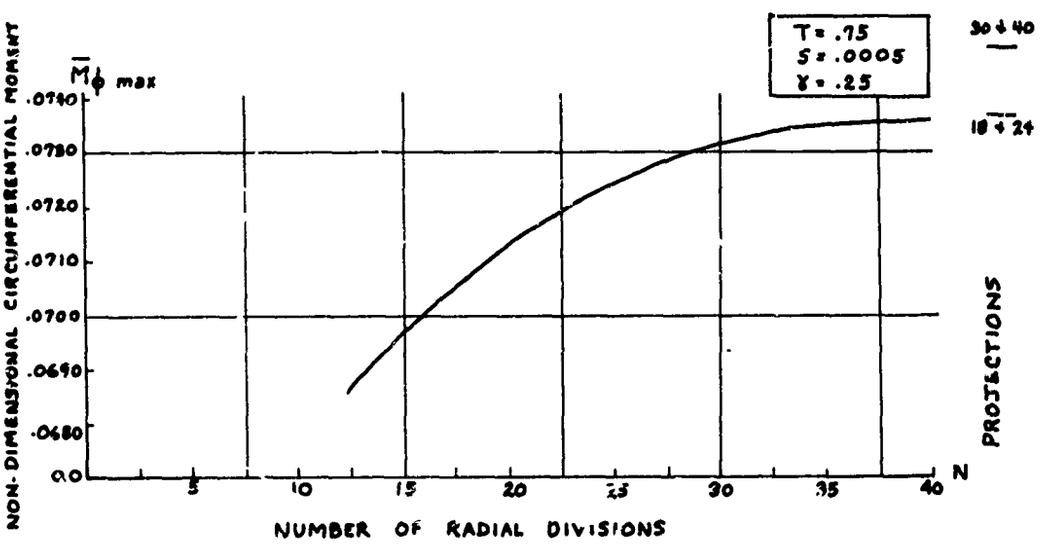

Fig. 6 - Convergence of Solution ($\bar{M}_\phi$) with N

radius to outer radius (γ) approaches unity, the system degenerates into the less complicated case of a ring on a foundation. This single degree-of-freedom problem is easily analyzed for maximum moments and deflections. If S is assigned a value of 0.001, T a value of 0.5, and γ a value of approaching units, it can be shown that $z_{max} \to \frac{\pi}{2}$, $\bar{M}_{r\,max} \to 0$, and $\bar{M}_{\phi\,max} \to \frac{1}{4\pi}$. Figure 7 clearly indicates the convergence of z_{max}, $\bar{M}_{r\,max}$, and $\bar{M}_{\phi\,max}$ to limiting values as γ approaches unity.

As the Component Stiffness Ratio (S) increases without limit, the system approaches the single degree-of-freedom case of a rigid plate on an elastic foundation. Again, the maximum deflection is easily obtainable. Figure 8 is a semi-log plot of maximum deflection versus Component Stiffness Ratio for T = 0.5 and γ = 0.25. The convergence to π/2 as S increases is well defined.

Finally, as the Pulse Duration Ratio (T) increases without limit the dynamic case degenerates to a static loaded annular plate on an elastic foundation. The conventional use of the finite-difference technique was used to obtain these limiting values of z_{max}, $\bar{M}_{r\,max}$, and $\bar{M}_{\phi max}$ these values are plotted as asymptotes on the response spectra.

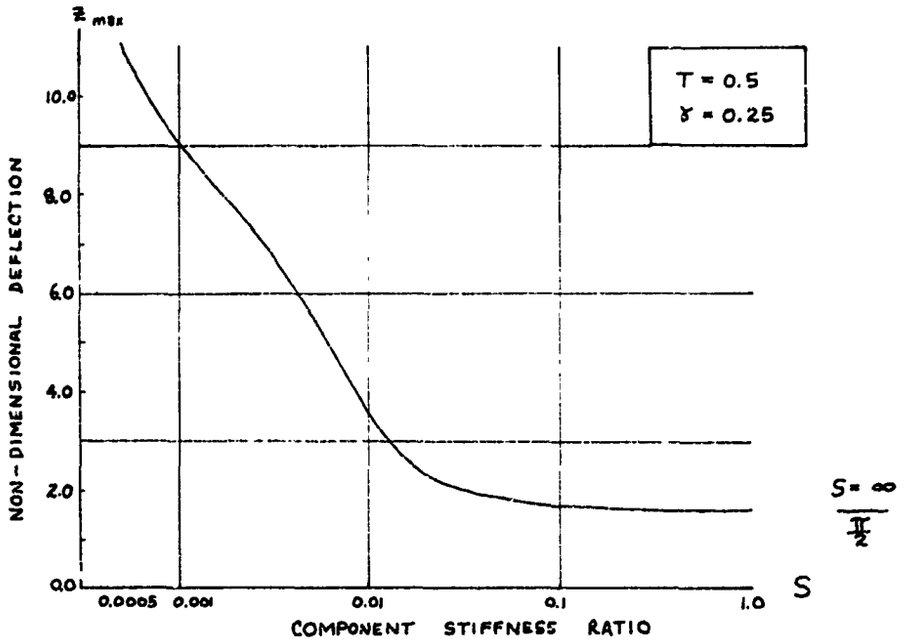

Fig. 7 - Convergence of Variables to Limits ($\gamma \to 1$)

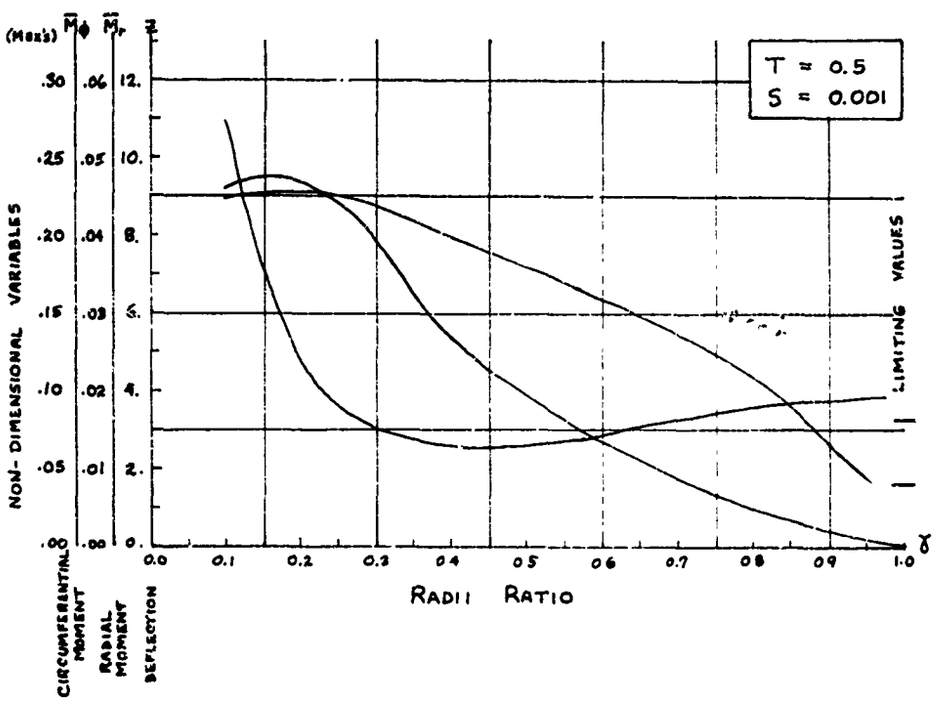

Fig. 8 - Conv ,ence of Solution ($\bar{z}$) with S

RESPONSE SPECTRA

The results of this investigation are perhaps most usefully presented in the form of response spectra, i.e., z_{max} versus T, $\bar{M}_{r\,max}$ versus T, and $\bar{M}_{t\,max}$ versus T. Response spectra provide the designer with the necessary information to predict maximum deflection, maximum radial moment, and maximum tangential moment for a given half wave sinusoidal pulse.

In order to depict the effect of the remaining two system parameters, γ and S, two sets of response spectra are drawn: one set holding γ constant and varying S as a family parameter (Figs. 9, 11, and 13); the other set holding S constant and varying γ as a family parameter (Figs. 10, 12, and 14). The constant values of $\gamma = 0.25$ and $S = 0.001$ were chosen from typical values of a, b, L, h, and q. Values used to plot the response spectra were projected using various values of N so that a consistent level of convergence was maintained.

CONCLUSIONS

The response spectra for deflection, radial moment, and tangential moment indicate consistent variation as the parameters are altered. A decrease in S results in a more flexible plate. This "softer" system results in larger deflections, smaller tangential moments, and somewhat less effect on radial moment. An increase in γ produces a plate of smaller dimension resulting in decreased curvature, therefore smaller deflections and smaller bending moments.

The maximax response, the maximum of the maxima for a given response quantity, for deflection of a single degree-of-freedom subjected to a one-half cycle sinusoidal pulse is known to be approximately 1.8 times the static deflection. The results of this paper indicate that similar maximax response for this multiple degree-of-freedom plate-foundation system may be many times that for the single degree-of-freedom system.

This study is part of a series of related studies of the response of nonlinear structural components to transient loadings [4, 5, 6, 7, 8, 9]. The results may be used in some specific cases of design or for a general understanding of plate-foundation response problems.

ACKNOWLEDGEMENT

This research was conducted under Research Initiation Grant GK 4813 from the National Science Foundation.

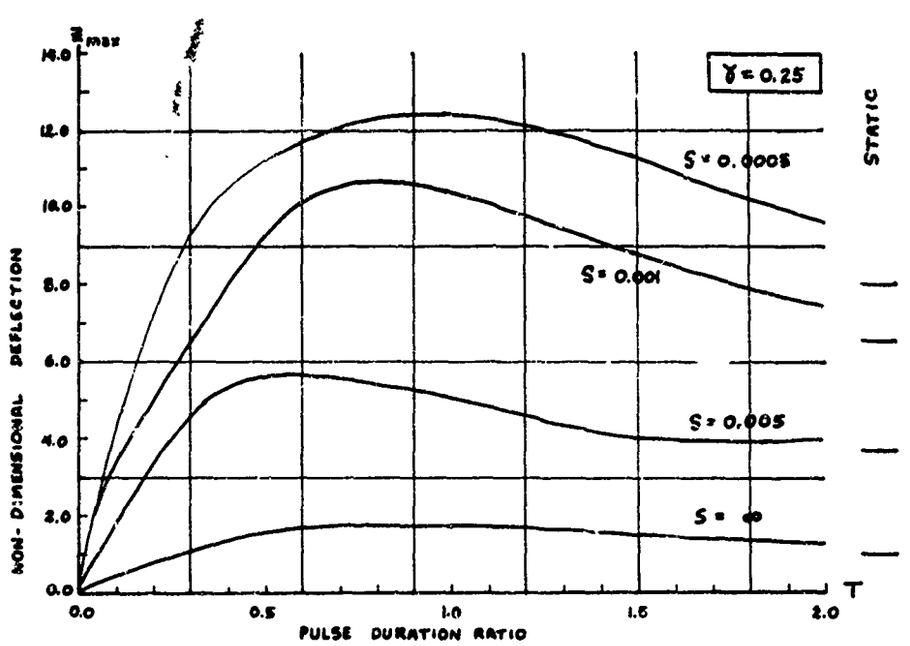

Fig. 9 - Response Spectra – Constant γ, Variable S

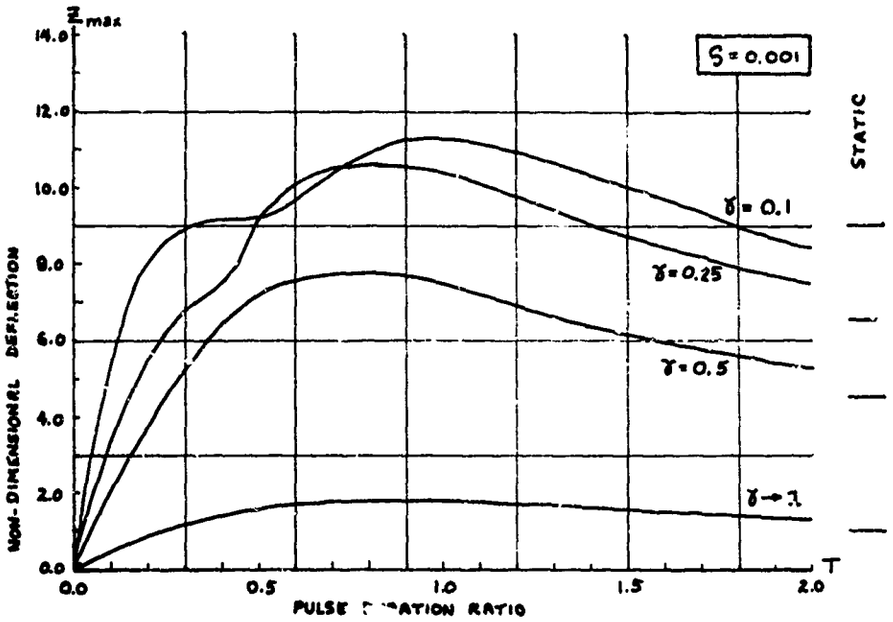

Fig. 10 - Response Spectra — Constant S, Variable γ

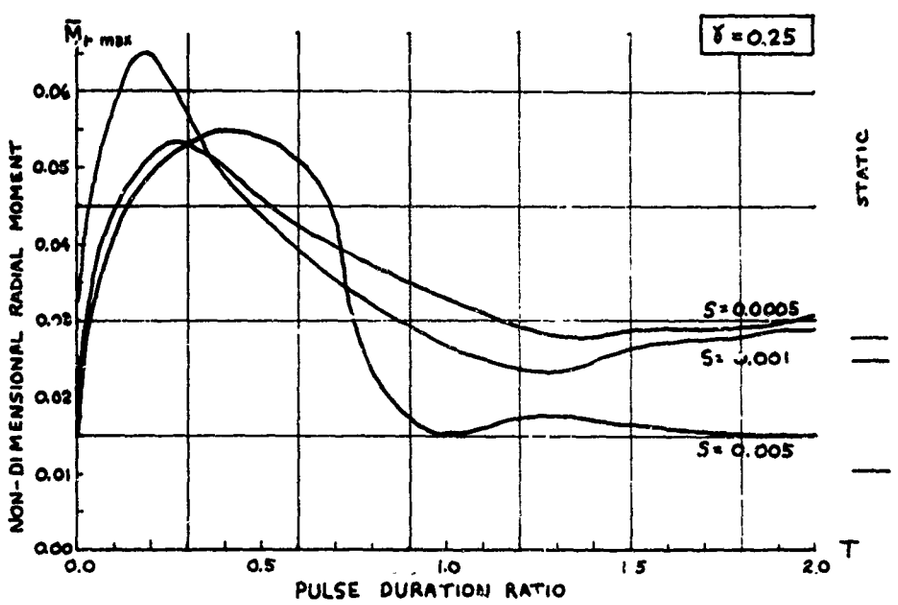

Fig. 11 - Response Spectra — Constant γ, Variable S

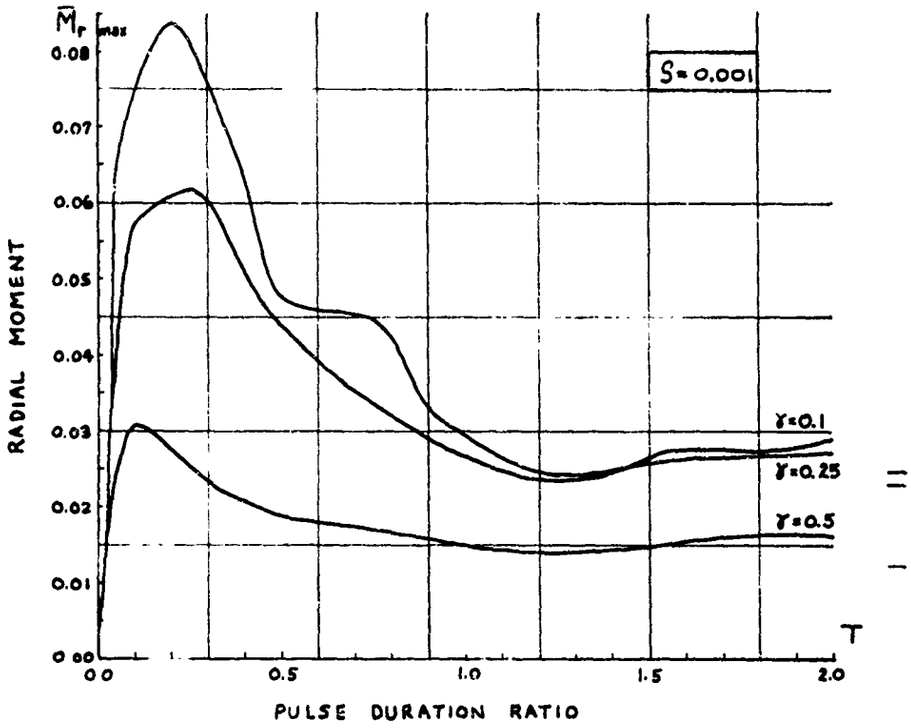

Fig. 12 - Response Spectra — Constant S, Variable γ

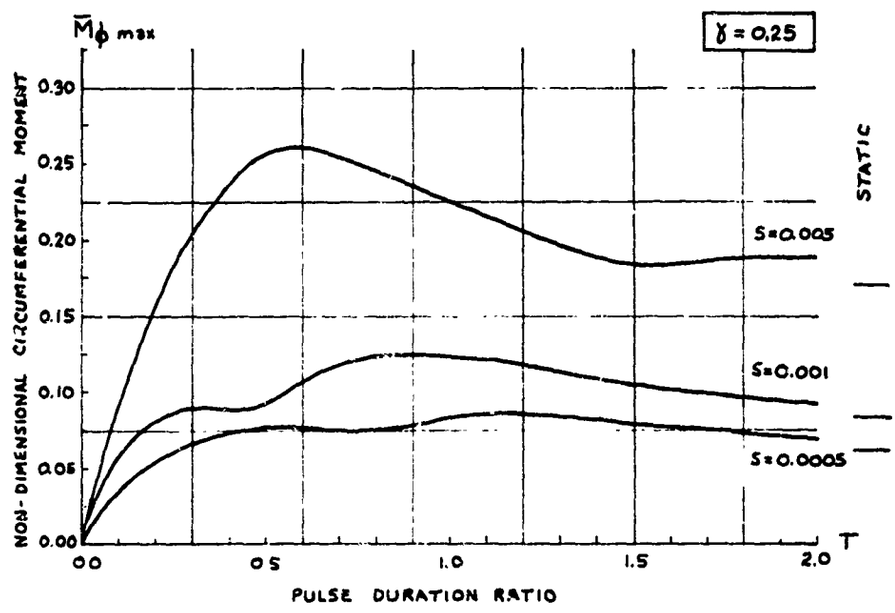

Fig. 13 - Response Spectra - Constant γ, Variable S

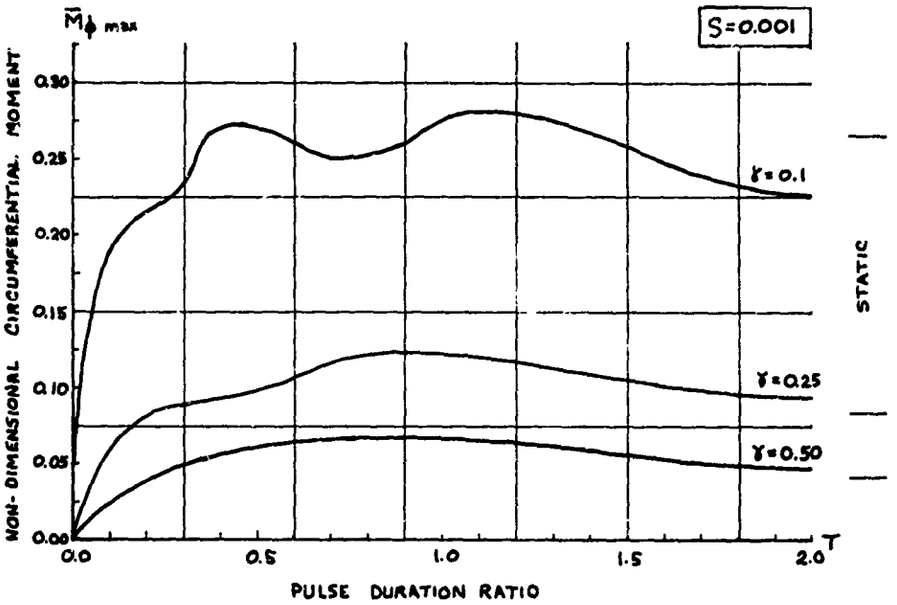

Fig. 14 - Response Spectra — Constant S, Variable γ

REFERENCES

1. E. Winkler, Die Lehre von der Elastizitat und Festigkeit, Prag, p. 182, 1867

2. J. W. Stafford, "Natural Frequencies of Beams and Plates on an Elastic Foundation with Constant Modulus," Journal of the Franklin Institute, vol. 284, pp. 262-264, Oct. 1967

3. S. Timoshenko and S. Woinowsky-Krieger, Theory of Plates and Shells, McGraw-Hill, New York, p. 259, 1959

4. J. R. Mays, "Propagation of Yielding in a Bilinear, Hysteretic, Beam and Distributed Foundation under Dynamic Pulse Loading," The Shock and Vibration Bulletin, Bulletin 40, Part 4, pp. 81-88, Dec. 1969

5. B. E. Burton, "Shock Response of an Elasto-Inelastic Beam on Elasto-Inelastic Supports," Thesis presented to the University of Colorado, July 1965

6. J. R. Mays and R. S. Ayre, "Shock Load Response of a Beam on a Distributed Foundation with Yielding, Bilinear, Hysteretic Action in Either Member," Proceedings, 10th Midwestern Mechanics Conference, pp. 681-701, Aug. 1967

7. T. R. Tauchert and R. S. Ayre, "Shock-Resistant Design of Simple Beams on Yielding, Nonlinear Supports," International Journal of Mechanical Sciences, Pergamon Press Ltd., Vol. 8, pp. 479-490, 1966

8. T. R. Tauchert and R. S. Ayre, "Shock Response of a Simple Beam on Nonlinear Supports," Journal of the Engineering Mechanics Division, A.S.C.E., Vol. 91, No. EM6, pp.91-109, 1965

9. A. B. Schultz, "Nonlinear Response of a Beam to Shock Pulse," Franklin Institute Journal, Vol. 276, No. 3, pp. 385-393, 1963

FRAGILITY

METHODOLOGY AND STANDARDIZATION FOR FRAGILITY EVALUATION

R. C. Rountree
Logicon
San Pedro, California

and

F. B. Safford
TRW Systems Group
Redondo Beach, California

Modern technology has broadened the meaning of the term fragility. Today it pertains to operational and functional aspects as well as to structural or packaging considerations. System and component hardness relative to dynamic environment is a concern to systems engineers and managers as well as to packagers and testers. Sophistication of modern and future systems and components has expanded the evaluation methods without maintaining any commonality between methods. A need for standardizing fragility methodology is shown to exist by means of examples from prior test and analytical endeavors. These samples point out that much analytical and experimental work is needed to relate fragility to parameters of wave shape and frequency content. This will permit fragility qualities to be abstracted to a wide range of dynamic environments. The examples further serve to emphasize a strong influence of environment on fragility and a need for fully understanding dynamic behavior of the system or component (subtle coupling between operational and structural modes may exist and models of this phenomena can be developed). A general philosophy of fragility methods is presented. The methodology is based on a knowledge of environment at free field, system, or component level; various interpretations of system or component interactions can be made. Standards tests are presented for shock, transient or vibration testing. Such tests will help accumulate data, provide statistical samples and indicate methods of upgrading. Techniques for enhancing decision processes for selecting off-the-shelf products are discussed. These include allocation of fragility budgets for components comprising a system and establishment of a controlled index of product/environment capability.

INTRODUCTION

Methods and standards are necessary for quantitatively measuring the ability of systems and system components to withstand dynamic environments. Systems and components herein refer in the broad sense to various equipments, process controls, humans, facilities, assemblies and parts. Dynamic environments considered for this paper involve mechanical shocks, transients, and vibrations. However, environments such as temperature, radiation and electromagnetic interference may be similarly treated in the total system picture either separately or as combined environments. The performance parameter selected to provide the quantitative measurement is termed fragility. Fragility is the threshold value of the dynamic environment at which the system/component exhibits operational failure, damage or malfunction[1].

Environmental effects on systems/components have consistently perplexed engineering designers. Means of evaluating these effects have covered a wide technological gamut[2]. Originally, a prime design consideration was the selection of materials to withstand various simple environments (e.g., static loads and impact). The advent of the missile/space age brought additional emphasis on determining the degradation of operational equipment performance when subjected to in-flight or ground environments[3,4,5]. The methods of evaluation therefore widened further.

Many of the systems requiring evaluation today include closed loop operations such as guidance equipment or process controllers. Furthermore, current ystem designs are incorporating failure detection computer software to enhance the system capability[6]. Evaluation methods involving test verifications of system performance are including on-line computing facilities[7,8]. These recent advances add more

dimensions to the evaluation picture. A need for standardizing fragility methodology clearly exists.

Knowledge of fragility or hardness levels permits an assessment to be made of an elementary component or complete system's probability of survival or vulnerability. Such assessments are made with respect to the expected dynamic environment. Fragility determinations also provide the following:

- Confirmation of system/component "weak links" early in the design cycle.
- Identification of unanticipated "weak links."
- Formal identification of the most critical fragile item in a system. This will provide an index of the system suitability for new applications or changed environments.
- Guidelines for upgrading fragility level.
- Minimization of needs for redesign, replacement and repair late in development cycles or even later in field usage.
- Datum basis for forensic applications, e.g., involving manufacturer/shipper/customer negotiations.

Standards for fragility determination are not without precedent. A beginning in formalizing fragility methods occurred with the publication of the Design of Vibration Isolation Systems(9,10) by the Society of Automotive Engineers in 1962. Since that time a committee was formed by the American National Standards Institute to develop a national fragility standard. That endeavor is still in progress*. Various individual attempts have been made to establish certain forms of fragility standards. For example, noise analysis and vibration were prescribed as indicators for preventive maintenance and for the acceptance of new equipment(11,12). Other attempts are being made by special interest groups such as the fragility standardization activities of the ASTM for packaging purposes(13,14,15). Current trends include legislative action to protect personnel from excessive noise exposure(16).

This paper summarizes some of the problems and objectives concerned with fragility standardization. Definitions are made regarding fragility/environment parameters and criteria. Specific examples indicating needs for different parameters and criteria are presented. The examples demonstrate the pitfalls of not recognizing the benefits or shortcomings of various simulation techniques. An initial approach to standardizing fragility is presented. Environmental simulation methods necessary to conduct this approach are outlined. These are based on previously and currently employed techniques. General comments are made regarding advantages of the methodology and the relationships between specific and general cases.

*Membership on the Fragility Standard Committee is open to those who have the interest and background to contribute.

FRAGILITY DEFINITIONS

Fragility of systems/components is categorized in terms of failure, malfunction and damage. These terms demonstrate that fragility is more comprehensive than expected after a cursory thought: its operational connotation extends the meaning well beyond structural breakage. However, even the fragility categories are subject to different interpretation in the range of technical fields involved. Therefore, the categories are defined as follows:

- Failure is defined as an irreversible environment-induced inoperative condition or operation outside of tolerances. Irreversible refers to the system/component remaining inoperative or out of tolerance after the environment is removed.
- Malfunction also represents an environment-induced inoperative condition or out-of-tolerance operation. However, the process is reversible, i.e., the system/component returns to satisfactory operation upon removal of the environment.
- Damage has multiple meanings. It may be considered as a mild form of failure (i.e., irreversible but borderline operation). It also represents permanent degradation in performance, reduction in hardness or survivability limitation. Damage also applies to system/component attributes that are unrelated to performance (e.g., damaged missile support resulting in tilted but unimpaired launch).

At least three versions of fragility arise in practice. Which of these is pertinent depends on the stage of the design cycle that exists or the state of knowledge of the system/component dynamic behavior. The fragility versions are discussed next.

Actual Fragility. Actual fragility(1) is defined as the dynamic environment magnitude and its variation with frequency and time which is just sufficient to cause failure, malfunction or damage. Below this limit is the hardness region, where systems/components are hard to the

environment. Figure 1 represents this concept in the form of a typical three-dimensional surface with uncertainty bands. The reduction in hardness along the time axis of Figure 1 is characteristic of fatigue. Such a fragility usually falls in the failure or damage category. Malfunctions are normally not long term duration dependent. They are sensitive to short term pulse rise time and system/component critical period relationships. When fragility is independent of time a two-dimensional plot of magnitude and frequency is appropriate.

Acceptable Fragility. If a specification states that a system/component must pass a given test to be qualified, the conditions of this test define the acceptable fragility surface. Parameters to designate acceptable fragility surfaces vary. One abscissa of the magnitude-frequency-time surface is often left to interpretation by prescribing a magnitude-time history. Alternately shock spectra together with a required number of repetitions are often specified[7]. It is pertinent that the ordinates of the acceptable fragility surface can at best be equal to or less than the ordinates of the actual fragility surface. This relationship is shown in Figure 2. However, unless the actual fragility is determined, it is impossible to determine if the difference between the two surfaces is large or small. Thus, the acceptable fragility surface establishes an arbitrary minimum and nothing more (unless a large number of test samples is involved). Use of probabilistic shock spectra would enhance this version[18,19].

Modeled Fragility. Early in the design cycle the system operations analyst usually attempts to make a best estimate of the system/component vulnerability or ability to survive a dynamic environment. Tradeoffs are required between using new system/components, upgrading off-the-shelf versions or protecting off-the-shelf versions to a higher degree. At this stage of the design cycle prototypes aren't available so he must rely on mathematical or empirically derived models. Some work has been done related to this line and it is reported in the References[3,20,21,22]. The three-dimensional fragility surface has been generated by statistical methods in some instances, with variations in both environment and operational behavior treated. The fragility surface in this case should be a best estimate, with conservatism removed to the greatest extent possible. The modeled fragility surface should be upgraded as better modeling or later empirical data become available. In any event, a model of the fragility mechanism provides a sound engineering basis for understanding the behavior of the system/component. It should supplement any fragility evaluation.

FRAGILITY PARAMETER SENSITIVITIES

Criteria that constitute failure, malfunction or damage are determined from the operating functions of the system/component under evaluation. Nevertheless, it must be recognized that, in general, fragility is a function of the dynamic character of the environment. Obviously, a constant 1 g application will have a different effect from 1 g for 1 millisecond or 1 g applied at a set frequency. Directional sensitivity is another variable to be strongly considered. Fragility evaluation requires a knowledge of various parameters. Examples that follow demonstrate this need.

Figures 1 and 2, while conceptually intended, were developed from sinusoidal frequency tests on components[3]. Figure 3 shows the actual fragility curves for each orthogonal axis of a motor-driven resolver subjected to sine wave excitation. The resolver function was coordinate transformation for rotations about an inertial guidance system gimbal axis[23]. Note that except for the regions 17-60 cps and above 1100 cps the vertical axis has the lowest, and therefore controlling, fragility level.

Figure 4 presents fragility curves for the same resolver but based on white noise random excitation. Note in this case that the lower and controlling level is that for the lateral axis, not the vertical axis. Notching the random at sensitive sine wave frequencies did not provide further insight. In both cases then, the resolver was not generally frequency sensitive. Performance of the resolver was dependent on the following:

- Geometrical location relative to the vehicle engine
- Nature of the engine power (i.e., rotary, jet, or thrust)
- Orientation of the resolver relative to the engine

A further conclusion[23] of this test series was that each wave shape provided useful design information even though different results were obtained for each. Also, it was recommended that components be excited with vibration shapes which simulate the environment at the attachment mounting.

Another case, this one demonstrating the performance of a highly frequency-sensitive device, is illustrated in Figures 4, 5, and 6. The device is an inertial quality pendulous accelerometer described as digital magnetic force rebalanced[24]. The intended closed loop operation of the accelerometer induced a high frequency limit cycle which "dithered" the pendulum to overcome friction and maintain constant temperature. Its expected acceleration range was 10 g's. However, specially designed sinusoidal vibration tests revealed a 1 g fragility level in the dither frequency region of 700 to 900 cps. One g applied in that region "quenched" the dither. This phenomenon is shown in Figure 5 for a 2 g case.

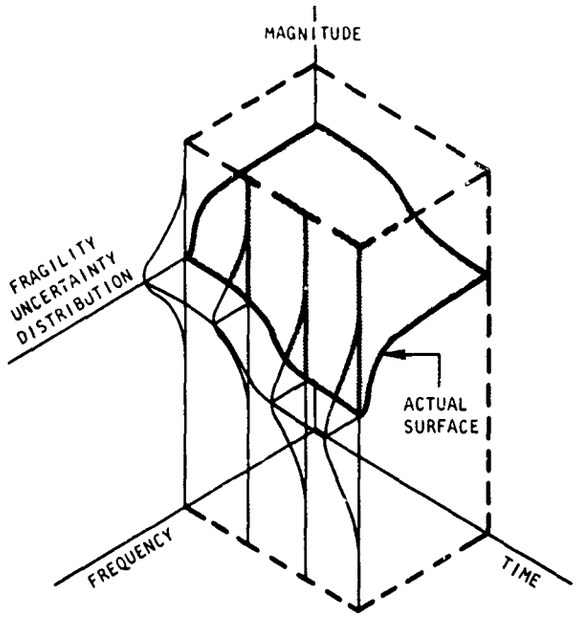

Figure 1. Actual Fragility Surface

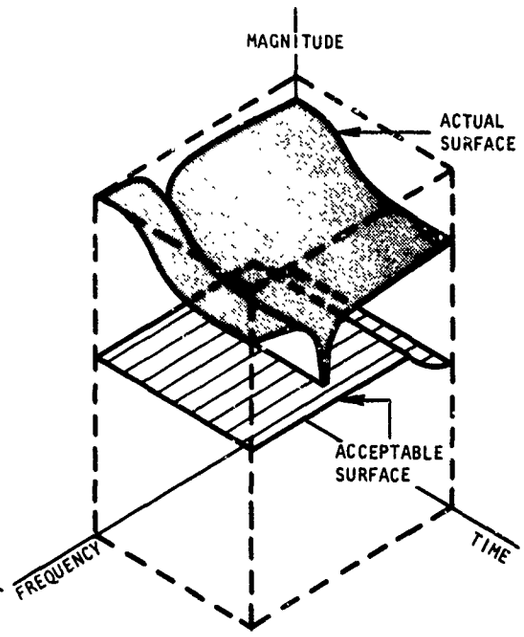

Figure 2. Comparison of Actual with Acceptable Fragility Surface

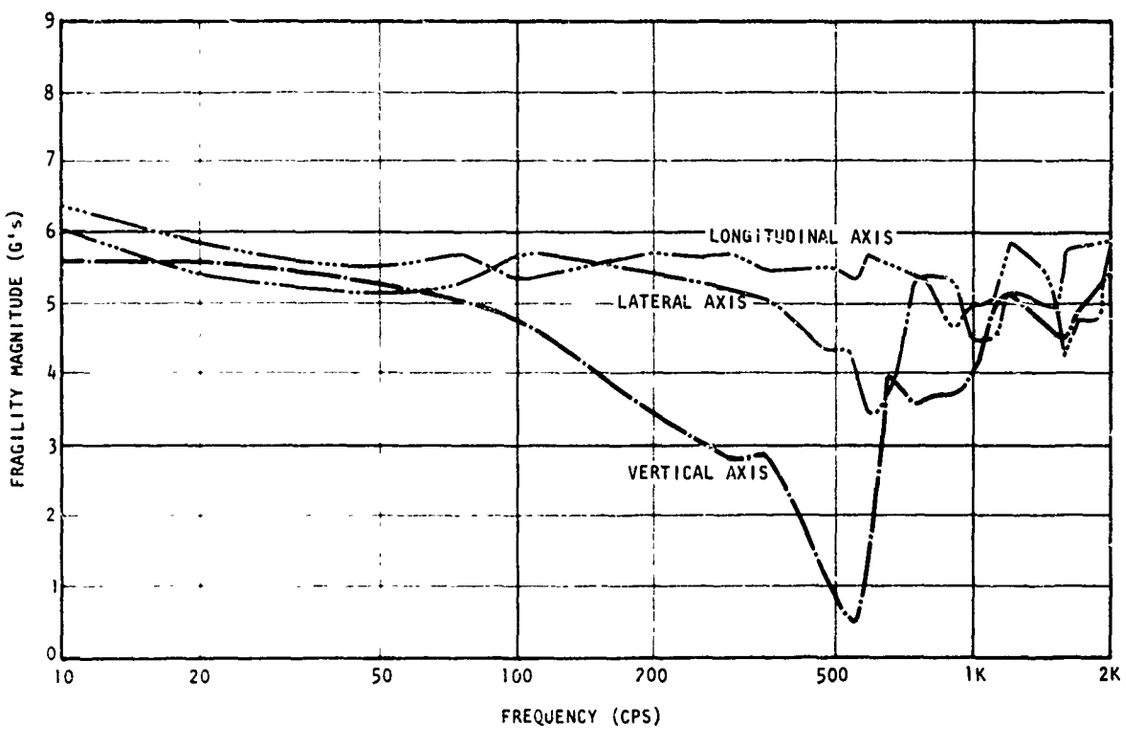

Figure 3. Sinusoidal Fragility Curves for a Motor-Driven Resolver

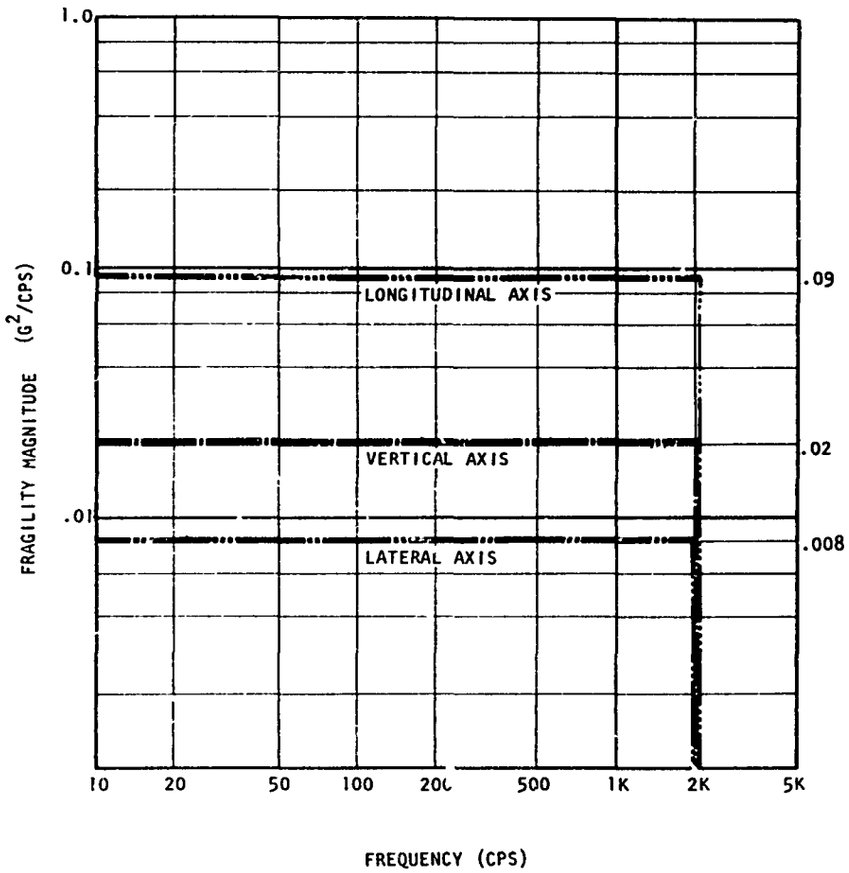

Figure 4. White Noise Random Fragility Curves for a Motor-Driven Resolver

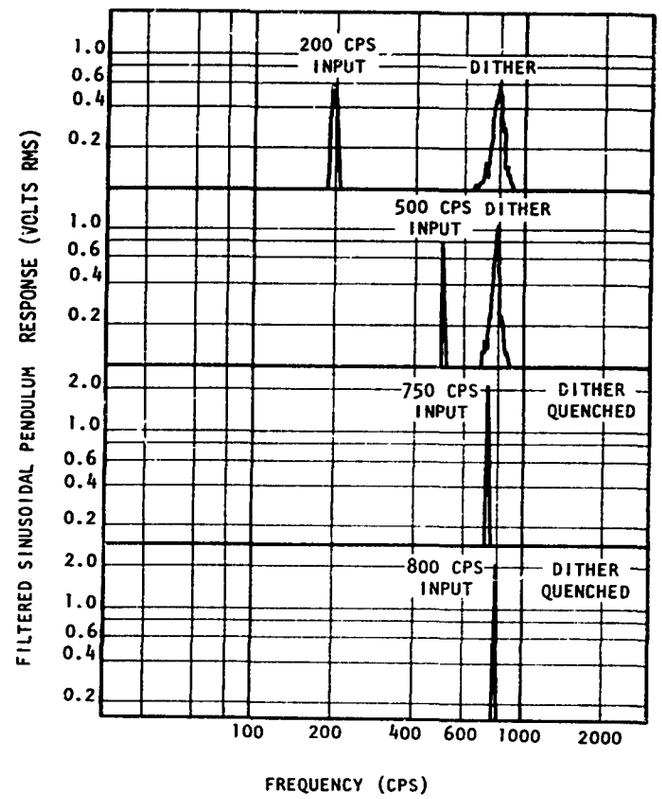

Figure 5. Experimental Verification of Dither Quench Phenomenon, Examples of 2g Input Case (Similar Results Found for 1g Input Case)

Similar phenomena resulted for random vibration excitation. Figure 6 shows the disturbance which is attenuated above 500 cps. The closed loop pendulum response to this excitation is shown in Figure 7. Note that an unquenched dither peak exists in the 700 cps region. The conclusion here was that a subtle but severely adverse operation results when the dynamic environment has frequency content in the critical dither region. Otherwise, the accelerometer performed in its intended manner.

Fragility parameter discussions involving random vibration are always subject to comparisons between broadband and narrowband results. Such comparisons are made in Figures 8 and 9. These figures were selected from fragility tests of 36 components for a Titan missile[25]. Tests were performed using both shaped broadband and narrowband (100 cps) random vibration. System/components tested were classified as launch essential. They included a 3 axis inertial reference system, autopilot and rate gyros, hydraulic actuators, command and control receivers, umbilicals, valves, and various electronics (e.g., relays and switches).

Figure 8 shows results for equipment mounted in the Stage I engine compartment. Broadband fragility is clearly well below that of the narrowband levels. Therefore, little correlation exists between them. This is somewhat contrasted in Figure 9, which shows results for the Stage I transition compartment containing the rate gyro system. Reasonable correlation occurred between shaped broadband and narrowband random vibration for this case. This was attributed to the fact that rate gyro drift modes were few in number.

Many operational types of modern system/components are often hybrid (i.e., analog and digital) in nature[26]. This class is prominent in the aerospace fields related to sophisticated guidance and control systems. Unusual failure phenomena were reported to result from dynamic environments. One such case[27] involved an astroinertial guidance system employing a sampled data loop for controlling a star tracking telescope. An excessive error was shown to propagate through the tracker loop at the beat frequencies between the tracker sampling rate and the tracker structural resonant frequency; see Figure 10. Furthermore, this effect was reportedly environment direction dependent. The conclusions were that electromechanical systems in general were subject to similar coupling problems. Use of actual environments was strongly recommended.

Guidance problems, such as that discussed above, became commonplace in the mid 1960's with the advent of strapdown guidance systems. In these systems, no shock or vibration isolation of the critical inertial sensors was permitted. The sensors were strapped directly to the vehicle and therefore subjected directly to translational and rotational environments. Considerable research was done to mathematically predict system malfunctions or failures when subjected to sinusoidal and random environments[20,21]. In many cases these predictions were verified by test. The successful Apollo 11 moon landing provided a major source of confirmation. A primary conclusion to date is that in order to accurately evaluate those effects, general vibratory levels are not enough. It was felt necessary that power spectral densities, cross-spectral densities and magnitude distribution data of the environment be made available. A second conclusion to be drawn is that accurate analytic and experimental models of fragility are feasible. These models depend upon good quality control to keep out-of-tolerance casing separations, misalignments or even loose screws or connections from being the "weak link."

In the mid and latter 1960's considerable aerospace emphasis was placed on shock pulse criteria[28]. The incentive for this was essentially twofold[29,30]: a) protection of missile silo equipment or personnel from nuclear blast; b) protection of missile-mounted equipment from pyrotechnic shock induced by staging. Results of tests that were transient in nature indicated that operational equipment was frequency sensitive as well as wave shape sensitive. Similar results were found for tests involving human operators[31,32].

The results and conclusions drawn from the above cases are summarized as follows:

- The shape of a fragility surface is dominated by the unique parameters of the particular dynamic environment simulated during the evaluation.
- Frequency content (broad or narrowband), axis selectivity and input wave shape can alter fragility results drastically.
- Unusual dynamic coupling can occur between system/component operational behavior and structural or packaged support response.
- Understanding of actual fragility is enhanced if modeled fragility is established and maintained by upgrading.
- Analytical and experimental work is needed to relate fragility to parameters of wave shape and frequency content. This will permit fragility qualities to be abstracted to a wide range of environments.

ENVIRONMENTAL REALISM

Since actual fragility is dependent on dynamic environment, the exact environment pertaining to system/component application should be used. Obviously this requirement is

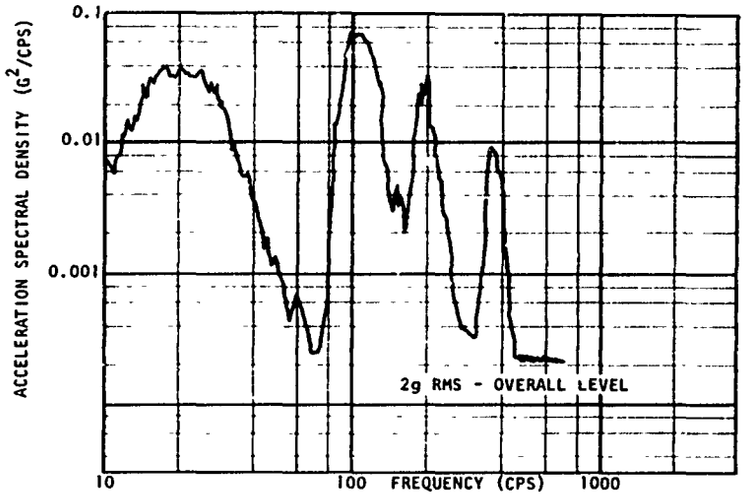

Figure 6. Acceleration Spectral Density of Random Vibration Disturbance

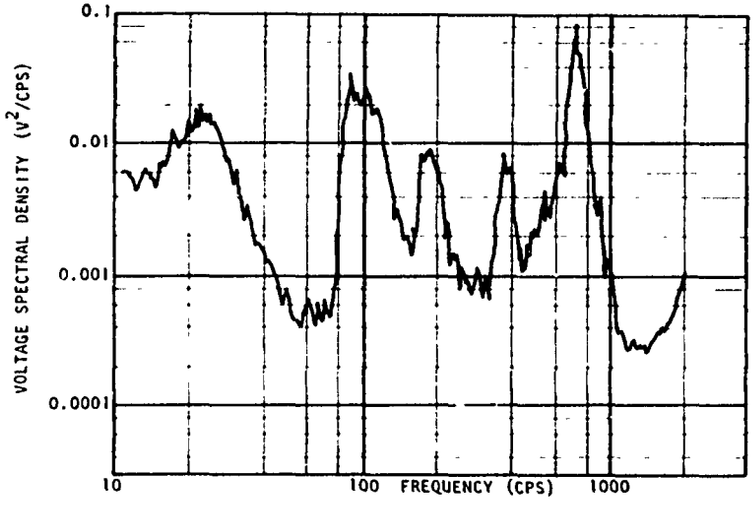

Figure 7. Experimental Voltage Spectral Density of Accelerometer Pendulum Analog Excursions - Unfiltered

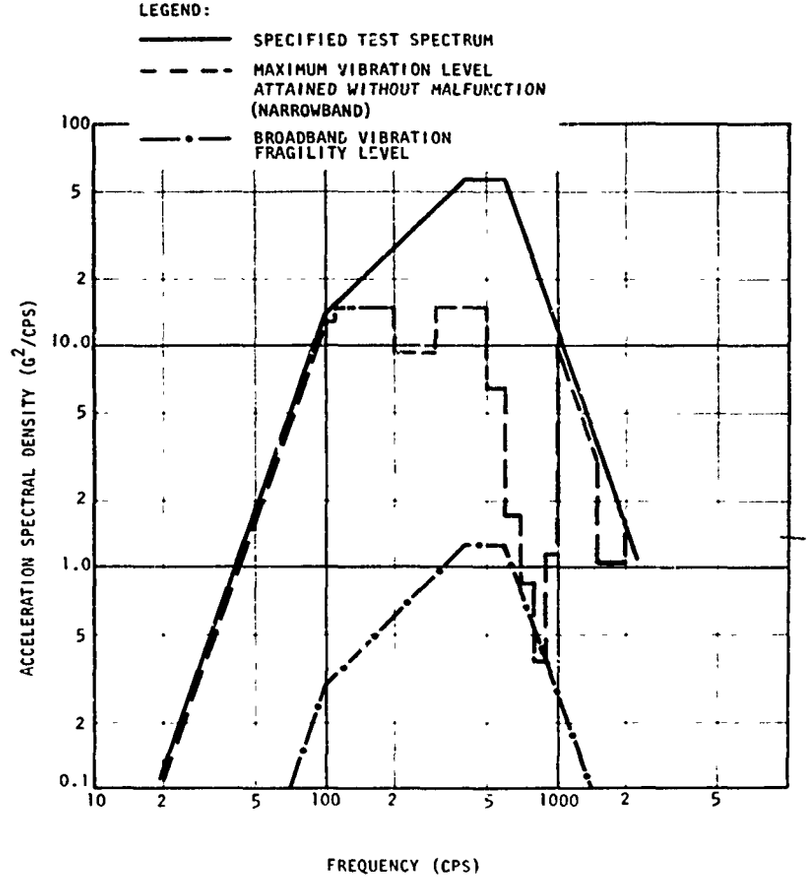

Figure 8. Compartment V (Stage 1 Engine) Vibration Test Spectrum, Structure-Mounted Equipment, Engine Control and Programmer Relay Panel, Y Axis

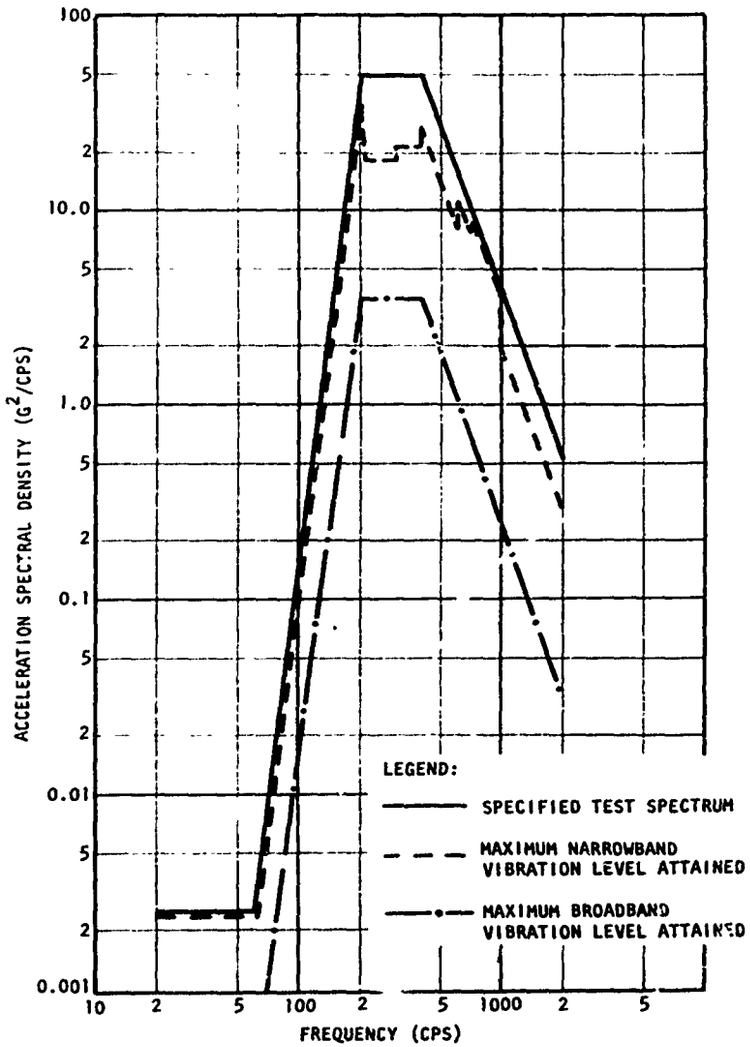

Figure 9. Compartment III B (Stage I Transition) Vibration Test Spectrum, Rate Gyro System on Vibration Isolators, X (Roll) Axis

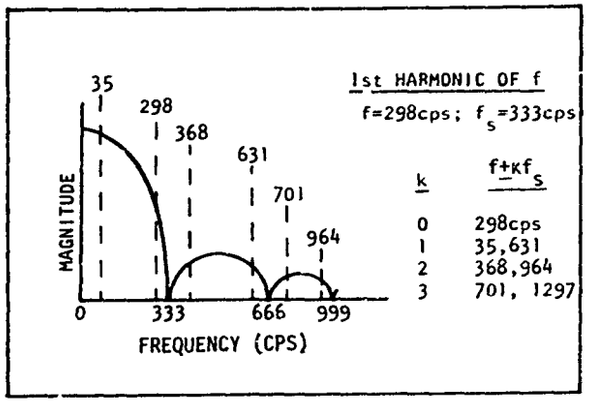

SAMPLE AND HOLD CHARACTERISTICS

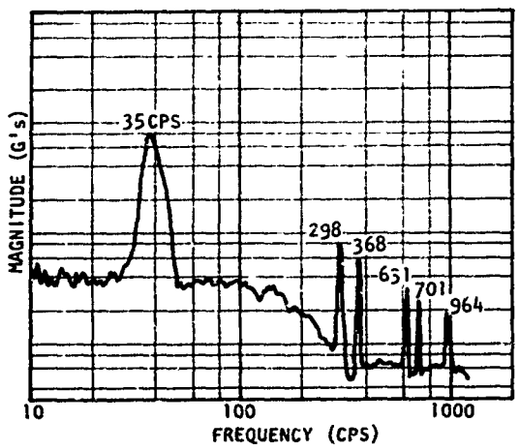

STRUCTURAL CHARACTERISTICS

Figure 10. Beat Frequency Phenomena Between Sample & Hold And Structural Resonance

impractical. Either the exact environment is unknown or it can't be accurately simulated in the fragility evaluation, or both. Furthermore, 'exact' is a misnomer since the intended application is generally in a statistically described environment. Impact conditions or mounting to rotary equipment are more definitive applications.

The issue of environmental simulation method revolves around such concepts as conservatism, simplicity or realism[15]. Conservatism, for example, holds a popular position in the packaging and structural design fields. Likewise, simplicity is essential to the testing field, especially when predominated by small business firms. Realism is generally supported by design/development proponents and system analysts. Their thinking is often prompted by technology needs for long term goals of business. This is a factor often overlooked. Testing or evaluation of a system/component for a given program or contract can often be efficiently designed to provide useful data for supporting analysis or future applications.

Immediate needs for exactness of dynamic environment where sensitive components are involved are mitigated to some extend by general representations and categorization of environments. Such a categorization of dynamic environments is shock, transients and vibrations. These certainly recognize the effect of various loadings on system/components. The need is also lessened by existing standardized test specifications. Experience and engineering judgement have often been used to fill in the uncertainties between simulated and realistic environments.

Special tests (intended to be somewhat more representative of service conditions) have also been developed. These include the Navy shock machines, shock barges, drop tests, high explosive simulation and road tests. However, much of this testing has been questioned for application, true representativeness, excessive levels and duration times. As answers to these questions become available improvements will come. Such was the case for random vibration[33] and transient testing.[35,37]

FRAGILITY DETERMINATION PHILOSOPHY

Standards, of necessity, lag technology. In the case of fragility, it is proposed to follow the well established categories of shock, transient and vibration. The dependent variable will be excitation magnitude as a function of failure, malfunction or damage. However, the means of establishing if any of these three occur are becoming more sophisticated as the technology rapidly advances. Therefore, in many instances monitoring methods are beyond those used in the past for shock, transient and vibration fragility tests[2]. In addition, a methodology is desired that will lead to a fragility index. Such an index would serve to indicate whether or not an existing and proven system/component is satisfactory for alternate application environments. Most missile/space contracts in recent years have emphasized "off-the-shelf" hardware. An analogy in the commercial field might be converting bus or train parts to use in a government funded rapid transit vehicle.

A generalization of a fragility methodology is illustrated in Figure 11. Ideally, any fragility evaluation is based on first establishing a free field environment for the system/component in question. Since this environment exists in the absence of the system/component, it must therefore be modified to account for insertion of the system/component. Impedance relationships are significant in this instance. The system is subjected to the modified free field environment, which is denoted E_s. In many practical cases a system fragility evaluation begins with the environment defined or specified at this level. It is necessary to interpret the system environment in terms of a nominal magnitude level and percentages of this nominal. The system environment is propagated to the component via a system transmission path. This path is designated T_s. The resulting component environment is designated E_c. Component fragility evaluations often begin at this point. The component will similarly have a transmission path, T_c, that propagates E_c to the location of a critical occurrence. Both transmission paths T_s and T_c may represent structural or functional characteristics. For example, mechanical-to-electrical energy conversion may be represented.

When E_c is sufficient to cause the component response to exceed a functional threshold then the E_c at that point forms a fragility surface. It may take several iterations of varying E_c to form a representative fragility surface. The comparison between the threshold indicator and the corresponding environment is obtained by means of the inverse path T_c^{-1}. This path also represents the feedback necessary for iterating E_c levels. The resulting fragility surface is then denoted as a function of magnitude, frequency and time, $E_c(M,f,t)$.

A similar situation exists for establishing a system level fragility surface. The inverse or feedback path is from the threshold exceeding response to E_s. This is designated $T_s^{-1}\,T_c^{-1}$. The corresponding system fragility surface is $E_s(M,f,t)$. Except for special cases (such as shipping container design) it is usually a system fragility surface that is desired.

Figure 11 may be readily extended by adding many branch points (for components) in a given system. These branches may be cascaded or in parallel. Further, the methodology may be simplified to a complete system level basis by setting T_c equal to unity. It becomes more representative as statistical uncertainty bands are added to both the environments and transmission functions. The versatility of the

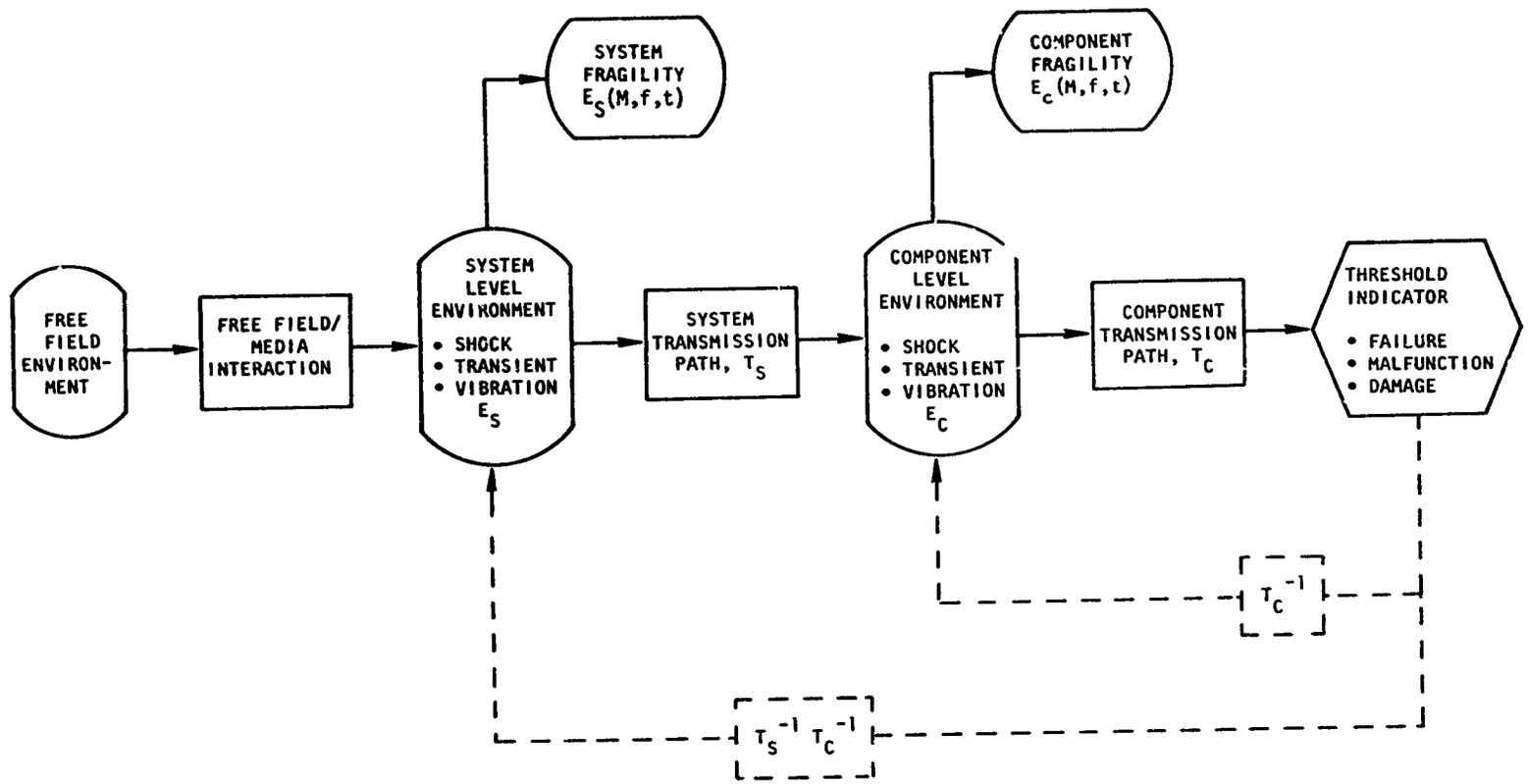

Figure 11. Generalized Fragility Methodology

methodology is summarized as follows:

- o Knowledge of environment can begin at free field, system or component level.
- o Specific cases may be interpreted as system, component, or combined evaluations by unitizing T_S or T_C or by adding additional branches.
- o Either system or component level fragility surfaces may be obtained. One may be obtained from the other by knowledge of T_S.

The establishment of the fragility surface E(M,f,t) then provides an answer to the question: Will the system/component survive the environment? The question is rephrased as: Is the system/component fragility surface above the expected environment surface? The answer incorporates differences of dynamic characteristics of the environment and provides a measure of goodness. For example, negative surface differences indicate system/component inadequacy while large positive surface differences indicate overconservativeness.

STANDARD SIMULATION TESTS

The preferred method of determining the fragility of a system is to test it with all components intact. The preferred method includes utilizing a realistic dynamic environment, while monitoring operations or functional parameters of each component. Unfortunately. this preferred method is seldom employed because of the unavailability of a complete system until late in the design cycle, or economical and technical limitations. Instead, tests are usually conducted at a component level. Failure, malfunction or damage criteria pertaining to a system specification must be interpreted as best possible for each component This implies that system fragility requirements be allocated to each component in the form of a fragility budget. Correspondingly, system fragility must be estimated from component fragility results. The accuracy of these estimates is primarily limited by testing constraints. Even system level fragility inaccuracy is predominated by testing constraints.

Constraints of testing apply to fragility determination in the same degree as to other testing (e.g., qualification). Interpretation and experience, supported by analysis, must be relied upon to properly account for best test conditions. A similar basis provides appropriate derating or enhancement of test results for field applications. The basis is reinforced by obtaining force measurements in addition to motion measurements at the test item/test fixture interface[34,35]. Such measurements are necessary to resolve the fragility curves for field installation. Test specifications generally imply unrealistically an "irresistible input motion" on the part of the test fixture. The major testing constraints are usually:

- Restriction to single axis testing
- Limitation of the test equipment (i.e., size, input capability)
- Lack of identification of the test fixture impedance
- Repeatability (i.e., lab-to-lab or day-to-day)
- Unavailability of sufficient numbers of test specimen
- Inaccessibility of operational or functional measurements
- Inability to generate combined environments.

Standard simulation tests are proposed for shock, transient and vibration environments. These are described next.

Shock Test

Shock tests are simple pulse tests. The most popular pulse shape used to date is the terminal peak sawtooth pulse[8]. Other pulses may be selected such as the rectangular pulse which has recently had a surge of interest[13] in the packaging field. Shock tests in the sense given here are a special case of a transient function described in the next subsection.

Overall control of the pulse with respect to frequency content is dictated by shock spectra. This relationship is shown in Figure 12. Any of the pulses on the right may be selected providing they generate the appropriate level shock spectrum. Levels begin at a sufficiently low value to be under fragility. This is identified in the figure as level 1. Levels are subsequently increased to level N, which corresponds to a failure, malfunction or damage.

Transient Test

Transient functions are defined as magnitude time histories (or amplitude time histories in the case of bilateral shaker motion) which are nonzero over a specified time interval[28,36,37]. This usage of transient includes the wide range of motions from the analytic pulse to the onset of stationary processes. The significance of this range is portrayed in Figure 13, which is a graph of amplification factor vs. quality factor (i.e., inverse of two times the damping ratio). The graph illustrates three pertinent relation ships between shocks, transients and vibrations.

- o Steady state vibration has a slope of unity

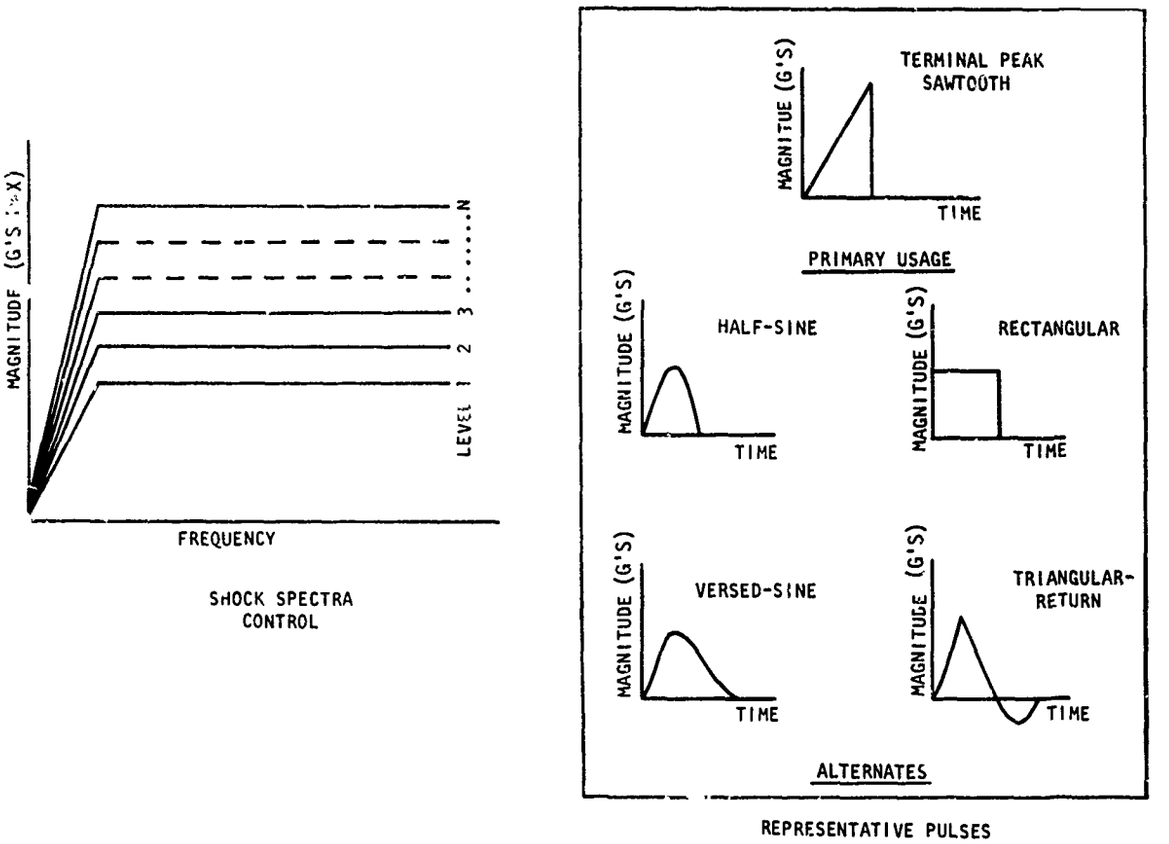

Figure 12. Standard Shock Fragility Test

- Shock has a slope of approximately zero
- Transients have slopes between the limits of unity and zero

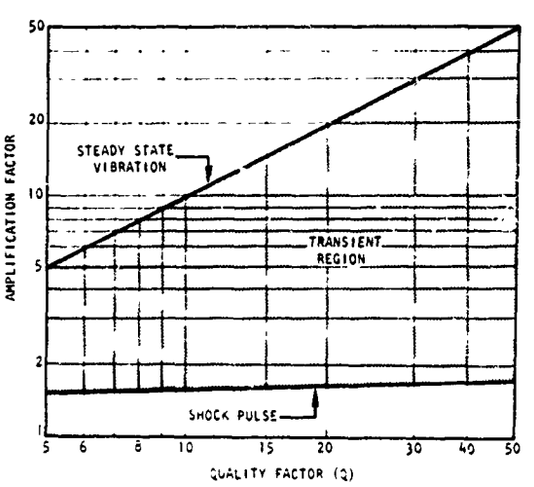

Figure 13. Amplification Versus Quality Factor

These relationships are highlighted in Reference (37), which developed a constant amplitude transient sine sweep test technique. The reference emphasizes the third relationship above, i.e. a wide variety of dynamic loadings fall into the transient category. This category also accounts for the number of cycles which occur at various frequencies in the transient spectrum.

Two types of transient tests are currently known to be in use. In one form[8,35], a transient is generated in a vibration shaker control system by a very short duration voltage pulse. This is used to trigger an array of band pass filters with separate gain controls. The filter outputs are summed and fed into the shaker system. Shaker motion time histories therefore have various frequencies at various times. Pulse duration is arbitrarily fixed. Shock spectra resulting from shaker motion are compared to field service shock spectra and corrected in a closed loop manner by means of shaker equalization. Shock spectra used in this case corresponds to a single quality factor (e.g. Q=10). This approach is illustrated in Figure 14. The above discussion pertains to each level of shock spectrum. Levels are increased from 1 to N where failure, malfunction or damage occurs.

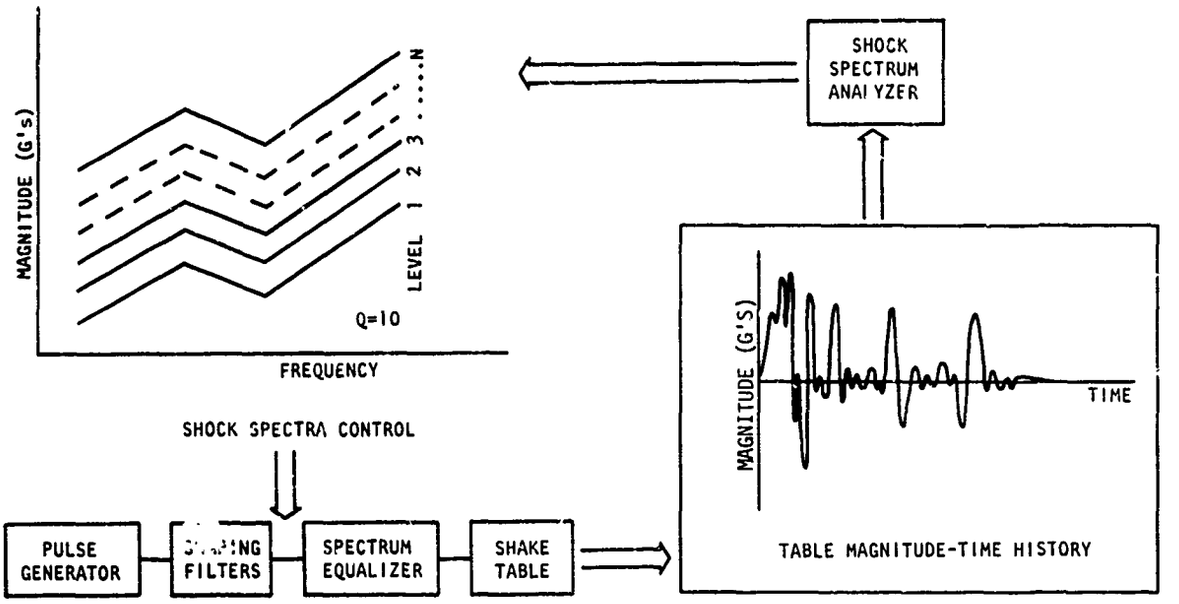

Figure 14. Standard Transient Fragility Test
Method 1 - Magnitude Time History Synthesis

The other transient technique[8,37] consists of a rapid sine sweep over the frequency range of interest. Predicted or measured shock spectra, based on two different quality factors (normally Q=5 and Q=25) are used to describe the environment. The ratio of these two shock spectra (i.e., $M_{Q=25}/M_{Q=5}$) governs the number of cycles occurring at each frequency. Sweep time over the frequency range is also controlled and usually varies from 1/2 second to 3 seconds duration. Sweeps are made both up and down the frequency scale. Figure 15 illustrates this type of transient test. Levels of the shock spectrum for each quality factor are increased to the point of fragility without changing the shock spectra ratio.

Vibration Tests

Standard vibration tests are proposed that will be composed of both sine and random tests. Both will have variable magnitudes (or amplitudes) as a function of frequency. Sine wave testing consists of slow sine sweeps over the frequency bandwidth. Such sweeps include resonance dwells. The approach is shown in Figure 16. Again, levels will be increased from an initially selected value to one causing failure, malfunction or damage.

Three options of random vibration testing are proposed. The first (and preferred option) is also shown in Figure 16. The power spectral density magnitude rolls off at both the high and low frequency ends of the test spectrum. Option B is used when the expected environment has predominant low frequency energy content. Option C pertains to predominant high frequency energy. All three options maintain an equivalent rms value for comparable levels and still cover the entire frequency range of interest (or practicality). The Option A graph is used to indicate the customary increasing of level until fragility is reached.

GENERAL COMMENTS

The above test concepts constitute the current general level of testing standardization. More detailed procedures are found in the literature. Standard fragility tests provide a number of advantages. Test results aid in situations involving comparisons between products. They also support diagnosis and identification of malfunction/failure mechanisms and help in determining system/component applicability to wide ranges of environments. Standard tests on widely used products conducted within a reasonable time period should provide meaningful statistical data.

Classification of the fault producing mechanism is particularly important. It helps determine whether the mechanism is under design/manufacturing control or a casual result of a production process. In the former case random fault occurrence and environment level are under control. In the latter case, extreme variability can result. Once identified, many faults may be eliminated or circumvented. Recent designs of computerized operational equipment are incorporating failure detection and correction software. Such concepts will influence fragility concepts more as the minicomputer enters the average household.

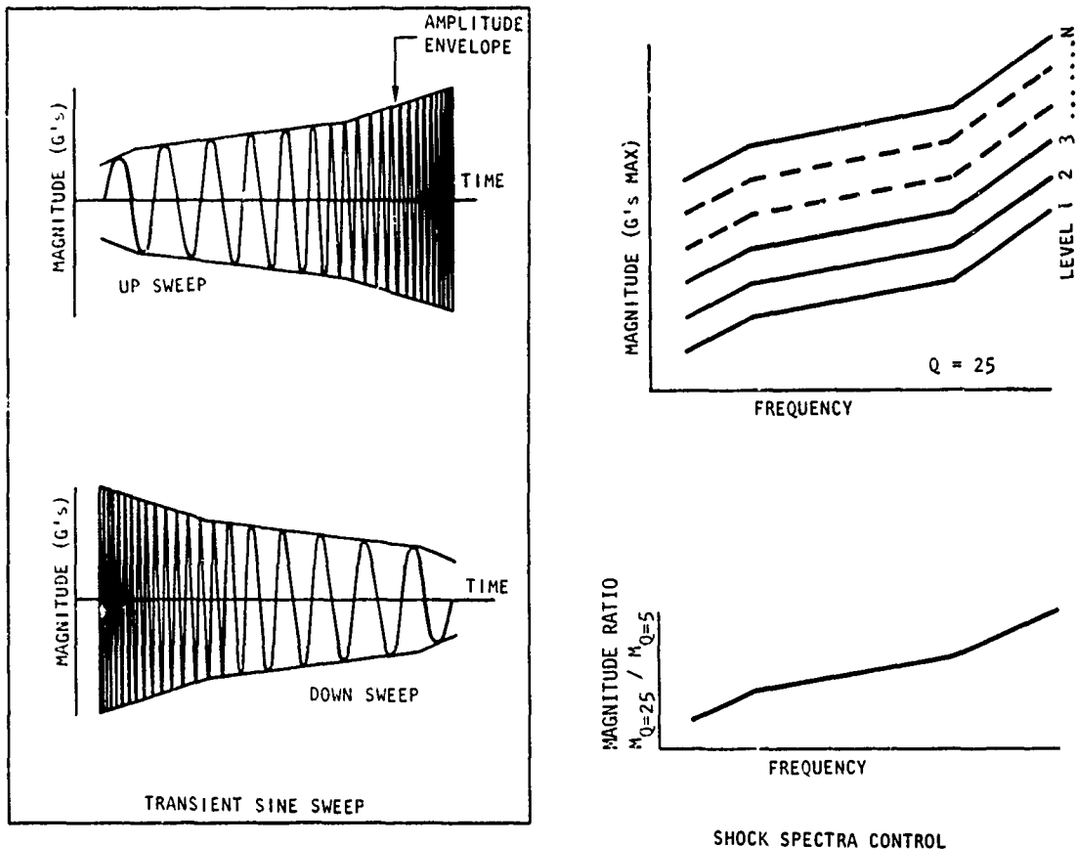

Figure 15. Standard Transient Fragility Test
Method 2 - Transient Sine Sweep

The non-standard phase of the methodology differs from that of standard testing by uniquely establishing the external environment and transmission characteristics. Also, appropriate uncertainty bands are assigned to these. Either a standard or specific fragility evaluation is conducted by subjecting the system/component to increasing percentages of transmitted environment (predicted or measured) until fragility is attained. Fragility levels with associated uncertainty bands are derived from these results by derating according to the constraints of the methods employed (e.g., impedance corrections). Subsequent to a malfunction determination, the degree of process control governing this undesirable effect should be established and repair or upgrade methods considered. Malfunction mechanisms are often readily eliminated once their nature is identified. Too often these mechanisms are careless design or assembly trivia with embarrassingly drastic results.

CONCLUSIONS

Definitions are made for fragility parameters and criteria that are general in nature. They are intended to encompass and satisfy various fields of technology. These include transportation, structural dynamics, packaging, guidance/control and operations/systems engineering and management.

Various examples of system/component unique sensitivities serve to indicate the strong influence of environment on the fragility surface. They also point out the need for fully understanding the system/component dynamic behavior and any subtle coupling between modes that may exist. These examples provide encouragement that modeled fragility is attainable and it adds technical insight to a fragility evaluation.

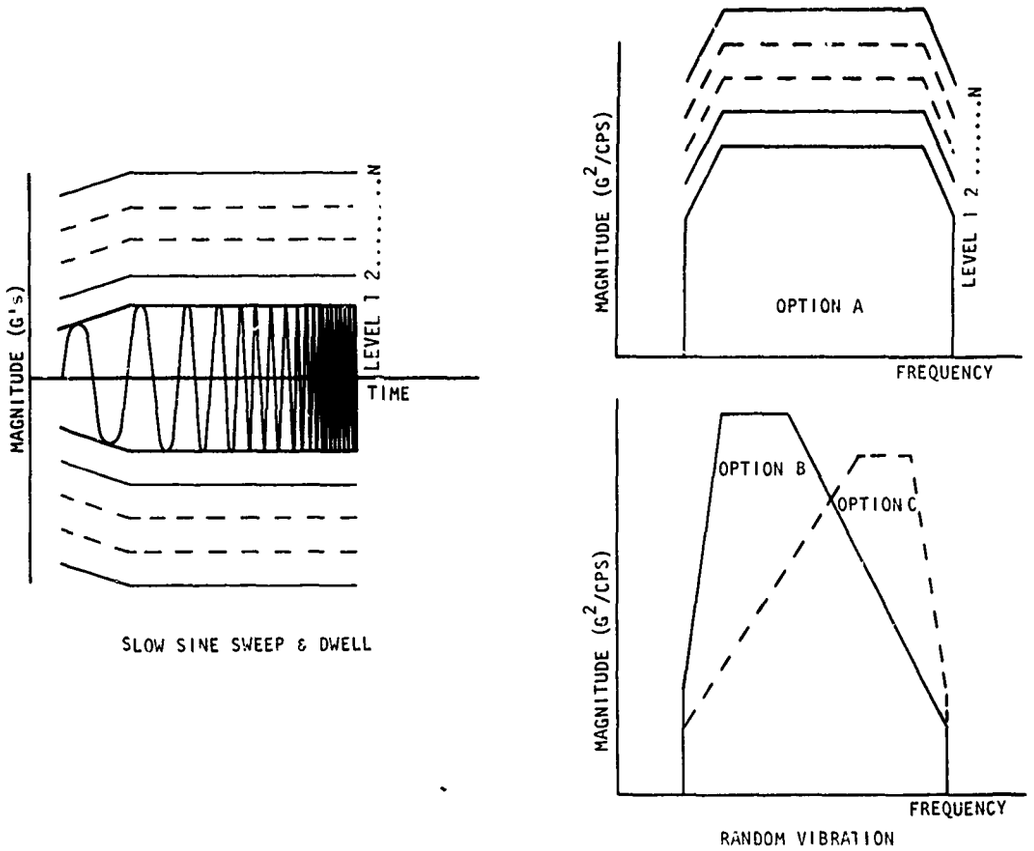

Figure 16. Standard Vibration Fragility Tests

Advantages and problems of obtaining realistic dynamic environment are discussed. A primary long term benefit is greater versatility in the application of the resulting evaluation data. Some alleviation of such realism requirements is justified by standardized test specifications.

A philosophy for determining fragility is presented. This philosophy pertains to unique or standard cases and allows treatment of system level or component level evaluations. Standard tests, evolved from past testing practices of shock, transient and vibration environments, are prescribed. At a minimum, fragility testing using standard environments presents a first cut. It helps to accumulate data, provide statistical samples and indicate methods of upgrading.

The authors have attempted to identify key areas that can be pursued further. Without proper guidelines inefficient testing usually occurs. Too often worthless or wasted data results. Establishment of a fragility budget for individual components will ensure desired fragility exists at the system's "moment of truth", the acceptance or qualification test. A national fragility index will permit greater versatility and insight when initial selections of hardened parts are made. This situation is gaining interest with changes in procurement and development philosophies. Off-the-shelf components and subsystems are being emphasized as in the B-1 Bomber and Space Shuttle programs. Similar emphasis can be expected on future Department of Transportation projects. Manufacturers producing components hardened to a wide range of environments will justifiably have a competitive advantage.

ACKNOWLEDGEMENTS

The authors appreciate the contributions of Mrs. P. Tilford for art work, H. M. Davis for typing, and Mr. A. H. Gibbs for editing.

REFERENCES

(1) F. F. Safford and J. S. Inouye, "Preventing Equipment Vibration Failures," Electronics, Vol. 31, No. 15, 11 April 1958, p. 92-94

(2) Environmental Test Methods, Military Standard, MIL-E-810B, 15 June 1967

(3) H. Himelblau, et al, "A Statistical Method for Determining Damage to Airborne Equipment," Paper No. 195, Society of Automotive Engineers, October 1957

(4) R. H. Jacobson and F. Mintz, "Evaluation of the Mechanical Design Level of Electronic Equipment Leading to Shock and Vibration Criteria," Armour Research Foundation Project K 044, TR R1, Appendix A, September 1953, (ASTIA No. AD 27207)

(5) H. N. Luhrs, "Electronic Component Vibration Sensitivity," National Electronic Packaging and Production Conference, New York, 11 June 1964

(6) J. P. Gilmore and R. A. McKern, "A Redundant Strapdown Inertial System Mechanization - SIRU," AIAA Guidance, Control and Flight Dynamics Conference, August 1970

(7) J. P. Favour and J. M. LeBrun, "Transient Waveform Control of Electromagnetic Test Equipment," Shock and Vibration Bulletin No. 40, December 1969

(8) "Specification of Shock Tests, Panel Session," Shock and Vibration Bulletin No. 36, part 2, January 1967

(9) F. B. Safford, "A Rational Procedure for the Design of Vibration Isolation Systems," Society of Automotive Engineers, SP-223, October 1961

(10) Design of Vibration Isolation Systems, Society of Automotive Engineers, Advances in Engineering, Vol. 3, 1962

(11) K. A. Bowen and T. S. Graham, "Noise Analysis: A Maintenance Indicator," Mechanical Engineering, p. 31-33, October 1967

(12) R. L. Baxter and D. L. Bernhard, "Vibration an Indicating Tool," Mechanical Engineering, p. 36-41, March 1968

(13) J. H. Goff and S. R. Pierce, "A Procedure for Determining Damage Boundaries," Shock and Vibration Bulletin No. 40, part 6, December 1969

(14) E. H. Schell, "Evaluation of A Fragility Test Method and Some Proposals for Simplified Methods," Shock and Vibration Bulletin No. 40, part 6, December 1969

(15) "Fragility Panel Session," Shock and Vibration Bulletin No. 40, part 6, p. 153-159, 1969

(16) M. Hirschorn, "The 90 dBA Guideline for Noise Control Engineering," Sound and Vibration, p. 25-29, April 1970

(17) C. T. Morrow, "The Shock Spectrum," Electrical Manufacturing, August 1959

(18) R. L. Barnoski, "Probabilistic Shock Spectra," NASA CR-66771, Measurement Analysis Corporation, 28032-FR-03, December 1968

(19) D. L. Cronin, "The Probabilistic Shock Spectrum," TRW Systems Group IOC No. 68-3343.2-49, Redondo Beach, California, 1968

(20) D. Sargent, "Dynamic Effects of Vibration on Guidance and Control System Performance," 15th Annual Meeting, Institute of Environmental Sciences, 20-24 April 1969, Anaheim, California

REFERENCES (Continued)

(21) D. Sargent and R. C. Rountree, "Rectification Errors in Strapdown Inertial Components Due to Random Vibrations, "Proceedings of Third International Guidance Test Symposium," MDC TR66-106 Volume I, October 1966

(22) B. Ishino, "The Use of Computers in Designing Shipping Container Suspension System," Presented to the Society of Packaging and Handling Engineers, May 1968

(23) J. M. Brust, "Determination of Fragility to Meet Random and Sinusoidal Vibration Environments," Society of Automotive Engineers, Paper No. 430A, October 1961

(24) L. R. Beuder and R. C. Rountree, "Dynamic Response of a Digital Magnetic Force Rebalance Rendulus Accelerometer to a Vibrational Environment," Shock and Vibration Bulletin No. 34, part 4, 1965

(25) "Lot vs. Component Vibration Test, Summary Report," The Martin Co., Report No. CR 61-257, October 1961

(26) G. A. Bekey and W. J. Karplus, Hybrid Computation, John Wiley and Sons, Inc., New York, 1968

(27) J. M. Brust and L. R. Beuder, "Analysis of the Effects of Dynamic Coupling Between Structural Resonances and Time Sampling Data Control Systems," Shock and Vibration Bulletin No. 35, part 3, 1966

(28) D. L. Cronin, "Response Spectra for Sweeping Sinusoidal Excitations," Shock and Vibration Bulletin No. 38, August 1968

(29) J. Wolkovitch, "Techniques for Optimizing the Response of Mechanical Systems to Shock and Vibration," SAE Paper No. 680748, October 1968

(30) E. Sevin and W. D. Pilkey, "Optimization of Shock Isolation Systems," SAE Paper No. 680749, October 1968

(31) J. N. Magduff, "Transient Testing of Man," Sound and Vibration, p. 16-21, August 1969

(32) T. J. Wittmann and N. S. Phillips, "Human Body Nonlinearity and Mechanical Impedance Analyses," Journal Biomechanics, Vol. 2, p. 281-288, 1969

(33) C. M. Harris and C. E. Crede, Shock and Vibration Handbook, Vol. 2 Chapters 22, 23, 24, McGraw-Hill Book Co., New York, 1961

(34) W. C. Ballard, et al, "Vibration Testing with Mechanical Impedance Methods," Sound and Vibration, p. 10-21, January 1969

(35) G. W. Painter and H. J. Parry, "Simulating Flight Environment Shock on an Electrodynamic Shaker," Shock and Vibration Bulletin No. 35, part 4, 1966

(36) R. E. Morse, "The Relationship Between a Logarithmically Swept Excitation and the Build-Up Steady-State Resonant Response." TRW Systems 7120-6154-R0-000, December 1964

(37) F. B. Fay, "A Transient Test Technique," TRW Systems Group Internal Report and Presentation Summary, Redondo Beach, California, October 1965

(38) G. W. Painter, "Use of Force and Acceleration Measurements in Specifying and Monitoring Laboratory Vibration Tests," Shock and Vibration Bulletin No. 36, part 3, 1967

Mr. Foley (Sandia Laboratories): Has your committee been doing any work related to the use of Falltree analysis techniques and associating them with fragility assessments?

Mr. Safford (TRW Systems): Not at this time. What we are basically doing is setting up a skeleton or you might call it a straw man. We want to broadcast that to anybody and everybody that has an interest in this business and look for contributions. Then we are going to go through a series of iterations. The main point is that we want to get the state-of-the-art as it is in the nation. So anybody that is interested and would like to participate is most welcome. I would like to talk to you later.

CONTROLLING PARAMETERS FOR THE STRUCTURAL FRAGILITY OF LARGE SHOCK ISOLATION SYSTEMS

Robert J. Port, Mechanical Engineer
Facilities Survivability Branch
Air Force Weapons Laboratory
Kirtland Air Force Base, New Mexico

A sensitivity study was performed on the design parameters of a large shock isolated equipment platform supported by six mechanical spring isolators that also function as pendulum arms. The analytic study was performed on a finite difference computer code that calculated the system response for increasing inputs until failure of the six isolators provided an estimate of the system structural fragility. The highly nonlinear system response at or close to the ultimate failure levels was displayed on a computer-made movie of the platform motion time history.

INTRODUCTION

A shock isolation system is normally designed for survivability against a severe dynamic input. The designer is provided with a maximum design level of the input environment, the maximum levels that can be tolerated by the internal system components, and the geometric and system constraints for the specific application. The shock isolation system is then engineered to attenuate the input motion to the acceptable internal levels.

Another consideration, which is not always addressed by the designer, is to determine the system vulnerability to levels above the specified design values, and to establish the ultimate failure level or fragility of the system. A study of this type can sometimes produce minor design changes which greatly increase the maximum system capability with little or no effect on the survivability at the original design levels. Ignoring the system vulnerability may produce a future requirement for major field modifications if the original design levels were incorrectly estimated, or future needs dictate a higher capability.

The determination of system fragility involves the analysis of failure modes and failure levels that are coupled in a highly nonlinear system response. The nonlinear characteristics usually make each situation unique, and prevents the development of general design procedures. In order to describe some of the inherent problems in fragility determination, this paper will be directed to a specific application involving a large shock-isolated equipment platform. The solution procedure relies heavily on the use of a digital computer to calculate and graphically display the nonlinear response characteristic near the system failure levels. In addition to providing conclusions for the specific application, the example is intended to show the ease in which the computer can be used to assimulate a nonlinear grouping of simple physical models and provide detailed design information.

PROBLEM DESCRIPTION

Consider the design of a shock isolation system for a hypothetical equipment platform shown in figure 1 with the dynamic characteristics listed in table I. The floor or platform is a rigid structure of steel plates and beams that is configured as a sector of an annulus. The equipment is contained in tall racks that are rigidly bolted to the platform.

The initial design process leads to an overhead support on six mechanical spring isolators (Fig. 2) that also act as pendulum arms. The spring constants listed as the standard case in table II will provide equal dead load deflection of 2.316 inches, and a vertical natural frequency of 2.1 Hertz. The above design will limit the acceleration at the equipment to levels below 3 g as long as the shock input does not cause the springs to exceed their linear range. The linear range or distance to solid height was made uniform to accommodate a shock spectra input of 5 inches without introducing nonlinearity. Damping was

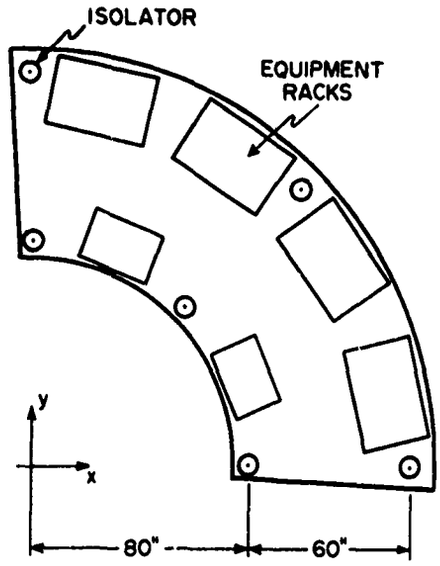

Figure 1. Shock Isolated Platform

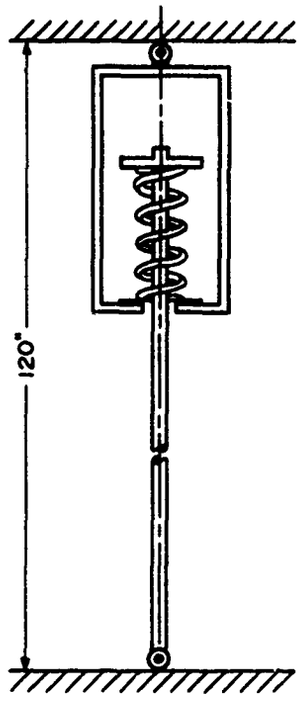

Figure 2. Isolator

not considered necessary to meet the design conditions, and a value of 1% of critical damping is assumed for the mechanical spring arrangement

FRAGILITY CONSIDERATIONS

The basic design configuration will provide a satisfactory solution to survive the given design levels. The next step is to determine the ultimate failure levels and the influence of the design parameters on the system vulnerability. Two modes of failure are possible: 1) malfunction of the acceleration sensitive equipment due to the high frequency signal generation when the isolator springs are driven to solid height; and 2) structural failure of the isolators due to increased tensile loads at solid height conditions. This paper will address only the latter structural failure mode.

Determination of the structural fragility requires the calculation of the three dimensional floor response after the springs are driven into the solid height condition. A computer program was developed to provide the nonlinear system response based on the following assumptions:

1) The platform responds as a rigid body.

2) The isolator has a linear force deflection curve up to the solid height position.

3) The isolator acts like a stiff linear spring beyond solid height.

4) The isolator fails abruptly when a given failure load is exceeded.

5) The isolator damping force is proportional to the platform velocity (viscous).

The isolator failure model is shown in figure 3 along with some datum points that were

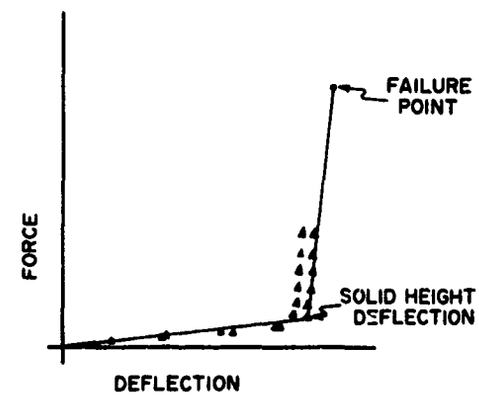

Figure 3. Isolator Model

TABLE I

PLATFORM CONSTANTS

PARAMETER	SYMBOL	VALUE	UNITS
TOTAL WEIGHT	W	8875.	Pounds
CENTER OF GRAVITY	X Y Z	62.15 72.11 32.00	Inches
MOMENTS OF INERTIA	I_{xx} I_{yy} I_{zz}	234500. 206500. 323300.	LB-IN-SEC^2
PRODUCTS OF INERTIA	I_{xy} I_{xz} I_{yz}	68370. 45740. 53070.	LB-IN-SEC^2
LENGTH OF ISOLATOR	D	120.	Inches

TABLE II

PARAMETER VALUES FOR SENSITIVITY STUDY

		STANDARD CASE	CASE 1	CASE 2	CASE 3	CASE 4	CASE 5	CASE 6
SPRING CONSTANTS OF THE SIX ISOLATORS (LBS/IN.)	1	483	500	520	500	500	500	500
	2	500	500	500	500	500	500	500
	3	625	667	690	667	667	667	667
	4	517	500	480	500	500	500	500
	5	1000	1000	1000	1000	1000	1000	1000
	6	708	667	644	667	667	667	667
DISTANCE FROM NEUTRAL POSITION TO SOLID HEIGHT CONDITION (IN.)	1	7.5			8.5			
	2	7.5			8.5			
	3	7.5			8.5			
	4	7.5			8.5			
	5	7.5			7.5			
	6	7.5			8.5			
PERCENT OF CRITICAL DAMPING (%)		1				2	10	
ISOLATOR FAILURE LOADS (LBS)		40000						80000
STEP INPUT LEVELS BETWEEN PASS AND FAIL (IN.)		7.5-8.0	8.0-8.5	8.0-9.0	6.0-7.0	8.0-9.0	10-11	13-14

obtained from a quasi-static loading of the pendulum spring isolators used in the Minuteman System [1]. No data is available near the failure level, but local yielding is expected to cause a reduction in the assumed spring constant just before failure. The simplified model that uses an abrupt failure criteria is an assumption that was selected for simplicity, and may or may not be validated by future studies.

A computer program was developed to assimilate the various physical models that represent the different components of the shock isolation system. A rigid body code that would solve the three-dimensional equations of motions expressed in terms of Euler angles would have been desirable but was not possible within the schedule constraints and available manpower. A less sophisticated but easier to program appraoch was adopted that consists of a lumped mass model of the floor. The mass points are connected by stiff springs and dash pots to maintain within a small error the initial rigid configuration. The equations of motion can then be solved by finite difference techniques to produce the three-dimensional system response. A brief description of the numerical method is given in the appendix.

DISCUSSION OF RESULTS

The computer program was used to conduct a parametric study for determining the sensitivity of system fragility to small changes in the designed solution. The calculated system response was found to contain a great deal of rotational motion in the form of pitching and yawing of the floor when solid height and isolator failure conditions were encountered. The nonlinear motion was impossible to analyze in the form of printed computer output, and created a need for visual display. A computer routine was incorporated to produce a 16-mm movie showing the motion of the floor as a function of time. The movie provides an excellent visual record for determining the sensitivity of some of the critical parameters and providing insight into requirements for design improvements. Unfortunately the movie cannot be incorporated into this report, which will tend to reduce the impact of the parametric study.

Table II displays the values of the various parameters that were used in seven cases of the sensitivity study. The no-entry positions in the table mean the parameter is identical to that of the standard case, and was omitted for clarity. The driving input to the system consisted of a step vertical displacement of the ceiling attachment point in the downward direction. The input displacement was increased incremently until the ultimate failure was reached (all six isolators had failed structurally). The largest input that did not produce failure and the minimum input that did produce failure are listed in the last row of table II.

The standard case, first column of table II, was designed to provide uniform vertical motion within the linear range of the isolator springs. This uniformity does not exist after the spring is reduced to solid height, as all the solid-height spring constants are assumed equal. At inputs greater than solid height the floor tends to pitch and yaw causing the outboard isolators to fail on the second or third cycle. Failure of one or two isolators will provide additional loads on those remaining, and tend to produce catastrophic failure several cycles later.

The first and second cases of table II were selected to study the effect of using slightly different spring constants. Case 2 involves a system design which uses only three types of isolators and would therefore be desirable for reducing the system production costs. Case 3 was considered as a worst case for a situation involving poor quality control during the manufacture and production of large springs. Although the ultimate failure levels did not vary significantly from that of the standard case, the actual motion time history as displayed in the movie is quite different. Case 3 produced the most out-of-plane motion and would be the worst case for an acceleration-sensitive equipment failure, as the solid height condition on the outboard isolators was reached at low input levels.

Case 4 was chosen to study the effects of changing the distance to solid height. Five of the solid height distances were increased by one inch over that of the standard case. The effect was to create a violent pitching motion when the one spring bottomed before the others. An isolator failure occurred on the second cycle of a 7-inch input, followed by the failure of the remaining springs on later cycles. Since the ultimate failure level was lower than that of the standard case, increasing the distance to solid height in a nonuniform manner can reduce the system fragility.

The next two cases, 5 and 6, were experiments to assess the advantages of introducing additional damping into the isolators. The resulting increase in the system fragility is not surprising since the minimum input failure occurs after several cycles, and the late time motion is strongly influenced by the amount of damping in the system. The increase from 1% to 2% of critical damping produced a slight change

[1] F. T. Krek, "Static and Shock Testing of Wing I, LER Shock Isolators," Technical Report No. AFSWC-TR-70-2, Vol I, Kirtland AFB, NM

in the fragility levels and system motion. In case 6 where the damping was 10%, a significant increase in fragility was obtained that would most likely shift the failure mode into that of an equipment failure.

The last study, case 7, had an increase of the spring failure force which almost prevented a structural failure. It would be almost impossible with standard inputs to introduce sufficient energy into the system to drive the solid height spring constant to the failure level for this case. In this situation, another mode would dominate the fragility.

CONCLUSIONS

The structural fragility determination of large shock isolation systems is complicated by three dimensional nonlinear motion that occurs when isolator springs are driven to their solid height conditions. Extreme pitching and yawing cause severe loading and then failure of outboard isolators, followed in many cases by failure of the remaining isolators on subsequent cycles. The intricate motion is most easily studied by the use of computer-made movies that display the time dependent solution of the basic equation of motion.

A parametric study on a pendulum spring-mounted equipment platform has produced the following conclusions:

1) Reasonable variations in spring constant values do not produce significant changes in the system structural fragility.

2) It is desirable to provide equal solid height distances for all springs, and thus reduce the energy coupled into rotational modes.

3) Small amounts of system damping can cause significant changes in the system fragility levels.

4) Strengthening the isolators will increase the system fragility, and may eliminate structural failure as the prime failure mode.

ACKNOWLEDGEMENTS

The author is indebted to Robert Thompson of the Facilities Survivability Branch, Air Force Weapons Laboratory, for his programming support and computer movie making talents.

APPENDIX - COMPUTER CALCULATIONAL MODEL

The shock isolated platform was divided into 12 lumped-mass points, six located at the isolator attachment points, and six at an 80-inch elevation above the attachment points. The arrangement provided a three-dimensional array of point masses that could be made dynamically similar to a given system by carefully selecting the values of the 12 unknown masses. Each mass was connected to each of the other masses by a stiff spring (60,000 #/in.) to limit the relative motion and provide an approximation to a rigid body. The equations of motion were expressed in cartesian coordinates and all vectors were expressed by their components along the coordinate directions.

The finite difference technique was a simple explicit scheme that defines the displacement on equal increments of time, and the velocity at the midpoint of the time increments. The procedure is most easily described by applying it to the simple one-dimensional equation of motion.

$$M\ddot{x} + C\dot{x} + Kx = 0 \quad (1)$$

where M = mass
C = damping coefficient
x = position coordinate
v = velocity

The calculation cycle starts with known values of the displacement, $x(t)$, and velocity, $v(t-1/2\Delta t)$, and provides an estimate for the updated velocity.

$$v(t+1/2\Delta t) = v(t-1/2\Delta t) - Kx(t)\Delta t \quad (2)$$

The estimated value is used to make a final prediction that includes damping effects

$$v(t+1/2\Delta t) = v(t-1/2\Delta t) - Kx(t)\Delta t - 1/2C(v(t+1/2\Delta t) + v(t-1/2\Delta t))\Delta t \quad (3)$$

Finally the position vector is updated

$$x(t+\Delta t) = x(t) + v(t+1/2\Delta t)\Delta t \quad (4)$$

The updated values then complete the calculations for the given time step, and provide the inputs for stepping off another time increment.

Mr. Bachman (Holmes and Narver): Are listings and the documentation of your computer program available?

Mr. Port: Not at the present time. I will be writing a report, which will be classified because it addresses the minuteman aspect itself.

Mr. Bachman: Will they still available to the public?

Mr. Port: They will be available through the Air Force Weapons Laboratory, but they are not written as yet.

Mr. Rymer (Naval Air Test Center): These are questions related more to the hardware that backs up your technique than the technique itself. How much core was required for this kind of program, and on what kind of machinery did you run it?

Mr. Port: We have a CDC 6600 with a 50,000 word storage. The entire program ran 6 minutes.

Mr. Safford: I think, as Mr. Rountree stated, once you have measured or analyzed fragility if you start playing games, you can very simply raise your fragility and often to very considerable lengths. The obvious question is: once you have all this fragility what does it really mean in assessing a system's, or a subsystems, resistance to environment, or its hardness.

HARDNESS EVALUATION

W. H. Rowan
TRW Systems Group
Redondo Beach, California

This paper presents a statistical approach to the evaluation of the failure of complex systems. The approach starts with a computation of the free field nuclear effects, the modification of these effects by such things as shock isolation and other protective equipment, and finally, the system response in terms of the probability of component failure due to the weapon induced environments. The component probabilities of failure are combined by means of system failure network logic to obtain the system probability of failure. An important characteristic of the approach is that it takes into account the many statistical uncertainties and correlations corresponding to the parameters involved.

INTRODUCTION

For over a decade, TRW Systems has been concerned with the survivability of hard and fixed strategic weapon systems. One of the tools which has been developed during this period is FAST — Failure Analysis Using Statistical Techniques. In a restricted sense, FAST is a family of computer codes for evaluating system hardness as a function of free field environments, transfer functions, and fragilities. In a more general sense however, FAST is a systematic and comprehensive methodology for evaluation of system survivability — giving clear perspective to priorities, sensitivities, alternatives, and risks. The purpose of this paper is to discuss briefly how the system engineering and system analysis techniques of the methodology can be used for a hardness evaluation of any military, civilian, or space system.

In the past the application of FAST methodology has been restricted to weapon systems in being for purposes of either assessment or upgrade, assessment meaning evaluation of the achieved hardness, and upgrade meaning changing of the system to improve hardness. The assessment of the hardness of a complex system due to nuclear attack requires calculation of the environment seen by each component, evaluation of how each component responds to the environment, and evaluation of how the probability of failure of these components contribute to the overall failure probability of the system.

The FAST methodology first identifies all of those components whose failure can contribute directly or indirectly to system failure. The individual failure mechanisms of the components are identified and related to the environment from the exploding weapon. The path of these effects from the weapon detonation to the failing component involves three basic steps (see Figure 1):

1) Weapons effects, such as ground shock, overpressure, debris, radiation, etc., are related to the size of the weapon and the distance from the burst to the facility;

2) Transfer functions are employed which account for the transmission of the nuclear environments through the structure including any shock isolating or protective equipment to the vicinity of the component;

3) The failure probability of the component is given by its fragility, which is the failure probability of the component as a function of the severity of the local environment.

Finally, the component failure probabilities are combined, by means of appropriate system network logic, to obtain the system failure probability. By repeating such calculations for several weapon misdistances, the system probability of survival as a function of overpressure can be obtained as diagramed in Figure 1.

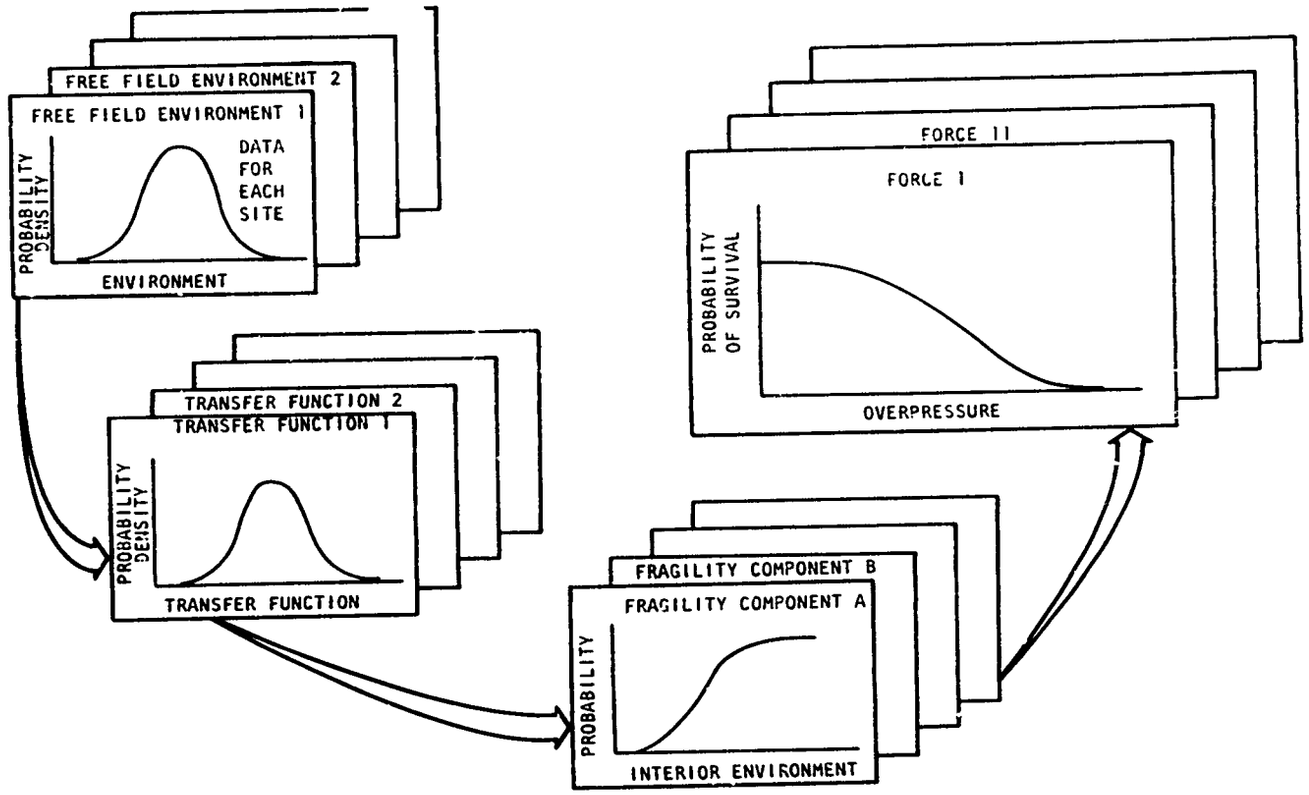

Figure 1. Assessment Methodology Overview

An important consideration which is treated by the FAST methodology, is that the failure of the system will never be known with certainty. No component failure level is ever known precisely, and the propagation of the weapon effects from the point of weapon detonation to the interior of a facility is subject to uncertainties due to soil inhomogeneities, manufacturing variabilities, and the uncertainties of weapon effects scaling laws.

Two categories of variation are recognized by the FAST codes. The first variation, physical uncertainties, is present in the input data because of statistical variation in the manufacturing process, soil properties, and meteorological phenomena. Such statistical variation in the input parameters is illustrated in Figure 1 (i.e., probability density functions).

The other variation arises from imprecise knowledge or uncertainties in the input data which may be associated with inadequate empirical data on significant parameters or the uncertainties associated with the mathematical models employed. Because of these uncertainties, biases will exist in the input parameters. Each bias is assumed to have a distribution appropriate to its uncertainty. A given bias will extend uniformly over a population of facilities and, hence, cannot be removed or suppressed by an averaging process. Such uncertainties are reducible by means of analyses to develop improved mathematical models or by means of test programs to provide improved data. It is a major objective of the survivability calculations to discriminate between these two kinds of variability.

METHODOLOGY

This section provides a description of the process used to generate the system survivability estimates using the FAST computer codes. The discussion is treated in three parts.

- Development of free field nuclear weapon environment estimates, including the probability of their accuracy which depends upon variations in physical properties such as soil characteristics across the weapon system and the uncertainty in these estimates which depends upon the accuracy of the estimating procedures such as calculational techniques and empirical relations.

- System analysis which yields probabilities/uncertainties in transfer functions, system failure networks, and probability/uncertainty in component hardness (or fragility).

- FAST calculations which combine the results of the free field and system analyses to yield the survivability estimates.

The relation of these three aspects of the FAST methodology are illustrated in Figure 2. The free field environment analysis and system analysis are depicted along with the seven (7) outputs from these two principal activities. Then these seven outputs become the inputs to the flow diagram which represents the sequence of FAST calculations.

FREE FIELD ENVIRONMENTS

Consider the environmental analysis in Figure 2. Here relations are developed which describe the free field weapon environments as a function of the physical properties of the facility location. Using these relations, calculations are done for a nominal range from ground zero, (GZ), and a specific yield, to obtain predictions of the nominal free field weapon environments at each site. All major categories of nuclear environment are considered, such as the following: nuclear radiation, EMP, ground shock, air blast, thermal, and debris. These major weapon effects categories can be broken down into further detail, such as neutrons, gammas, and x-radiation for nuclear radiation, and displacement, velocity and acceleration for ground shock. In addition, as necessary, additional subcategorization into such aspects as prompt, secondary, direct-induced, air-induced and outrunning are also treated. Details of the processing of these data are shown in Figure 3.

On the left side of Figure 3 is shown a matrix. The rows in this matrix are numbered 1 through n, where n is the number of sites. The columns correspond each to a single physical environmental property. For example, to support calculations of failure due to ground shock, the physical environment properties required are soil properties such as constrained modulus, Poisson's ratio, and densities at various levels below the surface.

The matrix of environmental properties is used as input to the relations for computing a matrix of local free field environments at each site. This is shown by the second matrix in Figure 3. The rows in this column are numbered 1 through n, corresponding to the same facilities in the paragraph above. The columns in this matrix correspond to individual environmental parameters. In the case of the ground shock environment, examples of such parameters include peak velocity, acceleration, and displacement at several ground depths. The elements within this matrix are the numerical values of the predicted local nuclear environments, represented in terms of physical parameters, at each site. The columns of this last matrix are examined for fit to a normal or log-normal probability distribution which is a convenience that simplifies calculation; however, it is not a necessary transformation. The completed matrix could be used if desired.

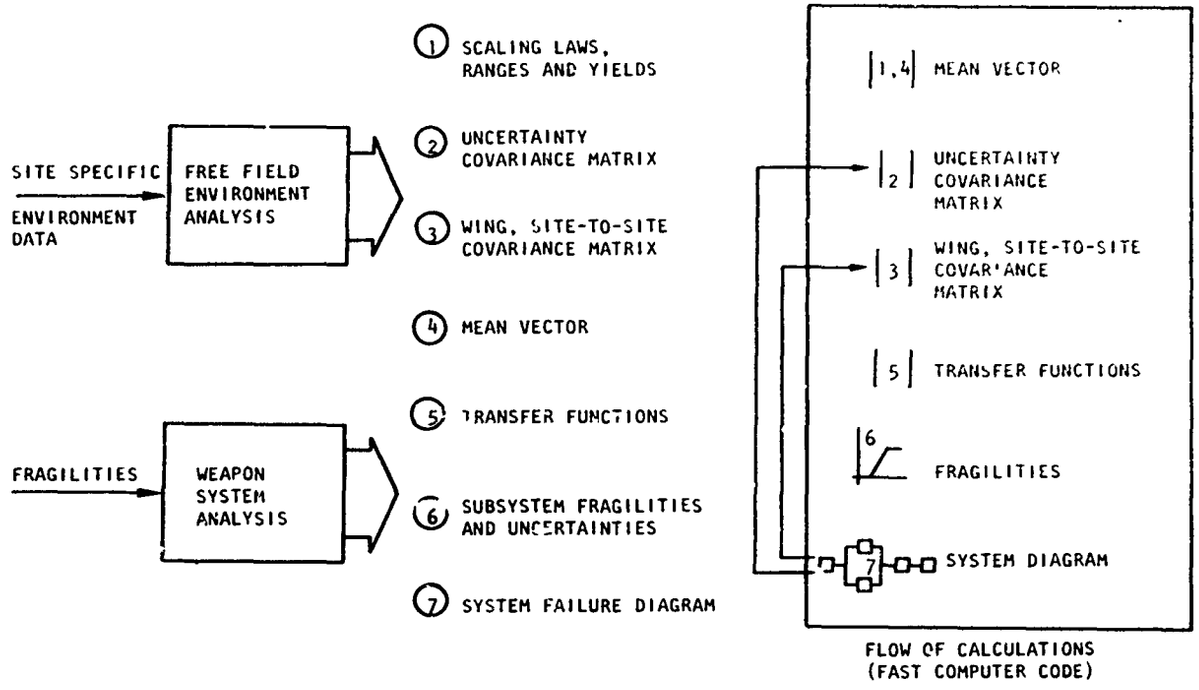

Figure 2. Assessment Methodology Data Inputs

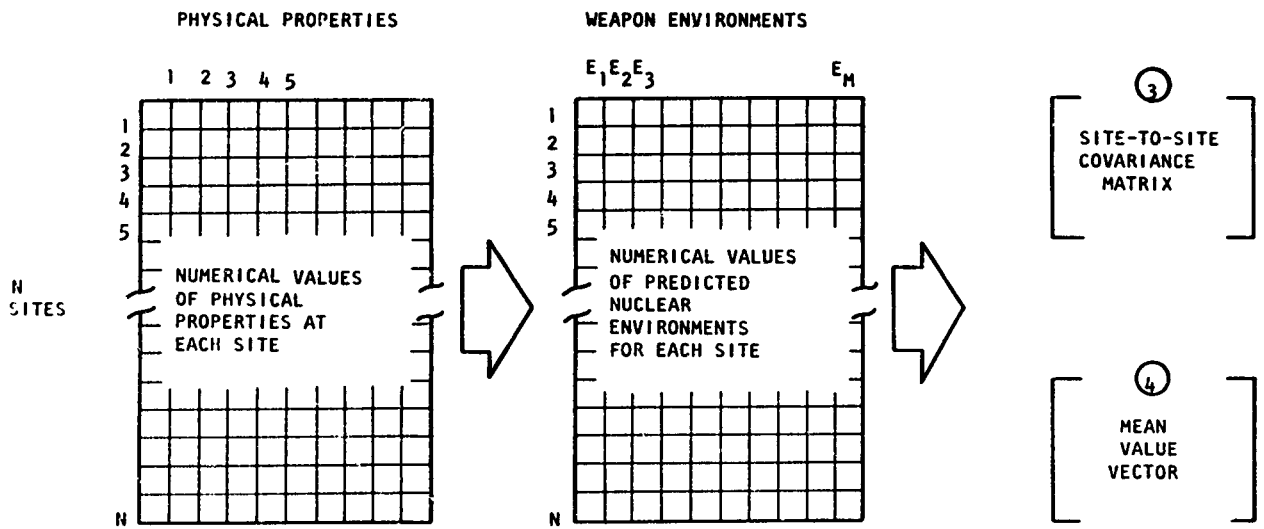

Figure 3. Nuclear Environment Data Inputs

The data in this matrix is then regarded as a distribution of n environments in N dimensional space (where "N" is the number of environmental parameters being treated). An N dimensional multivariate normal distribution is then fitted to the data. This calculation provides the data for Items 3 and 4 in Figure 3; namely, the covariance matrix and mean value vector representing site-to-site variation. The covariance matrix for a multivariate normal distribution is the analog of the variance for a normal distribution on a single variable. The mean value vector corresponds to the mean of a normal distribution defined for each individual environmental variable.

During the environment analysis, scaling laws are developed which provide a capability to predict the free field nuclear environments for varied ranges and yields. This is Item 1 in Figure 2.

Significant uncertainty is recognized in the prediction of the free field weapon environments. This is accounted for in Item 2 of Figure 2. These uncertainties result from both the imperfection of the mathematical models used to predict the weapons environments and from data uncertainties. As a part of the environment analysis, estimates of these uncertainties are made. The phenomenologist determines a range about the nominal value within which he is confident that the true value lies. This is expressed by "K" value. For example, if K=2, it is assumed that true value lies between one-half and two times the nominal value. It is assumed that the true value for the weapon effect is log-normally distributed about the predicted value and that the interval defined by the "K" factor has a width of plus or minus two standard deviations. This assumption provides the basis for obtaining the diagonal terms in a covariance matrix which describes the uncertainty in the weapon environment predictions. In some cases, the uncertainty in two weapon environments is correlated. The phenomenologist provides an estimate of the degree of correlation in the form of a correlation coefficient. This enables the off-diagonal terms in the covariance matrix to be determined.

SYSTEM ANALYSIS

The preceding discussion has been concerned with the procedure for generating the data necessary to predict free field environments. In addition, a procedure to develop the system response is performed. The start of this activity is represented by the box in Figure 2 below the environment analysis box.

The environments considered in the previous discussion are free field and not necessarily representative of internal or local environments within the facility. The internal environment may be attenuated, for example, by shock isolation, or in some cases even amplified. For each weapon effect, a transfer function is developed based upon the response characteristics of the appropriate subsystems (e.g., shock isolation subsystem). Uncertainty in the transfer function is recognized and is assumed to have a beta distribution unless some other frequency function is considered more valid. As with the free field environment uncertainty, a "K" factor is estimated to describe the width of the 2 sigma uncertainty band about the transfer function. This "K" factor, together with the transfer function defines the beta distribution for the uncertainty in the transfer function. The transfer functions for each weapon effect together with the associated uncertainty distributions provide the fifth item of data in Figure 1.

In several situations, there are quite complex transmissions from the free field into the system. For example, electronics may be vulnerable to the total ionizing radiation dose which could be due to free field neutrons, prompt gammas, secondary gammas and captured gammas. In other situations, the stress in a structure may be due to the air-induced and outrunning components of both displacement and velocity because of significant modal response from low-to-mid frequencies. In these situations, the FAST codes allow for appropriate modeling of these multiple component transfer functions.

The next step in the analysis develops the mathematical models for the system response to the internal environment--Item 7 of Figure 2. To this end, the system is partitioned into functional subsystems. Based upon this, a functional network for the system is constructed. This network is analogous to a reliability network for a system, and permits the derivation of an equation giving the system probability of failure as a function of the probability of failure of the subsystems. One difference between this equation and a system reliability equation is that in the case of the survivability equation, the subsystem probabilities of failure enter in the form of probability density functions rather than discrete numbers. The system probability of failure equation or diagram constitutes the seventh item in Figure 2. Another versatility of the FAST codes is the fact that a new network does not dictate a new code. The FAST codes have a compiling logic which writes that part of the code which represents the network equations. All that is necessary as input to FAST is a simple statement of what things are in series and parallel. Series elements are a sequence of things all of which must work to have the represented function work; parallel elements are redundancies such as commercial, standby and emergency power. In some instances, a given component or subsystem may appear more than once in the system network. (For example the guidance and

control system, which is used during ignition of each stage). The FAST codes contain appropriate logic to accommodate such networks.

For each of the components in the failure network, vulnerabilities or fragilities are constructed to represent their hardness. There may be more than one fragility for each component if they are vulnerable to more than a single environment. Thus, a piece of electronic equipment might have a shock and vibration fragility, a nuclear radiation fragility and an acoustic fragility. The fragilities are represented by Item 6 of Figure 2. Fragilities are represented as a cumulative probability of failure of the component as a function of environment level. Both the probability of failure and the uncertainty in these estimates are quantified.

The probabilities account for known physical variations such as strength of materials, manufacturing quality and construction tolerances. In some cases probability can also be used to account for azimuthal variations which might be manifested in such things as nonsymmetric shock isolation systems. The uncertainties account for the accuracy of the fragility estimate. The uncertainty may be due to inaccuracies in an analytic model, the lack of test data or a combination of the two.

It should be noted that the system analyses to derive transfer functions, failure network and fragilities can be carried out with or without an extensive data base on the particular weapon system of interest.

At a minimum, expected design criteria values for these parameters could be assumed to determine the expected system survivability if all requirements are met, and a series sensitivity analysis can be performed to determine the impact of not meeting or changing specific criteria. However, a great deal is known generically about transfer functions and fragilities so that engineering estimates can be made of these quantities even without the completion of component designs. The resulting analyses give a great deal of insight as to where the critical vulnerabilities of a system are and how survivability much like reliability can be allocated to either maximize survivability or minimize cost.

Thus, the data required for the FAST survivability analyses can be derived for a system in being, one being designed or even one being conceived.

FAST CALCULATIONS

The seven classes of data discussed above provide the basis for computation of the system failure probability, using the FAST computer codes. A simplified flow for this calculation is shown on the right in Figure 2.

The first step in the calculation involves scaling of the mean vector of free field weapon effects (Item 4) to the particular yield and range under consideration, by use of the scaling laws (Item 1). This vector together with the uncertainty covariance matrix (Item 2) defines a multivariate distribution for the uncertainty in the vector of predicted weapon effects. From the multivariate distribution, a vector is selected at random. This selected vector represents a mean weapon environment vector taking into account uncertainties in the predicted free field environments and scaling laws. This vector together with the covariance matrix for the variation in weapon effects due to variation in physical environment, such as soil properties (Item 3) defines a multivariate distribution for the weapon effects at randomly selected sites. A vector is then selected at random from this distribution, which represents a free field weapon environment at a specific site selected at random.

This vector of free field weapon environments is then modified by the transfer functions (Item 5) to obtain a vector of local or internal environments. Transfer function uncertainty is incorporated into this procedure.

The elements of the internal environments vector become the inputs to the functional subsystem fragilities (Item 6), permitting computation of the probability of failure for each of the functional subsystems. These probabilities are random in the sense that they depend on the particular combination of uncertain factors selected for the calculation. As with the transfer function, uncertainty in the functional subsystem fragilities is considered. Monte Carlo methods are used. A random number is drawn for each functional subsystem in order to determine the probabilities of survival.

The outcomes (in the form of probabilities of survival) are inserted into the system survival equation (Item 7) in order to determine the probability that the system survives for this particular Monte Carlo trial. At this point in the computation, the outcome for a particular randomly selected site, survival or failure, has been determined. This calculation is repeated many times, using the inner loop in Figure 2 to provide an accurate estimate of the probability of failure for a site. Iteration within this loop is performed to obtain the expected value arising from probabilities of hardness parameters such as variations in the hardnesses of components due to differences in the manufacturing processes. This is in contrast to uncertainty variations, such as errors in the mathematical modeling, transfer functions, and fragilities which will apply uniformly over the entire force.

Having determined the system probability of failure for the particular combination of

uncertainties, the process is repeated many times using the outer loop in Figure 2. Each time the outer loop is exercised, a new set of uncertainty factors are selected at random from the appropriate distributions. These include:

- Free field weapon environments using the multivariate distribution defined by the weapon environment mean value vector and the uncertainty covariance matrix.
- The nominal value for the transfer functions together with the associated beta distributions.
- Functional subsystem fragilities using the nominal fragility together with the associated beta distribution for each functional subsystem.

Each time the outer loop is exercised, a new value for system probability for failure is obtained, each of these values reflecting a different set of uncertainty factors resulting from randomization of the uncertainties. As the number of probabilities obtained by exercising the outer loop increases, a distribution of these values is built up. This process is continued until enough data has been collected so that the median of the distribution can be estimated accurately.

To derive the complete median or other "certainty" level of probability of system survival versus range curves, the program is run for other ranges and yields and the curve of interest is drawn through the median or other percentage points of the above distributions.

SUMMARY AND CONCLUSIONS

This paper has described a statistical approach to the evaluation of the failure of complex systems which was developed at the TRW Systems Group. The approach provides a standardized format for treatment of the many factors important to evaluation of system hardness. The methodology treats the propagation of the weapon effects from the exploding weapon to the vicinity of the facility, transmission of the effects into the facility taking into account modification of the effects by shock isolation or other protective equipment, and response of the system in terms of the probability of component failure due to the weapon induced environments. The components probabilities of failure are then combined by means of system failure network logic to obtain the system probability of failure.

One of the innovations involved in the approach is the treatment of uncertainty in the inputs and mathematical models. Estimates of these uncertainties are included in the inputs and their influence is displayed in the form of a distribution of the system failure probability.

The methodology has been employed for the assessment of the hardness of existing systems as well as for planning purposes. In the later case, the methodology has been used to evaluate alternative approaches to hardening the system to enable identification of the most cost effective alternatives.

FRAGILITY TESTING FOR HYDRAULIC SURGE EFFECTS

D. M. Eckblad
The Boeing Company
Seattle, Washington

and

W. L. Hedrick
TRW Systems Group
Redondo Beach, California

Hydraulic pressure pulses are induced in all fluid lines; such as water, fuel, brine, etc.; of a structure or facility that is subjected to transient motions as a result of the ground shock associated with a weapon attack. These pulses propagate through the plumbing system and impinge upon the various components attached thereto. A test was devised to subject various subsystems to hydraulic pressure pulses simulating that which would occur due to the ground motions in order to establish the failure levels of various components to this effect. This paper describes the components tested, derivation of the test pressure pulse, test procedure, and the test results.

INTRODUCTION

The system tested was composed of a liquid cooler, a heat exchanger for electronic equipment, and various storage tanks and interconnecting hoses. Portions of the cooling system were rigidly mounted to a wall of an equipment room, and portions were shock isolated as shown in Figure 1. Pressure pulses are induced in the tanks and plumbing due to the acceleration of the equipment room during an attack and these pulses are propagated throughout the cooling system. In order to determine the hardness of cooling system components to the shock, a test was devised to simulate the induced pressure pulses for various levels of ground shock.

The waveform and magnitude of the pressure pulses were determined from calculations based on the predicted motions of the equipment room and from measurements taken during previous field tests. The pulses were defined for an interface point some distance away from the test specimens. From this interface, the plumbing and hardware represented field installation.

The heat exchanger and the liquid cooler were the pressure sensitive subsystems. Because of the large spacial separations between the heat exchanger and the liquid cooler, the coupling of the hydraulic transients between the two units was assumed small and, therefore, each subsystem was tested independently. The test consisted of simultaneously inducing a given test pressure pulse into each hose leading to the subsystem, starting at a pressure level well below its anticipated capability and increasing monotonically in pressure level until a failure of a component occurred. Components were visually and, if necessary, functionally inspected after each test to identify component failures.

The heat exchanger subsystem controlled the temperature for four major components such as a computer, diode block, controller, and connector which were connected in series with medium pressure teflon hoses as shown in Figures 2 and 3. Two 3/8-inch diameter low pressure hoses service the subsystem which was located 15 feet from the interface where the test pressure pulse input was defined for the test. The liquid cooler subsystem consisted of two impeller pumps, a filter, a modulating valve, and a chiller which were interconnected with medium pressure hoses as shown on Figures 4 and 5. Two 3/8-inch diameter and

one 5/8-inch diameter low pressure rubber hoses service this unit which was located 6 feet from the interface where the test pressure pulse was defined for the liquid cooler test.

Four heat exchanger sets and two liquid coolers were tested until failure occurred. Pressure time histories were recorded at several points within the units and were correlated with component failure to aid in evaluating the system fragility in terms of ground shock level.

The pressure pulses were generated by dropping a weight on the piston of a hydraulic jack. By varying such parameters as drop height and weight, stiffness of crushable material between the drop weight and jack and piston travel, it was possible to calibrate the pulse generator to consistently reproduce the test pressure pulses for each level.

DERIVATION OF TEST PRESSURE PULSE

Hydraulic pressure pulses are generated in the hardmounted tanks and rubber hoses of the cooling system shown in Figure 1 when the equipment room is accelerated by the ground shock. Rather than subject the entire hardmounted plumbing system to the ground shock environment, it was obviously more desirable and economical to duplicate the hydraulic pressure pulse by other techniques. In order to accomplish this it was necessary to determine a realistic test pressure pulse waveform. To minimize the number of tests, a single test pulse was developed for a given ground shock level that represented the most critical pressure pulse that could be generated.

The pressure pulse generated in the hardmounted tank was assumed to be described by the short pipe equation for a closed end pipe, that is

$$P = 2 \rho a \ell \qquad (1)$$

where

- P - Peak pressure in the tank
- ρ - Density of fluid in the tank
- ℓ - Length of tank
- a - Step acceleration applied to tanks

For a given ground shock level, the acceleration of the equipment room was determined from analysis and previous full-scale tests. Because the tanks were rigidly attached to the wall, the accelerations associated with the high frequency environment were used in Equation (1) to determine the peak pressure generated in the tank. Since the pressure pulse definition desired was at the point of the hard/shock mounted interface, it was necessary to account for the modification of the pressure pulse in traveling to that point. Preliminary tests revealed that for the pressures propagating through the rubber hoses, the wave speed was reduced as shown in Figure 6; the peak pressure was attenuated by about 2 percent per foot as shown in Figure 7; and the rise time to peak pressure increased from about 2 ms to 9 ms. Thus, the contribution to the peak pressure at the point of test pulse definition from the tank consisted of the sum of the pressures calculated by Equation (1) for both the vertical and horizontal components of acceleration, reduced by an impedance factor in going from the tank to the hose, and further reduced by an attenuation factor of 2 percent per foot while traveling from the tank to the point of test pulse definition. Pressure pulses are also generated by motions of the hoses mounted to the wall or floor at points where bends or discontinuities exist. Since only 90° bends existed in the rubber hose plumbing, the pressure equation for each straight segment of rubber hose hardmounted was assumed to be

$$P = \rho a \ell \qquad (2)$$

The acceleration in this case was assumed to be the rigid body acceleration of the facility because the low frequency response of the rubber hose mounts. The contribution to the pressure at the point of the test pulse definition from each straight segment of the hardmounted rubber hose was calculated using Equation (2) and then attenuated by 2 percent per foot while traveling to the point of test pulse definition.

All sources contributing to the pressure at the point of the test pulse definition where summed together for the combined vertical and horizontal ground shock to define the peak pressure for the triangular test pressure pulse shown in Figure 8. Rise time to the peak pressure was determined from the transient time from the first 90° bend in the hose to the point of test pulse definition and the total pulse duration was evaluated from the duration of the rigid body acceleration of the equipment room.

TEST PULSE GENERATOR

The pressure pulse generator, shown schematically in Figure 3 and in the photograph of Figure 9, was used to generate the test pressure pulses defined above. It consisted of a 150 to 350 pound weight with a maximum drop height of 7 feet. The weight drops on the piston of a hydraulic jack having about a 6-inch stroke. A 7/8-inch diameter piston was used for the heat exchanger tests, but increased volume requirements for the simultaneous production of three pressure pulses in the liquid cooler (one for each line to the test specimen) required a 1½-inch diameter piston for the lower pressures and a 2½-inch diameter piston for the higher pressures. Additional plumbing was used for bleeding, filling, static pressure checking of the system, and smoothing out the generated pressure pulse.

Rise time of the pressure pulse was controlled by placing appropriately shaped styrofoam (density of 1 pound per cubic foot) between the jack piston and the drop weight. Peak pressure was controlled by the drop height and total piston stroke, while pressure pulse decay was primarily a function of stiffness of the weight arresting material (1 pound per cubic foot styrofoam). Additional tailoring of the pressure pulse was achieved by varying the length of rubber hose between the hydraulic jack and the point of pressure pulse definition.

Prior to testing, the pulse generators were calibrated by inserting hoses of sufficient length that end reflections did not influence the generated pulse. Typical correlations of the generated and calculated pressure pulse is shown by Figure 8. For a given setup the repeatability of the pulse generator was within ±8 percent on the peak pressures.

TEST PROCEDURE

The pulse generator was first calibrated as described above. It was then connected to the pressure hoses leading to a given test specimen at the subsystem hard/shock-mounted interface with the cooling system. The test specimen was then shocked, starting at the lowest test pressure pulse, and monotonically increased in shock level until a structural or functional failure occurred.

A hydrostatic pressure test was conducted before and after each shock to check for leakage in the test specimen. In addition, visual, and where necessary, functional checks were conducted after each shock level to determine if a failure had occurred.

Pressure transducers were used to measure the input pressure pulse out of the generator and the internal pressures in the subsystems.

TEST RESULTS

Preliminary impulse tests were conducted to determine the effect of bends in the rubber and teflon hoses on the pressure pulse propagation. This was accomplished by measuring the input and output pressures first of a straight section of rubber hose and then repeating the same pressure pulse with 4 to 5 complete coils with a number of short curvature bends. Results of the two tests were nearly identical confirming that it was not necessary to duplicate the actual hose routing for the shock tests.

Extreme care was required in bleeding the air out of test specimen and pulse generator. A small amount of air in the test setup resulted in erratic pressure measurements, generally in the form of shorter rise time to peak pressure and reduced peak pressures.

Failures of the four sets of heat exchanger components occurred in the soldered connection of the cover plate in the controller manifold and the epoxied connection of a 1/8-inch thick aluminum cover plate on the computer shown in Figure 10. Failures were easily identified by visual observation of the leakage and sudden drop of pressure on the pressure time history plots. One of the computer cover plates which did not fail during the impulse tests failed at about one-half the peak impulse pressures under a static pressure test. No leaks occurred in the quick disconnects of the teflon hoses or the connector during the pressure pulse tests.

It was useful to compare the pressure time histories measured in the heat exchanger subsystem to that which would occur in a simple linear system made up of a long rigid pipe with the test pulse input at each end of the pipe. The peak pressures at the center of this system would exactly double peak input pressure at each end. As shown on Figure 11, this phenomena occurred at the approximate center of the test specimen. This was surprising since 20 to 30 percent attenuation of the test input pulse was anticipated in traveling through 15 feet of rubber hose to the test specimen in addition to attenuation due to energy losses in the test specimen. Apparently there was an effective increase in impedance in going from the rubber hose to the test specimen which resulted in an increase in pressure at the interior of the test specimen.

Except for failures due to slippage of a set screw of the DC pump impeller seal shown on Figure 12, the liquid cooler withstood the maximum output of the 2½-inch diameter piston pulse generator with only minor leaks at the AC pump gasket during the pressure pulse test. Since there was no specification on the set screw torque requirements, it was decided to evaluate the fragility level as a function of the DC pump set screw torque and then determine the set screw torques of the DC pumps in the field from a statistical sample.

Peak pressures measured in the vicinity of the DC pump during the impulse tests were plotted as a function of set screw torques on Figure 13 along with results from static pressure tests.

CONCLUSIONS

The fragility test procedure, implementation, and data acquisition was of sufficient detail and accuracy to establish the fragility level of the cooling system for hydraulic pressure pulses.

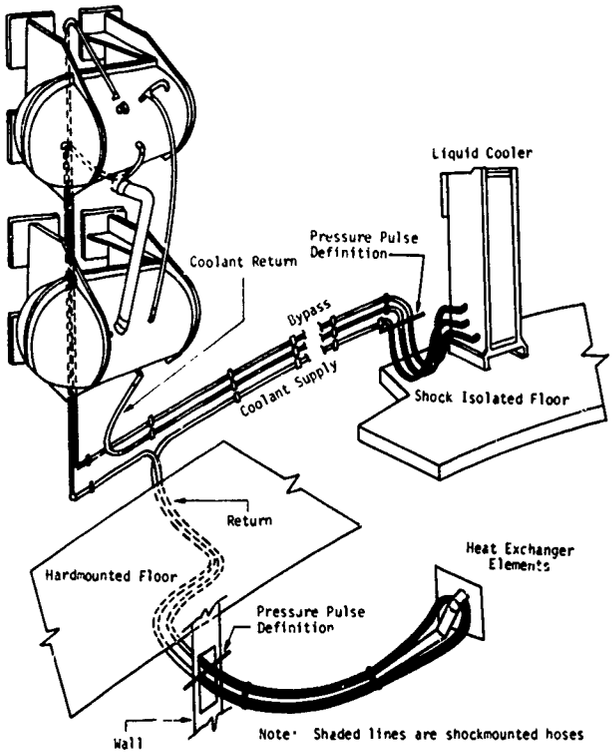

Figure 1. Schematic of Cooling System

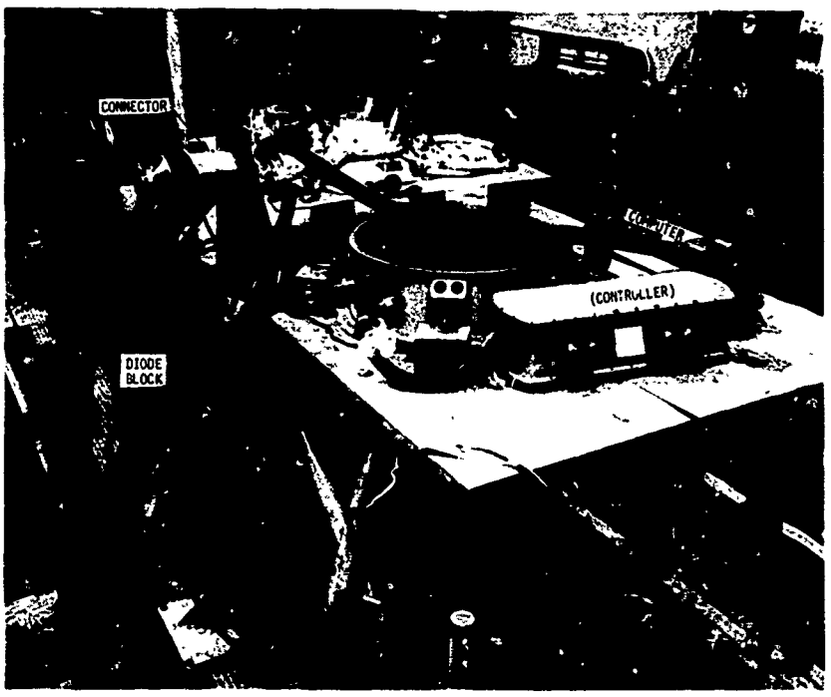

Figure 2. Photograph of Heat Exchanger Subsystem

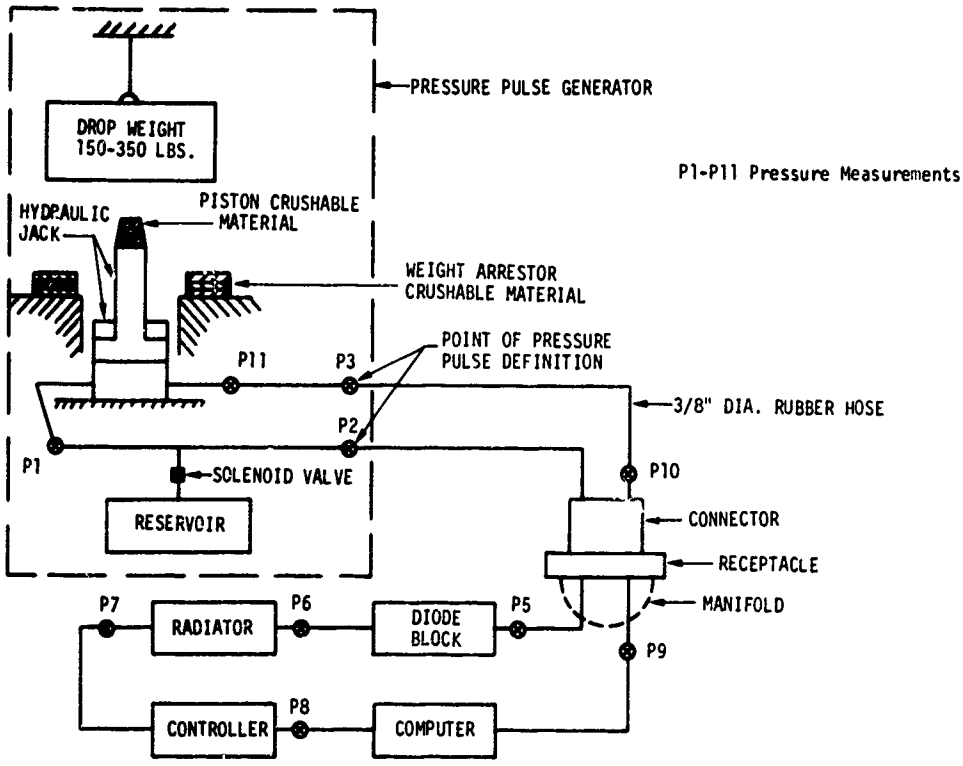

Figure 3. Schematic of Fragility Test Setup For Heat Exchanger Elements

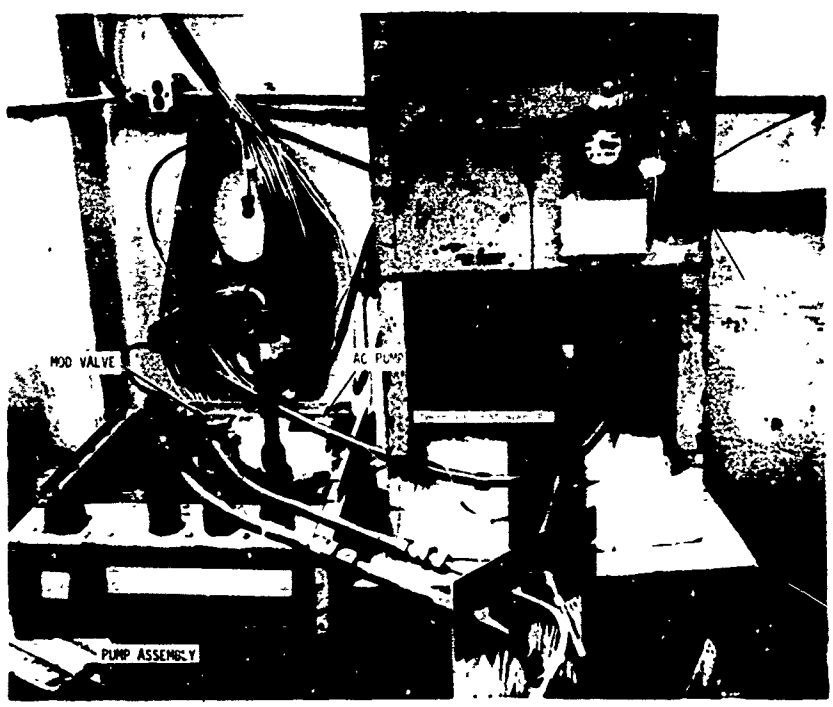

Figure 4. Photograph of Liquid Cooler Subsystem

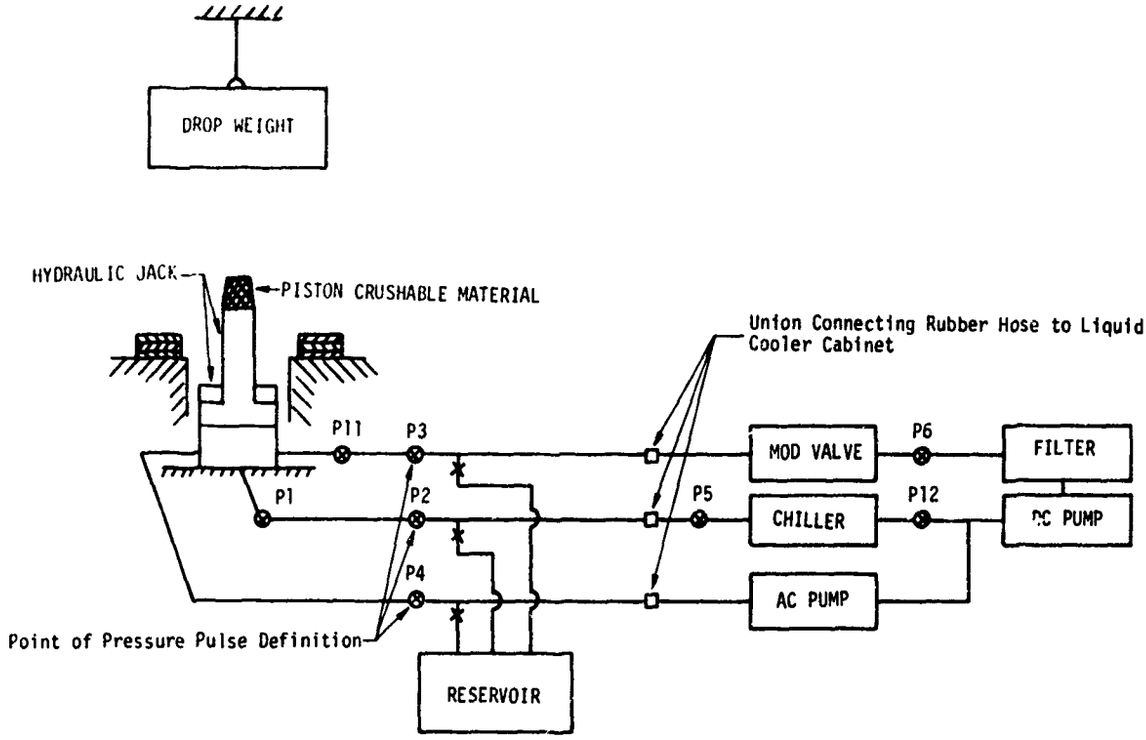

Figure 5. Schematic of Liquid Cooler Fragility Test Setup

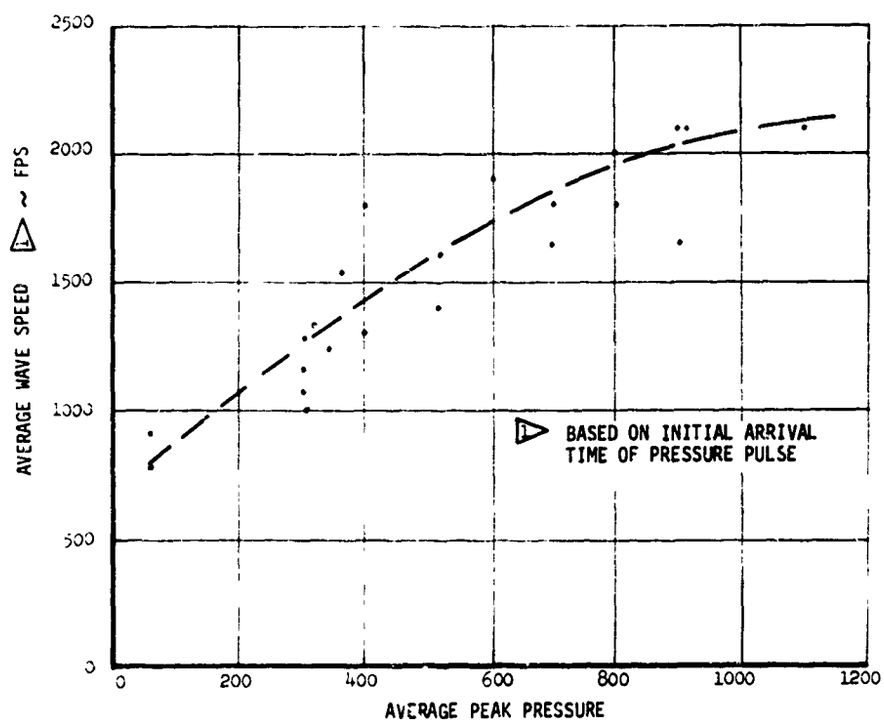

Figure 6. Wave Speed in Low Pressure Rubber Hose

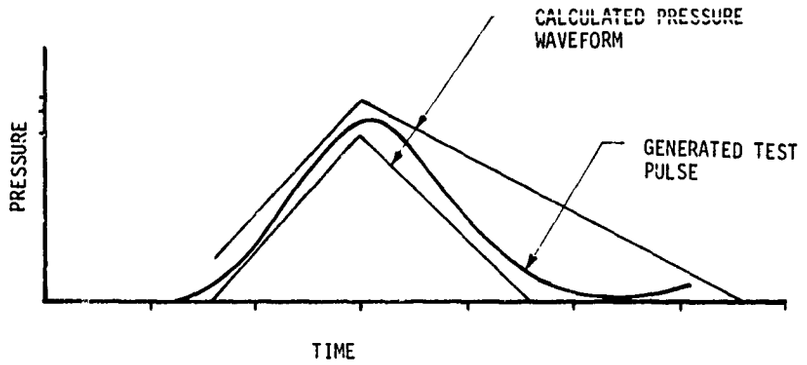

Figure 8. Test Pressure Pulse Shape

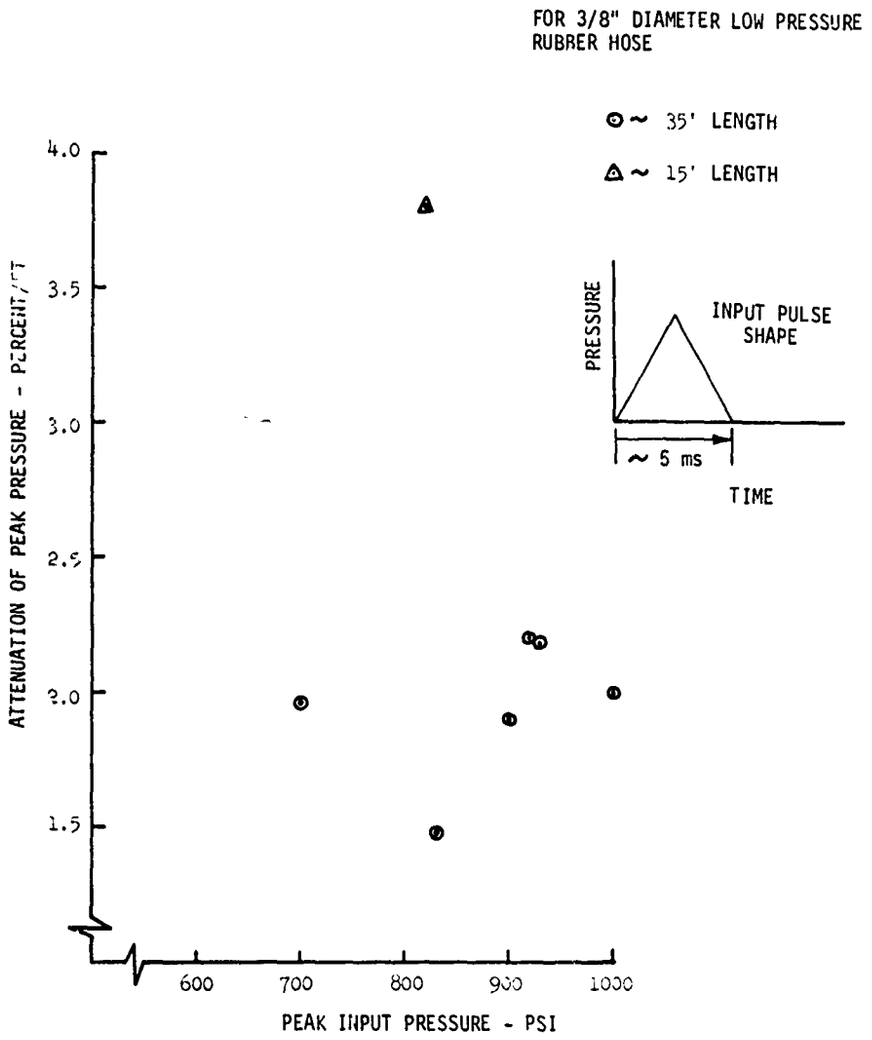

Figure 7. Attenuation of Peak Pressure in Low Pressure Rubber Hose

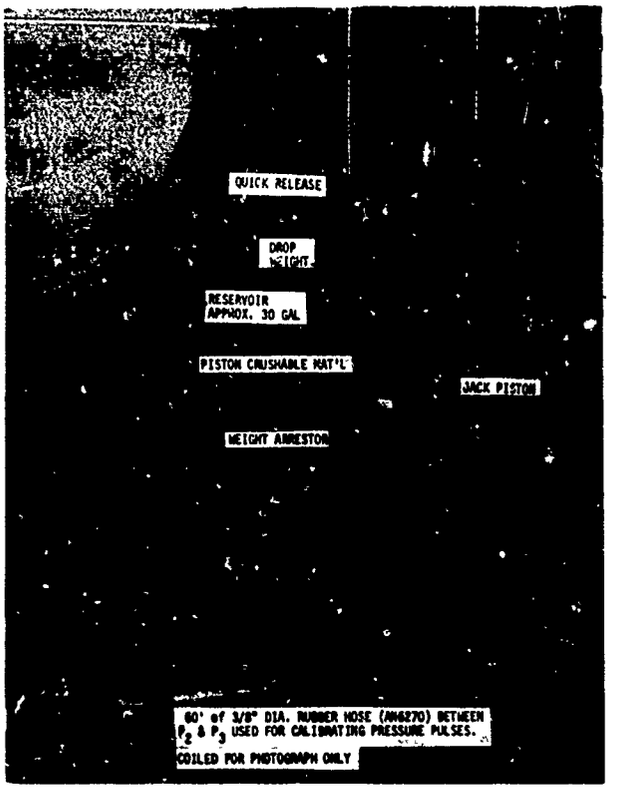

Figure 9. Photograph of Pulse Generator

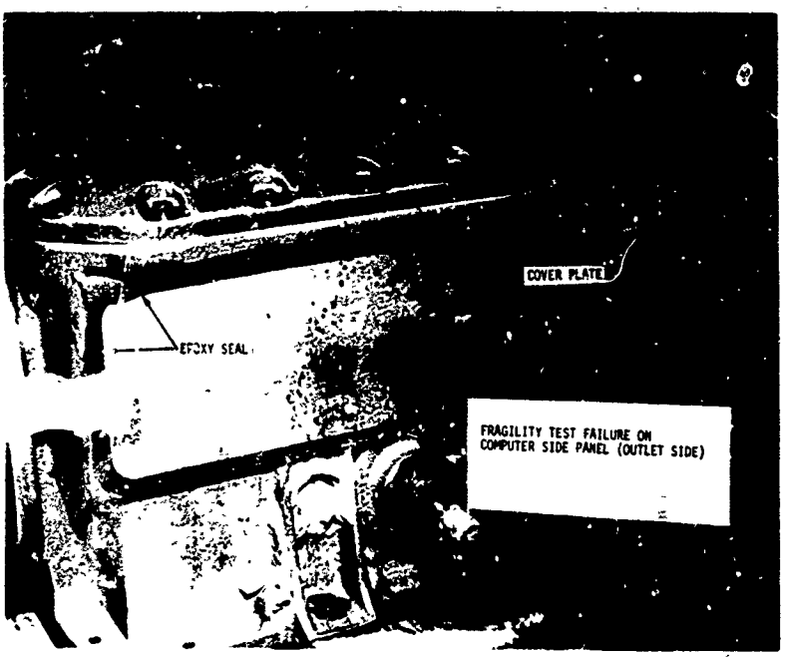

Figure 10. Photograph of Failed Computer Cover Plate

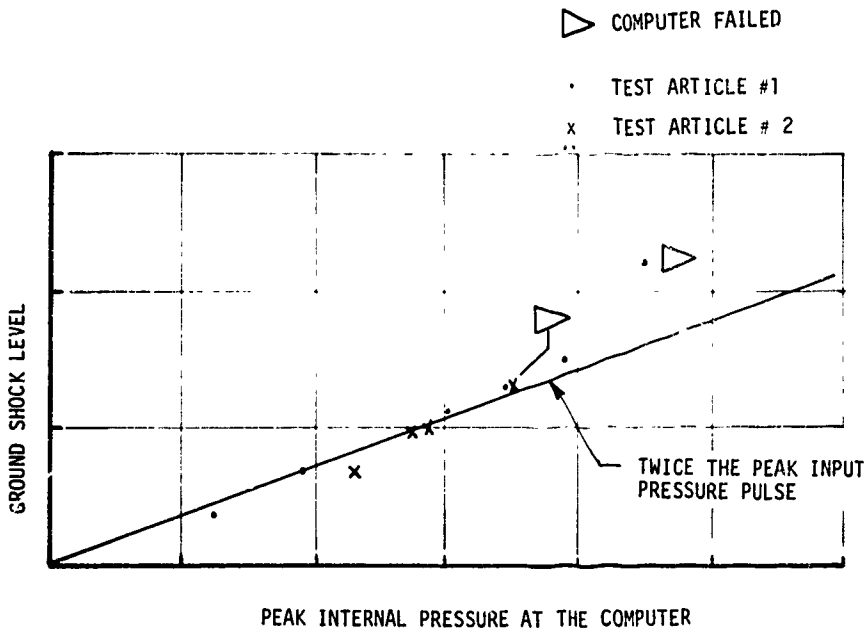

Figure 11. Internal Pressure Magnification in the Heat Exchanger

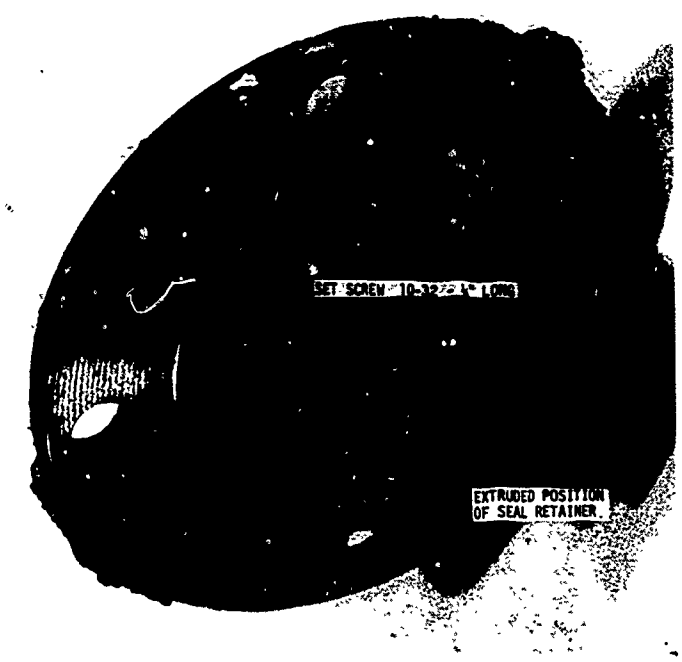

Figure 12. Photograph of DC Pump Retainer Seal

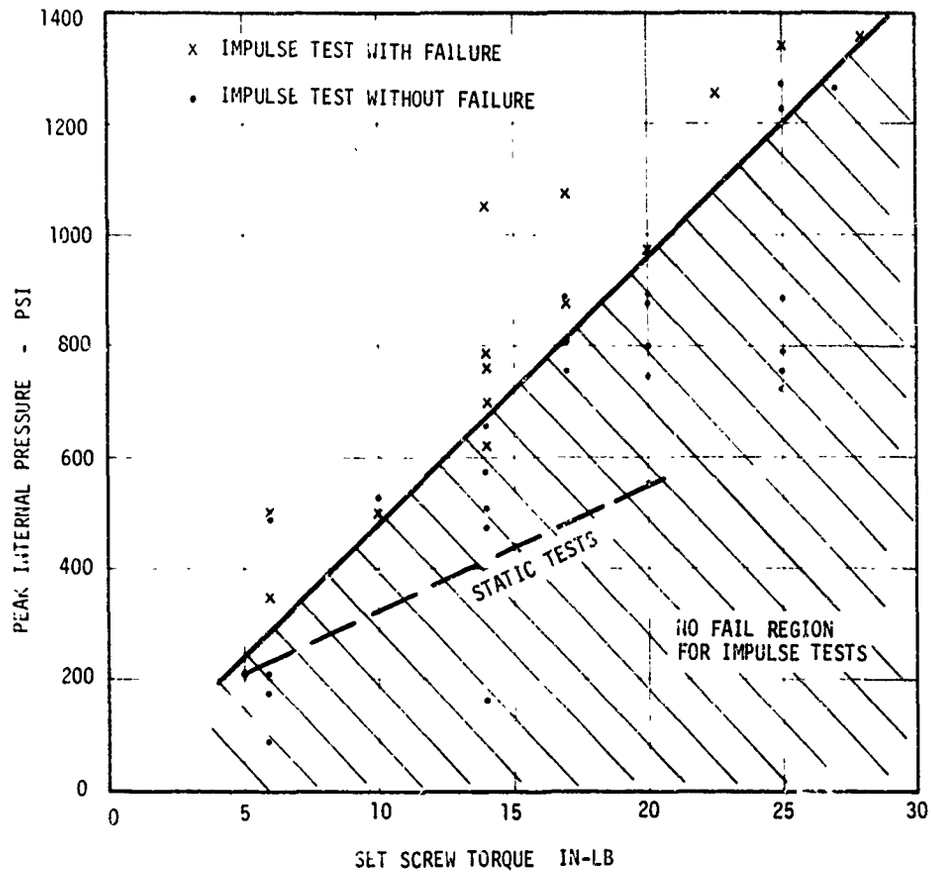

Figure 13. Peak Internal Pressure Versus Set Screw Torque at Failure of the DC Pump

Mr. Safford (TRW Systems, Chairman): Thank you very much. I think one of the things we are trying to stress here is the unanticipated, particularly in tests. Some of these failures are just silly, and they are very embarrassing, but you do not know until you make the test. Often when you do find them, you can easily rectify them. This test program was of substantial economic benefit to the Air Force. It permitted the Air Force to make a very good decision on a very sound basis.

(The following remarks were made by G. K. Dahmen, USAF Space and Missile Systems Organization, who was co-chairman of the session on which the preceding six papers were presented.)

In my field I am vividly aware of the fact that we get into a gray area whenever we even mention the word fragility. Questions that bother me are: what is the signature sensitivity of the item we are talking about; what is the test pulse—the input pulse, is it valid, what are the criteria, how do you define the criteria? What is the effect of using single-axis tests when you know in real life the items are going to get a multiple-axis signature. Well, this goes on and on and on, and I think today, this session has really indicated some very significant factors and considerations with regard to fragility testing and the definition of fragility. So, to sum it up, I think it is a wide open field and we have really only scratched the surface.

INITIAL DESIGN CONSIDERING STATISTICAL FRAGILITY ASSESSMENT

Richard L. Grant
The Boeing Co.
Seattle, Wash.

The discussions of this paper are largely philosophical, dealing with an approach to a pattern of technical confidence for a program of Research and Development. The program is concerned with development of shock isolation and equipment for underground nuclear attack resistant weapon systems. The program developed over the past two years, recognized the complexity of the overall task of shock isolation and the technology advances which had been made in the past 12 to 15 years. It also, however, recognized the uncertainties extant in the areas of high frequency transmissibility, the influence of the structural and mechanical details on transmissibility, the potential for signature sensitivity of equipment and the need to cope with these areas in assessment of the weapons system effectiveness.

The desire to do the best possible job of shock isolation is clearly not a new one. The requirements for statistical assessment either before, during or after the system is designed and built are relatively new; especially in terms of the scope and depth of the assessments which results from increased sophistication of analysis techniques and from the multiplicity of environments which must be considered. In these ways the statistical approach to fragility and the impact on the assessment differ from the normal reliability approach to the problem and warrant special consideration in the early conceptual and initial design phases.

INTRODUCTION

The discussion herein treats the initial design problem both from the standpoint of conceptual activities and from the standpoint of benefit derived during the actual design of hardware.

The most popular and practical means of providing shock isolation for critical equipment while also providing relatively easy access for checkout and maintenance is the shock isolated floor. This results in a fairly compact aggregate of several different kinds and types of equipment. It generally results in some degree of assymetry due to different equipment and due to the configuration of the facility housing the systems. The system then consists of shock isolators (sometimes of slightly different design and dynamic characteristics), a fairly stiff and usually structurally complex floor, a number of more or less flexible elements from the facility to the floor (cables, conduits, hoses, etc.) and finally a complement of equipment (usually housed in some kind of cabinet structure). For example, an underground hardened system with a shock isolated floor is configured as shown in Figure 1.

The difficulty in proceeding with a program for shock isolation systems, to present the best possible fragility picture to the ultimate assessment, is perhaps highlighted by looking at the two extreme cases; 1) the program could be initiated to develop equipment with such high capability that no isolation is required; or that what isolation is easily attained, is merely excess capability or 2) the program could be initiated to develop shock isolation capability such that the least capable off-the-shelf equipment could easily survive. Disregarding a number of other practical considerations not related to shock and vibration fragility, the input dynamic environment criteria for nuclear attack is so severe as to render the first case technically impractical for most delicate electronic equipment and the second case technically difficult and economically impractical. Therefore, the burden of providing a high capability to withstand the shock and vibration environment must be split reasonably between the isolation capability and the equipment tolerance for the isolated environments.

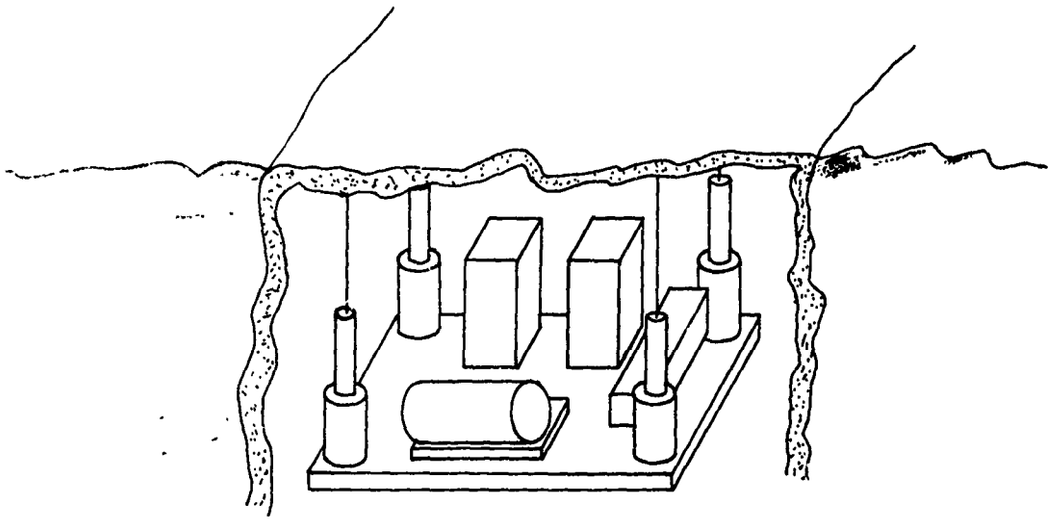

FIGUR 1

In order to better understand the overall dynamic behavior of shock isolation system elements, The Boeing Company conducted a comprehensive program of testing and analysis. This paper in intended to describe some of the motivation for this program and to explain how it fits into the goals of the statistical hardness assessment of the weapon system. A summary description of the test and analysis program is also contained herein.

DETERMINATION OF FRAGILITY

Now consider the requirements to determine the fragility of this system and to incorporate the fragility information into a statistical assessment of the composite system.

STRUCTURAL ELEMENTS

Basically the capability of structural elements of the system may be described by fairly straight forward structural dynamic analysis. The capability to perform the intended function in the presence of a dynamic environment is generally only limited by physical distress or yielding of the structural materials.

Solution of the equations of motion for the system including only the basic flexibilities and finite element analysis of support structure are generally adequate to permit description of the loads, stresses and strains in the structural elements.

The fragility of the structural system may then be derived as a function of any desired input parameters by performing the analysis enough times to establish the trends in the loads. The probability of failure (P_F) may be determined by prescribing an allowable range for the structural materials and relating these to the loads as a function of the input variables.

The only nuclear weapon effect requiring consideration is ground shock. But consider the relationships which may enter the solution of the fragility. Due to siting media, differences in weapon yield and distance to the detonation point, the isolation system may be subject to a large range of displacements. This range of displacements may occur with a large range of maximum velocities and accelerations and the input may be applied at any azimuth. The fragility data cannot be presented as unique, single valued parameter relations but must consider all the dependent variables.

Fortunately the structural fragility of the isolation systems are generally not much affected by variations in maximum acceleration so that a family of curves such as shown in Figure 2a may be developed.

Since the systems are fairly linear in the range of interest for the structural fragility, the azimuth sensitivity can generally be described in terms of a factor to be applied to the above P_F curve. The P_F curve may then be displaced to the right or left by an amount as indicated in Figure 2b.

Information of the type shown above can be derived at any point in the design activity. The accuracy will, of course, depend on the extent of the design informa-

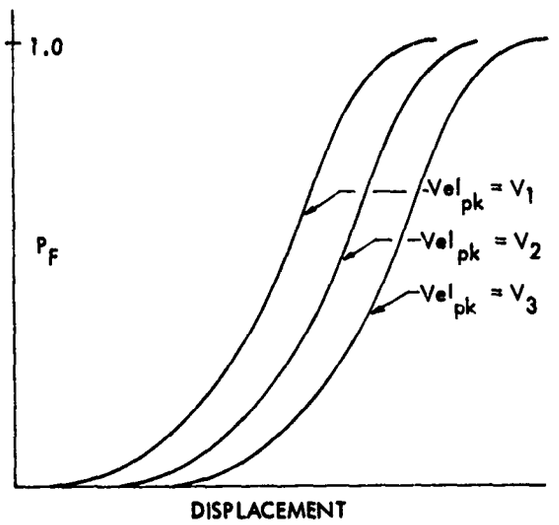

FIGURE 2a

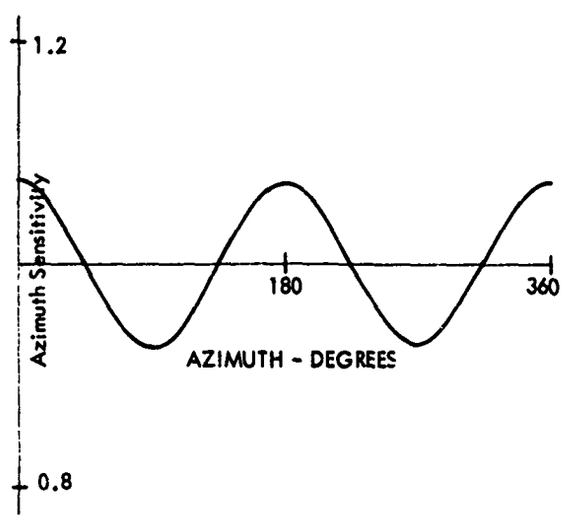

FIGURE 2b

tion and how well the input motion data represents the final requirements. Clearly, the design should strive to make the system fragility as insensitive as possible to input motion variations or should result in P_F curves so far to the right as to make then insignificant in the assessment.

Since weight limitations are not severe and since this portion of the system exists only to enhance the survivability of the remainder of the essential equipment, it is possible to design these structures with adequate excess capability. A much less straight forward determination is associated with the structural elements in their competence as isolation elements and the influence of the load path in establishing the character of the dynamic environment at the essential equipment items.

SHOCK ISOLATION ELEMENTS

Figures 3 and 4 show a collection of actual test results. These data are shown as the ratio of the output end acceleration response spectra to the input response spectra. There is no intent to defend these as true measures of transmissibility and obviously they should be normalized to the first response mode frequency for comparison. However, it is not intended that the numbers be useful. The point is to show that even the very good isolators such as the liquid spring or the foams, do not behave as ideal massless isolators but rather exhibit higher mode responses of their own structure as well as introducing environments due to the internal operation of their physical, material or design characteristics.

The precise nature of the entire frequency domain environment transmitted through or generated by the shock isolation is extremely dependent on the detailed design. The variation of environments with input are seldom linear and the variation with isolation element physical and geometric parameters are also not usually linear. However, insight into the most desirable features for incorporation into the design can be derived empirically from test data. At the outset of the program addressed in this paper very little data was available as a guide in this area. More importantly perhaps the guidance to effective design should be concerned with things to avoid as known problem areas.

FLOOR AND SUPPORT STRUCTURE ELEMENTS

Figure 5 shows some actual test data obtained for floor structures subjected to a transient dynamic environment. As noted above, the shock isolation elements do transmit high frequency environment to the floors. The floors and support structure do not, in general, attenuate these environments but rather modify the character of the environment and may introduce secondary environments due to local resonances, joint configuration and mechanical interfaces. These structures also tend to be non-linear with respect to input and physical variables.

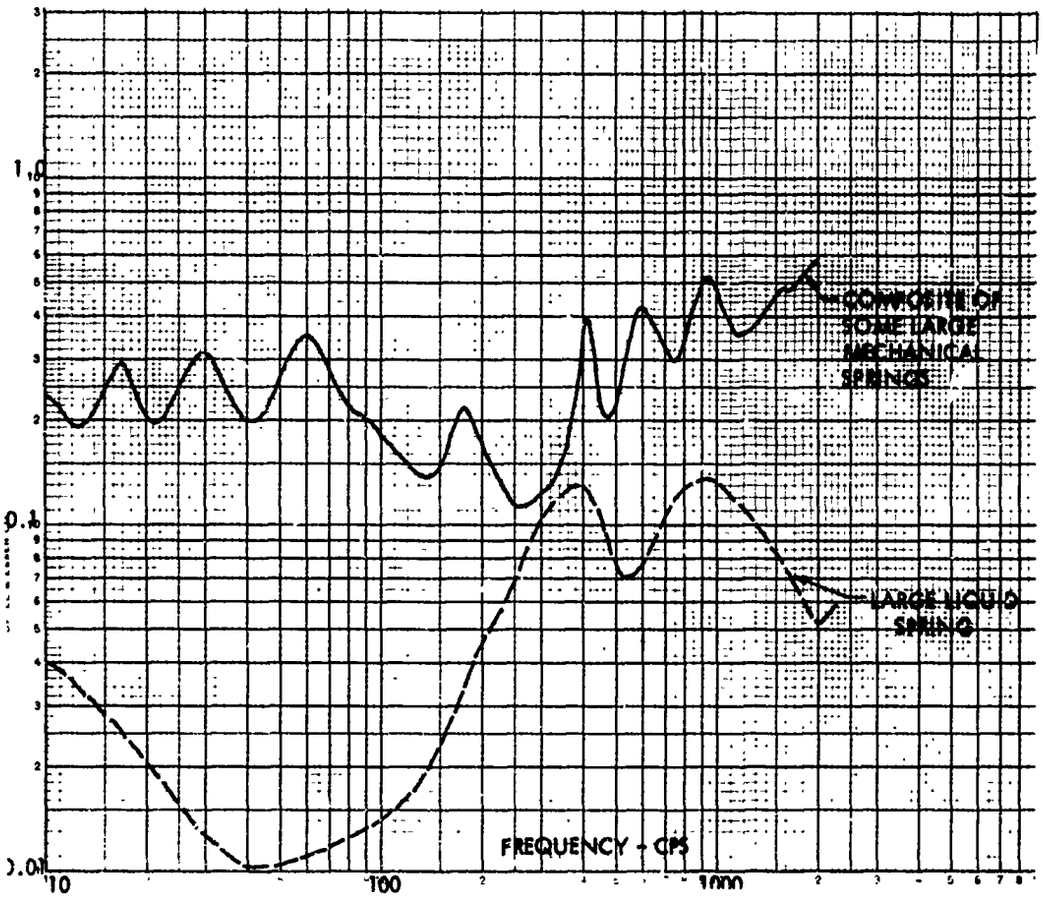
1.0
0.1
0.01
10
100
1000
FREQUENCY - CPS
COMPOSITE OF SOME LARGE MECHANICAL SPRINGS
LARGE LIQUID SPRING

FIGURE 3

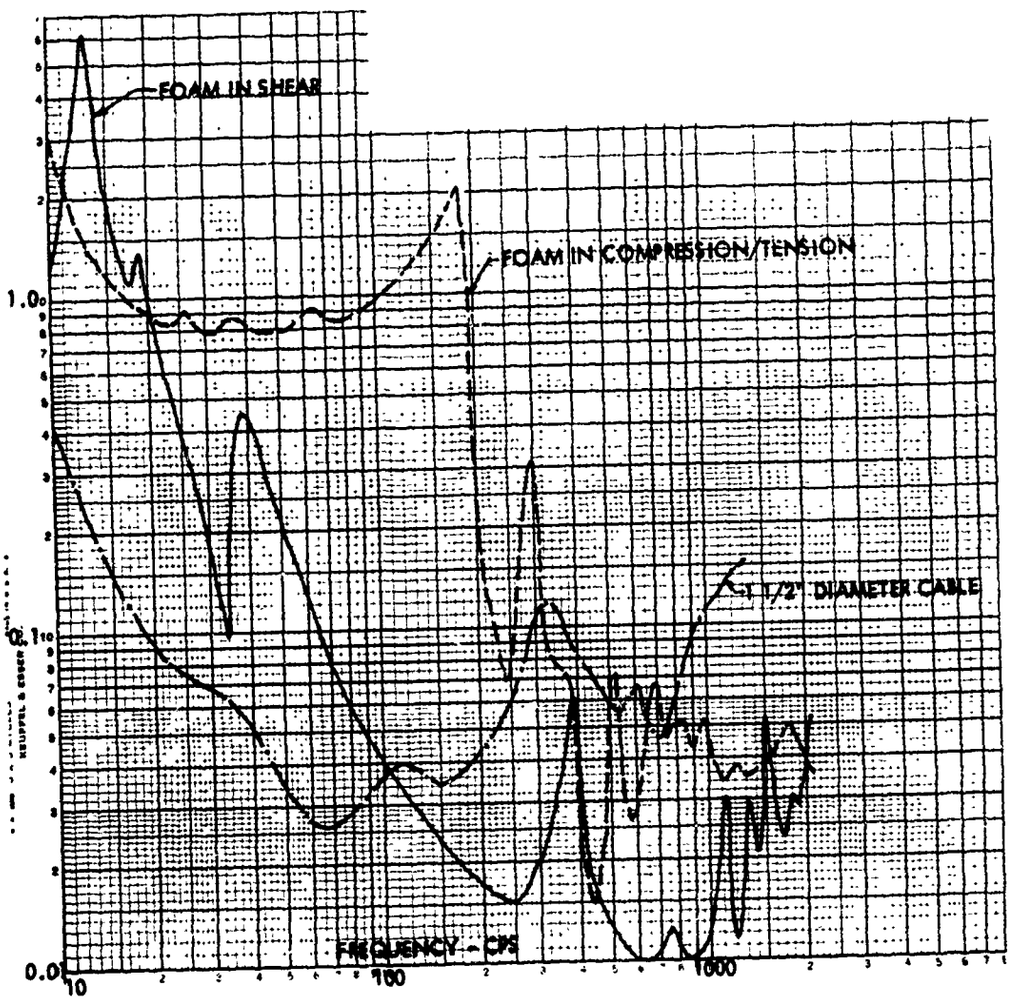
FOAM IN SHEAR
FOAM IN COMPRESSION/TENSION
1 1/2" DIAMETER CABLE
1.0
0.1
0.01
10
100
1000
FREQUENCY - CPS

FIGURE 4

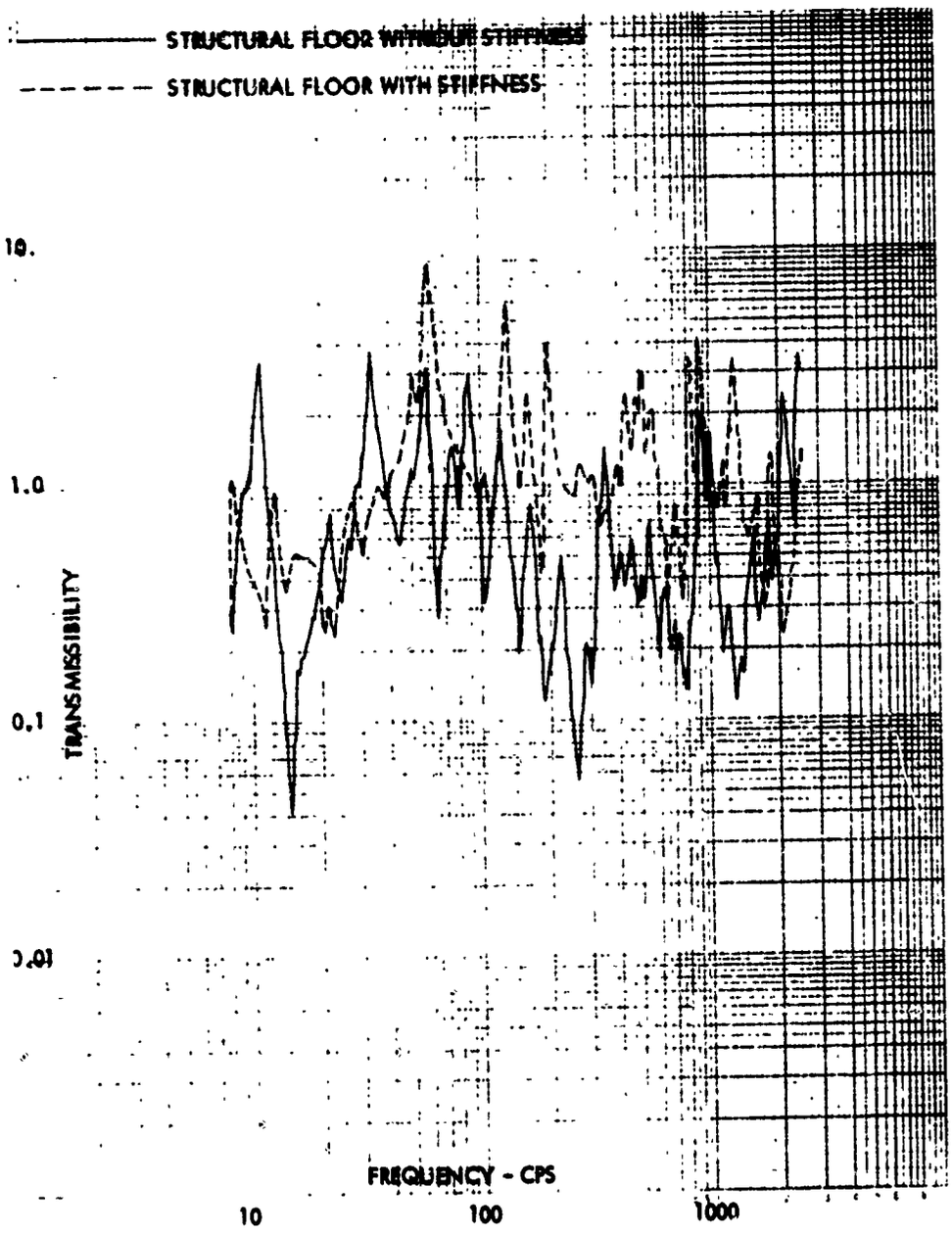
STRUCTURAL FLOOR WITHOUT STIFFNESS
STRUCTURAL FLOOR WITH STIFFNESS
10.
1.0
0.1
0.01
TRANSMISSIBILITY
FREQUENCY - CPS
10
100
1000

FIGURE 5

Here again the design process can benefit from empirical information indicating desirable design features and things to avoid.

EQUIPMENT ELEMENTS

As previously mentioned the complement of equipment found on the shock isolated floor is made up of a number of different kinds and types. Electronic equipment predominates but a number of mechanical items and mechanical/electrical items are also included. Each of these items possess more or less unique characteristics which lead to different fragility levels for the different items. The failure modes are different as are failure levels and the frequency domain sensitivity is also different. In the above sense the equipment exhibits the classical examples of dynamic environment signature sensitivity. An example of this behavior from actual test data is shown in Figures 6a and 6b. Figure 6a depicts a case where a transient vibration input which produced a flat response spectrum caused the first failure of an equipment item to be a capacitor and its bracket. A transient vibration input which produced the variable response spectrum, caused the first failure of an identical equipment to be a circuit breaker. Figure 6b depicts a case where identical transient vibration pulses were input to the same equipment except that the frequency was increasing with time in the first case and decreasing with time in the second. At a specific level, the first case did not produce failure, the second did.

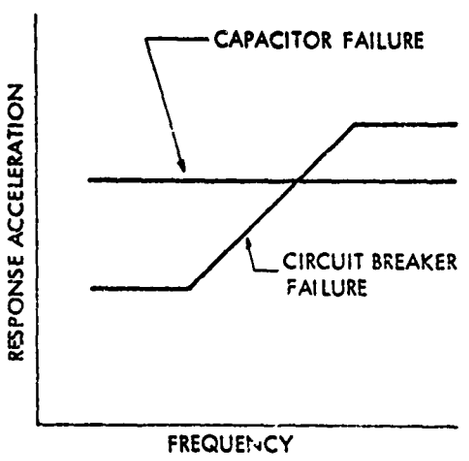

FIGURE 6a

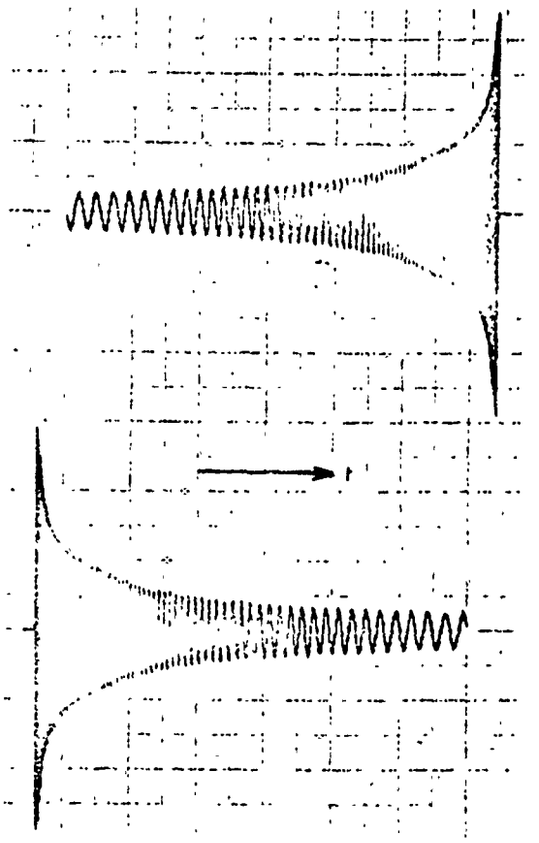

FIGURE 6b

IMPACT ON ASSESSMENT

Ideally, one must account for all the dynamic environments in the assessment. As shown in Figure 7, acoust and systematic air pressure pulses enter the picture in addition to the shock and vibration environment. This not only places the added burden on the assessment of deriving equipment fragility to these environments, but also requires that the appropriate set of shock and vibration environments be combined with a consistent set of acoustic and pressure environments.

This, of course, introduces another set of variables requiring definition of the interactions. In addition, the input now requires consideration not only of displacement and velocity, but acceleration as well. These data must then also be placed in the frequency domain, but this will be discussed later.

Assume for the moment that single valued descriptions of the fragility can be made; then the fragility curves as shown in Figure 8 could be generated. These sketches depict the fragility curves for all the fundamental parameters. If these were uniquely attainable, then it is still necessary to describe each parameter in

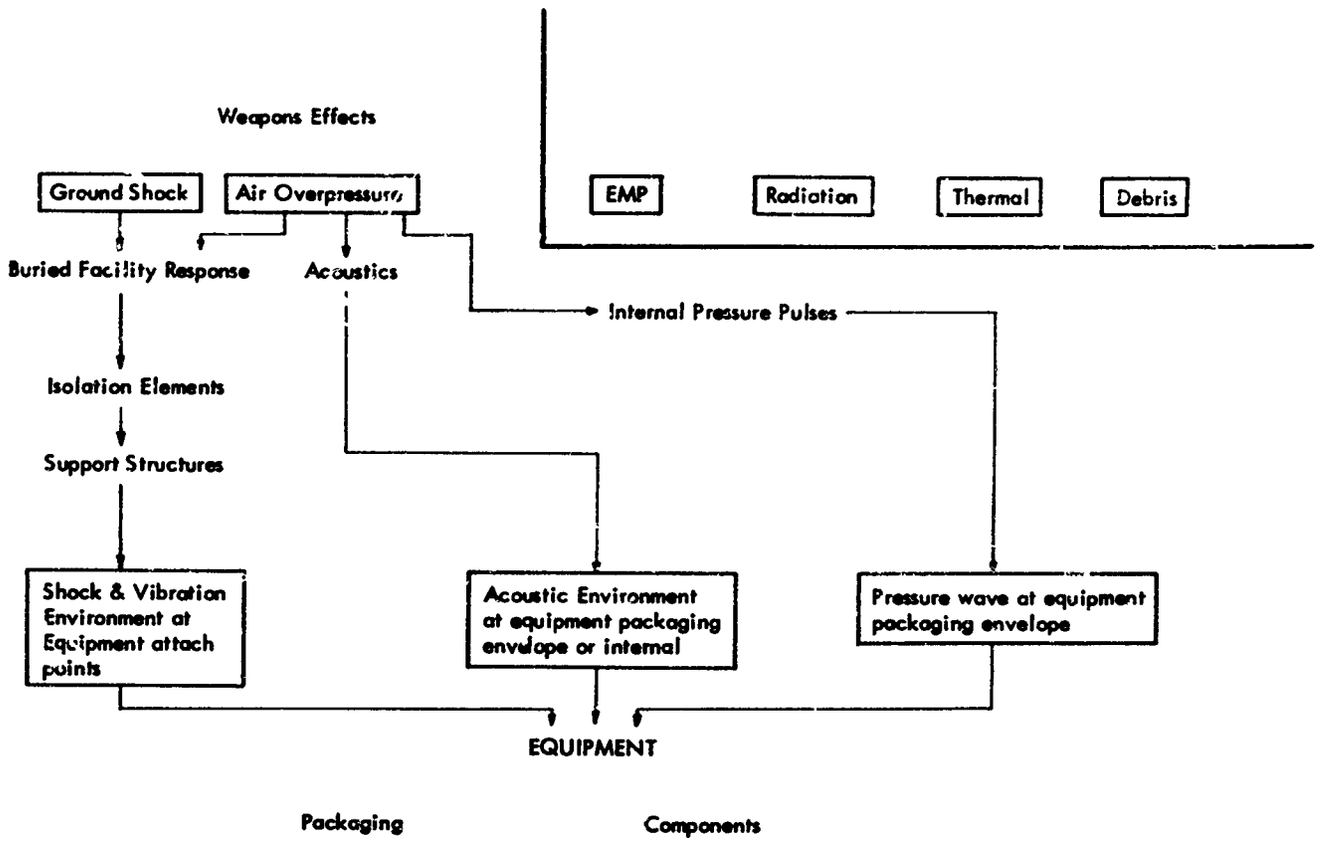
Weapons Effects
Ground Shock
Air Overpressure
EMP
Radiation
Thermal
Debris
Buried Facility Response
Acoustics
Internal Pressure Pulses
Isolation Elements
Support Structures
Shock & Vibration Environment at Equipment attach points
Acoustic Environment at equipment packaging envelope or internal
Pressure wave at equipment packaging envelope
EQUIPMENT
Packaging
Components

FIGURE 7

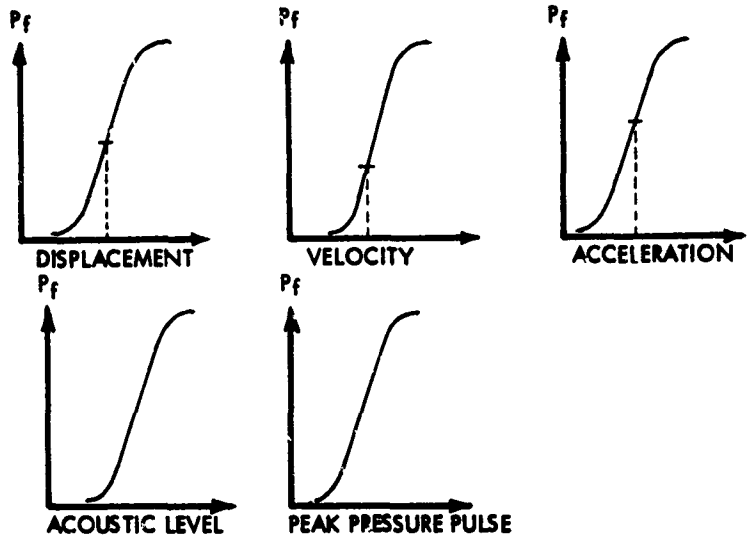

TYPICAL PROBABILITY OF FAILURE PARAMETRIC CONSIDERATIONS

FIGURE 8a

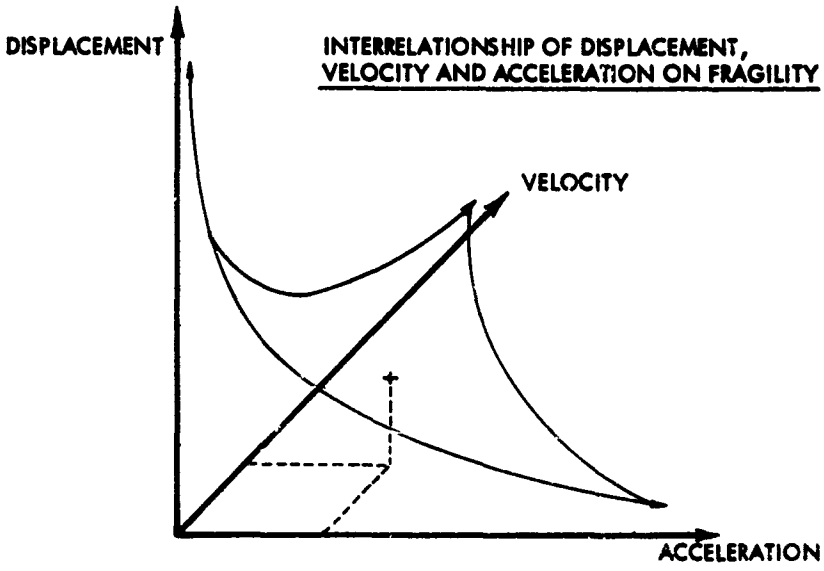

FIGURE 8b

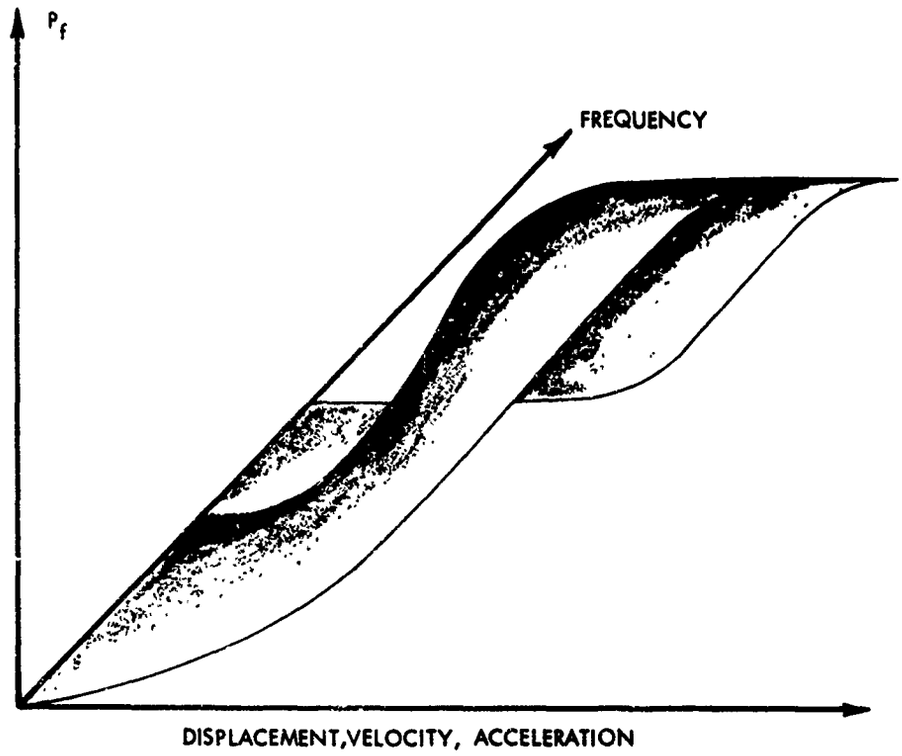

FIGURE 9

terms of the other so that a three dimensional surface such as Figure 8b might be developed for purposes of assessment. This would then permit all the degrees of freedom in the statistical analysis to be utilized. Finally consider Figure 9 where the frequency dimension has been added. The extreme complexity of the evaluation with this dimension added to the concepts of Figure 8 is obvious.

The above discussions are addressed to highlight the desirability of approaching the design of any new shock isolated system with the goal of making the system either insensative to several of the input parameters, or so capable that simplifying assumptions will not significantly impact the assessment.

TRANSMISSIBILITY TEST PROGRAM

Understanding the benefits to be derived in terms of increased capability to withstand attack and the desired simplification of the assessment it was clear that attention to the higher frequency characteristics of a shock isolation system could enhance the strategic value of a hardened weapon system. Following extensive literature searches it was evident that little information was available which could guide the analyst and designer in the choice of elements and detailed design to minimize the impact of high frequency dynamic environments.

Following the literature searches the previously mentioned test and analysis program identified as the Concept Development Transmissibility program was planned and initiated.

TEST PROGRAM PHILOSOPHY

Three specific goals for the Concept Development Transmissibility test program, were as follows:

(1) Provide a basis for comparison of alternate media and a figure of merit which can be assigned for trade studies. Early eliminationof materials or concepts with undesirable characteristics will result.

(2) Provide information indicating the influence of design details on system performance and provide insight into the depth to which isolation parameters need be known for meaningful analysis in support of concept selection.

HIGH FREQUENCY TRANSMISSIBILITY TEST AND ANALYSIS

ISOLATION ELEMENT	TYPE		CONFIGURATION VARIABLE	TEST CONDITION	
	NO.	VARIABLE		TYPE	DIRECTION
Foam	4 7	Materials Densities	4 Preloads	Load-Deflection Vibration	Compression Shear Tension/Compression Shear
	2 5	Materials Densities	8 Preloads	Shock	Tension/Compression Shear
Elastomers	3 5	Materials Durometers	3 Preloads	Shock	Compression Shear
Cables	4 2 3	Materials Diameters Lengths	3 Preloads	Shock	Vertical Horizontal
Liquid Isolators	2	Single Chamber	3 Fluid Types 3 Fluid Viscoscities 4 Damping Designs 5 Chamber Volumes 2 Piston Areas 3 Mountings 4 Preloads	Shock	Vertical Horizontal
		Dual Chamber 20 KIPS	3 Fluid Viscoscities 3 Preloads	Vibration Load-Deflection Shock Twang	Longitudinal Vertical Vertical Horizontal Vertical
		60 KIPS	2 Preloads 2 Mountings	Shock	Vertical Horizontal
Floors	2 6 4	Materials Structures Damping Designs	3 Loadings	Vibration Transient Special Impulse	Vertical Vertical Vertical Vertical
Equipment Rack	2	Rack/Drawer Designs	4 Loadings	Transient Vibration	3 orthogonal axes

FIGURE 10

(3) Provide empirical data and improved techniques for the prediction of isolation system dynamic environment and required equipment capability.

TEST PROGRAM SUMMARY DESCRIPTION

The program was postured to look carefully at individual elements and configurations which were candidates for inclusion in most practical designs of shock isolation. Figure 11 depicts the variables which have been investigated and the types of tests performed. The data from these tests were reduced in a variety of ways, trying to anticipate a number of potential uses. As appropriate, time histories, x-y plots, shock spectra, Fourier spectra, Fourier Transfer Functions and filtered signatures were constructed.

In each case, analysis was performed to attempt correlation with test results in the basic and low mode flexible operating regimes. The depth and form of the analysis varies for the different elements depending on the confidence in the ability to analyze and the interest in the particular elements as the program evolved. The analysis served two purposes 1) to estimate confidence in the system analysis validity and 2) to indicate the regime beyond which empirical results would have to be accepted.

Mr. Eshelman (IIT Research Institute): I was particularly interested in the fragility curve which measures failure, the one with probability versus frequency versus acceleration, velocity and displacement. Did you say that you do not know which one—velocity, displacement or acceleration—is the measure of failure, or are you saying it is different for different components?

Mr. Grant: The latter. The particular element of the environment to which it is sensitive varies with the piece of equipment. It varies with the particular isolation element and the other system parameters involved.

Mr. Eshelman: You say you cannot use one measure. The ISO uses velocity as their figure of merit for failure but that is a different situation, because it is a long time fatigue failure type of thing, where your's is a short time-duration type of failure.

Mr. Grant: Very true.

Mr. Eshelman: You showed some high frequency characteristics with the liquid spring. Do you have any idea whether they came from the fluid or from the structure that contains the fluid?

Mr. Grant: Yes, I do. The fluid column effects in the liquid spring tests are almost entirely indistinguishable. The other elements of the liquid spring, in this case a less general or more specific liquid spring, are the ones that control these high frequency environments. Elements such as damper valves are generally discreet operating items that open and close, and they cause their own internal environment. Seals on liquid springs are of different designs for different liquid springs. The stiffer ones transmit well. We ran some vibration tests on a liquid spring and of course as long as you do not break friction a liquid spring does not behave as an isolator. It behaves simply as another structural element and very linearly I might add. Very little of the environment for the liquid spring is directly transmitted under the normal shock approximation of the environment. However, unfortunately, the characteristics of our ground shock environment at the input to the liquid spring are such that, before it can start to get out of its own way, the sealing starts to transmit high amplitude, high frequency oscillatory inputs through the spring before friction is overcome, and therefore it is not really acting as an isolator. Once friction is broken, it goes into its low frequency normal operation, and becomes an excellent isolator. None that we have tested recently are better.

Mr. Eshelman: Did you do any work on pneumatic springs?

Mr. Grant: Very little.

TRANSIENT PULSE DEVELOPMENT

Jerry D. Crum & Richard L. Grant
The Boeing Company
Seattle, Washington

Over the years, standard industry requirements have specified slow sine sweep or random vibration testing for development and qualification testing of electronic equipment. Several simulated nuclear tests of large shock isolated subsystems determined that these requirements were overly severe, not from an amplitude standpoint, but rather from the duration of environment as related to expected nuclear attack considerations. The problem was that long duration testing generated responses of high Q responding systems much greater than the short duration "real world" environment would allow. The full scale simulated nuclear response environments were generalized by shock spectra techniques, and a transient vibration pulse developed to meet the resulting shock spectra criteria. These results, along with generalized considerations of development of a transient vibration test pulse are presented here.

INTRODUCTION

This paper summarizes the past five years of development of a transient test technique and its evolution with expanded knowledge of the real world response of a shock isolated subsystem to a nuclear attack environment. A considerable amount of data gathered in this time period substantiated the technology concern that slow sine sweep testing has little applicability to verification of the ability of an equipment design to survive a nuclear attack environment. It has always been understood that the nuclear blastwave itself is transient: That a hardened facilities response would then also be transient, and finally, that the equipment shock isolated within this facility would also be subjected to a transient environment not at all consistent with a slow sine sweep environment. However, the general assumption of beneficial conservatism as well as reliance upon existing specifications for testing of Air Force qualified equipment led to the continued use of the slow sine sweep test. As a practical matter this was a perfectly acceptable approach in lieu of specific knowledge of the environment, and as long as no undue penalty was imposed on the equipment particularly to the extent that signature sensitivity did not become important.

This paper discusses the relative damage potential of variaous classes of environments in terms of shock spectra. In turn, the rationale for development of shock spectra criteria for shock isolated equipment is presented, and finally the development of a transient test pulse which satisfies the criteria is shown. Practical usage of the technique using various control techniques is summarized.

BACKGROUND

The arguments for and against using shock spectra techniques for measuring damage potential to electronic equipment are many, varied and fundamentally too often discussed to repeat here. Basically, the authors feel that the variations of predicted weapons effects, the free field response, the facility response as well as the shock isolated subsystem responses negate any reasonable considerations to a more precise method of assessment of the design requirement for the shock isolated element. Shock spectra techniques fall short of a precise definition of the real world environment, but so also do the sources of the environment fall short of yielding a precise and predictable real world definition. No further defense is offered.

In further consideration of damage potential, it is first necessary to consider the fundamental response of single degree of freedom oscillator to sinusoidal excitation at its resonant frequency.

For the single degree of freedom oscillator response to sinusoidal excitation at its natural frequency, and for

light damping (i.e. $4Q^2 \gg 1.0$), the following equation is given.

$$\ddot{X}_r = Q\ddot{X}_o\left(1 - e^{-\omega_n t/2Q}\right)\cos\omega_n t \qquad (1)$$

Since the excitation is at the oscillator natural frequency, then

$$\omega_n t = 2\pi f_n t = 2\pi f_o t = 2\pi N \qquad (2)$$

where N is the number of cycles impressed on the oscillator in the time period 0 to t. Allowing equation (1) to be maximized, we have

$$\ddot{X}_r = Q\ddot{X}_o\left(1 - e^{-\pi N/Q}\right) \qquad (3)$$

which when considering the ratio of oscillator response acceleration to the input acceleration appears as

$$\frac{\ddot{X}_r}{\ddot{X}_o} = Q\left(1 - e^{-\pi N/Q}\right) \qquad (4)$$

Terms:

$Q = \frac{1}{2\zeta}$, Damping quality factor

ζ = The percent of critical damping

N = Number of sinusoidal cycles

W_n = Oscillator natural circular frequency

$\ddot{X}_o$ = Input peak acceleration

$\ddot{X}_r$ = Oscillator response peak acceleration

t = time

Thus it is seen that the oscillator ratio of response to input acceleration for sinusoidal excitation is a function only of the number of cycles of impressed motion (N) and the oscillator damping (Q).

A plot of Equation (4) for various values of Q is shown in Figure 1.

Now, using Figure 1, a second graph is derived which qualitatively classifies the kinds of environments considered in terms of their effect of the single degree of freedom oscillator response.

Referring to Figure 1, it is seen that for very small values of N (N=1/2, simple half sine excitation) the oscillator response ratio is virtually independent of Q. For large values of N, the oscillator response becomes independent of N and dependent only on the value of Q. For all cases within these limits, the response ratio is a function of both N and Q. It is this class that is termed the region of transient vibration. Figure 11 depicts this classification of environments.

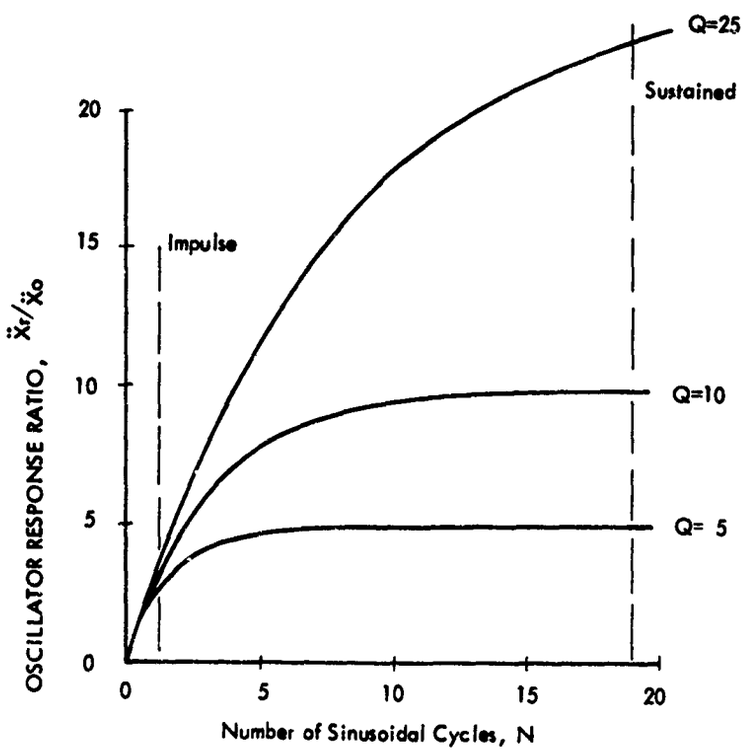

FIGURE I
OSCILLATOR RESPONSE TO SINUSOIDAL BASE MOTION

As was mentioned, a considerable amount of data has been gathered which was utilized to derive a transient test criteria of shock isolated equipment. This data resulted from tests of single coil spring type isolators, dual-isolator tests with beam segment floor simulation, and full scale high explosive simulation technique tests of hardened facilities. Data from these tests were usually reduced to shock spectra for two different damping values: Usually ζ's of 10% and 2% (Q=5 and 25 respectively) were used in these shock spectra analyses. A typical example is shown in Figure III.

It is this type of data in conjunction with the approaches defined by Figures I and II that were used to develop the test criteria. Inspection of Figure III leads to several observations. Specifically, at some frequencies the ratio of a Q=25 oscillator response to a Q=5 oscillator approaches the maximum of 5.0. This is the "near sustained" condition as depicted in Figure II. At other frequencies, the ratio of Q=25 to Q=5 oscillator response approaches 1.0, or the "impulse region" as shown in Figure II.

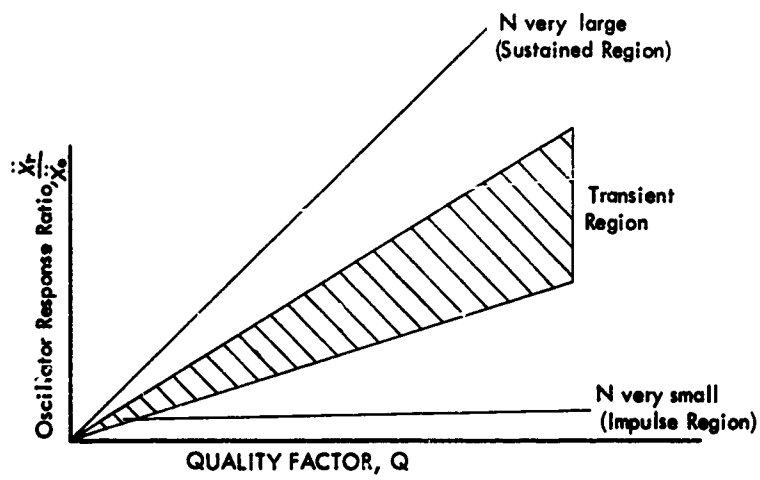

FIGURE II

CLASSIFICATION OF ENVIRONMENTS

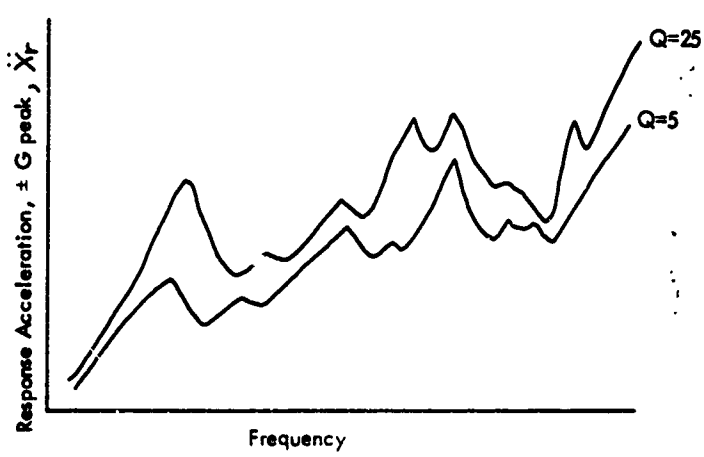

FIGURE III

TYPICAL ISOLATION SYSTEM TEST SHOCK SPECTRA (EXAMPLE)

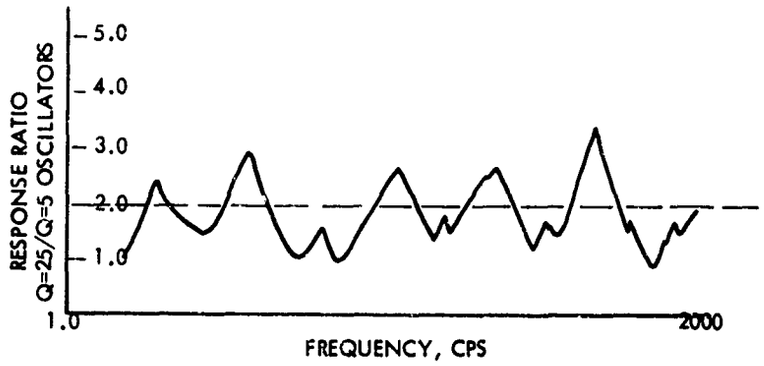

FIGURE IV

RATIO OF Q=25 TO Q=5 SHOCK SPECTRA (Example)

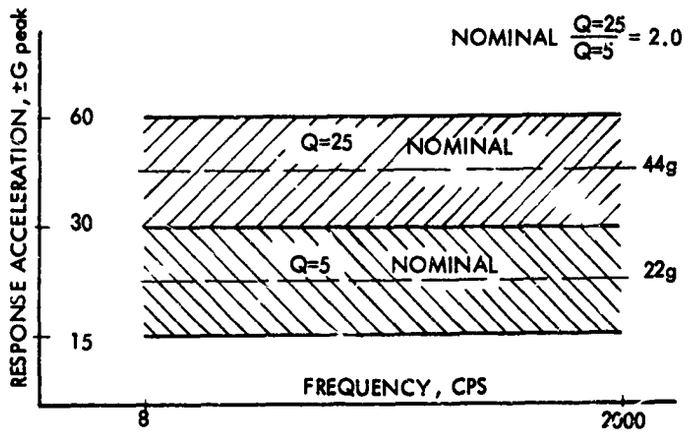

FIGURE V

ORIGINAL TRANSIENT TEST CRITERIA

By ratioing the Q=25 response to Q=5 response as a function of frequency, the graph shown in Figure IV is derived.

This was the final step towards the development of the original transient test criteria. The amplitude shock spectra were enveloped to develop the amplitude criteria. The ratio of Q=25/Q=5 oscillator responses were enveloped to derive the transient condition (or class) to be met. The results were presented as shown by Figure V.

It was this criteria that led to the development of the first transient test pulses by Boeing. Other variations have since been considered as are summarized later.

TECHNICAL APPROACH

Given the definition now of the class of transient vibration criteria, it was necessary to decide if a quasi-random or systematic test pulse definition would best meet the criteria. The most important factor in the choice of method was the fact that the nominal spectrum criteria established a fixed ratio between Q=25 and Q=5 oscillator responses. Specifically, all Q=25 oscillators were to respond to 2.0 times the Q=5 oscillator response. What this implied was that every oscillator in the frequency domain of the test criteria must see exactly the same number of cycles. In the time domain, the damped oscillator if subjected to a quasi-random environment would alternately reach peaks and dampen out as the frequencies of the quasi-random pulse were at or near the oscillators natural frequency. Controlling the response amplitude of Q=25 oscillators to Q=5 oscillator responses did not seem feasible with a quasi-random approach. Thus, the systematic test pulse approach was selected. This permitted development of analytical analyses which would approach the desired realism and also afford the opportunity for a more exact engineering evaluation of observed results. The development of these concepts is expanded as follows.

The requirement was to develop the analytical express-

ion for an acceleration pulse which would generate the desired shock spectrum responses as specified by the established criteria. The general form of the expression was selected as

$$\ddot{x}(t) = \ddot{X}_o \sin\left[\theta(t)\right] \tag{5}$$

Repeating equation (4) here

$$\frac{\ddot{X}_r}{\ddot{X}_o} = Q\left(1 - e^{-\pi N/Q}\right)$$

It is reiterated that the single degree of freedom oscillators response is a function only of the numbers of cycles of impressed motion (N) and the oscillators damping (Q). Thus, the ratio of response for two oscillators with the same natural frequency, but different values of damping may be expressed as follows:

$$R = \frac{\ddot{X}_{r_2}}{\ddot{X}_{r_1}} = \frac{Q_2}{Q_1}\left[\frac{\left(1 - e^{-\pi N/Q_2}\right)}{\left(1 - e^{-\pi N/Q_1}\right)}\right] \tag{6}$$

It is seen then that to control the responses of oscillators with different damping to be a specified ratio depends only on the value of N. Further, since the above expression holds for all oscillators independent from their natural frequency, the N must be constant for all oscillators in the frequency domain to maintain a constant value for the ratio R. This background allows us to proceed to the development of the sine function argument, $\theta(t)$.

The specific requirements for the transient pulse imply that it contains all frequencies within the specified range of frequencies of the criteria. That is to say, the argument $\theta(t)$ must have both first and second derivatives defined as follows:

$$\frac{d\theta(t)}{dt} = 2\pi f(t) \tag{7a}$$

$$\frac{d^2\theta(t)}{dt^2} = 2\pi \dot{f}(t) \tag{7b}$$

It is understood now that the transient pulse must yield the same results as a multitude of individual sinusoidal forcing functions applied at the natural frequencies of an ensemble of single degree of freedom oscillators. The term, N′, is introduced to represent the pseudo number of transient test cycles impressed in the bandwidth of a resonant oscillator.

We must assume that the function f(t) above is continuous in the time domain from t_o to t. Thus, the instantaneous frequency at time $t = t_1$, will be f_1 and at a different time $t = t_2$, the instantaneous frequency will be f_2. If the assumption that f(t) is continuous holds, then we may consider a small Δt in time before and after t_1 and establish the instantaneous frequencies of these times. This may also be done at time t_2. Figure VI illustrates this approach.

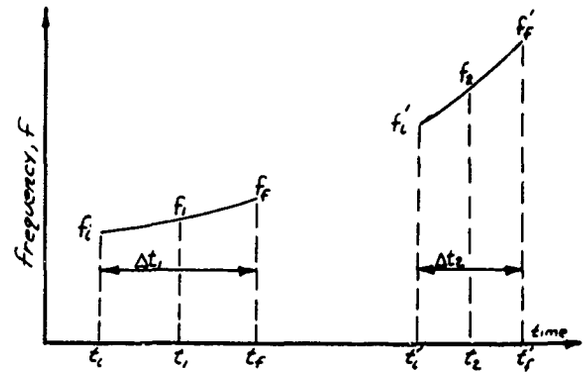

FIGURE VI

If all the frequencies in the time domain t_i and t_f can be assumed to act at the center frequency f_1, then we can establish the effective number of cycles, N′, in the elapsed time $\Delta t_1 = (t_f - t_i)$.

$$N' = f_1(t_f - t_i) = f_1 \Delta t_1 \tag{8}$$

At another time $t = t_2$, the same thing may be found

$$N' = f_2 \Delta t_2 \tag{9}$$

and since we have established that N′ must be constant for all frequecies in the domain, we may consider Δt_2 to be fixed by

$$\Delta t_2 = \frac{N'}{f_2} \tag{9a}$$

Now, by determining the difference in elapsed times Δt_1 and Δt_2 required to generate the same number of cycles, N′, at center frequencies f_1 and f_2, the change in elapsed time as a function of center frequency is found.

$$\Delta t = (\Delta t_2 - \Delta t_1) = \pm N'\left(\frac{1}{f_2} - \frac{1}{f_1}\right) \tag{10}$$

The plus or minus sign is necessary since it is not known whether Δt_2 is larger or smaller that Δt_1. We may write the above expression as

$$\Delta t = \frac{N'(f_1 - f_2)}{f_1 f_2} = \frac{N'\Delta f}{f_1 f_2} \tag{10a}$$

and

$$\Delta t = \frac{-N'\Delta f}{f_1 f_2} \tag{10b}$$

where the expression is negative if f_1 is less than f_2 (increasing frequency) and positive if f_1 is greater than f_2 (decreasing frequency).

In the limit

$$\Delta t \rightarrow dt \tag{11}$$

$$\Delta f \rightarrow dt$$
$$t_1 t_2 \rightarrow f_1^2 \rightarrow f_2^2 \rightarrow f^2 \qquad (11)$$

so that the above expression may be written as

$$dt = \pm N \frac{df}{f^2} \qquad (12)$$

To find then an expression for the instantaneous frequency, it is necessary to integrate the above expression and establish boundary conditions.

Thus

$$\int_0^t dt = \pm N' \int_{f_0}^{f} \frac{df}{f^2} \qquad (13)$$

$$t = N'\left[\frac{1}{f_0} - \frac{1}{f}\right] \quad \text{increasing frequency} \qquad (13a)$$

$$t = -N\left[\frac{1}{f_0} - \frac{1}{f}\right] \quad \text{decreasing frequency} \qquad (13b)$$

where f_0 is in each case the starting frequency of the sweep.

Solving the above expression for frequency, f,

$$f = \frac{f_0}{1 - \frac{f_0 t}{N'}} \quad \text{increasing frequency} \qquad (14a)$$

$$f = \frac{f_0}{1 + \frac{f_0 t}{N'}} \quad \text{decreasing frequency} \qquad (14b)$$

It is now simply a matter of integrating these expressions to find the sine function argument, $\theta(t)$

$$\frac{d\theta(t)}{dt} = 2\pi f(t) \qquad (7a)$$

$$\int_0^t d\theta(t) = 2\pi \int_0^t f(t)\,dt \qquad (15)$$

$$\theta(t) = 2\pi \int_0^t \frac{f_0}{1 \pm \frac{f_0 t}{N'}}\,dt \qquad (15a)$$

$$\theta(t) = -2\pi N' \ln\left(1 - \frac{f_0 t}{N'}\right) \quad \text{increasing frequency} \qquad (15b)$$

$$\theta(t) = 2\pi N' \ln\left(1 + \frac{f_0 t}{N'}\right) \quad \text{decreasing frequency} \qquad (15c)$$

Thus, the complete expressions for the transient pulses become:

$$\ddot{X}(t) = \ddot{X}_0 \sin\left[-2\pi N' \ln\left(1 - \frac{f_0 t}{N'}\right)\right] \qquad (16a)$$

for increasing frequency

$$\ddot{X}(t) = \ddot{X}_0 \sin\left[2\pi N' \ln\left(1 + \frac{f_0 t}{N'}\right)\right] \qquad (16b)$$

for decreasing frequency

PRACTICAL APPLICATIONS AND TESTING

Given the form of the equation for a transient pulse, it is still necessary to develop the values to be used in input for the parameters of the equation. Specifically, the values of N', $\ddot{X}_0$ and the starting and final frequencies must be selected.

The authors developed empirical relationships for derivation of these parameters. Some recent work within Boeing has used a more classical approach for solution of the parameters in the transient pulse equation. This work is not presented here, but it is hoped that it may be presented in the future.

The selection of the values of $\ddot{X}_0$ and N' are interrelated unilaterally. That is, the value of $\ddot{X}_0$ is a function of N', but the value of N' is dependent only on the ratio between the two shock spectra with different damping values, and not a function of the pulse amplitude, $\ddot{X}_0$. Therefore, we will develop a selection criteria for N' first, and leave $\ddot{X}_0$ and the frequency range to follow.

A number of shock spectra analyses were performed for transient pulses with a unit value for $\ddot{X}_0$ and a set of values of N'. Spectra analyses were performed for oscillator damping values of 2% and 10% of critical, or Q's of 25 and 5. Figure VII shows the results in terms of the ratio of Q=25 oscillator response to Q=5 oscillator response as a function of N'. This curve may be used directly then to select a value of N' for any specified ratio of Q=25 to Q=5 oscillator response.

The results of the shock spectra analyses were also presented in a second manner. Specifically, the amplification of a Q=5 oscillator to the input amplitude $\ddot{X}_0$ is plotted as a function of N'. This is shown in Figure VIII. Thus after selecting N' from the spectrum ratio criteria, the amplification of a Q=5 oscillator is found from Figure VIII as a function of the selected N'. Given the criteria amplitude for the Q=5 spectrum, the value of $\ddot{X}_0$ may be selected.

Finally, the frequency range of the transient pulse must be selected. It is the nature of the transient pulse that the resonant oscillators are affected by the frequencies preceeding and following the center frequency of the oscillator. There is a resonant build up and decay as the transient pulse sweeps through the oscillators resonant frequency. Thus, the established criteria spectrum's end frequecies cannot coincide with the starting and final frequencies of the transient pulse. The empirical relationship defined for selecting the pulse end frequencies is as follows. Given the end frequencies of the shock spectrum criteria, extend the transient pulse frequencies to 25% below the lower spectrum frequency and 25% above the upper spectrum frequency.

Using these three empirical relationships, the following example is given for selecting the transient pulse

parameters.

Using the criteria shown in the backgound statements (Q=5 spectrum nominal of 22 g's: Ratio of Q=25/Q=5 spectrum = 2.0: Spectrum end frequencies of 8 and 2000 cps) a value of N' of 10 is selected from Figure VII to provide the spectrum ratio of 2.0. Figure VIII is then used to determine that the Q=5 oscillator amplifies the input acceleration 4.25 times for a N' of 10. Thus, dividing the nominal Q=5 spectrum value of 22 g by the amplification of a Q=5 oscillator of 4.25 yields a pulse amplitude of $\pm$ 5.1 g's. Using the empirical rule for end frequencies, the pulse should cover the range from 6 to 2500 cps. The total transient pulse definition then becomes

$$\ddot{X}_t = 5.1 \sin \pm(10 \times 2\pi) \ln\left[1 \pm \frac{6t}{10}\right] \qquad (17)$$

and the time required to traverse the frequency range from 6 to 2500 cps is

$$t = N'\left(\frac{1}{f_o} - \frac{1}{f_f}\right) \qquad (18a)$$

$$t = N'\left(\frac{1}{6} - \frac{1}{2500}\right) = 1.663 \text{ seconds} \qquad (18b)$$

This pulse and the resulting shock spectra are shown in Figure IX.

The use of the developed test pulse in equipment testing has taken two approaches. Originally, the pulse with the specified parameters was generated by an analog computer and recorded on FM tape. This tape was then played through a set of passive filters and then to the power amplifier at a shaker system. The system was equalized by trial and error by pulsing the system, computing the shaker output shock spectrum, adjusting the passive filters, and re-running until adequate equalization was obtained.

More recently, the pulse has been generated solely by digital computer, and test system equalization and control performed by using a digital transient waveform control system (ref. 1). This system uses Fourier Transform and convolution techniques to derive a synthesized waveform which when played through the shaker system yields a shaker output very closely approximating the desired transient waveform. This system effectively performs the shaker system equalization automatically.

Elements tested have included electronic equipment racks up to 1200 pounds in weight, and other electrical equipment weighing over 2000 pounds. The results of the testing using the transient test pulse and the evaluations relative to the ability of the equipment to survive nuclear attack have been, overall, very successful.

Variations to the basic pulse defined above have since been developed and used for equipment tests. These include programming a variable pulse amplitude to achieve shock spectra with variable amplitudes, and programming a variable value for N' to achieve shock spectra with a variable ratio of Q=25 to Q=5 oscillator responses. The development of these variations has not been reported here, but were fairly straight forward. A later paper could be written to report on these and other developments.

CONCLUSIONS

A more realistic environment to simulate the expected response of a shock isolated subsystem to nuclear attack has been formulated. The result is a more precise definition of the equipment fragility and ultimately, a better definition of overall system survival. The transient test technique is a straight forward and reasonable alternative to slow sine sweep tests for equipment intended to be located in a hardened facility.

ACKNOWLEDGEMENTS

The authors wish to acknowledge to previous unreported work of R. N. Paczkowski and G. J. Czajkowski, former Boeing Structures Staff Engineers, for their contributions to this paper.

REFERENCES

1) Favour, J. D., LeBrun, J. M., and Young, J. P., "Transient Waveform Control of Electromagnetic Test Equipment", 40th Shock and Vibration Symposium, 1969.

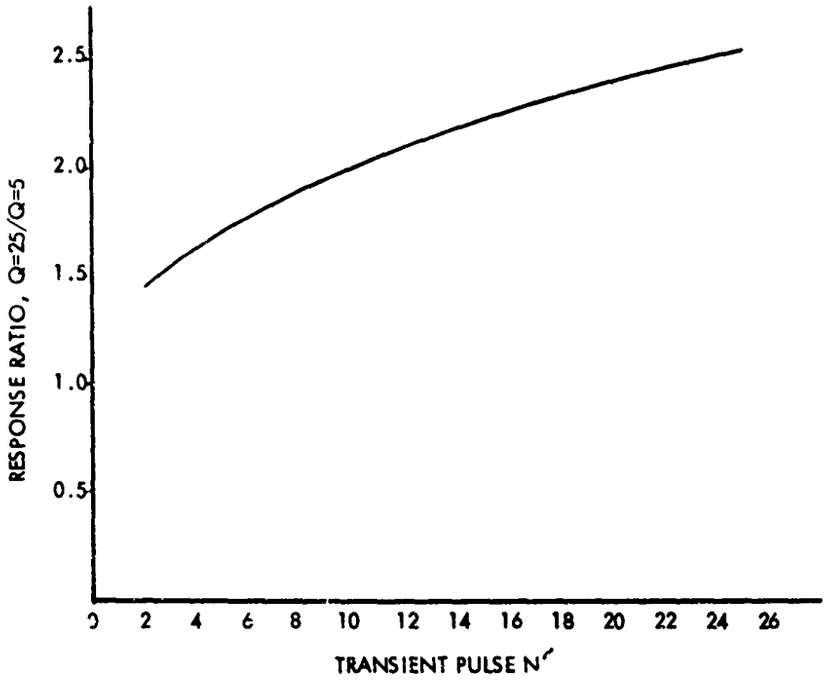

Q=25/Q=5 RESPONSE VS. PARAMETER N′ FOR TRANSIENT PULSE UPSWEEP
FIGURE VII

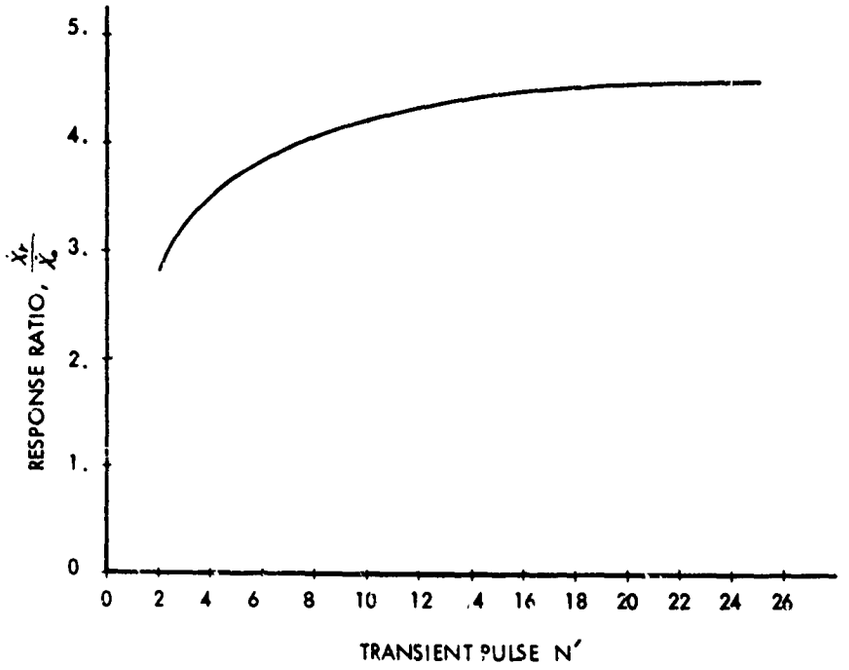

Q=5 OSCILLATOR RESPONSE VS. PARAMETER N′ FOR TRANSIENT PULSE UPSWEEP

FIGURE VIII

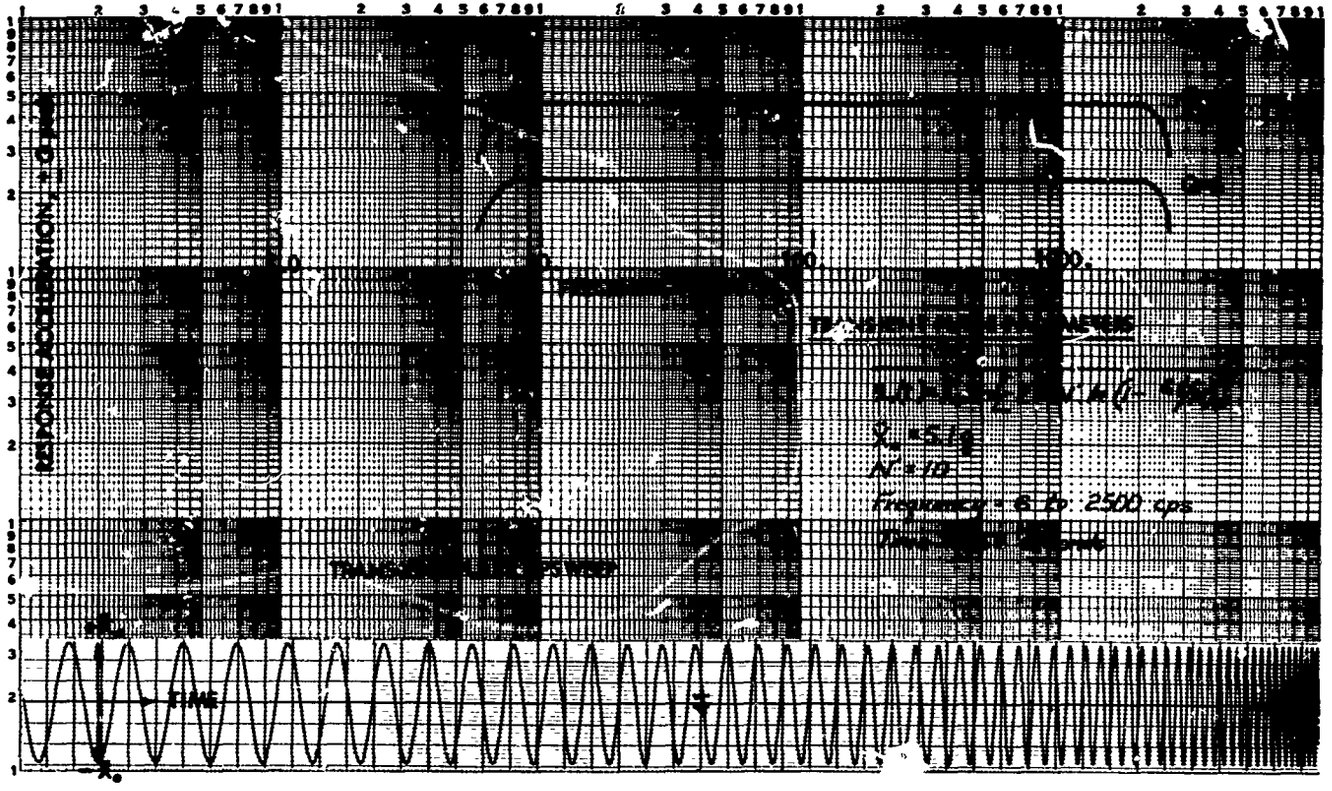

TRANSIENT PULSE AND SHOCK RESPONSE SPECTRA

FIGURE IX

Mr. Schell (Shock and Vibration Information Center): Would you comment on the type of environment and the durations of the transients being simulated?

Mr. Crum: They are generally extremely short. I cannot be specific without getting classified, but we do have environments which are long in duration relative to the low frequency response of the system. We have environments of very short duration, for example, when an isolator tops out against a can. As a practical matter, when we are testing the equipment, we apply the pulse a prescribed number of times so we achieve a total test time in excess of the 1.6 seconds it would take for one pulse.

Mr. Duel (Motorola): What rationale did you use to choose a ratio of two between the Q of 25 and of 5 oscillator?

Mr. Crum: This was developed based on the measured responses of the shock isolation tests that were performed. Specifically, we took measured shock spectra of Q of 25 and Q of 5 values, performed the ratio, plotted it as a function of frequency and then enveloped this, or selected a nominal of these data.

Mr. Keith (Kaman Sciences) You referenced a paper by Favour in which he used a shaker and Fourier transform techniques and had quite good success in actually reproducing these transient pulses. I am curious as to why you went back to this sine sweep technique when you could actually reproduce a pulse?

Mr. Grant: I will field that one. One of the points which I made previously that deserves some attention here, perhaps, is that the transient character of the pulse is not single valued. It depends on the input, on the peculiarities of the shock isolation system, on where the equipment is sitting on the floor, on how it is mounted and on the particular equipment item itself. On that basis, if we could uniquely describe it, there would be as many different transient pulses to simulate as there are pieces of equipment, locations on the floor, and types of shock isolation systems. In this sense, we had to use some expedient to approximate all those environments and come up with something that was more or less standard to be applied across all the systems we were testing.

Mr. Schell: I think there is also another reason. You also have a shock spectrum specification to meet for these items, do you not?

Mr. Grant: On the input, not necessarily on the response. We never really had criteria on the equipment itself except for design goal purposes. As it turned out it was specified as a shock spectrum. However, it did not have associated with it any necessary transient qualities.

Mr. Safford: I think several years ago at a Shock and Vibration Symposium, Warren Painter, Lockheed Company, developed a complex time-history transient in a paper* to which you might wish to refer. He was trying to simulate pyrotechnic shock, but you could still run into the problems that Dick discussed for multiple environments and transmission paths.

*Editors note: Shock and Vibration Bulletin 33, Part 3, p85, March 1964.